Selection of new therapeutic targets in relation to lipid metabolism in Mycobacterium abscessus

Tonia Dargham

NNT : 0000AIXM0000

THÈSE DE DOCTORAT

Soutenue à Aix-Marseille Université
Le 10 Avril 2024 par

Tonia DARGHAM

Sélection de nouvelles cibles thérapeutiques en lien avec le métabolisme lipidique de *Mycobacterium abscessus*

Discipline
Biologie-Santé

Spécialité
Microbiologie

École doctorale 62
Sciences de la vie et de la santé

Laboratoire d'ingénierie des systèmes macromoléculaires UMR7255

Centre National de la Recherche Scientifique

Composition du jury

Caroline DEMANGEL INSERM, Institut Pasteur, Paris	Rapportrice
Jérôme NIGOU CNRS, IPBS, Toulouse	Rapporteur
Oana DUMITRESCU CNRS, CIRI, Lyon	Examinatrice
Gérarld LARROUY-MAUMUS Imperial college, Londres	Examinateur
Nathalie WINTER ISP, INRAE, Tours	Présidente du jury
Stéphane CANAAN LISM, CNRS, Marseille	Directeur de thèse
Laurent KREMER IRIM, CNRS, Montpellier	Co-encadrant de thèse

Affidavit

Je soussigné, Tonia DARGHAM, déclare par la présente que le travail présenté dans ce manuscrit est mon propre travail, réalisé sous la direction scientifique des *Dr. Stéphane CANAAN et Dr. Laurent KREMER*, dans le respect des principes d'honnêteté, d'intégrité et de responsabilité inhérents à la mission de recherche. Les travaux de recherche et la rédaction de ce manuscrit ont été réalisés dans le respect à la fois de la charte nationale de déontologie des métiers de la recherche et de la charte d'Aix-Marseille Université relative à la lutte contre le plagiat.

Ce travail n'a pas été précédemment soumis en France ou à l'étranger dans une version identique ou similaire à un organisme examinateur.

Fait à Marseille, le 02 février 2024.

Liste de publications et/ou brevets et participation aux conférences

1) Liste des publications réalisées dans le cadre du projet de thèse :

1. Dargham T., Mallick I., Raze D., Kremer L., Canaan S., “Intrabacterial lipid inclusions: overview of an amazing organelle”, Biology of Mycobacterial Lipids book Juin 2022, DOI : 10.1016/B978-0-323-91948-7.00003-8

2. Dargham T., Mallick I., Kremer L., Santucci P., Canaan S., “Intrabacterial lipid inclusion-associated proteins: A core machinery conserved from saprophyte Actinobacteria to the human pathogen Mycobacterium tuberculosis?” FEBS open Bio, Octobre 2023, DOI : 10.1002/2211-5463.13721

3. Avellan R*., Lehoux J*., Dargham T*., Celik L., Guy A., Poncin I., Point V., Kremer L., Durand T., Audebert S., Camoin L., Spilling CD., Crauste C., Canaan S., Cavalier J-F., (*contribution égale) “Mapping of lipolytic enzymes involved in triacylglycerol accumulation as intrabacterial lipid inclusions using multi-target inhibitor-like affinity-based probes”. Manuscrit en preparation.

4. Dargham T*., Jairo Aguilera-Correa J*., Avellan R.*, Mallick I., Celick L., Brasseur G., Camoin L., Audebert S., Poncin I., Point V., Daher W., Cavalier J-F., Kremer L., Canaan S., (*contribution égale) “Deciphering the ILI proteome dynamics during the synthesis phase: unveiling novel therapeutic targets against mycobacteria”. Manuscrit en preparation.

2) Participation aux conférences et écoles d'été au cours de la période de thèse :

1. Présentation de poster : Mise en place de APEX2 dans le modèle d'accumulation des lLI chez *M. abscessus*. T. Dargham, I. Mallick, L. Kremer, S. Canaan. Journée de l'infectiopôle, Marseille le 01 juillet 2021.
2. Présentation orale : Sélection de cibles potentielles pendant la biogénèse des lLI chez *M. abscessus*. T. Dargham, I. Mallick, L. S. Audebert, L. Camoin, Kremer, S. Canaan Junior Scientists of Marseille JSM3, Marseille le 05 mai 2022.
3. Présentation orale : Sélection de cibles potentielles pendant la biogénèse des lLI chez *M. abscessus*. T. Dargham, I. Mallick, L. S. Audebert, L. Camoin, Kremer, S. Canaan. Mycodays 2022, Lyon le 22 juin 2022.
4. Présentation de poster : Sélection de cibles potentielles pendant la biogénèse des ILI chez *M. abscessus*. T. Dargham, I. Mallick, L. S. Audebert, L. Camoin, Kremer, S. Canaan. Journée de l'infectiopôle, à Marseille le 03 juillet 2022.
5. Présentation orale : Validation des protéines impliquées dans le métabolisme lipidique chez *M. abscessus*. T. Dargham, I. Mallick, L. J. Jairo Aguilera-Correa, S. Audebert, L. Camoin, V. Point, I. Poncin, W. Daher, Kremer, S. Canaan. Civis Summer School, Tubingen, Allemagne le 08 juillet 2022.
6. Présentation de poster : Validation des protéines impliquées dans le métabolisme lipidique chez *M. abscessus*. T. Dargham, I. Mallick, L. J. Jairo Aguilera-Correa, S. Audebert, L. Camoin, V. Point, I. Poncin, W. Daher, Kremer, S. Canaan. Microbes 2022, 17^{e} Congrès de la SFM « La microbiologie dans tous ses états », Montpellier, le 05 octobre 2022.
7. Présentation de poster : Sélection et validation des cibles thérapeutiques en lien avec le métabolisme des triacylglycérols chez *M. absccesus*. Dargham T., Jairo Aguilera-Correa J, Avellan R., Mallick I., Celick L., Brasseur G., Camoin L., Audebert S., Poncin I., Point V., Daher W., Cavalier J-F., Kremer L., Canaan S. Junior Scientists of Marseille JSM3, Marseille du 10-12 mai 2023.
8. Présentation orale : Sélection et validation des cibles thérapeutiques en lien avec le métabolisme des triacylglycérols chez *M. absccesus*. Dargham T., Jairo Aguilera-Correa J, Avellan R., Mallick I., Celick L., Brasseur G., Camoin L., Audebert S., Poncin I., Point V., Daher W., Cavalier J-F., Kremer L., Canaan S. Journée de l'infectiopôle, Marseille le 07 juillet 2023.

Résumé

Les gouttelettes lipidiques sont des organites conservés dans un grand nombre d'organismes ayant un rôle essentiel dans le stockage de l'énergie et dans le renouvellement des membranes. Parmi les procaryotes, les actinobactéries, notamment le genre *mycobacterium*, sont les plus connus comme étant capables d'accumuler des triacylglycérols sous forme d'inclusion lipidique intrabactérienne (ILI). En plus de leur rôle de source de carbone, les ILI sont impliquées dans la tolérance aux antibiotiques, la persistance et la virulence. Ces organites sont entourés d'une monocouche de phospholipides au niveau de laquelle des protéines sont ancrées. Malgré de récentes études réalisées sur le protéome des ILI, peu de choses sont connues sur les principaux acteurs protéiques chez *M. tuberculosis* et *M. abscessus*, deux pathogènes responsables d'infections pulmonaires chez l'homme. Dans ce contexte, ma thèse a été centrée sur l'identification du protéome des ILI au cours de leur synthèse et de leur dégradation chez *M. abscessus*. En utilisant un modèle réversible *in vitro* développé au laboratoire couplé à une technique de marquage de proximité « APEX2 » et la spectrométrie de masse, j'ai pu identifier les protéines qui seraient présentes à la surface de ces ILI au cours de leur synthèse et de leur dégradation. J'ai pu également montrer qu'il s'agissait d'un processus dynamique impliquant des échanges de protéines en fonction de la taille des ILI. Enfin, j'ai validé une partie de mes résultats et déterminé l'implication des quelques protéines dans la biogénèse de ces ILI. Au cours de ma thèse, seule une partie des résultats que j'ai générés a pu être exploitée dans le temps imparti mais l'ensemble des données (biogénèse et dégradation des ILI), une fois validé, pourrait ouvrir de nouvelles perspectives sur le rôle physiologique de ces protéines comme étant de potentielles cibles thérapeutiques permettant de contrer la persistance des mycobactéries.

Mots clé : *Mycobacterium abscessus*, inclusions lipidiques intrabactériennes, APEX2, protéome, cibles thérapeutiques, métabolisme lipidique.

Abstract

Lipid droplets are conserved organelles in a large number of organisms, playing an essential role in energy storage and membrane renewal. Among prokaryotes, actinobacteria, notably the genus *mycobacterium*, are known for their ability to accumulate triacylglycerols in the form of intrabacterial lipid inclusions (ILIs). In addition to their role as a carbon source, ILIs are involved in antibiotic tolerance, persistence and virulence. These organelles are surrounded by a phospholipid monolayer to which proteins are anchored. Despite recent studies on the ILI proteome, little is known about the main protein players in *M. tuberculosis* and *M. abscessus*, two pathogens responsible for lung infections in humans. In this context, my thesis focused on identifying the ILI proteome during synthesis and degradation in *M. abscessus*. Using a reversible *in vitro* model developed in the laboratory, coupled with an APEX2 proximity labeling technique and mass spectrometry, I was able to identify the proteins that would be present on the surface of these ILI during their synthesis and degradation. I was also able to show that this was a dynamic process involving protein exchanges depending on ILI size. Finally, I validated some of my results and determined the involvement of a few proteins in the biogenesis of these ILIs. During my thesis, only a part of the results I generated could be exploited, but the data set (ILI biogenesis and degradation), once validated, could open up new perspectives on the physiological role of these proteins as potential therapeutic targets for countering the persistence of mycobacteria.

Keywords: *Mycobacterium abscessus*, intrabacterial lipid inclusions, APEX2, proteome therapeutic targets, lipid metabolism.

Remerciements

Je tiens à remercier tout d'abord mon directeur de thèse, le docteur Stéphane Canaan, pour son soutien, ses conseils et ses encouragements tout au long de mon doctorat. Je suis reconnaissante de sa patience, de sa disponibilité et de sa confiance en moi. Je remercie également mon co-directeur de thèse, le docteur Laurent Kremer pour toutes les discussions inspirantes et les contributions scientifiques qu'on a eu pendant ces trois années. C'est grâce à une offre de thèse dans son laboratoire que j'ai eu l'opportunité de commencer cette aventure à Marseille dans l'équipe « Lipolyse et Pathogénie Bactérienne ».

Je remercie les membres de mon jury de thèse, Dr Nathalie Winter d'avoir accepté d'en présider le jury, Dr Caroline Demangel et Dr Jérome Nigou de m'avoir fait l'honneur d'évaluer ce travail en tant que rapporteurs. Je tiens aussi à exprimer ma gratitude à Dr Gérald Larrouy-Maumus et Dr Oana Dumitrescu pour avoir examiné ces travaux de thèse.

Je voudrais adresser un grand Merci aux membres de jury de mon comité de suivi de thèse, Pr Siya Bun-Sok, Dr Thierry Doan, Dr Emilie Layre et Dr Stéphane Audebert. Vos conseils ont été essentiels pour le bon avancement de ma thèse.

Mes sincères remerciements s'adressent aux membres de l'équipe « Lipolyse et Pathogénie Bactérienne », qui sans eux, ce travail n'aurait pas pu se réaliser dans de bonnes conditions.

Parmi eux, merci Jef (Dr Jean-François Cavalier) pour le café de chaque matin, toutes les discussions de protéomique, tous les tableaux Excel infini, et l'attention que tu as portée à mes travaux.

Merci Pierre (Dr Pierre Santucci) pour toutes les discussions enrichissantes, les critiques intéressantes pour l'avancement de mes résultats, les Mr Freeze et Haribo, et surtout pour mon premier article !

Merci Isa pour avoir partagé avec moi les dures matinées de dissection de souris, pour ton aide en biologie cellulaire et en microscopie, pour ta bonne humeur, ta bienveillance, et les discussions hors-science des vendredis. Merci Vanessa pour tous les moments rigolos, toutes les analyses de TLC et de lipides. Vous êtes les « tampons » de l'équipe !

Je tiens à remercier aussi tous les étudiants avec qui j'ai beaucoup interagit, appris, et partagé les bons et les durs moments. Merci Romain et Emma. Janis, et Clémentine je n'oublierai jamais le voyage de Rome sans moi, mais cava vous êtes adorables et « exceptionnelles » même si votre arrivée à l'équipe un peu « too late ». Merci Thomas, pour toutes les discussions « libanaises » et scientifiques, ainsi que pour le support. Merci à Léa, avec qui on a partagé les manips, les réussites et le projet ! Je tiens à remercier Morgane « Maurice » pour les nuits qu'on a passées ensemble au laboratoire, mais aussi les week-ends et les jours fériés, les gouters de 16h, les trajets à pieds lors des matches de l'OM… Et pour parler un peu de science, merci pour les discussions sur nos résultats, et le soutien réciproque de fin de thèse.

J'aimerais aussi remercier tous nos collaborateurs qui nous ont aidés à avancer plus rapidement sur le projet. Merci Dr Gaël Brasseur, Dr Valéry Matarazzo, Dr Luc Camoin, et Dr Stéphane Audebert. Une petite dédicace à toutes les souris mortes pour le « bienfait de la Science ». Enfin et surtout merci au Dr Wassim Daher et Dr John Jairo Aguilera-Correa pour toutes les longues discussions qui ont permis la transmission de leurs compétences, pour tout le partage des tâches et tous les résultats intéressants.

A Ivy,
Ancien ingénieur de recherche dans l'équipe, avec qui j'ai partagé des moments de science mais aussi personnels, merci pour tout. Merci pour l'accueil dès mon arrivée, pour le transfert des compétences nécessaires à la réussite de ce projet, à toutes les données préliminaires que tu as générées avant mon arrivée, pour toutes les sorties extra-labo qu'on a faites. Merci pour ton amitié même après ton départ.

Je remercie enfin toutes les personnes que j'ai rencontrées pendant ces 3 années, Dr Christine Kellenberger, Dr Magali Casanova, Inès, Graziella, Rumeyza, Elora, tous les membres du JSM3 et les étudiants du LISM et de l'IMM.

Plus personnellement, ces remerciements ne seraient pas complets sans une pensée à mes amis d'enfance, de l'université avec qui j'ai partagé la passion pour la Science, mes amis au Liban, on ne s'est pas vu durant ces années mais vous savez votre importance. Merci Nour, Wendy, Marina, Myriam, Paloma, Nour, Elissa, Karen, Micho, Ralph, et Rima.

Bib, ta présence et ton soutien indéfectible tout au long de ces années étaient une source de force, d'encouragement, et de motivation. Merci d'avoir supporté avec moi les périodes difficiles et de m'avoir aidée à les franchir. Merci d'avoir fait avec moi des jours meilleurs, pleins d'aventures, de nouvelles découvertes et d'amour.

Je tiens à exprimer ma profonde gratitude envers ma famille, ma mère et mon père, spingo et mimi, sans vous je n'en serais jamais arrivée là, merci pour votre soutien, votre amour inconditionnel, et vos encouragements constants. C'est grâce à ces éléments déterminants que j'ai pu réaliser ma thèse. Merci d'avoir été à mes côtés à chaque étape, dès les classes primaires jusqu'à aujourd'hui. Je vous adresse mes plus sincères remerciements pour tout ce que vous avez faits et que vous faites encore pour moi, et pour avoir toujours cru en moi, et j'espère avoir été à la hauteur ! ***Bhebkon****…*

Je voudrais rendre hommage à teta Jeannette, j'aurais aimé que tu sois encore parmi nous, pour voir le fruit de mon travail de thèse, mais je sais que tu nous surveilles de là-haut.

Pour finir, une pensée à mon Cher Liban, malgré tout… je t'aime !

Au final, j'ai réalisé que la thèse n'est pas un travail solitaire, je n'aurai jamais pu réaliser ce travail sans le soutien d'un grand nombre de personnes, qui m'ont montré la générosité et l'intérêt à l'égard de ma recherche, pour cela :

Merci à tous ! **Choukrann**

Finalement, pour toutes ces années, toutes les rencontres, pour tous les dons que ***Tu*** *m'as offerts, pour tout ce que j'ai vécu en* ***Ta*** *présence, à* ***Toi*** *mille mercis !*

Abréviations

AM	Acide mycolique	**MS**	Macrophage spumeux
ACAD	Acyl-CoA deshydrogénase	**MTBC**	Complexe *Mycobacterium tuberculosis*
Acc	Acyl-CoA carboxylase	**NES**	"Nuclear export signal"
aft	Acyltransferase	**NK**	"Neutral killer"
AG	Arabinogalactane	**NO**	"Nitric oxyde"
AMC	Amikacine	**OMS**	Organisation mondiale de la santé
APEX2	Ascorbate péroxydase 2	**PAMP**	"Pathogen-Associated molecular patterns"
BAAR	Bacille alcoolo acido résistant	**PAT**	Polyacyltréhalose
BC	Biotine carboxylase	**PCR**	"Polymerase chain reaction"
BCG	Bacille Calmette Guérin	**PDIM**	Phtiocérol Dimycocérosate
BDQ	Bédaquiline	**PE**	Phosphatidyléthanolamine
BPCO	Bronchopneumopathie obstructive	**PG**	Peptidoglycane
CD	Cellule dendritique	**PGL**	Glycopeptide phénolique
CEMOVIS	"Cryo-Electron microscopy of vitreous section"	**PGly**	Phosphatidylglycérol
CFTR	"Cystic fibrosis transmembrane conductance regulator"	**PHA**	Polyhydroxyalcanoate
CL	Cardiolipine	**PHB**	Acides poly (3-hydroxybutyriques
CMI	Concentration minimale inhibitrice	**PI**	Phosphatidylinositol
COVID	Corona virus	**PIM**	Phosphatidylinositol-myo-mannoside
CT	Carboxyltransférase	**PL**	Phospholipase
DAG	Diacylglycérol	**PLIN**	Périlipine
DAT	Diacyltréhalose	**PS**	Phosphatidylsérine
DGAT	Diacylglycérol acyltransférase	**R**	"Rough"
EC	"Enzyme Commission"	**RE**	Reticulum endoplasmique

GL	Gouttelette lipidique
GPL	Glycopeptidolipide
ILI	Inclusion lipidique intrabactérienne
LAM	Lipoarabinomannane
LDL	"Low density lipoprotein"
LM	Lipomannane
LOS	Lipooligosaccharide
LTBI	"Latent tuberculosis infection"
MABC	Complexe *Mycobacterium abscessus*
ManLAM	Lipoarabinomannane coiffé de mannose
MCL	Mycobactérie à croissance lente
MCR	Mycobactérie à croissance rapide
MDR	"Multi drug resistant"
MDR RRTB	"Multi drug resistant rifampicin resitant tuberculosis"
MFS	"Major facilitator superfamily"
MLDS	"Microorganism Small Lipid Droplet"
MMDAG	Monoméromycolate diacylglycérol
MNT	Mycobactéries non tuberculeuses
RFLP	"Restriction fragment length polymorphism"
RGO	Reflux gastro-oesophagien
ROS	"Reactive oxygen specie"
S	"Smooth"
SL	Sulfolipide
TAG	Rriacylglycérol
TAT	Triacyltréhalose
TB	Tuberculose
TCA	"Tricarboxylic acid cycle"
TDM	Tréhalose dimycolate
Tgs	Triacylglycérol synthase
TLR	"Toll like receptor"
TM	Transmembranaire
TMM	Tréhalose monomycolate
TNF	"Tumor necrosis factor"
TPP	Tréhalose polyphléate
VIH	Virus d'immunodéficience humaine
WS/DGAT	"Wax ester/ diacylglycerol acyltransferase"
XDR	"Extremely drug resistant"

Introduction

Malgré tous les efforts déployés pour éradiquer cette maladie, la tuberculose demeure l'une des dix principales causes de décès dans le monde. Selon de rapport de l'Organisation Mondiale de la Santé en 2023, 1,3 millions de patients sont décédés de la tuberculose en 2022, tandis que l'apparition de nouveaux cas aurait diminué dans le monde. Cette diminution ne reflète pas la réalité à cause de l'émergence du Coronavirus (COVID-19) et le passage des tests de diagnostic de la tuberculose au second plan. Le danger d'une infection à *Mycobacterium tuberculosis*, agent étiologique de la tuberculose, se traduit tout d'abord par le pourcentage de plus en plus élevé des cas résistants aux antibiotiques, généralement prescrits contre cette bactérie. Une autre forme du danger causé par *M. tuberculosis* réside dans sa persistance dans les poumons de l'hôte, au sein d'une structure multicellulaire appelée granulome. Celle-ci n'est pas strictement limitée à l'espèce *M. tuberculosis*, et peut se retrouver aussi chez d'autres espèces du genre *Mycobacterium*, qu'elles soient pathogènes (*M. tuberculosis, Mycobacterium leprae*) ou même opportunistes (*Mycobacterium abscessus*). Malgré la présence d'une multitude de stress (pH, hypoxie, carence en nutriments, espèces réactives de l'oxygène), le bacille est capable de s'adapter à l'intérieur d'un granulome et de survivre dans cet environnement hostile. Pour cela, il modifie l'expression de certains de ces gènes, notamment ceux impliqués dans le métabolisme des acides gras et du cholestérol afin de métaboliser les lipides abondants dans le caséum, centre nécrotique du granulome. Toutes ces modifications dans le métabolisme des mycobactéries peuvent aboutir à l'accumulation d'inclusions lipidiques intrabactériennes (ILI) permettant ainsi à la bactérie de rentrer dans un état de dormance et de se protéger de l'action du système immunitaire.

Cette capacité à accumuler des ILI peut en fait être généralisée à l'ordre des actinobactéries auxquelles appartiennent les espèces mycobactériennes. Qu'elles soient pathogènes, opportunistes ou saprophytes, toutes ces espèces mycobactériennes, sont capables d'accumuler des lipides en grande quantité sous la forme d'ILI.

En plus de leur rôle de réserve nutritive et de source de carbone, les ILI participeraient à la réduction des stress oxydatif et métabolique et seraient impliqués dans la tolérance aux antibiotiques ainsi que dans le renouvellement des lipides de l'enveloppe.

Depuis quelques années, plusieurs études sur le métabolisme des lipides ont été réalisées et il apparait clairement que la présence des ILI revêt une importance fonctionnelle majeure pour la physiologie bactérienne. De manière générale, les gouttelettes lipidiques, leurs rôles et leurs caractéristiques ont été particulièrement bien décrits et étudiés chez les eucaryotes. Cependant comme chez ces derniers, les inclusions lipidiques des procaryotes sont composées d'un corps de lipide neutre (triacylglycérol (TAG) et d'ester de cholestérol) délimité par une monocouche de phospholipides dans laquelle sont enchâssées des protéines dont le rôle reste à définir. En effet, l'identification des protéines associées à ces ILI ainsi que leur rôle dans la synthèse et/ou la dégradation des ILI ont été peu étudiés jusqu'à présent. La plupart des études concernant l'identification du protéome des ILI ont été menées sur les actinomycètes, notamment le genre *Rhodococcus*, et, à ce jour, seulement deux études ont été réalisées chez les mycobactéries.

La compréhension et l'identification de ce protéome chez les mycobactéries permettrait d'obtenir de nouvelles informations particulièrement utiles pour lutter contre l'apparition des formes de persistance/résistance au cours du processus d'infection. Afin de répondre à cette problématique, nous avons utilisé de nouvelles technologies dites « spatio-temporelles » pour étudier les interactions protéine-protéine dans des compartiments cellulaires vivants, visant à déterminer les interactants de nombreux complexes protéiques. Plusieurs marquages de proximité sont actuellement disponibles et sont basés sur l'utilisation soit d'une ligase soit d'une peroxydase. Pour étudier le protéome des ILI, notre choix s'est orienté vers le marquage de proximité en utilisant une peroxydase, l'APEX2.

Pour la réalisation de ces travaux, un modèle réversible d'accumulation et de consommation des ILI élaboré au laboratoire a été utilisé.

En effet, l'excès du carbone et la carence en azote induisent de façon significative l'accumulation des ILI chez *M. smegmatis* et *M. abscessus* et à l'opposé, la suppression de la source unique de carbone contenu dans le milieu, induit la dégradation des ILI formées, dont les produits de dégradation deviennent leur seule réserve nutritive.

Dans ce contexte, ma thèse s'est articulée autour de 3 axes, avec comme principal objectif l'identification du protéome/proxysome des ILI, c'est-à-dire l'ensemble des protéines impliquées dans la formation et la dégradation de ces structures.

Les principaux axes sont :

i) L'identification du protéome total dans notre modèle d'accumulation et de dégradation des lipides,
ii) La mise au point de la technologie APEX2 appliquée à la formation et à la dégradation des ILI, la purification et l'identification par spectrométrie de masse des protéines présentes à la surface des ILI en fonction du temps,
iii) La caractérisation biochimique des protéines cibles sélectionnées et l'étude de leur rôle physiopathologique.

Table de matière

"A model is a lie that helps you see the truth"

~ H. Skipper

Introduction bibliographique

Chapitre I

La tuberculose et les mycobactéries

“I felt so distressed when people avoid talking to me because of tuberculosis”

Halima

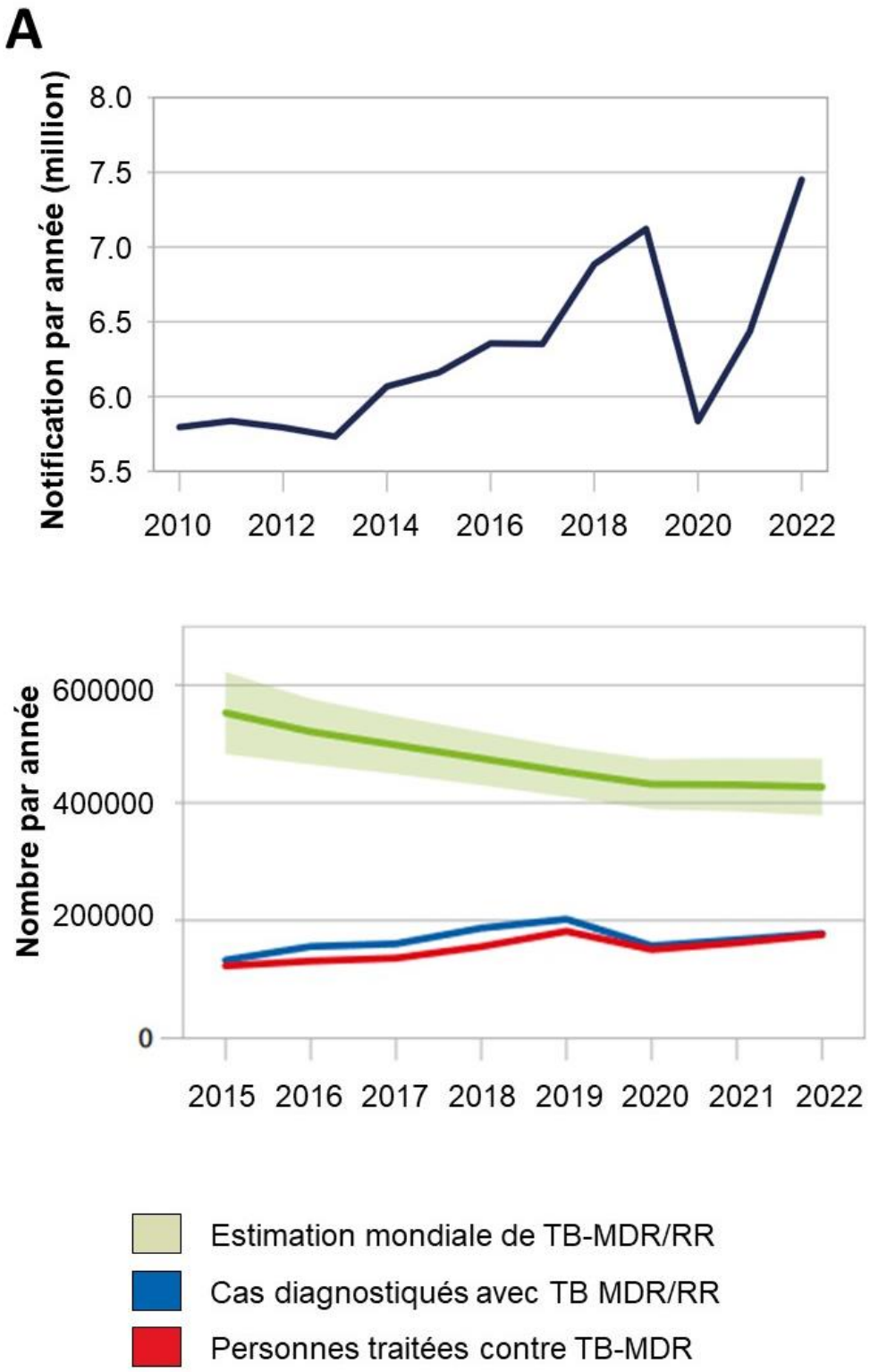

Figure 1. Données épidémiologiques de la tuberculose*. A) Tendance mondiale des notifications de cas de personnes nouvellement diagnostiquées avec la tuberculose entre les années 2015 et 2022. B) Représentation schématique et estimation de cas de tuberculose MDR au niveau mondial. MDR/RR : « multi drug resistant/rifampicin resistant ». Données adaptées de (WHO 2023).*

Parmi les mycobactéries, la plus connue d'entre elles est *Mycobacterium tuberculosis*, le pathogène responsable de la tuberculose (TB). En effet, TB reste à l'heure actuelle une des principales causes de décès dans le monde due à un agent infectieux unique. Selon l'Organisation Mondiale de la Santé (WHO 2023), près de 7,5 millions de personnes étaient atteintes de tuberculose en 2022. Pendant la pandémie du COVID-19, les services de diagnostic de TB ont été perturbés, expliquant la chute du nombre nouveaux cas en 2020 et la ré-augmentation de nouveaux cas en 2021 (**Figure 1A**). En effet, l'augmentation du nombre de patients non diagnostiqués et par la suite non traités, a entrainé un nombre plus élevé de décès. Globalement, en 2022, 1,3 millions de personnes sont décédés dont 88% étaient séronégatifs. Parmi les patients testés en 2022, une augmentation de 6,4% de cas infectés par des souches résistantes a été observée par rapport à 2019 (**Figure 1B**). Cela est équivalent à une personne sur trois qui serait atteinte d'une Multi Drug Resistant / Rifampicin Resistant TB (MDR/RR TB) chaque année.

En termes de santé publique, une autre mycobactérie pose de plus en plus de problème. Cette mycobactérie nommée *Mycobacterium abscessus* est une mycobactérie non tuberculeuse à croissance rapide, responsable d'un large spectre de manifestations cliniques. Son traitement est aussi compliqué que celui d'une infection à *M. tuberculosis,* principalement à cause de sa résistance, induite ou acquise, à la plupart des anti-tuberculeux ; antibiotiques généralement prescrits contre *M. tuberculosis* mais également contre d'autres mycobactérioses.

Depuis des dizaines d'années, *M. abscessus* est considérée comme un pathogène opportuniste de l'homme ayant la capacité d'infecter la peau, les poumons, les tissus mous et pouvant causer des infections disséminées. Les formes les plus graves des infections causées par ce bacille se retrouvent chez les patients immunodéprimés, notamment ceux atteints de mucoviscidose.

Ce chapitre a donc pour objectif de définir le genre *Mycobacterium*, ses classifications ainsi que ses caractéristiques physiopathologiques. Une partie de ce chapitre sera consacrée à l'espèce *M. abscessus*, qui est le modèle d'étude que j'ai utilisé tout au long de ma thèse.

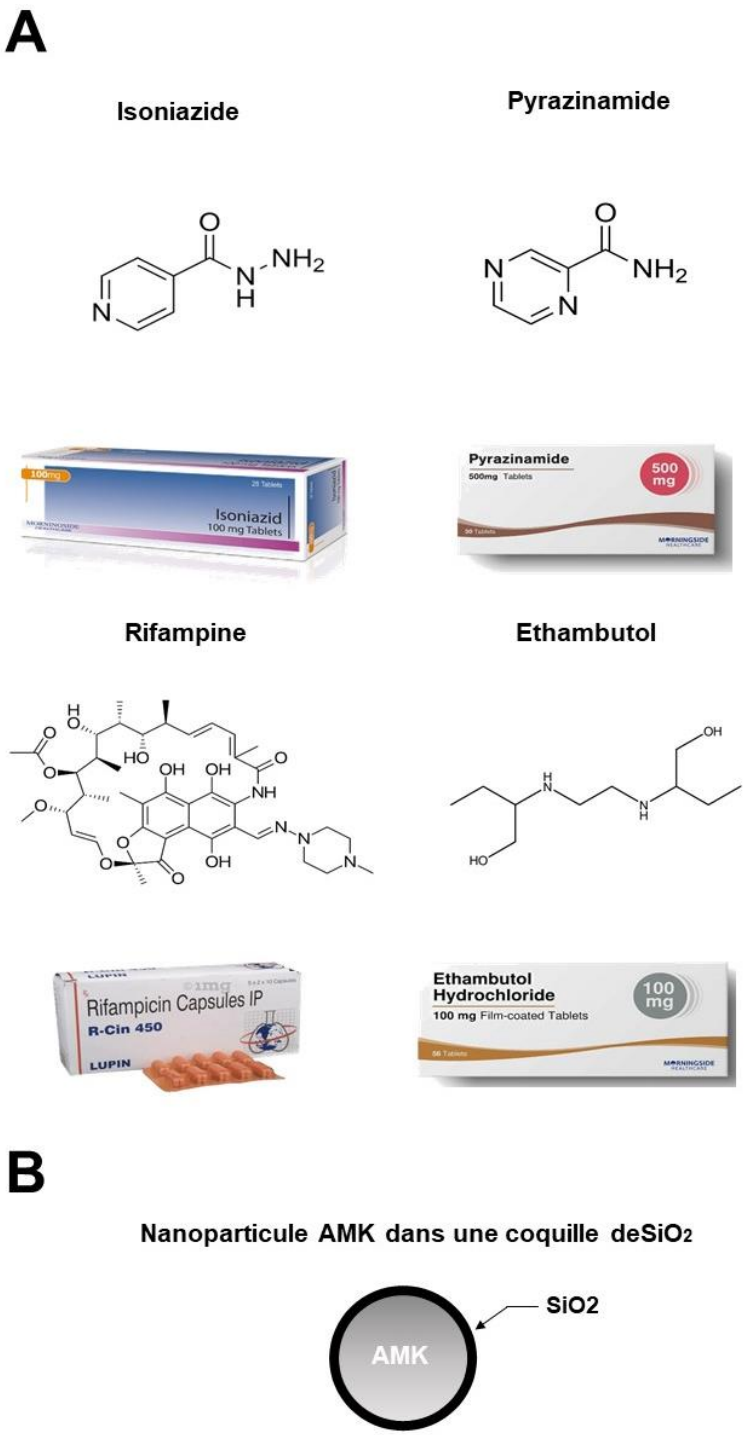

***Figure 2. Traitements contre la tuberculose**. A) Antibiotiques de première ligne avec représentation de leur formule chimique. B) Nanoparticule d'amikacine (AMK) stabilisée par une couche de silice (SiO_2) pour une application pulmonaire sous forme d'aérosol. Adaptée de (Rutschmann, Redinger et al. 2023).*

1.1 La tuberculose

L'Organisation Mondiale de la Santé « OMS » a mis en place, depuis 2015, un programme « End TB Program » pour réduire l'incidence de la tuberculose d'ici 2035, dont un de ses objectifs était de réduire le taux de mortalité de 35% dès 2020. Malheureusement, cet objectif n'a pas pu être atteint en partie à cause de la pandémie due au COVID-19 (WHO 2023).

Jusqu'au 19e siècle, le traitement contre la tuberculose était assez aléatoire, aucun médicament spécifique n'était utilisé et il se basait sur l'isolement des patients dans des cures de repos, avec des régimes alimentaires spécifiques, une pratique d'exercices physiques et une exposition au soleil pour stimuler le système l'immunitaire (Brennan and Fruth 2001). Depuis, de nombreux progrès ont été réalisés, non seulement au niveau des traitements médicamenteux mais aussi grâce au développement et à l'administration du bacille Calmette-Guérin (BCG), utilisé comme vaccin à partir de 1921. Sa très large diffusion dans le monde a permis de faire diminuer le nombre de mort lié à cette maladie. Cependant depuis cette date, de nombreuses études ont montré que ce vaccin avait une efficacité hétérogène, en particulier chez les adultes et les patients immunodéprimés, nécessitant ainsi le développement de nouveaux candidats vaccinaux (Hernàndez Pando, Aguilar et al. 2006). Dès lors, de nouveaux vaccins ou BCG modifiés ont vu le jour et sont actuellement en cours de développement (Romano, Squeglia et al. 2023; Srivastava, Dey et al. 2023). D'autres études ont montré une possibilité d'utiliser des composants de la paroi mycobactérienne, la capsule par exemple, comme vaccin contre *M. tuberculosis* (Prados-Rosales, Carreño et al. 2016; Sarmiento, Alvarez et al. 2019).

Le traitement par antibiotique est lourd, long, et entraine des effets toxiques chez les patients car il s'étend sur un minimum de 6 mois et associe des antibiotiques dits de première ligne (Izoniazide, Rifampicine, Ethambutol et Pyrazinamide) (**Figure 2A**). Les molécules antituberculeuses de première ligne présentent des rapports bénéfiques pour le patient. Durant les deux premiers mois du traitement, les 4 antibiotiques sont prescrits, suivi d'une période de 4 mois consistant en une bithérapie combinant la rifampicine et l'isoniazide. Outre sa toxicité hépatique, ce type de traitement génère l'apparition, selon les cas, de souches résistantes (Pai, Behr et al. 2016).

Des mécanismes d'adaptation et de nouvelles mutations élaborés par les bacilles ont favorisé l'apparition des souches résistantes suite à l'utilisation répétée et massive de ces antibiotiques. Par conséquent, il est important de développer de nouvelles stratégies thérapeutiques en ciblant des mécanismes de résistance chez le pathogène.

Après avoir séquencé le génome complet de *M. tuberculosis*, le développement des approches thérapeutiques a beaucoup évolué (Cole, Brosch et al. 1998). Récemment, une preuve de concept de nanoparticules d'amikacine a été développée par Rutschmann *et al.* contre les infections pulmonaires (**Figure 2B**). En effet, ces nanoparticules sont formées d'un noyau de 200 nm contenant de l'amikacine (AMK), encapsulé par une enveloppe de silice de 20 nm. Cette dernière protège le principe actif et favorise sa dispersion dans le poumon ainsi que son internalisation dans les macrophages. Quand la pression osmotique de la cellule pulmonaire augmente, la nanoparticule se casse et libère l'AMK sur une durée de 80 minutes. L'AMK libérée peut alors être absorbée par les macrophages pour être transportée vers les phagosomes contenant les bactéries, tandis que les résidus de silice sont éliminés du poumon avec le mucus. Des études préliminaires portant sur les infections de macrophages dérivés de moelle osseuse par *M. tuberculosis* et *M. abscessus* ont montré des résultats prometteurs pour ce type de traitement (Rutschmann, Redinger et al. 2023).

1.2 Les mycobactéries

1.2.1 Caractéristiques physiologiques

Les mycobactéries sont des bacilles droits ou légèrement incurvés non flagellés immobiles, ayant une taille de 1,4 µm et un diamètre allant de 0,3 à 0,5 µm. Il s'agit d'aérobies stricts ne pouvant pas former de spores (Cook, Berney et al. 2009). Ces dernières se caractérisent par une masse lipidique d'environ 40% du contenu cellulaire, provenant essentiellement de leur paroi (Chiaradia, Lefebvre et al. 2017).

***Tableau 1. Différentes classifications utilisées pour les mycobactéries**. Adaptée de (Runyon 1959).*

	Mycobactérie tuberculeuse	Mycobactérie non tuberculeuse	Lèpre
Mycobactérie à croissance lente (MCL)	*M. tuberculosis* *M. africanum* *M. canettii* *M. bovis* *M. microti*	*M. marinum* *M. ulcerans* *M. avium* *M. kansasii* *M. simiae*	*M. leprae*
Mycobactérie à croissance rapide (MCR)		*M. abscessus* *M. chelonae* *M. fortuitum* *M. smegmatis* *M. vaccae*	

Cette abondance en lipide, notamment la présence d'acides mycoliques (détaillé dans le **§ 2.1.4**) augmente l'hydrophobicité de la membrane et donc leur résistance à de nombreuses molécules chimiques (antibiotiques), solutés ou solvants (alcools, acides) ce qui permet de qualifier les mycobactéries de bacilles-acido-alcoolo-résistants (BAAR), rendant la coloration de Gram classiquement utilisée inappropriée. La mise en évidence des mycobactéries se fait spécifiquement par la coloration de Ziehl-Neelsen qui est basée sur la rétention de la fuchsine au niveau des lipides complexes de la paroi mycobactérienne (Vilchèze and Kremer 2017). Une autre caractéristique typique de ce genre bactérien est que leur génome possède un pourcentage de GC (coefficient de Chargaff) élevé de près de 70%, leur permettant ainsi une adaptation à l'environnement et une stabilité génétique (Cole, Brosch et al. 1998).

1.2.2 Phylogénétique et classification

Les mycobactéries sont un genre de bactéries appartenant à la classe des *Actinomycètes* qui sont des bactéries filamenteuses. Ce genre comprend 190 espèces dont 66% sont pathogènes pour l'homme.

En 1959, Runyon a proposé une classification des mycobactéries selon une observation visuelle (**Tableau. 1**). Cette classification se base sur la séparation des espèces en fonction de leur vitesse de croissance, celles à croissance rapide (MCR) qui ont un temps de dédoublement inférieur à 6 h et qui forment des colonies sur gélose au bout de 7 jours, et celles à croissance lente (MCL) dont le temps de dédoublement est supérieur à 6 h avec une formation des colonies après 7 jours (Rastogi, Legrand et al. 2001). En plus, les mycobactéries sont classées en trois sous-catégories selon la pigmentation : les non chromogènes, les scotochromogènes, et les photochromogènes (Runyon 1959).

Initialement, les MCL sont considérées comme des mycobactéries pathogènes alors que les MCR, étant essentiellement environnementales, sont considérées comme opportunistes (Cowman, van Ingen et al. 2019). Ces dernières se retrouvent dans des systèmes de plomberies, jardins, sols et eaux, (De Groote and Huitt 2006; Thomson, Tolson et al. 2013) et sont transmises aux humains *via* les infrastructures de santé (Bryant, Grogono et al. 2016).

Récemment, une nouvelle classification reposant sur des marqueurs moléculaires et des approches phylogénomiques a permis d'obtenir cinq clades monophylétiques séparés : *Tuberculosis-Simiae*, *Terrae*, *Triviale*, *Fortuitum-Vaccae* et *Abscessus-Chelonae* (Gupta, Lo et al. 2018).

Cette nouvelle classification des mycobactéries, proposée en 2019, est controversée dans la communauté scientifique. Elle n'est pas encore utilisée par les cliniciens et les microbiologistes, et plusieurs études suggèrent que la reconstitution du genre unique *Mycobacterium* reste plus appropriée (Tortoli, Brown-Elliott et al. 2019; Armstrong and Parrish 2021; Meehan, Barco et al. 2021).

1.2.2.1 Mycobactéries tuberculeuses

Les mycobactéries tuberculeuses, connues sous le nom des mycobactéries pathogènes strictes, se multiplient en infectant un hôte, sans avoir besoin d'une source environnementale. Cette famille comprend le complexe MTBC, responsable des infections tuberculeuses chez les humains et les animaux. Il inclut les espèces *M. tuberculosis*, *M. africanum*, *M. canettii*, *M. bovis* et la souche vaccinale *M. bovis* BCG. La virulence de ce complexe semble provenir d'une espèce environnementale ayant subi un grand nombre de mutations génétiques (Orgeur and Brosch 2018).

1.2.2.2 La lèpre

M. leprae est un pathogène strict, appartenant au MCL avec un temps de dédoublement allant de 12 à 13 jours. En plus de sa lente vitesse de croissance, la difficulté d'étudier ce pathogène est liée à son incapacité à croître *in vitro* (Salipante and Hall 2011). Par rapport à *M. tuberculosis*, cette espèce est caractérisée par une taille plus réduite de son génome (~3,3 Mb), un nombre réduit de gènes codant pour des protéines, et un très grand nombre de pseudogènes (Cole, Eiglmeier et al. 2001).

En effet, l'analyse de son génome a révélé qu'il possède près de 1 133 pseudogènes (~38% du génome), qui sont des gènes tronqués ou interrompus par des codons stop, expliquant probablement pourquoi ce pathogène nécessite un hôte pour se développer.

1.2.2.3 Mycobactéries atypiques

Les mycobactéries atypiques sont des mycobactéries à croissance lente ou à croissance rapide dites « non tuberculeuses « (MNT), qui comprennent près de 170 espèces. Elles sont la plupart du temps environnementales, et la majorité est saprophyte, c'est-à-dire qu'elles n'entrainent pas d'infections humaines. Cependant, certaines d'entre elles sont considérées comme des pathogènes opportunistes, capables d'infecter des patients présentant des facteurs à risque (détaillé dans le **§1.3.3.1**) (Wu, Aziz et al. 2018; L. Marsollier 2020). Les maladies causées par ces dernières sont appelées des mycobactérioses qui sont le plus souvent des infections cutanées et pulmonaires (Koh 2017).

Parmi ces nombreuses MNT, j'aborderai l'espèce *M. abscessus* plus en détail dans le chapitre suivant, car elle représente la bactérie modèle utilisée dans le cadre de mon projet de thèse.

1.3 Mycobacterium abscessus

1.3.1 Historique et caractéristiques de l'espèce abscessus

Isolée en 1953 de l'abcès d'une patiente, *M. abscessus* était considérée comme une sous-espèce de *M. chelonae* ou *M. chelonei* jusqu'en 1970. Ce n'est qu'en 1992, suite à des études d'hybridation de l'ADN que ces deux espèces ont pu être réellement séparées en deux espèces distinctes (Moore and Frerichs 1953; Kusunoki and Ezaki 1992). Cette distinction a permis d'améliorer la prise en charge des patients, car *M. chelonae* et *M. abscessus* ayant des sites d'infection et des sensibilités aux antibiotiques différents, les échecs des traitements, étaient particulièrement fréquents (Swenson, Wallace et al. 1985; Wallace, Brown et al. 1997). En plus d'un génome de 5 Mb, *M. abscessus* possède également un plasmide de 23 Kbp qui renferme un locus de résistance au mercure, présentant une identifié de 99,9% avec celui identifié chez *M. marinum* (Schué, Dover et al. 2009).

Cette identité de séquence suggère qu'il y a dû avoir une cohabitation entre les 2 espèces qui ont pu s'échanger cet élément mobile au cours du temps.

D'autre part, le séquençage des gènes codant pour les protéines Hsp65 et RpoB a permis de diviser l'espèce *abscessus* en différentes sous-espèces (Garsia, Hellqvist et al. 1989). En effet, Hsp65 est une des protéines les plus immunoréactives des mycobactéries et contient des épitopes uniques à chaque espèce. De son côté, *rpoB* code la sous-unité β de l'ARN polymérase bactérienne qui est également spécifique à chaque sous espèces. Par conséquent, l'analyse de la séquence de *hsp65* et la PCR sur le polymorphisme de la longueur de fragments de restriction (RFLP) ont classé, selon les profils de digestion, *M. abscessus* en deux groupes I (AY603553) et II (AY603554) (König, Tammer et al. 2005). Le séquençage du gène *rpoB,* quant à lui, a permis d'identifier deux nouvelles sous-espèces chez *M. abscessus* ; *M. abscessus sous-espèce bolleti*, *et M. abscessus sous-espèce massiliense*, qui ensemble, forment le complexe de *Mycobacterium abscessus* « MABC » (Adékambi, Colson et al. 2003; Simmon, Pounder et al. 2007), et qui appartiennent au groupe II (Kim, Kook et al. 2008). Une des différences entre ces 3 sous-espèces est la présence d'un gène codant pour une érythromycine ribosome méthyltransférase Erm41 qui peut être responsable d'une résistance induite aux macrolides. Les macrolides représentent une famille d'antibiotiques très largement utilisée pour le traitement des infections à *M. abscessus* (Nash, Brown-Elliott et al. 2009; Shallom, Gardina et al. 2013), d'où la nécessité d'identifier correctement la sous-espèce avant d'initier un traitement (Benwill and Wallace 2014)**.**

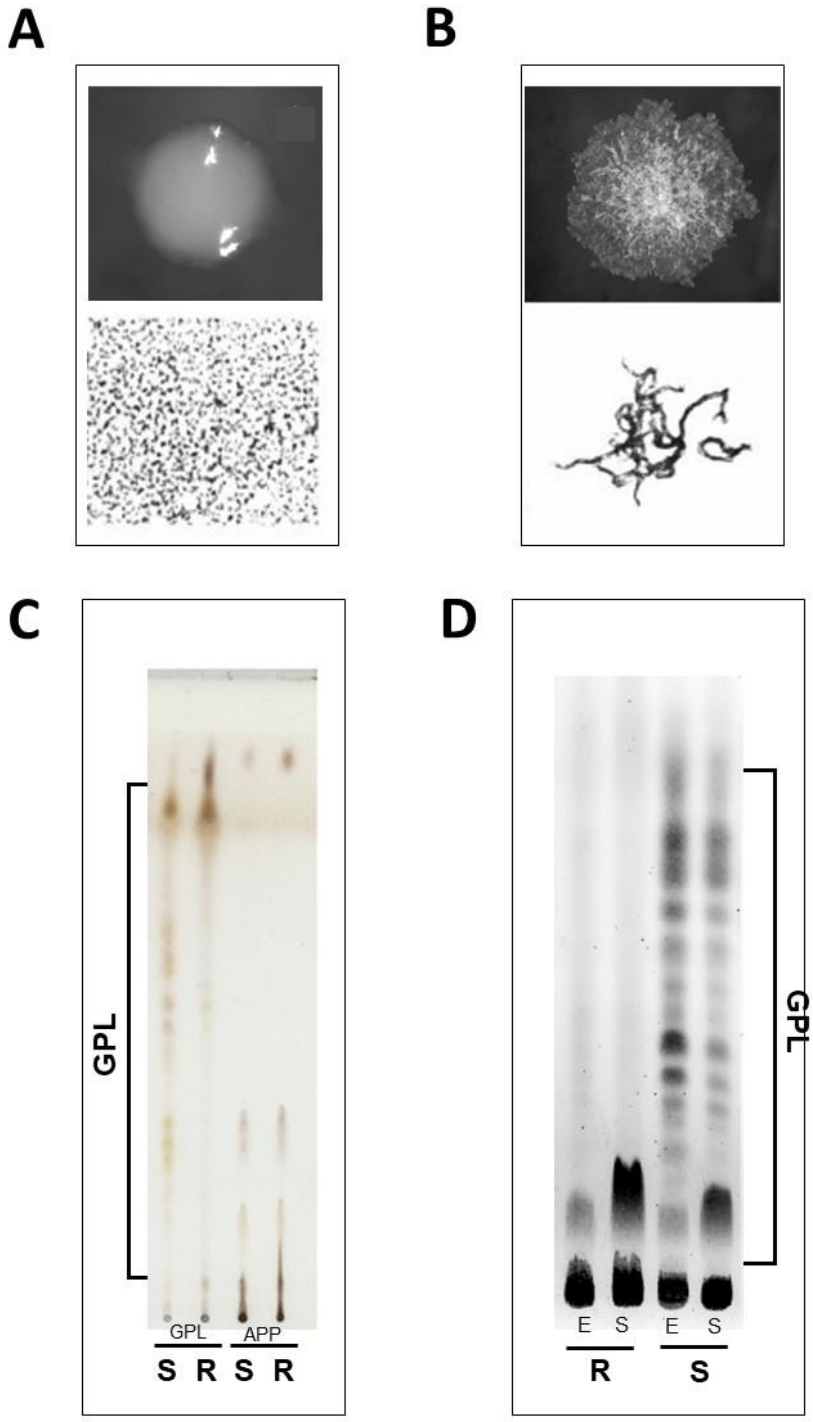

***Figure 3. Les morphotypes des MNT**. A) morphotype lisse de M. abscessus sur gélose et en suspension liquide. B) morphotype rugueux de M. abscessus sur gélose et en liquide. C) chromatographie sur couche mince des glycopeptidolipides (GPL) et des lipides totaux issus des culots précipités (APP) de deux souches S et R de M. abscessus. D) chromatographie sur couche mince des GPLs de deux souches S et R de M. intercellulare en phase exponentielle (E) et stationnaire (S). Adaptée de (Howard, Rhoades et al. 2006; Whang, Back et al. 2017).*

Comme les autres MNT, *M. abscessus* est une bactérie environnementale et se trouve dans le sol, l'eau naturelle, potable, et usée, et dans les végétaux (Moore and Frerichs 1953; Brown-Elliott and Wallace 2002; Thomson, Tolson et al. 2013). Partageant les mêmes niches, il a été montré que *M. abscessus* était capable d'infecter et de se propager dans les amibes, suggérant que ces protozoaires seraient des véhicules potentiels pour infecter l'homme (Delafont, Mougari et al. 2014). Le modèle des amibes a même permis dans certains cas, l'isolement et l'identification par co-culture, d'espèces mycobactériennes non identifiables par culture simple (Adékambi, Reynaud-Gaubert et al. 2004), mais aussi l'étude de certains facteurs de virulence tel que la phospholipase C, ainsi que des facteurs nécessaires pour la croissance intracellulaire de la bactérie (Lamrabet, Mba Medie et al. 2012; Le Moigne, Rottman et al. 2015).

1.3.2 Les morphotypes

M. abscessus peux exister naturellement sous deux morphotypes bien distincts, la forme S pour « Smooth » ou lisse et R pour « Rough » ou rugueux. Sur un milieu solide, les colonies du variant S apparaissent rondes et crémeuses et forment en milieu liquide une suspension homogène. En revanche, les colonies du variant R sont déshydratées et forment en cultures liquides des agrégats importants (Byrd and Lyons 1999) (**Figure 3A, B**).

Cette différence de phénotype est attribuée à la présence (variant S) ou à l'absence (variant R) des Glyco-Peptido-Lipides (GPL) dans la paroi mycobactérienne (**Figure 3C**). En effet chez un variant S de *M. abscessus subsp bolletii*, une mutation au niveau de MmpL4a, le principal transporteur des GPL, entraine une disparition des GPL à la surface et conduit à l'apparition du morphotype R et à sa capacité de former des cordes (Bernut, Viljoen et al. 2016). Les cordes sont de longues chaines de bacilles collés bout à bout formant un réseau compact permettant à la bactérie de résister plus facilement à la phagocytose des macrophages et les neutrophiles, ce qui représente un mécanisme d'échappement au système immunitaire inné (Bernut, Herrmann et al. 2014) (**Figure 4**).

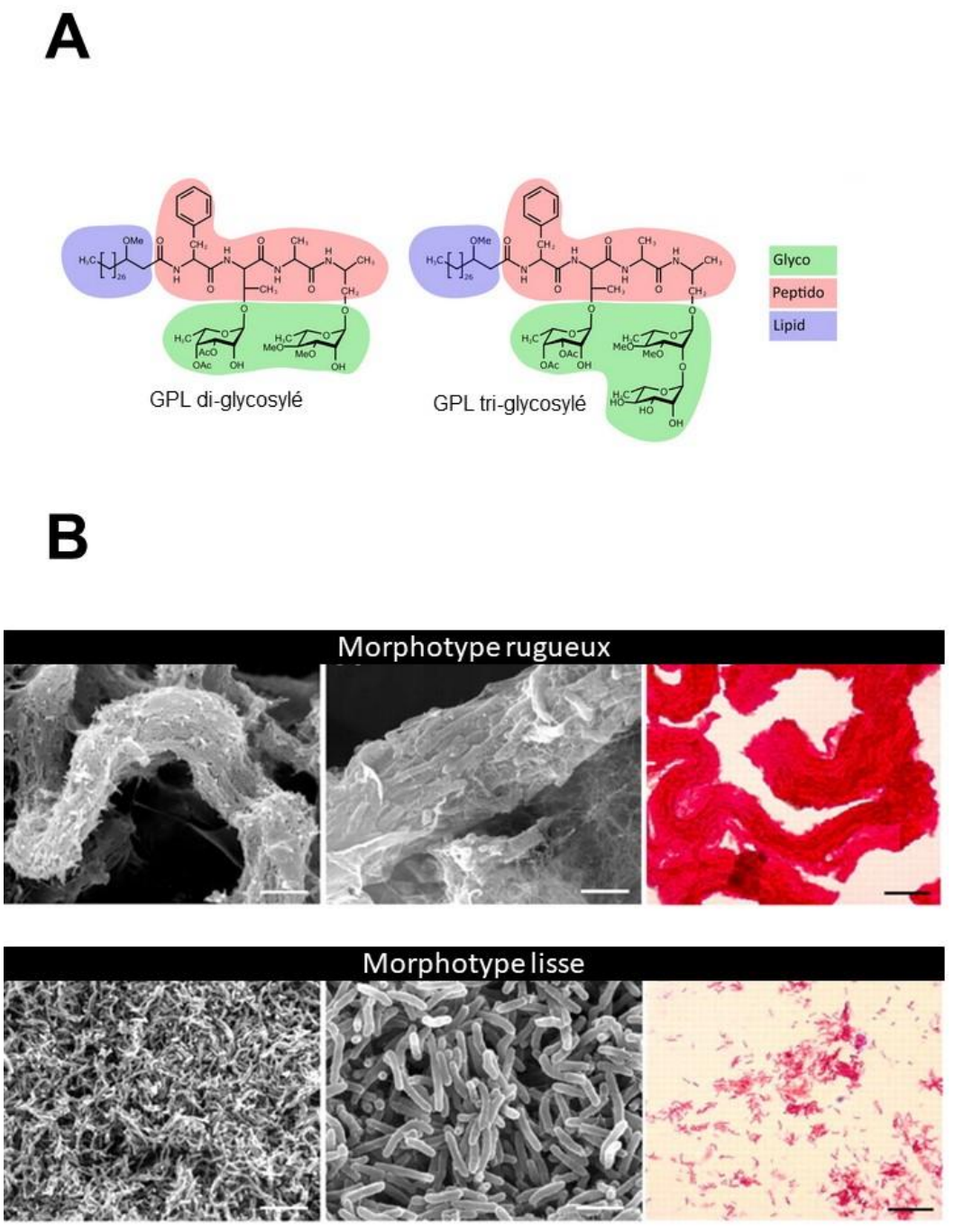

Figure 4. Morphotypes S et R chez M. abscessus*. A) Images de microscopie électronique à balayage et coloration de Ziehl-Nelseen des deux morphotypes de M. abscessus. B) Structure de GPL produits chez M. absccesus contenant une partie glucidique (vert), protéique (rose), et lipidique (mauve). Adaptée de (Sánchez-Chardi, Olivares et al. 2011; Gutiérrez, Viljoen et al. 2018).*

D'une façon similaire, il a été montré chez *M. avium*, *M. smegmatis*, ainsi que *M. intercellulare* (**Figure 3D**), qu'un déficit en GPL dans les variants S est à l'origine du morphotype rugueux (Barrow and Brennan 1982; Belisle, McNeil et al. 1993; Etienne, Villeneuve et al. 2002). La structure des GPL varie selon la longueur de la chaine, la méthylation et l'hydroxylation des glycosides (**Figure 4A**). *M. abscessus,* comme *M. smegmatis* et *M. chelonae,* produisent des GPL polaires et di-glycosylés (Gutiérrez, Viljoen et al. 2018). Le morphotype R d'une souche CIP104536^T se caractérise par des mutations au niveau du locus *gpl* condant pour des protéines de synthèse et de transport de GPL (Pawlik, Garnier et al. 2013). Par conséquent, différentes études se sont enchainées pour étudier la différence génétique entre les deux variants, S et R. Tout d'abord, Nessar *et al,* ont montré que les colonies rugueuses sont issues d'une perturbation de *mmpl4b* qui affecte le transport des GPL (Medjahed and Reyrat 2009), ensuite Bernut *et al* ont montré que l'inhibition de la production de GPL est liée à une mutation dans Mmpl4a ou Mmpl4b, responsable de l'export des GPLs (Bernut, Viljoen et al. 2016). Pour des stades avancés en infection par *M. abscessus*, des mutations supplémentaires ont été identifiées chez le morphotype R, allant d'un indel d'une seule paire de bases à une délétion de 3,1 kbp dans le cluster *mps1-mps2*, impliqué dans la synthèse des GPL, ou dans les gènes *mmpS4-mmpL4a* responsables de l'export de GPL (Park, Hsu et al. 2015). Des délétions des gènes codant les glycosyltransférases Gtf1 et Gtf1 qui ajoutent le 6-déoxy-talose et le premier rhamnose sur les GPL induisent également la transition d'une forme lisse vers une forme rugueuse (Daher, Leclercq et al. 2022)**.**

Cependant, les mécanismes par lesquels les GPL sont transloqués du périplasme jusqu'à la membrane externe demeurent inconnus. En outre, ce changement de morphotype est associé à des phénotypes *in vitro* et *in vivo*.

1.3.2.1 Caractéristiques phénotypiques *in vitro*

Les mycobactéries se caractérisent par une mycomembrane qui leur confère une forte hydrophobicité (**Voir chapitre 2**). Dès lors, ces propriétés hydrophiles et hydrophobes affectent la formation des biofilms. A la différence des cordes, les biofilms sont des amas de bactéries attachées à une surface et entourées d'une matrice polymérique (Etienne, Villeneuve et al. 2002) (**Figure 4B**).

Les GPL étant des lipides polaires, leur présence favorisent la formation de biofilm, ainsi que la motilité par glissement sur agar ; caractéristiques du morphotype S (Recht and Kolter 2001; Howard, Rhoades et al. 2006; Bernut, Herrmann et al. 2014; Bernut, Viljoen et al. 2016). En revanche, le morphotype R est peu motile et forme préférentiellement des cordes (**Figure 4B**) (Howard, Rhoades et al. 2006). La présence de cordes n'est pas spécifique à *M. abscessus* et se retrouvent chez *M. tuberculosis* comme chez d'autres MNT (*M. kansasii*, *M. avium*, et *M. marinum*) et ont été décrits comme facteur de virulence (Middlebrook 1945; Tortoli, Fedrizzi et al. 2017; Degiacomi, Sammartino et al. 2019; Johansen, Herrmann et al. 2020; To, Cao et al. 2020).

La transition du morphotype S en morphotype R est assez fréquente et se traduit par une hyper-virulence (Bernut, Herrmann et al. 2014; Bernut, Viljoen et al. 2016; Halloum, Carrère-Kremer et al. 2016). Ce phénomène de transition a été notamment observé chez des patients immunodéprimés ou encoreatteints de mucoviscidose (Bernut, Herrmann et al. 2014; Bernut, Viljoen et al. 2016; Halloum, Carrère-Kremer et al. 2016; Koh, Jeong et al. 2017). La mucoviscidose est une maladie génétique autosomale récessive qui a été décrite initialement en 1940 chez les enfants atteints de lésions pancréatiques sévères. Ce n'est qu'en 1989 que l'origine de cette maladie a pu être identifiée (Wilmers, Mackay et al. 1950; Kerem, Rommens et al. 1989). Il s'agit d'une maladie liée à une anomalie du gène codant pour le canal « *Cystic Fibrosis Transmembrane Conductance Regulator* » (CFTR) porté par le chromosome 7. Ce canal permet les échanges d'ions chlorures entre l'intérieur et l'extérieur de la cellule. Cependant lorsque son gène est muté, le canal est dysfonctionnel et cette altération se traduit notamment par une diminution de l'eau excrétée au niveau des muqueuses conduisant à une inflammation et un épaississement du mucus bronchique. Le canal étant présent dans tous les types cellulaires, la mucoviscidose touche principalement les poumons, mais aussi le système digestif et reproducteur (Shteinberg, Haq et al. 2021).

Une transition du variant S au variant R peut également se faire suite à des concentrations sub-inhibitrice d'amikacine qui entrainent un changement de morphotype (Lee, Kim et al. 2017). En outre, une étude récente a suggéré un lien entre le régulon dosR activé lors d'un stress issu des conditions hypoxiques et la transition de S en R (Simcox, Tomlinson et al. 2023).

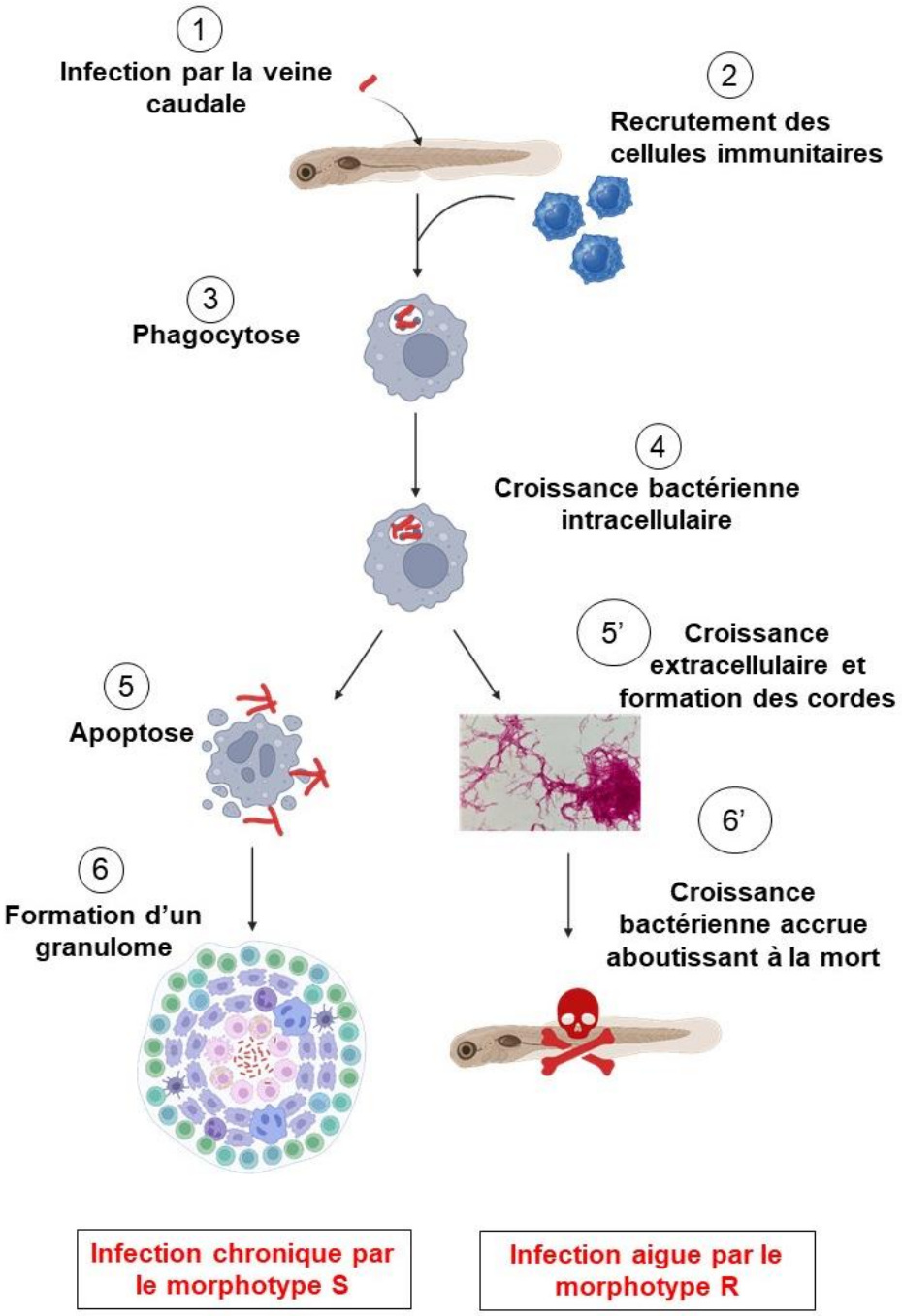

Figure 5. Évènements immunopathologiques d'une infection par M. abscessus dans un modèle de zebrafish. *1) infection du poisson zèbre par voie intraveineuse iv, 2) recrutement des cellules immunitaires au site de l'injection, 3) phagocytose, 4) croissance intracellulaire du pathogène, 5) apoptose des macrophages et libération des bactéries, 6) le morphotype S est de nouveau phagocyté par de nouveaux macrophages, et après la formation d'un granulome, une infection chronique se met en place. 5') Une transition vers le morphotype R induit la mort des cellules immunitaires grâce à la formation des cordes et abcès 6') et induit une infection aiguë aboutissant à la mort de l'embryon infecté. Adaptée de (Bernut, Herrmann et al. 2014).*

Cependant, plus de recherches sont nécessaires pour comprendre les mécanismes moléculaires et les conditions de changement de morphotype chez *M. abscessus*, ainsi que chez d'autres MNT. La transition inverse de R vers S a été décrite une seule fois (Howard, Rhoades et al. 2006) mais cette étude reste controversée.

1.3.2.2 Caractéristiques phénotypiques *in vivo*

En plus des différences morphologiques, les deux morphotypes se comportent différemment au sein des cellules hôtes. En général, le morphotype S est considéré comme un microorganisme responsable des infections chroniques (**Figure 5**) (Bernut, Nguyen-Chi et al. 2016), alors que le morphotype R est responsable d'infections aigues (**Figure 5**) (Jönsson, Gilljam et al. 2007; Catherinot, Roux et al. 2009; Bernut, Herrmann et al. 2014). Ce dernier a été décrit à partir d'un isolat clinique qui a présenté une capacité de persistance et de multiplication dans un modèle d'infection murin à l'inverse du morphotype S qui est la plupart du temps éliminé par le système immunitaire (Byrd and Lyons 1999). Cependant, une étude récente publiée par Touré *et al.*, a démontré chez la drosophile ainsi que chez la souris que le variant S de *M. abscessus* est capable d'échapper à la réponse immunitaire innée de l'hôte(Touré, Galindo et al. 2023). En effet, ils ont suggéré que l'infection de la drosophile par *M. abscessus* induit l'apoptose des phagocytes par la voie dépendante de caspase. D'autre part, chez la souris, les Natural killers (NK) tuent les phagocytes par la voie de la granzyme ou la voie de la perforine-granulysine sans affecter la viabilité des mycobactéries intracellulaires. Par conséquent, la réponse inflammatoire diminue à cause de l'épuisement des macrophages, favorisant ainsi la survie bactérienne et la propagation des bacilles. Chez les poissons zèbres, des infections par le morphotype R ont montré une formation de cordes ce qui se traduit par une forme plus agressive et plus virulente que la forme S (**Figure 5**) (Bernut, Herrmann et al. 2017). D'autre part, Catherinot *et al*., ont mentionné la prédominance des infections par *M. abscessus* R chez les patients atteint de mucoviscidose bien que la proportion d'infection de S et R dans les populations sont largement inconnues (Catherinot, Roux et al. 2009).

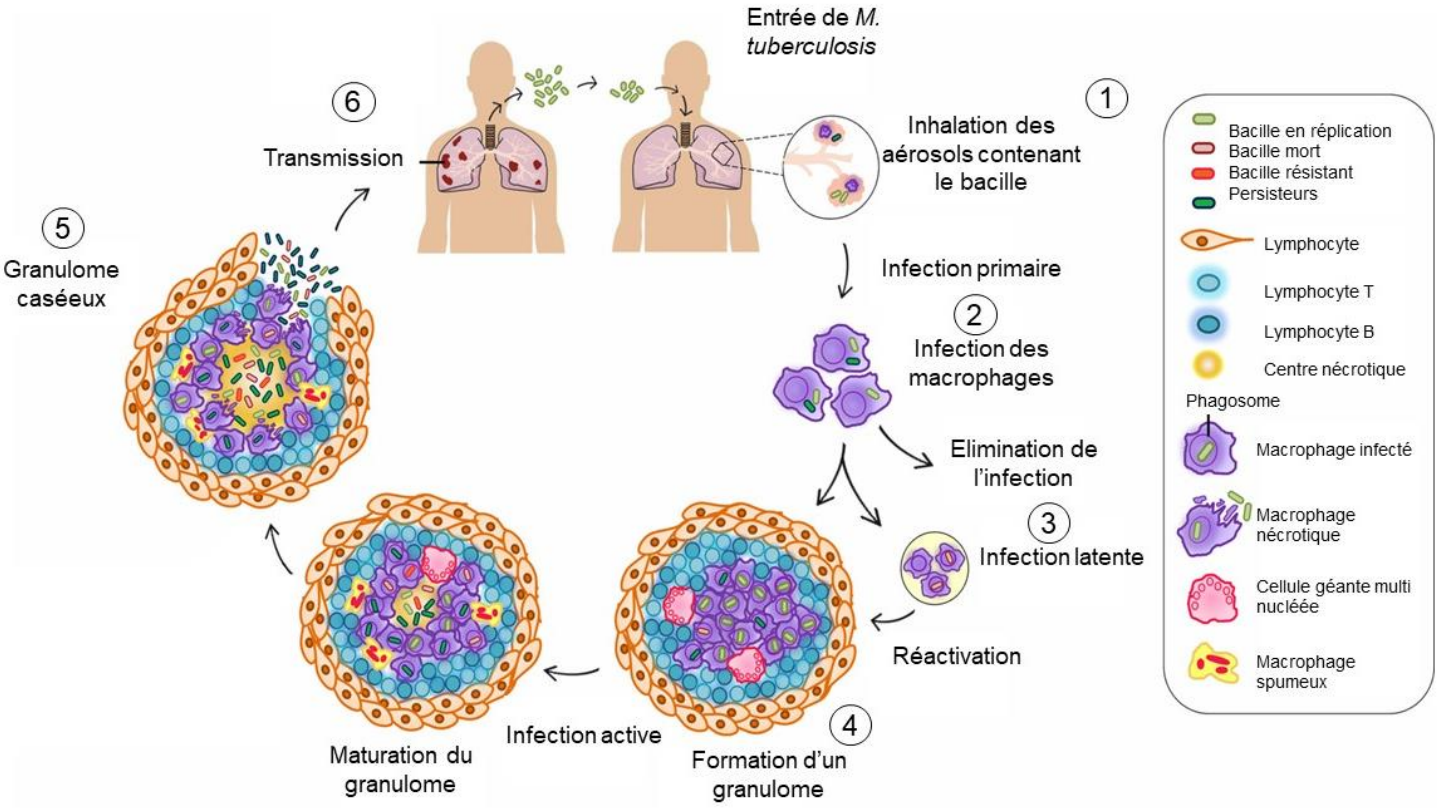

Figure 6. Schéma représentatif de la formation d'un granulome tuberculeux*.1) L'infection primaire implique l'inhalation de M. tuberculosis dans les poumons. 2) Après phagocytose des bacilles par les macrophages alvéolaires, l'infection peut rester latente (3) pendant des décennies, avec un potentiel de réactivation. 4) Lors d'une infection active, les macrophages infectés déclenchent une réponse inflammatoire, recrutant des cellules de l'immunité pour contenir l'infection dans un granulome. Les macrophages se différencient en cellules géantes multinucléées et en macrophages spumeux, lesquels sont entourés de lymphocytes B et T. Dans cet état l'infection peut être éliminée ou persister. 5) Cependant, la dégradation nécrotique accrue des cellules immunitaires entraîne la formation de caséum et favorise la dissémination des bacilles (6). Adaptée de (Parbhoo, Sampson et al. 2020).*

Au niveau des événements immunopathologiques, les GPL favorisent les premiers stades de colonisation. Par contre, les molécules immunogènes (phosphatidyl-*myo*-inositol-mannoside « PIM2 » et les lipoprotéines) sont masqués par les GPL, ce qui retarde l'activation de la réponse immunitaire et facilite par la suite la colonisation et l'inhibition de la signalisation des Toll Like Receptors « TLR2 » (Davidson, Nessar et al. 2011). En revanche, ces molécules sont exposées chez le morphotype R et par conséquent la voie de facteur de nécrose tumorale « TNF » est plus rapidement activée, ce qui aboutit à des lésions tissulaires (Rhoades, Archambault et al. 2009; Roux, Viljoen et al. 2016).

Par contre, bien que la phagocytose assurée par les monocytes soit similaire pour les deux variants, une différence importante est observée au niveau de la membrane des phagosomes formés. En effet, des observations faites par microscopie électronique sur des macrophages infectés avec *M. abscessus* S a révélé que la membrane du phagosome n'entre pas en contact avec la bactérie laissant ainsi apparaitre une zone translucide qui pourrait être liée à la présence des GPL. En revanche l'observation de cellules infectées par le variant R montre un contact étroit entre la membrane et le bacille, typique d'un phagosome contenant des mycobactéries pathogènes strictes (Byrd and Lyons 1999; Roux, Viljoen et al. 2016).

De la même façon, l'acidité des phagosomes varie selon le morphotype. Les monocytes THP1 infectés par le morphotype R présentent des phagosomes plus acides et plus apoptotiques que les cellules infectées par le morphotype S (Roux, Viljoen et al. 2016). Ceci peut s'expliquer par les résultats obtenus par Whang *et al.* , qui ont montré que la présence des GPL inhibait cette apoptose en éliminant les ROS et en protégeant le potentiel mitochondrial des cellules hôtes (Whang, Back et al. 2017).

1.3.2.3 Le granulome

Les infections pulmonaires sont caractérisées souvent par la formation d'un granulome. Une fois inhalés, les aérosols contenant le bacille vont atteindre les poumons et déclencher une réponse immunitaire innée locale (**Figure 6-1)**.

Le recrutement des cellules immunitaires vers le site d'infection forme une masse amorphe appelée granulome et composée de macrophages, de monocytes, de neutrophiles, de cellules dendritiques, de lymphocytes, de NK, de cellules épithéliales, et de cellules géantes multinuclées (**Figure 6-4)**. Bien que cette structure soit une caractéristique fondamentale d'une infection à TB, elle n'est toutefois pas exclusive et on peut retrouver ce type de granulome suite à l'infection d'autres pathogènes, tels que *Schistosoma* ou *Brucella* (Jeong, Lee et al. 2004).

Décrit initialement en 1912 par Ghon *et al*. lors d'une incidence tuberculeuse infantile, le granulome est une réponse immunitaire de l'hôte qui a pour but initial de contrôler la propagation de l'infection (Ghon 1912; Silva Miranda, Breiman et al. 2012).

La structure primaire ou granulome solide est formée par les cellules immunitaires qui sont entourées par un tissu conjonctif de fibroblastes, du collagène et de vaisseaux sanguins nouvellement formés (Mariano 1995). Une fois formé, le granulome est stable et est associé à une infection latente, ou tuberculose latente (LTBI) (**Figure 6-3)** (Dutta and Karakousis 2014). Avec le temps, la vascularisation autour du granulome se réduit, et la disparition progressive de l'afflux sanguin entraine la mort d'une sous-population de cellules et de bactéries, et permet en même temps la formation du caséum au centre du granulome (**Figure 6-5**). Au centre de cette structure, et plus précisément au niveau du caséum, des bacilles extracellulaires se confrontent au stress de cette zone et survivent en accumulant des lipides provenant des débris cellulaires du caséum. Ce comportement est mimé par un modèle *in vitro* représentant une carence en élément nutritif (détaillé dans le **§ 3.2**) (Santucci, Johansen et al. 2019). Cette différence entre les deux constituants du granulome lui confère des propriétés immunitaires variables car le centre nécrotique a un rôle pro-inflammatoire (Marakalala, Raju et al. 2016), alors que les cellules de la périphérie, au contraire, sont anti-inflammatoires. Dans cet environnement qui devient « stringent » du fait de l'appauvrissement en nutriments, en oxygène et de la baisse du pH, les mycobactéries parviennent à survire (Gengenbacher and Kaufmann 2012).

Au moment de la maturation du granulome, le métabolisme d'une sous-population de macrophages infectés peut être modifié, conduisant à une accumulation de triacylglycérol (TAG) sous forme de gouttelettes lipidiques dans leur cytoplasme formant ainsi des macrophages spumeux (MS) (Russell, Barry et al. 2010; Yuan and Sampson 2018).

Ces MS peuvent non seulement servir de niche aux bacilles mais aussi de source de carbone qui favorisera la persistance et la réactivation mycobactérienne (Bloch and Segal 1956). En effet, Peyron *et al.*, a montré par des approches de microscopie électronique, que *M. tuberculosis* induit l'accumulation des lipides chez les macrophages et par la suite était capable de consommer les lipides stockés dans les MS afin de les accumuler sous formes de réserves dans des inclusions lipidiques intrabactériennes (ILI) (Peyron, Vaubourgeix et al. 2008).

Ce phénomène physiologique est également mimé par un modèle expérimental *ex vivo* (détaillé dans le **§ 3.2**) (Caire-Brändli, Papadopoulos et al. 2014; Santucci, Bouzid et al. 2016).

Gorgées de lipides, les bactéries peuvent rester dans cet état au sein du granulome pendant plusieurs décennies mais peuvent parfois se réactiver suite à un déséquilibre anti/pro inflammatoire, à l'inefficacité des lymphocytes T, ou suite à des signaux d'activation émis par des bacilles « scouts». Ces derniers sont des bactéries dormantes ayant la capacité de détecter si l'environnement est propice pour se réactiver (Gengenbacher and Kaufmann 2012). Quand cela se produit, l'intégrité du granulome est rompue et le granulome devient cavitaire, permettant ainsi la pénétration de l'oxygène et favorisant alors la réplication des bacilles.

A ce stade, les bactéries peuvent se disséminer dans les alvéoles pulmonaires, dans le sang, et infecter d'autres personnes (**Figure 6-6)** (Gengenbacher and Kaufmann 2012). A l'exception de *M*. *ulcerans*, toutes les espèces de *mycobacterium* semblent être capables d'induire la formation des granulomes. Bien que les cellules épithéliales soient une caractéristique commune à tous les granulomes tuberculeux, le centre nécrotique est, en revanche, spécifique de l'hôte infecté (Bouley, Ghori et al. 2001; Cosma, Sherman et al. 2003). Chez *M. abscessus*, on retrouve également la formation de granulome qui pourra être représenté sous trois formes ; granulome pulmonaire nécrotique, granulome pulmonaire non nécrotique, et granulome extra-pulmonaire / abcès. En effet, un granulome pulmonaire non nécrotique avec des zones réticulo-ondulaires, a été observé chez une femme atteinte d'un cancer gastrique (Okazaki, Takato et al. 2013). La biopsie pulmonaire de cette patiente a révélé que ce granulome était composé par des cellules épithéliales géantes surmontées par des lymphocytes, type cellulaire majoritaire du granulome induit par une infection à *M. abscessus*.

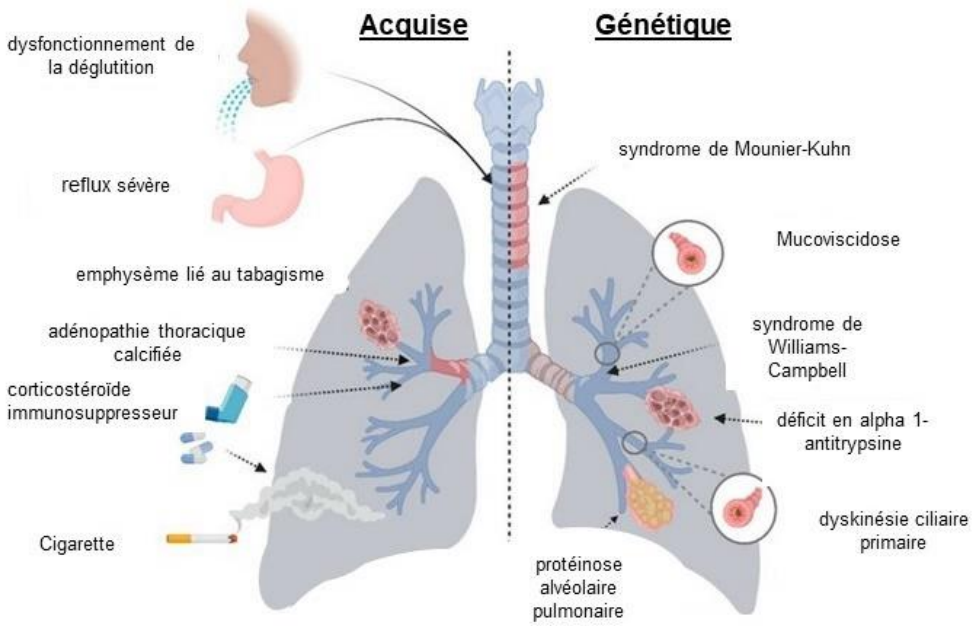

Figure 7. Les facteurs de risque contre M. abscessus. *Schéma représentatif des facteurs génétiques et acquis favorisant les infections à M. abscessus. Adaptée de (Abdelaal, Chan et al. 2022).*

D'un autre côté, des biopsies pulmonaires réalisées chez différents patients immunocompétents ont révélé des granulomes avec des centres nécrotiques (Han, Lee et al. 2003). Ces derniers sont identiques à ceux induits par *M. tuberculosis*. En effet, ils sont formés, tous les deux, par des macrophages et des cellules géantes, avec un centre nécrotique délimité par une capsule fibreuse (Jeong, Lee et al. 2004). Cependant, les étapes clés de la formation d'un granulome faisant suite à une infection *par M. abscessus* ainsi que les évènements immunopathologiques sous-jacents restent à peu connus.

D'autre part, des infections cutanées par *M. abscessus* induisent la formation de nodules granulomateux avec une majorité de cellules immunitaires de type neutrophile. Ces granulomes extra-pulmonaires sont de type tuberculoïde, sarcoïde ou rhumatoïde, et sont moins abondants chez les patients immunodéprimés (Jeong, Lee et al. 2004; Sardiña, Kaw et al. 2020).

1.3.3 Les infections et les facteurs de risque

1.3.3.1 Facteurs de risque

Les manifestations cliniques d'une infection à *M. abscessus* sont diverses et sont soit des infections pulmonaires, soit extra-pulmonaires et plus rarement disséminées dans tout l'organisme. Malheureusement la prévalence des infections aux MNT, et particulièrement à *M. abscessus*, a fortement augmenté ces dernières années (Prevots and Marras 2015; Sharma and Upadhyay 2020) jusqu'à éclipser celle de la tuberculose dans les pays industrialisés où la majorité de ces infections sont décrites. Cette augmentation peut tout simplement s'expliquer par le fait que le diagnostic de *M. abscessus* était beaucoup moins performant et souvent confondu à tort, comme des infections à *M. tuberculosis,* en particulier dans des pays en développement fortement touchés par la tuberculose (Shahraki, Heidarieh et al. 2015). Outre les personnes immunocompétentes ainsi que des patients à immunité réduite*, M. abscessus* peut infecter les patients atteints de mucoviscidose.

D'ailleurs, les personnes les plus vulnérables sont, d'une part, celles ayant des complications pulmonaires, notamment la bronchopneumopathie chronique obstructive (BPCO), et les pneumoconioses, et d'autre part, celles ayant des complications digestives comme le reflux gastro-œsophagien (RGO) (Dawrs, Kautz et al. ; Kubo, Yamazaki et al. 1998; Mojica, Richards et al. 2018) (**Figure 7**).

Enfin, la malnutrition, le tabagisme, l'âge, les personnes souffrant de maladies immunosuppressives ou ayant subi un transplant d'organes sont des facteurs pouvant faciliter les infections à *M. abscessus* (Lee, Ryu et al. 2014; Wakamatsu, Nagata et al. 2015; Adjemian, Frankland et al. 2017; Ruis, Bryant et al. 2021; Fifor, Krukowski et al. 2022).

Des facteurs héréditaires comme la dyskinésie ciliaire primitive, le syndrome de Mounier-kuhn, ou encore la protéinose alvéolaire peuvent également augmenter les risques d'infection et de propagation de *M. abscessus* (Noone, Leigh et al. 2004; Chan, Kaminska et al. 2007) (**Figure 7**).

Dans certains cas, les infections à *M. abscessus* peuvent survenir chez des personnes ne prédisposant d'aucun de facteur aggravant. C'est le cas, notamment, des personnes maigres et anorexiques pouvant être infectées plus facilement que les personnes ayant des poids adaptés à leur taille, et la plupart du temps les femmes sont plus touchées que les hommes (Chan and Iseman 2010; Portillo and Morera 2012).

1.3.3.2 Transmission

A l'inverse de *M. tuberculosis* qui ne se transmet que par voie directe entre les personnes infectées, la transmission des MNT est encore mal comprise mais se ferait principalement à partir de réservoirs environnementaux et donc par voie indirecte.

Cependant depuis 2013, le génotypage des plusieurs isolats cliniques issus de patients atteints de mucoviscidose, a suggéré une possibilité de transmission interhumaine (Bryant, Grogono et al. 2013; Howard 2013; Bryant, Grogono et al. 2016). Bien qu'il ait été montré chez *M. tuberculosis*, que l'hydrophobicité améliore la transmission, aucune étude sur les mécanismes de transmission du variant S *versus* R n'a été réalisée (Jankute, Nataraj et al. 2017).

***Tableau 2. Exemples d'infections extra-pulmonaires par M. abscessus**. Adaptée de (Piersimoni and Scarparo 2009).*

Infection	Effet clinique
Ostéomyélite	Traumatisme du dos
Infections des plaies post-traumatiques	Abcès sous-cutanés, cellulite
Injections sous-cutanées, intra-articulaires ou péri-articulaires	Abcès sous-cutanés, nodules douloureux, sinusites multiples, infections articulaires, fièvre, frissons après l'injection
Acupuncture	Papules érythémateuses, nodules, lésions ulcéreuses, abcès, plaques confluentes, sinus drainants avec écoulement, ténosynovite du poignet
Chirurgie cardiaque	Infection de la plaie sternale, endocardite
Perçage du mamelon	Nodules asymptomatiques, nodules sensibles
Implantation des prothèses	Abcès
Pose d'un stimulateur cardiaque	Abcès
Cathéter de dialyse péritonéale	Abcès

1.3.3.3 Infections pulmonaires

La première infection pulmonaire causée par des MCR a été décrite en 1933, dans les expectorations d'une patiente atteinte d'achalasie (Griffith, Girard et al. 1993). Depuis, ces infections étaient associées à des tumeurs ou des maladies. Bien que les infections pulmonaires sont une caractéristique des patients vulnérables, ayant des pathologies pulmonaires (détaillé dans le **§ 1.3.3.1**) (Lee, Sheng et al. 2015), dans certains cas, *M. abscessus* peut causer des infections pulmonaires à des personnes sans antécédent pulmonaire ou gastrique (Griffith, Girard et al. 1993; Jeong, Lee et al. 2004; Varghese, Shajan et al. 2012).

1.3.3.4 Infections extra-pulmonaires

Les infections extra-pulmonaires causées par *M. abscessus* peuvent conduire à des infections cutanées locales, disséminées ainsi que dans des tissus les plus profonds (Wongkitisophon, Rattanakaemakorn et al. 2011). Les atteintes cutanées comme le tatouage (Falsey, Kinzer et al. 2013; Sousa, Cruz et al. 2015; Griffin, Schmitz et al. 2019), la chirurgie esthétique, les injections de botox, et la pose de cathéters (Deng, Luo et al. ; Wang and Pancholi 2014; Eustace, Jolliffe et al. 2016; Levy, Du et al. 2016) sont autant d'exemples qui peuvent être des points d'entrée pour des infections à *M. abscessus*. Également, des cas d'infections cutanées en particulier pour la sous-espèce *massiliense* ont été recensés suite à des séances de spas ou d'exposition à des sources d'eaux thermales (Nakanaga, Hoshino et al. 2011). Ces infections sont issues d'un contact direct d'une plaie ou d'une blessure avec une source d'eau ou de matériel contaminé (Chadha, Grover et al. 1998; Lee, Sheng et al. 2015) (**Tableau. 2**).

Plus rarement, les infections extra-pulmonaires touchent les patients atteints du Virus d'Immunodéficience Humaine (VIH) et ceux ayant subi des chirurgies cérébrales ou encore des patients atteints de maladies otologiques. Elles entrainent essentiellement des méningites et des atteintes du système nerveux central (Lee, Cheng et al. 2012).

1.3.3.5 Infections disséminées

Les infections disséminées à *M. abscessus* sont des cas rares, et bien qu'elles soient peu connues, elles sont définies par au moins une des caractéristiques suivantes : atteinte de plus d'un organe ou de plus de deux ganglions lymphatiques, hémocultures positives, et sont associées à un taux de mortalité très élevé (Chetchotisakd, Mootsikapun et al. 2000).

1.3.4 Diagnostic, traitement, et obstacles

1.3.4.1 Diagnostic

Selon la société américaine des maladies infectieuses, le diagnostic d'une infection pulmonaire à *M. abscessus* nécessite une démarche spécifique : la présence des symptômes cliniques, la présence des lésions par radiographie, les résultats de culture positive d'expectorations, et l'exclusion appropriée d'autres maladies (Lee, Sheng et al. 2015). Cependant, le diagnostic varie selon le pays et les moyens financiers mis en œuvre.

Le diagnostic basique repose sur les techniques de microbiologie (Griffith, Aksamit et al. 2007; Floto, Olivier et al. 2016; To, Cao et al. 2020; Griffith and Daley 2022) qui consistent dans un premier temps à analyser des échantillons respiratoires par la coloration de Ziehl-Neelsen, mais qui ne donne aucune information sur l'espèce et la viabilité du pathogène (Somoskovi and Salfinger 2014).

Pour distinguer entre le complexe *M. abscessus* et les MCR, l'OMS recommande l'utilisation de milieux liquides comme le MGIT pour la culture-détection et l'antibiogramme des mycobactéries (Demoulin, Médard et al. 1983; Pfyffer, Welscher et al. 1997). Dans les pays industrialisés, l'agent pathogène est recherché par un test de détection de l'interféron gamma, identique à celui utilisé pour le diagnostic de la tuberculose (Steindor, Stehling et al. 2021).

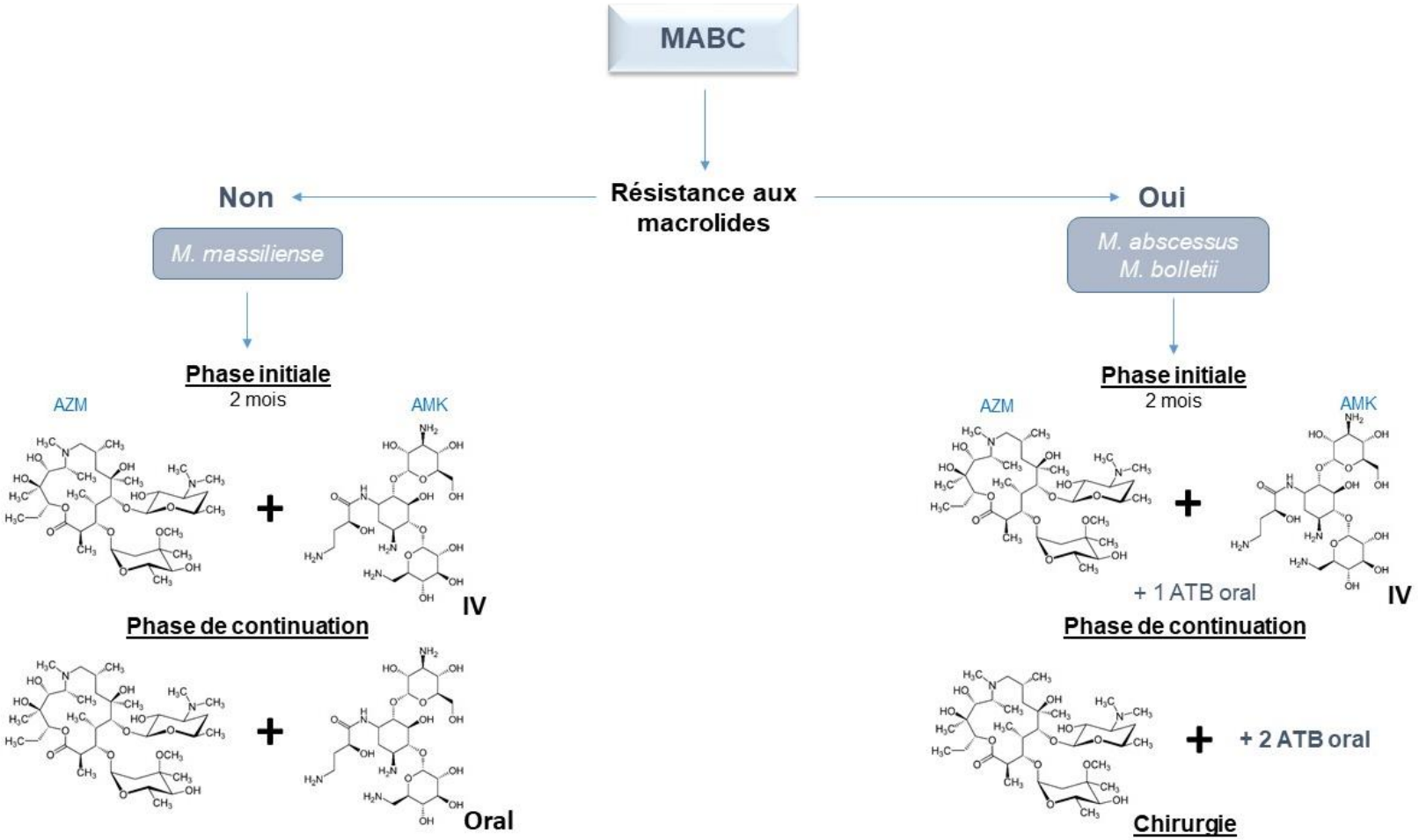

Figure 8. Régime thérapeutique contre M. abscessus. *AZM : azithromycine, AMK : amikacine, IV : intraveineuse, ATB : antibiotique. Adaptée de (Abdelaal, Chan et al. 2022).*

D'autres approches de diagnostic basées sur la réponse sérologique vis-à-vis de la phospholipase C (PLC), de la fraction enrichie du récepteur TLR2, et du taux de l'immunoglobuline A (IgA) ont été développées mais ne sont pas encore utilisées en clinique (Le Moigne, Roux et al. 2020; Le Moigne, Roux et al. 2022).

L'observation phénotypique n'étant pas suffisante pour différencier les sous espèces, des techniques ont été développées pour résoudre ce problème, notamment séquençage du gène *rpoB* et du gène *erm41*, la spectrométrie de masse et le typage de séquences multi-loci (Teng, Chen et al. 2013; Sassi and Drancourt 2014).

1.3.4.2 Antibiothérapie

La pharmacothérapie ne permet pas toujours de traiter les infections dues à *M. abscessus,* en particulier infections pulmonaires, c'est pourquoi elle est souvent couplée à une chimiothérapie spécifique, et selon les cas, à une chirurgie. Le choix d'antibiotiques contre *M. abscessus* est limité à cause de sa résistance. Le traitement est basé donc sur une phase d'initiation avec un cocktail d'antibiotiques, plus spécifiquement une association d'un macrolide (de préférence l'azithromycine) par voie orale, avec un agent antimicrobien (l'amikacine) administré par voie intraveineuse, et une phase de continuation comprenant un macrolide oral, l'amikacine nébulisée et deux à trois antibiotiques (clofazimine, moxifloxanine, linézolide, minocycline) (**Figure 8**) (Ripoll, Pasek et al. 2009; Lee, Sheng et al. 2015; Haworth, Banks et al. 2017).

Toutefois, ce type de combinaison présente de nombreux effets toxiques, qui varient en fonction de la durée d'exposition et des effets secondaires liés à chaque antibiotique (**Figure 8**). Une autre famille d'antibiotiques peut être prescrite contre *M. abscessus* ; les β-lactamines, caractérisé par un noyau β-lactame. Cette famille, comprenant les céphalosporines, les monobactames, les carbapénèmes, et les pénicillines, agit sur la synthèse de la paroi cellulaire en inhibant la formation des liaisons peptiques par les transpeptidases du peptidoglycane (détaillé dans le **§ 2.1.3**) (Zapun, Contreras-Martel et al. 2008). Dans le traitement contre ce bacille, la céfoxitine et l'imipenème sont utilisés.

Il est important de noter que l'identification des sous-espèces affecte le choix du traitement parce qu'elles présentent des symptômes et des clichés de radiographie similaires, ce qui rend la discrimination difficile. En effet, *M. abscessus* présente une résistance induite aux macrolides dû à la protéine Erm41 (détaillé dans le **§ 1.3.1**). Cette dernière est tronquée chez *M. abscessus subsp massiliense* ce qui la rend sensible à la clarithromycine, antibiotique appartenant à la famille des macrolides (Lee, Sheng et al. 2015; Wu, Aziz et al. 2018). De nouveaux agents anti-microbiens sont testés et doivent être pris en compte pour les schémas thérapeutiques, comme la tigécycline, la seule tétracycline efficace pour le traitement de *M. abscessus*, ayant une faible concentration minimale inhibitrice (CMI) *in vitro* (Kwon, Levin et al. 2019). Elle est généralement prescrite pour sauver les patients présentant une maladie grave parce qu'elle a des effets secondaires.

Pour les infections non curables par antibiotiques tel que la lymphadénite cervicale ou les infections oculaires, une chirurgie est recommandée si l'état du patient le permet. Cette thérapie n'exclue pas un long traitement mais aussi les risques post-opératoires (Griffith, Aksamit et al. 2007; Lee, Sheng et al. 2015).

Récemment, un traitement à base d'inhalation d'oxyde nitrique NO a été utilisé contre les infections causées par MABC. En effet, le NO est bactéricide et facilite la dispersion des biofilms sans induire de résistance (Chiarelli, Degiacomi et al. 2021).

Avec l'évolution de la médecine, de nouvelles voies thérapeutiques ont été étudiées, notamment l'utilisation de vaccins qui pourraient protéger les patients contre les infections aux MNT. Le vaccin du BCG principalement utilisé contre la tuberculose permet d'induire un effet protecteur contre les infections aux MNT, notamment contre *M. abscessus* et *M. avium* (Abate, Hamzabegovic et al. 2019). Dans ce contexte d'autres candidats vaccins ont été testés, notamment la phospholipase C ou le facteur de virulence MgtC (transporteur de magnésium) qui semblent protéger la souris contre *M. abscessus* (Le Moigne, Rottman et al. 2015; Le Moigne, Belon et al. 2016).

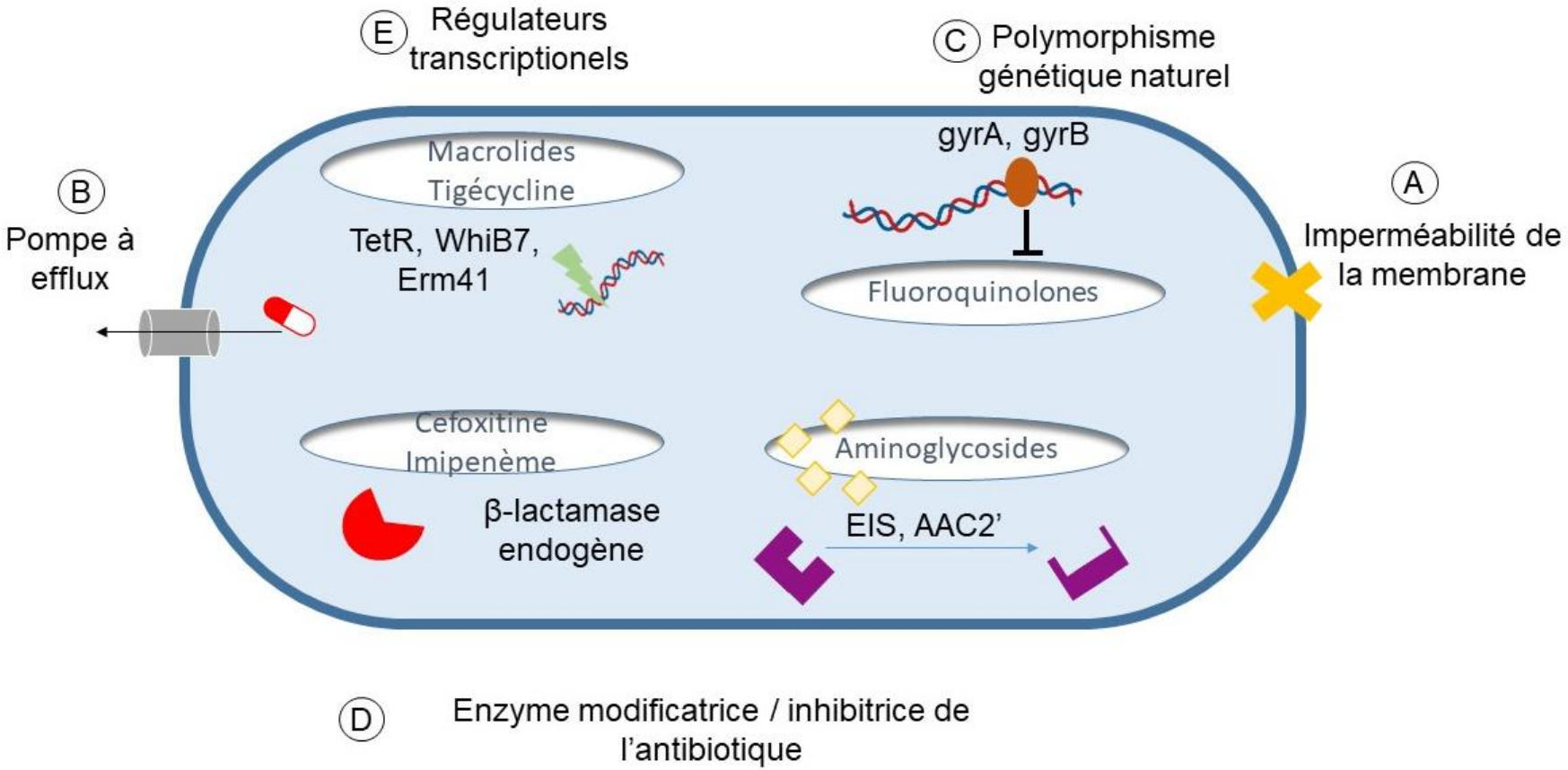

Figure 9. Mécanismes de résistance chez M. abscessus. *Différents types des mécanismes impliquant différents processus physiologiques, enzymatiques et génomiques contribuent au profil de résistance aux antibiotiques. Adaptée de (Lopeman, Harrison et al. 2019).*

Récemment, un cocktail de trois mycobactériophages modifiés a été utilisé contre *M. abscessus,* et l'étude a montré une amélioration de l'état des patients sans effet secondaire (Dedrick, Guerrero-Bustamante et al. 2019). Une autre étude prometteuse a démontré que les phages peuvent être internalisés par certains types cellulaires, les macrophages et les cellules épithéliales pulmonaires et atteindre les *M. abscessus* intracellulaires (Schmalstig, Wiggins et al. 2023). Cependant l'utilisation de la phagothérapie est encore controversée et nécessite des investigations supplémentaires avant de pouvoir être généralisée. Contrairement aux recherches sur les thérapies liées aux infections pulmonaires causées par ce pathogène, les études sur les infections extra-pulmonaires restent encore peu nombreuses.

1.3.4.3 Obsctacles : mécanismes de résistance

M. abscessus est considérée comme étant un cauchemar pour les antibiotiques car cette bactérie présente des résistances, naturelles et acquises, contre la plupart des antibiotiques recommandés.

Cette résistance est tout d'abord due à sa paroi hydrophobe imperméable (**Figure 9A**) ainsi qu'à la présence des pompes à efflux (**Figure 9B**), mais aussi à un polymorphisme génétique (**Figure 9C**). En effet, *M. abscessus* présente des mutations aux niveaux des pompes à efflux et des gènes cibles ce qui modifie ou empêche leur interaction avec les antibiotiques correspondants (**Figure 9D**) (Zaunbrecher, Sikes et al. 2009; Burian, Ramón-García et al. 2012; Maurer, Rüegger et al. 2012; Dubée, Soroka et al. 2015; Dal Molin, Gut et al. 2017; Richard, Gutiérrez et al. 2018; Richard, Gutiérrez et al. 2018). Par conséquent, elle n'est sensible qu'aux antibiotiques suivants, amikacine, céfoxitine et imipénème (Griffith, Girard et al. 1993). En premier lieu, *M. abscessus* présente un polymorphisme naturel au niveau de certains gènes codant pour des protéines ciblées par des antibiotiques. En effet, une résistance naturelle aux fluoroquinolones (antibiotique bactéricide) est remarquée par un polymorphisme génétique au niveau des sous unités de l'ADN gyrase (*gyrA*, *gyrB),* inhibant ainsi l'interaction de l'antibiotique avec l'ADN (**Figure 9C**) (Guillemin, Jarlier et al. 1998). En plus de cette résistance naturelle, ce bacille présente un polymorphisme génétique acquis suite à une longue exposition aux antibiotiques, résultant en des mutations ponctuelles dans les gènes ciblés par ces molécules.

Une autre forme de résistance est développée par *M. abscessus*, cette fois-ci contre deux β-lactames (céfoxitine et imipenème), impliquant une β-lactamase (MAB_2875) capable de dégrader le noyau β-lactame, conduisant à l'inactivation de l'antibiotique (**Figure 9D**) (Soroka, Dubée et al. 2014). Cependant, l'association des inhibiteurs de β-lactamases (tel que l'avibactam) permet d'améliorer l'efficacité de ces molécules en contournant la résistance (Dubée, Bernut et al. 2015). De même, une résistance contre les aminoglycosides implique des enzymes capables de modifier cette classe d'antibiotique (**Figure 9D**) (Magnet and Blanchard 2005).

Également, la mycobactérie présente des mécanismes de résistance contre la tigécycline notamment au niveau des régulateurs transcriptionels (TetR) (Ng and Ngeow 2022), ainsi que contre les macrolides, à cause du régulateur transcriptionel WhiB7 médié par une érythromycine ribosome méthyltransférase Erm(41) (**Figure 9E**) (Nash, Brown-Elliott et al. 2009)

Chapitre II

Les lipides chez les mycobactéries

"The self-organized bacterial membrane has constantly, over very long time lines, increased the complexity of its structure in order to stabilize itself and to more effectively deal with perturbations to the system"

~*Stephen Harrod Buhner*

Comme décrit précédemment, le genre *Mycobacterium* se caractérise par une enveloppe particulière composée de lipides complexes. Ces derniers jouent un rôle crucial dans l'adaptation du bacille, ainsi que dans sa pathogénicité et son interaction avec le système immunitaire de l'hôte infecté. Suite à des études de génomique, de protéomique et bio-informatique, la plupart des enzymes impliquées dans la biosynthèse de cette enveloppe ont été identifiées.

En plus de ces lipides membranaires, les mycobactéries abritent d'autres types de lipides intrabactériens, connus sous le nom d'inclusions lipidiques intrabactériennes (ILI), principalement composées de triacylglycérols. Ces structures jouent un rôle important dans la virulence et la survie des bacilles. Elles associent des protéines, parmi lesquelles on trouve des enzymes impliquées dans le métabolisme lipidique, et contribuant vraisemblablement leur biosynthèse et/ou dégradation.

Ainsi, l'objectif de ce second chapitre consiste à présenter les mécanismes associés au métabolisme des lipides chez les mycobactéries, notamment la composition hydrophobe de la membrane, le métabolisme du triacylglycérol et les enzymes associées.

Comme le génome de *M. tuberculosis* a été le premier annoté (~ 4 173 gènes) et le plus largement étudié parmi les mycobactéries, il sera utilisé comme génome de référence pour l'identification des enzymes lipolytiques putatives chez *M. abscessus*.

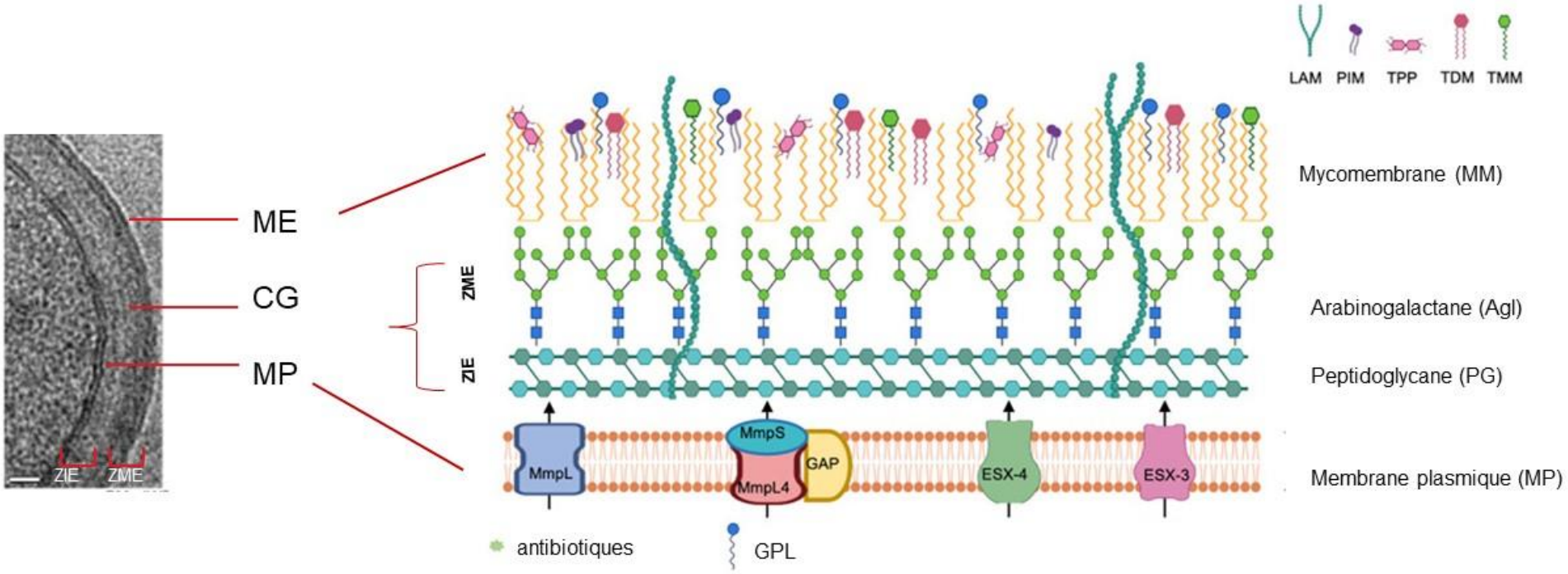

***Figure 10. Structure de l'enveloppe des mycobactéries**. Micrographie électronique de l'enveloppe de M. smegmatis obtenue par microscopie cryo-électronique de coupes de vitrées (CEMOVIS), avec une représentation schématique de l'enveloppe de M. abscessus ME : membrane externe, CG : couche granulomateuse, contenant ZIE : zone interne d'électrons, et ZME : zone médiane d'électrons, qui correspondent à la couche de peptidoglycane-arabinogalactane, MP : membrane plasmique. LAM : lipoarabinomannane, PIM : phosphatidylinositol-myo-mannoside, TPP : tréhalose polyphléate, TDM : tréhalose dimycolates, TMM : tréhalose mono-mycolates, GPL : glycopeptidolipides. Adaptée de (Zuber, Chami et al. 2008; Parmar and Tocheva 2023).*

2.1 La paroi mycobactérienne

Les mycobactéries se distinguent principalement par leur abondance en lipides, en particulier au sein de leur membrane. Ces bacilles sont des BAAR en raison de la complexité de leur membrane. En effet, il a été montré que la paroi des mycobactéries est 100 fois moins perméable que celle de *Pseudomonas aeruginosa*, bactérie imperméable à Gram négatif (Jarlier and Nikaido 1990). Cette imperméabilité est assurée essentiellement par la présence d'acides mycoliques (Liu, Barry et al. 1996; Jackson, Raynaud et al. 1999; Dubnau, Chan et al. 2000). De plus, plusieurs familles de lipides composant la paroi cellulaire sont essentielles pour la survie du bacille et jouent un rôle déterminant dans sa pathogénicité ainsi que dans sa résistance aux antibiotiques.

Des études de cryo-microscopie électronique, ont permis de déterminer la structure de l'enveloppe, révélant que cette dernière est composée de cinq couches concentriques, de l'intérieur vers l'extérieur (**Figure 10)** :

a) Membrane plasmique
b) Espace périplasmique
c) Couche de peptidoglycane/arabinogalactane
d) Mycomembrane
e) Capsule (selon les espèces)

2.1.1 Membrane plasmique

L'épaisseur de la membrane plasmique des mycobactéries est identique à celle des autres bactéries, et mesure environ 7 nm (Hoffmann, Leis et al. 2008). Elle est composée essentiellement de protéines et de lipides. Ces derniers sont des glycérophospholipides comme le phosphatidylinositol (PI), phosphatidylsérine (PS), phosphatidyléthanolamine (PE), phosphatidylglycérol (PGly), et la cardiolipine (CL) (Brennan and Nikaido 1995). Les PI peuvent se trouver sous forme mannosylés connus sous le nom de phosphatidylinositol mannosides (PIMs), caractéristiques des actinobactéries. Quatre types de PIM (PIM_2 - PIM_6) existent selon les ramifications du mannose (Brennan and Nikaido 1995; Gilleron, Nigou et al. 1999; Guerin, Korduláková et al. 2010).

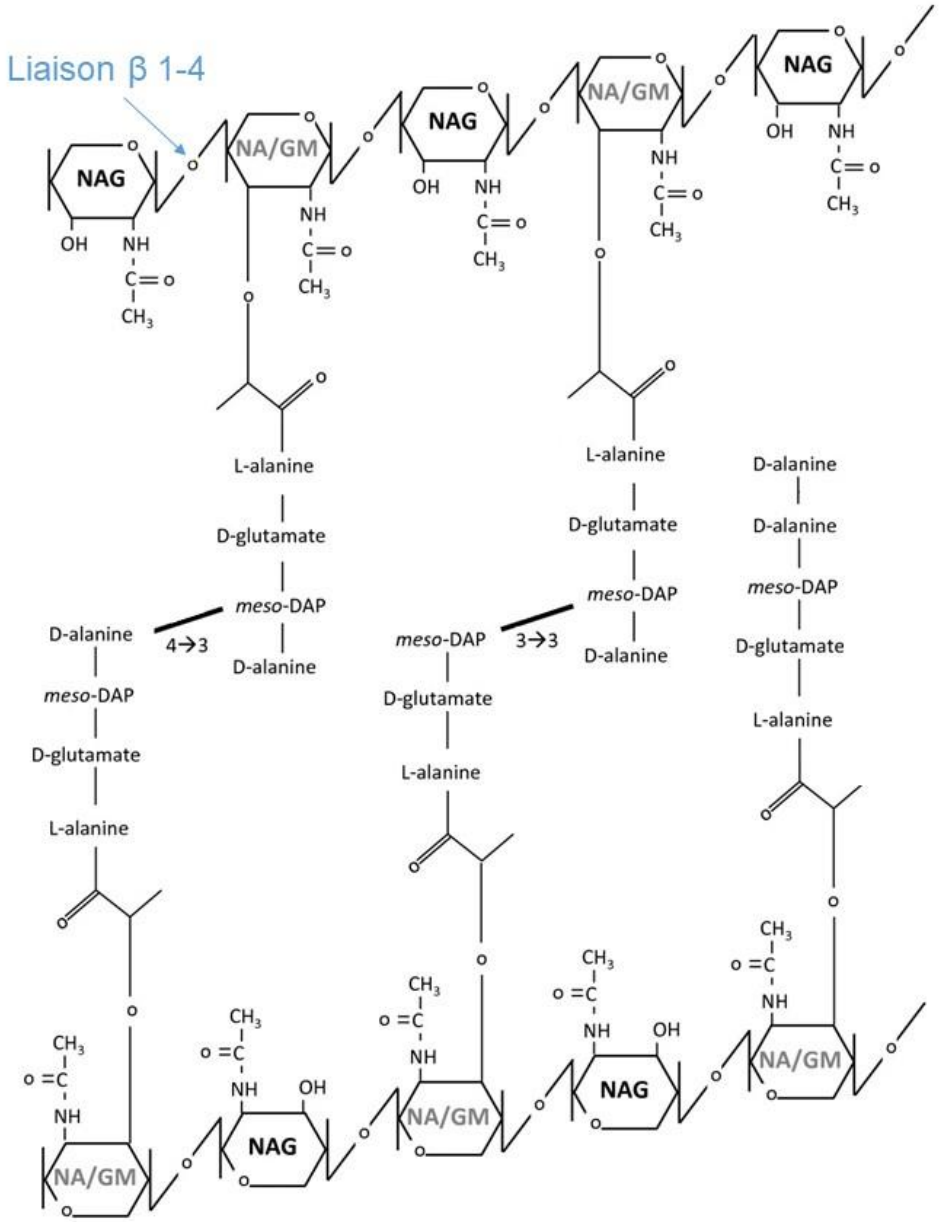

Figure 11. Représentation schématique du peptidoglycane mycobactérien. *Les résidus glycoliques NAG et NA/GM sont reliés par des liaisons ß-1,4. Les tiges pentapeptidiques opposées se trouvent aux positions 4,3 (L-Ala à méso-DAP) ou 3,3 (méso-DAP à méso-DAP). NA/GM : acide N-acétyl-muramique avec ou sans les modifications glycolyles, NAG : N-acétyl-glucosamine. Adaptée de (Machowski, Senzani et al. 2014).*

Bien que la localisation précise de ces molécules demeure en cours de validation, elles peuvent être présentes dans la membrane plasmique, l'espace périplasmique voire même dans la capsule.

Outre leur implication dans la synthèse d'autres composés (LM, LAM), les PIMs et les PI sont essentiels pour la viabilité *in vitro* de *M. tuberculosis* et agissent comme des activateurs des réactions immunitaires (Gilleron, Quesniaux et al. 2003; Guerin, Korduláková et al. 2010). Aucune différence significative n'a été observée entre les MCR et les MCL au niveau de la composition de leur membrane plasmique (Minnikin, Minnikin et al. 1982; Daffé 2008).

2.1.2 Espace périplasmique

Cet espace, d'une largeur de 16 nm, abrite diverses protéines solubles et enzymes, offrant ainsi un environnement propice aux échanges biochimiques (Daffé and Draper 1998; Hoffmann, Leis et al. 2008). Chez *M. smegmatis*, 3308 protéines ont été identifiées dans cet espace, ayant un rôle dans la néoglucogenèse, l'énergie, la transcription, et la dégradation des acides gras (Chiaradia 2018).

2.1.3 Complexe peptidoglycane-arabinogalactane

Cette couche a essentiellement un rôle structural et est majoritairement composée de peptidoglycane « PG », un polymère présent dans la plupart des bactéries. Ce PG confère la rigidité caractéristique des bacilles, tout en assurant la stabilité osmotique. En effet, il est constitué d'acides aminés et des unités d'oses répétées qui sont liés entre eux par des ponts osidiques de type $\beta_{1\text{-}4}$ (**Figure 11**) (Crick, Mahapatra et al. 2001). Ce peptidoglycane s'associe de manière covalente à l'arabinogalactane (AG) par le biais d'une liaison phosphoester et d'un linker disaccharide phosphate. L'AG, composé d'arabinose et de galactose, contribue également à la rigidité membranaire (McNeil, Daffe et al. 1990) et représente une molécule essentielle pour la survie des mycobactéries (McNeil, Wallner et al. 1987). Les enzymes impliquées dans leur voie de synthèse sont donc considérées comme des cibles thérapeutiques intéressantes à exploiter.

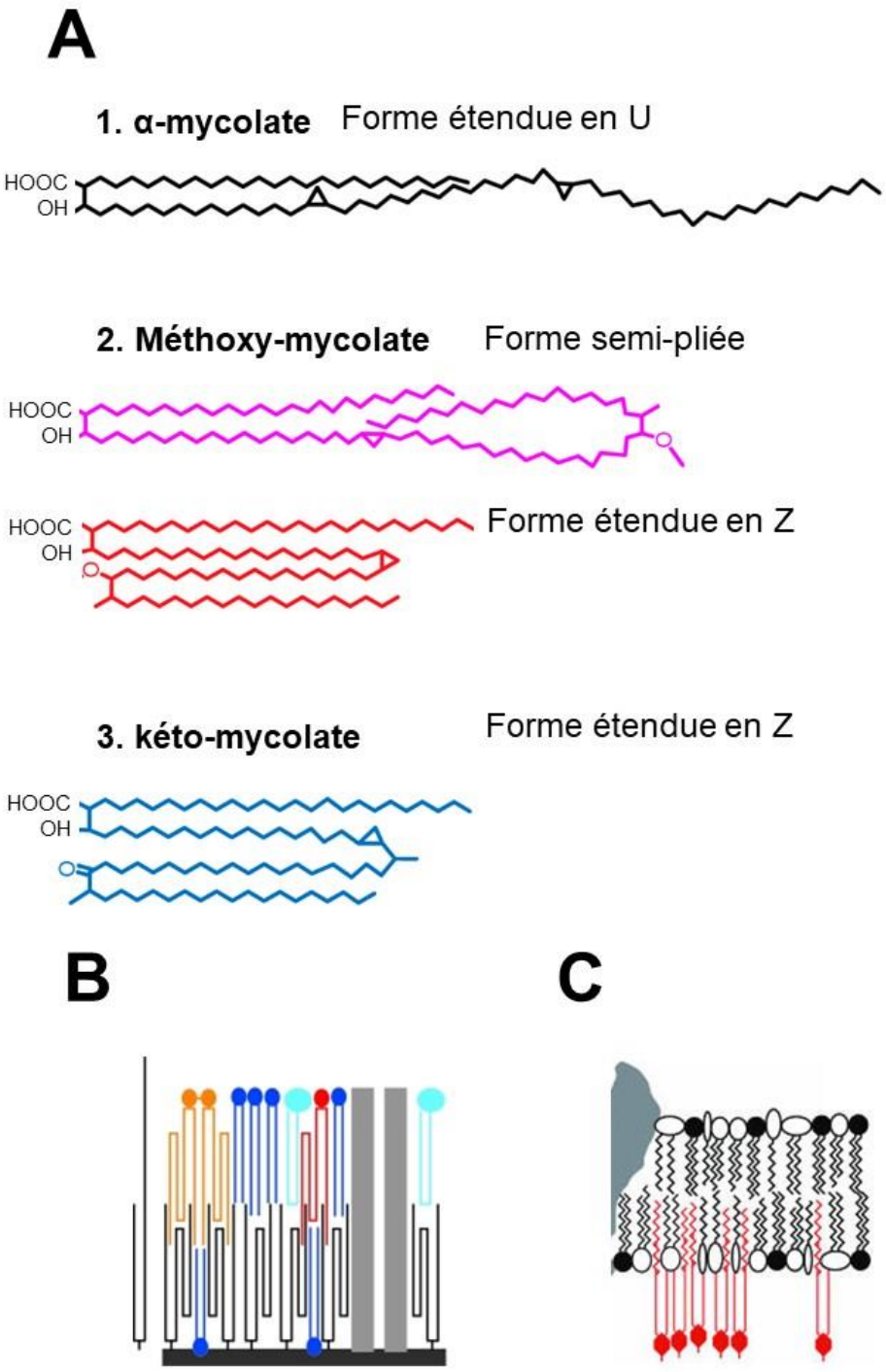

Figure 12. Représentation schématique des acides mycoliques. *A) différents types d'acides mycoliques retrouvés chez M. tuberculosis. B) organisation des acides noir, acide mycolique ; bleu foncé, phospholipides (chaînes de 16 à 18 carbones) ; gris foncé, peptidoglycane-arabinogalactane ; bleu clair, GPL ; orange, dimycolate de tréhalose ; rouge, monomycolate de tréhalose ; gris clair, porine. C) organisation dans l'enveloppe des acides mycoliques en modèle W. rouge : la liaison des acides mycoliques au polymère arabinogalactane. Adaptée de (Hoffmann, Leis et al. 2008; Zuber, Chami et al. 2008; David, Oona et al. 2015).*

2.1.4 Mycomembrane

Des études de microscopie électronique ont permis de montrer que cette mycomembrane a la même épaisseur que la membrane plasmique 6-7 nm et est constituée de deux feuillets distincts. En effet, le côté interne considéré moins fluide, renferme les acides mycoliques (AM) qui sont des acides gras α-ramifiés β-hydroxylés composés de 60 à 90 atomes de carbone, et liés l'AG par une liaison covalente. En revanche, le côté externe (plus fluide) renferme quant à lui, des glycolipides, essentiellement des mono-mycolates de tréhalose (TMM), des di-mycolates de tréhalose (TDM) et des monoméromycolates-diacyglycérol (MMDAG) (**Figure 12A**). Le TDM est un facteur de virulence essentiel favorisant la survie intracellulaire en induisant la formation de cordes qui facilitent la lyse des phagocytes. C'est ainsi qu'il est couramment désigné sous le nom de "cord factor" (Hunter, Olsen et al. 2006). Outre ces molécules, des protéines telles que les porines, sont présentes dans la membrane externe, mais peu d'entre elles ont été caractérisées (Trias, Jarlier et al. 1992; Trias and Benz 1994; Liu, Rosenberg et al. 1995; Liu, Barry et al. 1996).

Au sein de cette mycomembrane, pendant longtemps il s'est avéré difficile de combiner la longueur des chaines d'acides mycoliques dans un modèle structural complet, principalement parce que les données ultrastructurales disponibles reposaient sur des coupes en microscopie électronique conventionnelle, qui peuvent induire des artefacts. Cependant l'existence d'une bicouche de la membrane externe avait été postulée mais n'avait jamais été directement étudiée et confirmée. Ce n'est qu'en 2008 que la technique de CEMOVIS (Cryo-Electron Microscopy Of Vitreous Sections) réalisée sur *M. bovis* BCG et *M. smegmatis* a permis de montrer que les acides mycoliques adopteraient une structure en W (**Figure 12C**). En effet, cette structure est tout à fait compatible avec l'épaisseur de 7-8 nm de la mycomembrane observée par la Cryo-EM. Cependant deux types d'agencement ont été proposé, soit un modèle en « zipper like » (Hoffmann, Leis et al. 2008), soit le modèle en W proposé par Zuber *et al*. (Zuber, Chami et al. 2008)(**Figure 12B, C**). Toutefois, l'organisation des acides mycoliques dans la mycomembrane de *M. tuberculosis* n'a pas encore été définitivement établie.

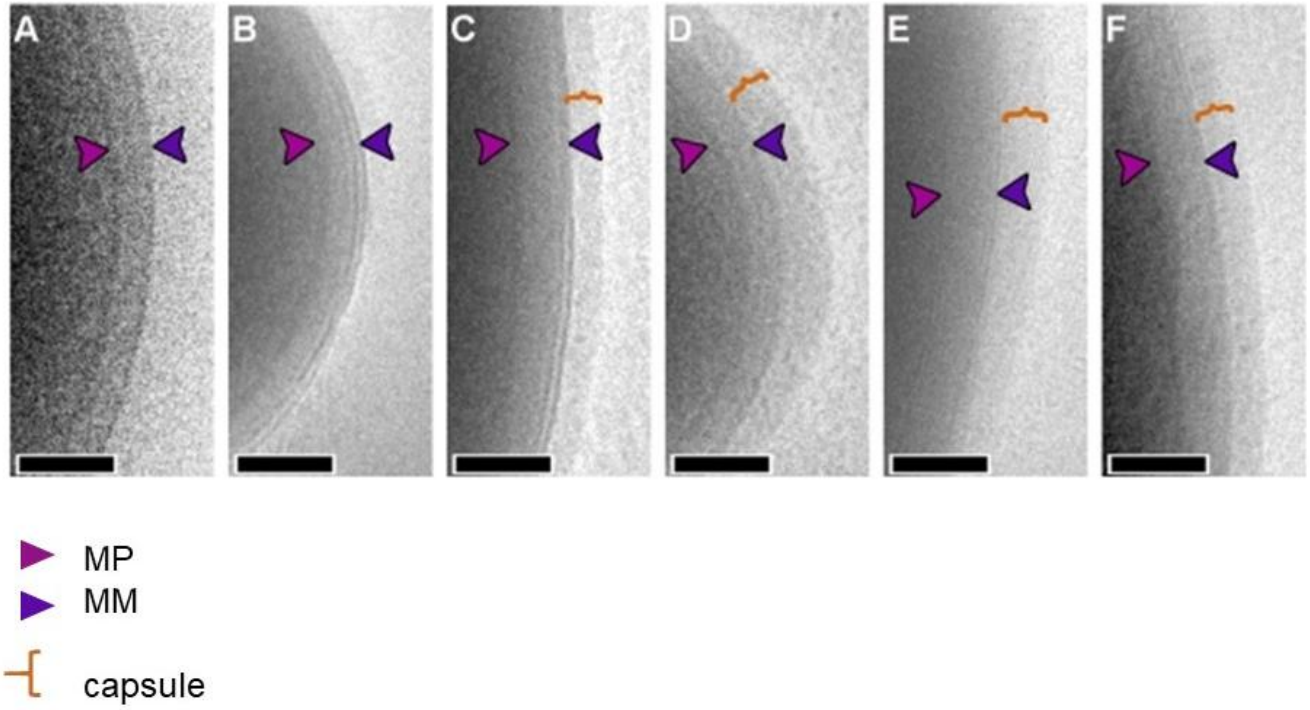

Figure 13. Visualisation de la capsule par cryo microscopie électronique*. A) enveloppe cellulaire d'une bactérie à Gram négatif S. flexneri. B) enveloppe de M. smegmatis cultivées avec des perturbations chimiques et mécaniques, similaire à une bactérie à Gram négatif C) capsule (accolade orange) chez M. smegmatis en croissance normale, D) capsule chez M. tuberculosis (accolade orange) E) capsule chez M. marinum (accolade orange), F) capsule chez M. bovis BCG (accolade orange). MP : membrane plasmique, MM : mycomembrane. Adaptée de (Sani, Houben et al. 2010).*

Cette bicouche asymétrique est également composée de divers lipides extractibles (liés de manière non covalente) qui ne sont pas indispensables à la survie de la bactérie, mais qui, chacun à leur manière, contribuent à sa virulence. Parmi ces molécules on trouve les sulfolipides (SL), les diacyltréhaloses (DAT), les triacyltréhaloses (TAT), les polyacyltréhaloses (PAT), les GPL, les lipo-oligosaccharides (LOS), les glycolipides phénoliques (PGL) et les dimycocérates-phtiocérol (PDIM) sous forme majoritaire avec une fonction méthoxy, ou sous forme minoritaire avec une fonction cétone (Cambier, Falkow et al. 2014; Jackson 2014; Boritsch and Brosch 2016). Il est important de noter que ces divers types de lipides ne se retrouvent pas systématiquement dans toutes les espèces mycobactériennes et chaque groupe peut se distinguer par des compositions spécifiques et distinctes.

2.1.5 Capsule

La capsule forme la couche la plus externe de l'enveloppe bactérienne. En 1961, la présence de la capsule a été identifiée par microscopie électronique, tout d'abord chez *M. leprae* puis chez *M. tuberculosis, M. bovis* BCG, et *M. smegmatis*, et définie comme une matrice amorphe entourant des bacilles individuels (**Figure 13**) (Hanks 1961; Sani, Houben et al. 2010).

D'une épaisseur d'environ 35 nm, la capsule est principalement composée de polysaccharides (glucane), de protéines et de lipides, avec des proportions variables selon l'espèce considérée : les mycobactéries pathogènes se distinguent par une prédominance de lipopolysaccharides (LAM, LM), tandis que les non-pathogènes présentent une plus grande proportion de protéines. Ces composants ne sont pas liés à l'enveloppe par des liaisons covalentes. Par conséquent, cette faible interaction permet aux mycobactéries d'éliminer la capsule dans le milieu (Lemassu, Ortalo-Magné et al. 1996). Généralement, la capsule bactérienne existe sous quatre formes distinctes, rigide, flexible, intégrale, ou périphérique, et son apparence est étroitement liée aux conditions de croissance (Costerton, Irvin et al. 1981; Sani, Houben et al. 2010).

Des études ont montré que le rôle de cette capsule ne se limite pas à la survie des bacilles dans les cellules hôtes, mais qu'elle participe également au niveau des interactions hôte-pathogène, en favorisant la reconnaissance et l'internalisation du pathogène dans les macrophages, les cellules dendritiques, et les phagocytes (Kalscheuer, Palacios et al. 2019).

2.1.6 La paroi chez M. abscessus

Des différences significatives sont observées dans la paroi de *M. abscessus* par rapport à *M. tuberculosis*. Contrairement à ce dernier, *M. abscessus* ne présente pas de DAT, PAT, PDIM, ni de SL, mais d'autres glycolipides spécifiques comme le tréhalose polyphléate (TPP) et les glycopeptidolipides (GPL) ont été identifiés. En effet, les GPL se trouvent essentiellement chez les mycobactéries opportunistes ou non-pathogènes (Medjahed, Gaillard et al. 2010; Parmar and Tocheva 2023). La présence ou l'absence de ces GPL est responsables de deux morphotypes distincts chez ce bacille (**voir Chapitre I**). Pour *M. abscessus*, seuls les AM α et α'-mycolates sont présents (Halloum, Carrère-Kremer et al. 2016).

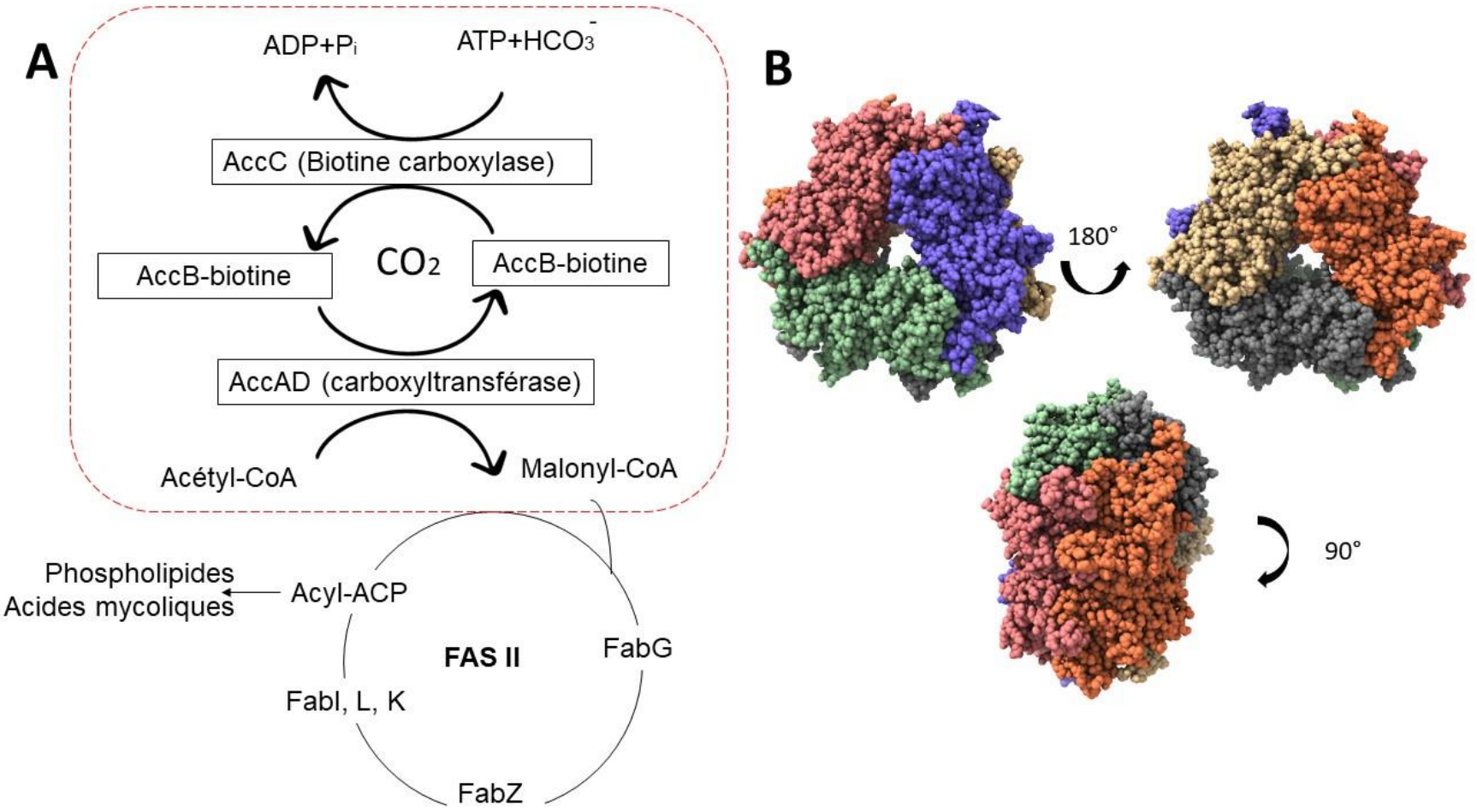

Figure 14. La carboxylester hydrolase. *A) Mécanisme d'action du complexe acétyl-CoA carboxylase (AccC). La biotine attachée à AccB est carboxylée via la consommation de l'ATP. Le groupe carboxyle est transféré de l'acétyl-CoA au malonyl-CoA par AccC, composée de 2 sous-unités AccA et AccD pour entrer dans le cycle de synthèse des acides gras (FASII). B) (Code PDB 2bzr) Structure 3D de l'AccD5. A gauche le premier trimère, à droite, le 2ème trimère visualisé après rotation de 180°, empilement visualisé après rotation de 90, cristallisation 2,9A°. Adaptée de (Freiberg, Brunner et al. 2004; Lin, Melgar et al. 2006).*

2.2 Les enzymes lipolytiques

Outre la complexité structurelle de la membrane des mycobactéries et son implication dans le métabolisme lipidique, le séquençage du génome de *M. tuberculosis* a permis d'identifier 250 enzymes lipolytiques, représentant 6% du génome, tandis qu'*E. coli* n'en possède que 50 (1,2%) (Friesen 1988; Cole, Brosch et al. 1998; Camus, Pryor et al. 2002). Selon l'Union Internationale des Biochimistes, les enzymes sont divisées en sept classes enzymatiques « EC » selon les réactions qu'elles catalysent :

EC1 : les oxydoréductases
EC2 : les transférases
EC3 : les hydrolases
EC4 : les lyases
EC5 : les isomérases
EC6 : les ligases
EC7 : les translocases

2.2.1 Les hydrolases

2.2.1.1 Les carboxylester hydrolases

La famille des carboxylester hydrolases est formée de deux sous-familles ; les carboxylestérases et les lipases.

Les carboxylestérases (CT) sont des enzymes qui possèdent différents rôles *in vivo* mais qui partagent un substrat commun : l'acide carboxylique. Elles catalysent l'addition d'un groupe carboxyl COOH à une autre molécule, tout en ayant la possibilité d'agir sur la synthèse ou l'hydrolyse des lipides (Luppa and Andrä 1983). Ces enzymes catalysent uniquement des molécules hydrosolubles comportant des chaînes acyles courtes. La réaction chimique qu'elles déclenchent est la suivante :

$$RCOOR' + H2O \leftrightarrow RCOOH + CoA$$

Avec RCOOR' : carboxyl ester RCOOH : acide carboxylique

L'acyl-CoA carboxylase (Acc) intervient dans le métabolisme des lipides, notamment dans la biosynthèse d'acide gras, en catalysant la carboxylation de plusieurs substrats d'acyl-CoA (**Figure 14A**) (Salaemae, Azhar et al. 2011). L'Acc est formé par deux sous-unités : la biotine carboxylase et la carboxyltransférase. Chez *M. tuberculosis*, la structure de la carboxyltransférase de l'AccD5 a été étudiée : il s'agit d'un homohexamère en anneau composé de deux trimères empilés l'un sur l'autre (**Figure 14B**) (Lin, Melgar et al. 2006).

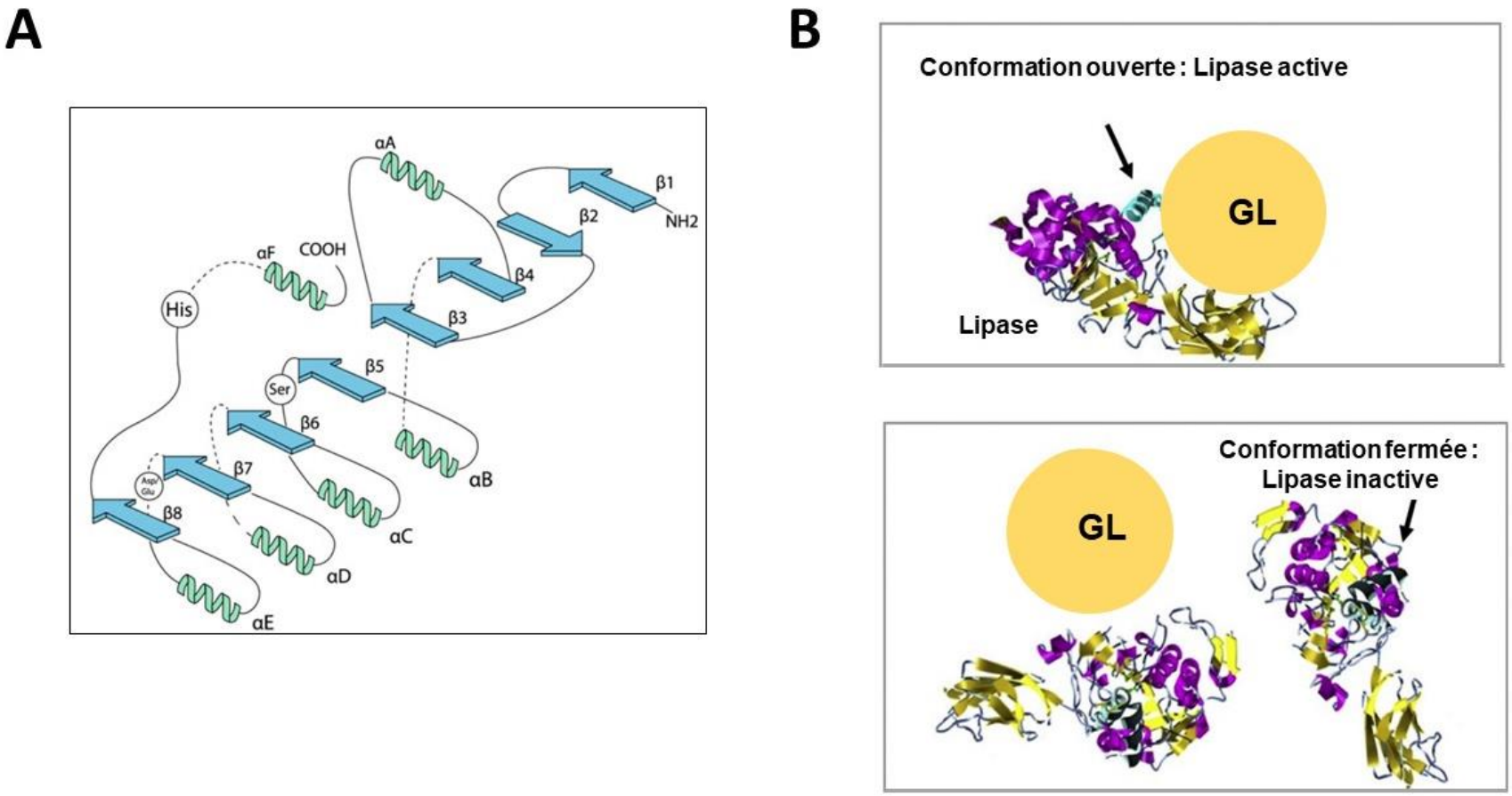

Figure 15. Structure et mode d'action d'une lipase. *A) Représentation sous forme canonique du repliement des enzymes de la famille des α/β hydrolases. Les hélices sont représentées en vert et les brins β en bleu. La triade catalytique est représentée par les acides aminés dans les cercles. B) Structure 3D d'une lipase active exposant son volet amphiphile face au substrat : gouttelette lipidique (GL) et d'une lipase inactive à conformation fermée. Adaptée de (Joyce, Kempson et al. 2016; Casas-Godoy, Gasteazoro et al. 2018).*

Les lipases, quant à elles, hydrolysent la liaison ester d'acylglycérides ayant de longues chaines d'acides gras. Des molécules d'acide gras et de glycérol sont issues de cette réaction. Cette famille d'enzymes se caractérise par la présence d'une organisation tridimensionnelle commune avec un cœur formé par huit brins β, dont 7 sont parallèles et un antiparallèle, reliés par 6 hélices α. Cette conformation est appelée un repliement α/β hydrolase, qui peut également être trouvé chez d'autres familles d'enzymes. Ce repliement permet de positionner dans l'espace la triade catalytique qui est composée des trois acides aminés, sérine, histidine, acide glutamate ou aspartate, et qui seront impliquées dans l'acte catalytique (**Figure 15A**).

Dans certaines lipases, ce site actif n'est pas toujours accessible au substrat et peut être couvert par un volet amphiphile qui s'ouvre et qui se ferme en présence du substrat (Ollis, Cheah et al. 1992) (**Figure 15B**). Chez *M. tuberculosis* la monoglycéride lipase Rv0183 et la lipase LipY sont jusqu'à présent identifiées comme lipases extracellulaires ainsi que la cutinase Cfp21 (Rv1984c) à activité lipasique (détaillé en dessous)(Schué, Maurin et al. 2010). La Rv0183 été retrouvée dans la paroi cellulaire ainsi que dans le milieu de culture et cette protéine étant capable dégrader essentiellement des monoacylglycérides (MAG), il a été proposé qu'elle dégraderait les lipides de l'hôte permettant aux acides gras libérés d'être utilisés par la bactérie pour former ses réserves en lipides (Côtes, Bakala N'goma J et al. 2008). D'autre part, la LipY aurait une activité de triacylglycérol (TAG) hydrolase qui contribuerait à la dégradation des lipides de l'hôte, et dans certains cas les lipides intracytoplasmiques des mycobactéries (Mishra, de Chastellier et al. 2008; Daleke, Cascioferro et al. 2011; Santucci, Diomandé et al. 2018). De plus, cette enzyme qui est une des 21 lipases identifiées chez *M. tuberculosis*, possède deux domaines : un domaine catalytique et un domaine PE ou PPE. En effet, des études ont validé que le domaine PE de cette TAG hydrolase affecte négativement l'hydrolyse et la liaison à la monocouche. Le domaine PE permet de réguler l'activité de la protéine et *via* le système de sécrétion de type VII ESX5, et la translocation du domaine catalytique de LipY à la surface de la bactérie lui permettant ainsi d'agir sur la dégradation des lipides de l'hôte (Garrett, Broadwell et al. 2015; Santucci, Smichi et al. 2019).

Parmi les protéines appartenant à la famille des Lip, 8 sont considérées comme étant des estérases strictes (hydrolysent les liaisons ester) LipC, LipF, LipH, LipI, LipN, LipR, LipU, et LipW (Delorme, Diomandé et al. 2012; Shen, Singh et al. 2012). Concernant LipF, en plus de son activité estérasique, elle possèderait une activité de type phospholipase C (Zhang, Wang et al. 2005; Richter and Saviola 2009; Delorme, Diomandé et al. 2012).

LipG est une thioestérase aux rôles variés impliquées dans le métabolisme des phospholipides, le remodelage de la membrane ainsi que dans l'immunité. En effet, LipG est essentielle pour la survie du bacille dans les poumons de souris (Santucci, Point et al. 2018).

Les cutinases constituent également un sous-groupe de cette famille d'enzymes, dégradant les liaisons esters de la cutine, et ayant une origine bactérienne ou fongique. Cependant, des activités de type lipase et estérase ont été associées à cette famille (Schué, Maurin et al. 2010). Comme les lipases, les cutinases possèdent le repliement α/β hydrolase avec la triade catalytique, et hydrolysent les esters et les TAG, avec des longueurs des chaines variables. Sept gènes codant pour des cutinases ont été identifiés et étudiés chez *M. tuberculosis* et qui sont homologues aux cutinases de *Fusarium solani pisi* (West, Chow et al. 2009). Cut4 et Cfp21 sont secrétées et possèdent chacune une activité spécifique. Cpf21 hydrolyse des esters carboxyliques à chaine moyenne, alors que Cut4 a une activité de PLA_2 (détaillé dans le **§ 2.2.1.3**) (Schué, Maurin et al. 2010). L'enzyme Cut6 joue un rôle important dans le métabolisme lipidique et est essentielle chez *M. tuberculosis*. Elle se retrouve dans la fraction membranaire et possède une activité de type phospholipase A_2 et thioestérase et contribue de façon significative à la synthèse des AM (Parker, Barkley et al. 2009; Goins, Schreidah et al. 2018).

2.2.1.2 Les thioestérases

Les thioestérases (ou thioester hydrolases) sont responsables de l'hydrolyse des liaisons thioesters, produisant un acide carboxylique et une fonction thiol. Cette famille comprend 27 sous-groupes identifiés en fonction du substrat, mais qui ne sont pas entièrement classifiés (Cantu, Chen et al. 2010).

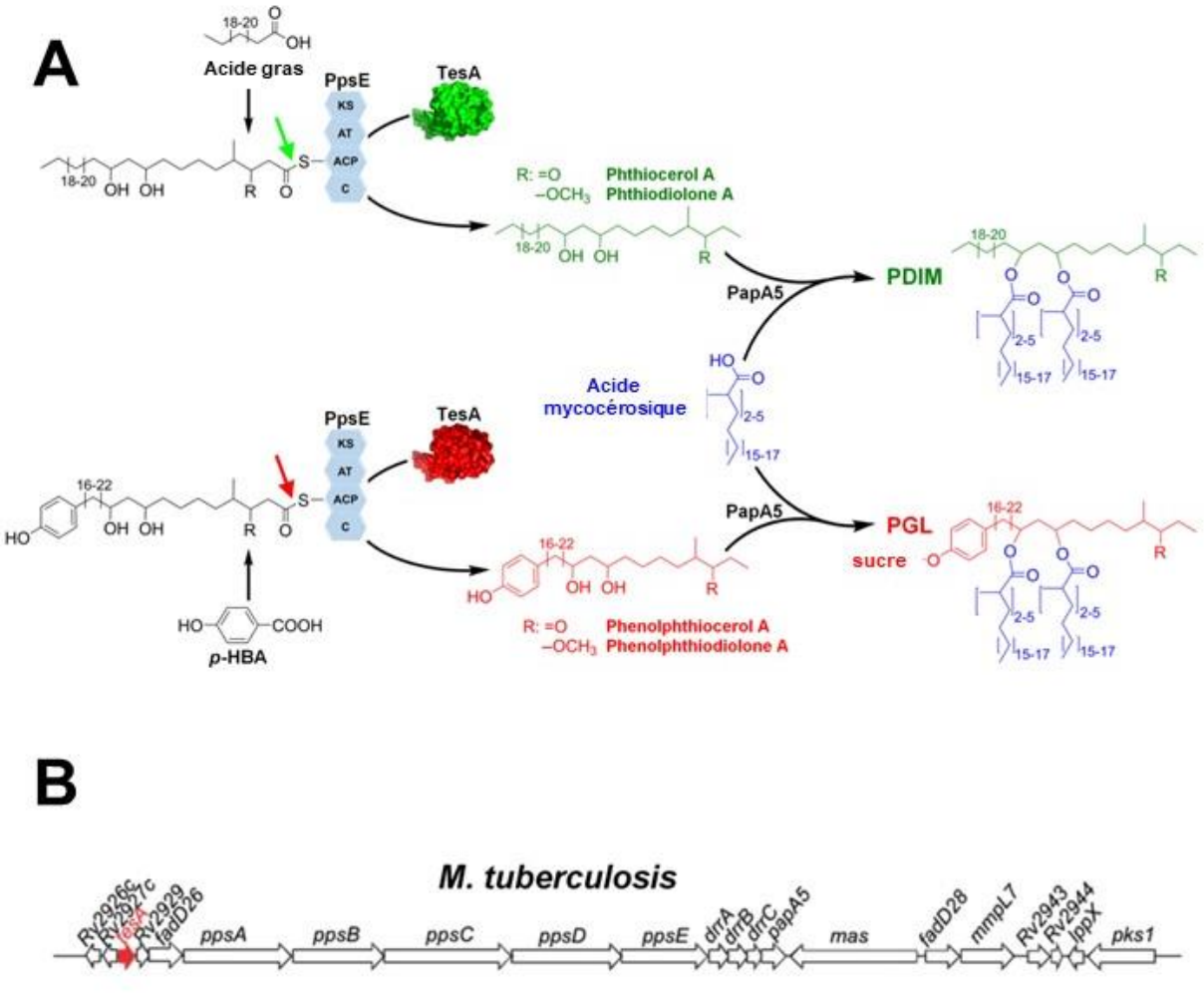

Figure 16. La thioestérase TesA*. A) Représentation schématique de la voie de biosynthèse du PDIM et du PGL chez M.tuberculosis en mettant en évidence le role de TesA et son interaction avec la polykétide synthase PpsE. B) Cluster des gènes codant la synthèse du PDIM chez M. tuberculosis, le gène codant pour TesA est représenté en rouge. Adaptée de (Alibaud, Rombouts et al. 2011; Nguyen, Nguyen et al. 2018).*

Parmi eux se trouvent le sous-groupe des acyl-CoA hydrolases et celui des oleyl-ACP hydrolases, qui permettent la libération d'un acide gras et d'un CoA qui peuvent être les précurseurs de la synthèse de nombreux autres lipides.

Chez *M. tuberculosis*, la thioestérase TesA annotée Rv2928 , est une thioestérase de type II qui joue un rôle important dans la synthèse des PDIM et des PGL, effecteurs importants pour la virulence (**Figure 16A**). (Waddell, Chung et al. 2005; Nguyen, Nguyen et al. 2018; Yang, Vandenbussche et al. 2020). En effet, un mutant de délétion de TesA chez *M. marinum* produit une faible quantité de PDIM et PGL et présente une sensibilité accrue aux antibiotiques (Chavadi, Edupuganti et al. 2011). Le gène codant pour TesA appartient au cluster de biosynthèse et d'export des PDIM (**Figure 16B**) (Rao and Ranganathan 2004). De plus, un mutant de *M. marinum* Δ*tesA* injecté par voie intraveineuse dans l'embryon de zebrafish est beaucoup plus atténué que lors d'une injection dans la notochorde, cette dernière représentant l'endosquelette ou la ligne médiane du zebrafish (Alibaud, Rombouts et al. 2011).

Une autre thioestérase TesB, similaire à des enzymes chez présentent chez *E. coli,* semble avoir un rôle dans l'homéostasie lipidique (Swarbrick, Bythrow et al. 2017). Sa structure a été caractérisée, cependant son rôle dans les voies métaboliques n'est pas encore résolu. Cette thioestérase peut se trouver sous forme active ou non selon les résidus dans son site catalytique. En effet, la substitution de l'aspartate du site actif (détaillé dans le **§ 2.2.1.1**) en alanine rend l'enzyme incapable d'hydrolyser les acyl-CoAs. Un autre exemple de thioestérase bien étudiée chez les mycobactéries est la protéine LipG (détaillé dans le **§ 2.2.1.1**).

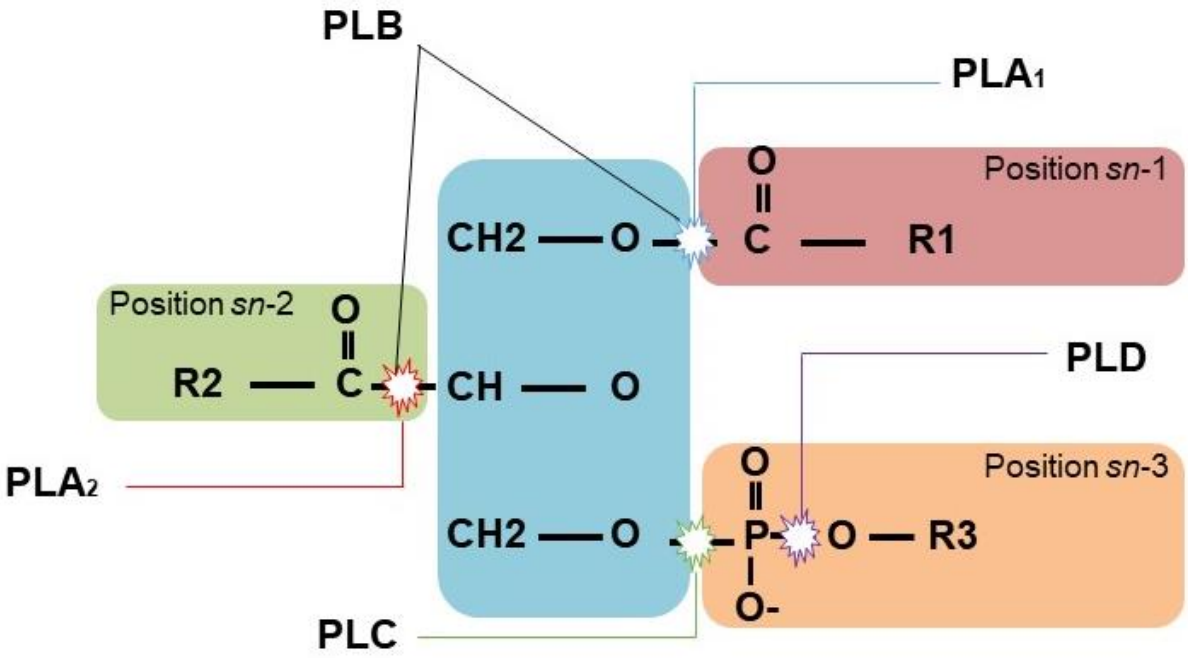

Figure 17. Représentation schématique de la structure d'un phospholipide ainsi que le mode d'action des phospholipases en fonction de leurs positions spécifiques.

2.2.1.3 Les phospholipases

Les phospholipases (phosphodiester hydrolases), qui se caractérisent par la capacité d'hydrolyser les phospholipides, sont présentes chez les bactéries à Gram positif et Gram négatif. Quatre groupes ont été décrits selon la position du clivage (**Figure 17**) ;

- ✓ Phospholipase A (PLA) ; qui hydrolyse de la liaison entre le glycérol et la chaine d'acide gras, soit en position *sn-1* (PLA_1), soit en position *sn-2* (PLA_2).
- ✓ Phospholipase B (PLB) ; qui présente une activité de phospholipase A et de lysophospholipase (Maeda and Kashiwabara 1996). Cette dernière libère une lysophosphatidylcholine et un acide gras.
- ✓ Phospholipase C (PLC) ; qui hydrolyse la liaison ester du groupe phosphate, libérant ainsi un diacylglycérol et un phosphoalcool. Ce groupe d'enzymes est uniquement présent chez les espèces pathogènes des mycobactéries, y compris *M. abscessus* (Raynaud, Guilhot et al. 2002; Bakala N'Goma, Le Moigne et al. 2015; Le Chevalier, Cascioferro et al. 2015).
- ✓ Phospholipase D (PLD) ; génère un acide phosphatidique.

Les phospholipases demeurent sous-étudiées chez les mycobactéries, bien qu'une action synergique entre la PLC et une lipase ait été démontrée chez *P. aeruginosa* (Cortes, Nessar et al. 2010). Chez *M. abscessus*, seule la PLC a jusqu'à présent été identifiée et caractérisée biochimiquement (Bakala N'Goma, Le Moigne et al. 2015).

2.2.2 Autres classes enzymatiques

2.2.2.1 Les déshydrogénases

Le génome de *M. tuberculosis* code pour 35 acyl-CoA déshydrogénases putatives « ACAD » codées par les gènes *fadE.* Elles appartiennent à la classe des oxydoréductases, et sont impliquées dans la β-oxydation, la principale voie métabolique de dégradation des molécules d'acides gras (Cole, Brosch et al. 1998). Ce sont des flavoprotéines qui catalysent l'insaturation α,ß des acyls-CoA thioesters quel que soient les longueurs de chaine des acides gras (Wipperman, Yang et al. 2013).

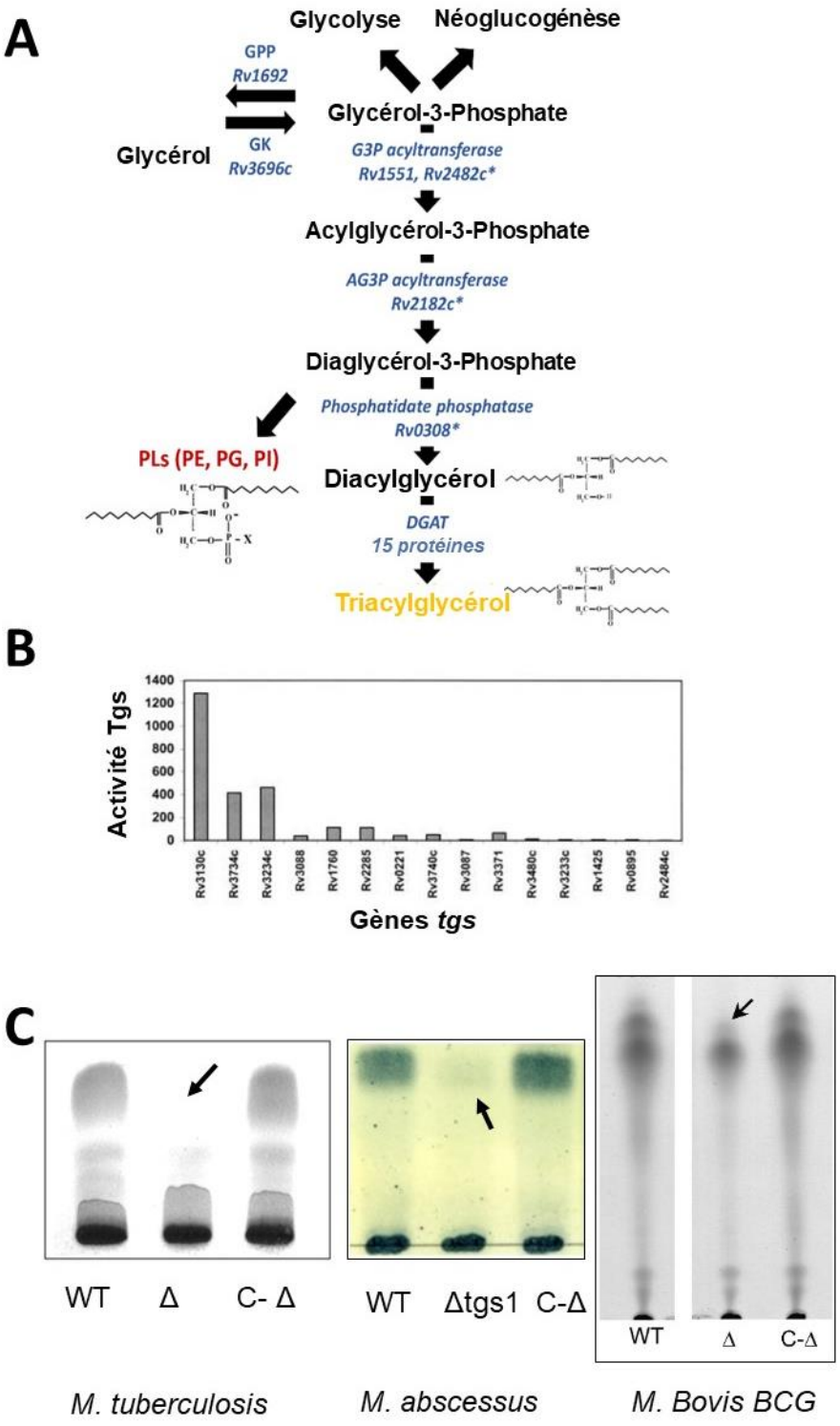

Figure 18. Implication des triglycérides synthases dans la synthèse des TAG. *A) Représentation schématique de la voie de Kennedy de synthèse des TAG chez les actinobactéries. B) Estimation de la contribution relative potentielle des produits des gènes tgs à l'activité TGS totale. C) Role de Tgs1 dans la synthèse des TAG chez différentes espèces mycobactériennes. GPP : glycérol phosphate phosphatase, GK : Glycérol kinase, GPAT : Glycerol 3 Phosphate acyltransferase, PAP : Phosphatidate phosphatase, DGAT : Diacylglycérol acétyl transférase, PL : Phospholipides. Adaptéee(Daniel, Deb et al. 2004; Sirakova, Dubey et al. 2006; Low, Shui et al. 2010; Viljoen, Blaise et al. 2016; Mallick, Santucci et al. 2021).*

L'existence d'un motif structural commun à toutes les ACAD basé sur la présence de α_4 homotétramères ou α_2 homodimères, a été proposée. Cependant, une étude menée par Wipperman *et al.* a identifié une sous-famille d'ACAD dotée d'une structure différente composée d'hétérotétramères $\alpha_2\beta_2$. Ces dernières semblent jouer un rôle dans une sous-voie du métabolisme du cholestérol (Kim and Battaile 2002; Wipperman, Yang et al. 2013). A l'issue de cette étude, les 35 ACAD identifiées par Cole *et al.*, sont remises en question. En effet, ils ont montré que 2 *fadE* codent pour un même complexe protéique d'ACAD, et c'est le cas pour 4 autres complexes holoprotéiques, d'où la réduction du nombre des ACAD dans le génome de *M. tuberculosis* de 35 à 30.

2.2.2.2 Les synthases

Les synthases ou synthétases font partie de la famille des ligases (EC6). Chez les procaryotes, une enzyme responsable de la synthèse des TAG nommée WS/DGAT pour wax synthase/ diacylglycérol acyltransférase, et agissant comme acyl-CoA acyltransférase (Aft) à chaine longue dans l'étape finale de la synthèse, a été identifiée en 2003 (Kalscheuer and Steinbüchel 2003). Chez les mycobactéries, une dizaine de protéines apparentées à WS/DGAT ont été répertoriées.

Les Aft se trouvent chez les actinomycètes ainsi que chez certains Gram négatif, comme *A. calcoaceticus* (Wältermann, Hinz et al. 2005; Alvarez, Alvarez et al. 2008; Hernández, Arabolaza et al. 2013). Chez *M. tuberculosis*, 15 gènes *aft* ont été identifiés et sont exprimés lors de différents stresses auxquels le bacille est soumis (**Figure 18A**) (Daniel, Deb et al. 2004; Sirakova, Dubey et al. 2006). Parmi ces 15 Aft, 4 étaient purifiées et leur activité de triglycéride synthase a permis de les nommer triglycéride synthase (Tgs1-4) (Daniel, Deb et al. 2004; Sirakova, Dubey et al. 2006), les 11 protéines restent des Tgs putatives (**Tableau 3**). La Tgs1 (Rv3130c) exprimée chez *E. coli* a montré l'activité triglycéride synthase la plus importante parmi les autres (**Figure 18B**).

Basé sur ces résultats, une étude a montré que la surexpression de *tgs1* fait augmenter l'accumulation des TAG dix fois plus d'une souche sauvage, indiquant ainsi le rôle de Tgs1 dans le métabolisme des TAG (Gerasimova, Kazakov et al. 2011).

La délétion du gène de Tgs1 chez différentes espèces mycobactériennes, notamment chez *M. tuberculosis* (Sirakova, Dubey et al. 2006), *M. bovis* BCG (Low, Shui et al. 2010), et *M. abscessus* (détaillé dans le **§ 2.3**) (Viljoen, Blaise et al. 2016) a montré une réduction significative au niveau des TAG synthétisés (**Figure 18C**). Toutes ces investigations mettent en valeur le rôle de Tgs1 parmi les 15 Tgs de *M. tuberculosis* dans la synthèse des TAG. D'ailleurs, le régulon de la dormance Dos, activé au cours de période de stress, est composé de 48 gènes dont celui codant la triglycéride synthase Tgs1, ce qui favorise la relation entre la persistance et l'accumulation des TAG. Certaines Tgs (Rv0895, Rv3087, Rv3480) sont essentielles pour la croissance *in vivo* dans certains modèles (Moorey and Besra 2022).

***Tableau 3. Les 15 Tgs identifiées chez M. tuberculosis et leurs orthologues chez M. abscessus**. Adapté de (Daniel, Deb et al. 2004; Viljoen, Blaise et al. 2016).*

Gène chez *M. tuberculosis*	Protéine	*M. abscessus*	Gène	Protéine
Rv3130c	Tgs1	*MAB_3551c*	*Rv0895*	Tgs putative
Rv3734	Tgs2	*MAB_1917*	*Rv0221*	Tgs putative
Rv3234c	Tgs3	*MAB_0507*	*Rv3371*	Tgs putative
Rv3088	Tgs4	*MAB_4544c*	*Rv2285*	Tgs putative
Rv1760	Tgs putative (Tgs5)	*MAB_3964*	*Rv3480c*	Tgs putative
Rv3740c	Tgs putative (Tgs6)	*MAB_1278*	*Rv3087*	Tgs putative
Rv2484c	Tgs putative (Tgs7)	*MAB_0854*	*Rv1425*	Tgs putative
			Rv3740c	Tgs putative

Tableau 4. Les enzymes lipolytiques chez M. abscessus selon leur orthologues chez M. tuberculosis. Adaptée de (Stehr, Elamin et al. 2012)

Gène	Protéine	Orthologue chez *M. abscessus*	% d'identité	Fonction (selon KEGG)
Rv0220	LipC	MAB_3447c	34%	Putative lipase/esterase
Rv3487c	LipF	MAB_1194	54%	Putative LipU
Rv1399c	LipH	MAB_2814	55%	Putative LipH
Rv1400c	LipI	MAB_2814	54%	Putative LipH
Rv2284	LipM	MAB_2814	28%	Putative LipH
Rv2970c	LipN	MAB_3270c	56%	Putative LipN
Rv1426c	LipO	MAB_2814	28%	Putative LipH
Rv2485c	LipQ	MAB_0078	29%	Putative lipase/esterase
Rv3084	LipR	MAB_0141c	35%	Putative esterase
Rv1076	LipU	MAB_1194	54%	Putative LipU
Rv0217c	LipW	MAB_0826c	59%	Putative LipW
Rv3097c	LipY	MAB_2584	25%	Putative esterase
Rv2045	LipT	MAB_3453c	61%	Putative carboxylesterase LipT
Rv3203	LipV	MAB_3517	59%	Putative LipV
Rv0183	Rv0183	MAB_4548	57%	Probable O-methyltransferase
Rv2715	Rv2715	MAB_3034	71%	Probable hydrolase
Rv3171c	Hpx	MAB_3738c	30%	Putative hydrolase
Rv1984c	Cfp21	MAB_3272c	47%	Probable cut1
Rv1758	Cut1	MAB_3272c	53%	Probable cut1
Rv2301	Cut2	MAB_3763	50%	Probable cutinase cut2 precursor
Rv3451	Cut3	MAB_3766	47%	Probable cutinase cut3 precursor
Rv3452	Cut4	MAB_3763	44%	Probable cutinase cut2 precursor
Rv3724B	Cut5b			
Rv3802c	Cut6	MAB_0178	64%	Hypothetical cutinase precursor
Rv2351c	PlcA	MAB_0555	38%	Phospholipase C (Bakala N'Goma, Le Moigne et al. 2015)
Rv2350c	PlcB	MAB_0555	40%	
Rv2349c	PlcC	MAB_0555	40%	
Rv1755c	PlcD			
Rv1592c	Rv1592c	MAB_2676	62%	Conserved hypothetical protein (lipase?)
Rv1683	Rv1683	MAB_2348	65%	Possible long-chain acyl-CoA synthase
Rv0646c	LipG	MAB_3880	54%	Probable LipG
Rv3130c	Tgs1	MAB_3551c	32%	Tgs1 (Viljoen, Blaise et al. 2016)
Rv3734c	Tgs2	MAB_1917	51%	Tgs2 (Viljoen, Blaise et al. 2016)
Rv3234c	Tgs3	MAB_0507	63%	Conserved hypothetical
Rv3088	Tgs4	MAB_4544c	28%	Conserved hypothetical
Rv1760	DGAT	MAB_1917	56%	Tgs2 (Viljoen, Blaise et al. 2016)
Rv2285	DGAT	MAB_4544c	31%	Conserved hypothetical
Rv3804c	Ag85A	MAB_0176	63%	Ag85A precursor
Rv1428c	DGAT	MAB_4002c	33%	Putative acyltransferase
Rv2224c	Rv2224c	MAB_1918	60%	Conserved hypothetical
Rv0467	ICL1	MAB_4095c	84%	Isocitrate lyase (AceA)
Rv1915	ICL2	MAB_4095c	36%	Isocitrate lyase (AceA)
Rv1916	ICL2	MAB_4095c	38%	Isocitrate lyase (AceA)

2.2.3 Les enzymes lipolytiques chez M. abscessus

Le génome de *M. abscessus* n'est pas encore aussi bien caractérisé que celui de *M. tuberculosis*, et notre compréhension des enzymes lipolytiques reste encore limitée. Grâce à des *études* bioinformatiques, les orthologues des enzymes lipolytiques déjà connues dans le génome de *M. tuberculosis* ont pu être identifié chez *M. abscessus.*

Par ailleurs, nous avons recherché les homologues des enzymes lipolytiques de *M. tuberculosis* en exploitant la base de donnée KEGG (https://www.kegg.jp/) ainsi que les protéines répertoriées dans la revue de Stehr (Stehr, Elamin et al. 2012).

Les résultats sont répertoriés dans le **Tableau 4**.

2.3 Le métabolisme des triacylglycérols

Chez les mycobactéries, le carbone est métabolisé selon 4 voies ; la glycolyse, le cycle de l'acide tricarboxylique (TCA), la néoglucogenèse ou la voie du pentose phosphate (**Figure 19**). A l'opposé des autres bactéries, les mycobactéries ne sont pas diauxiques, par contre elles sont capables de co-cataboliser les sources de carbone provenant de ces voies avec le carbone résultant du métabolisme des acides gras (de Carvalho, Fischer et al. 2010).

Au cours de la β-oxydation, les acides gras sont décomposés en $FADH_2$, NADH, et acétyl-CoA, qui sont ensuite pris en charge par le cycle TCA. S'ils ne sont pas dégradés, les acides gras peuvent subir des modifications de type élongation ou polymérisation par la voie de synthèse des acides gras I (FAS I), ou bien une estérification au glycérol pour former les DAG et les TAG (**Figure 19**) (Talley and Mohiuddin 2023). Deux protéines ont été identifiées pour contribuer à l'import des métabolites, facilitant ainsi la synthèse des TAG, le canal Mce1/LucA qui transporte les acides gras de l'extérieur vers le cytosol bactérien, et la Rv3723/LucA, une protéine membranaire qui interagit avec Mce4 et facilite l'absorption des acides gras et du cholestérol (Nazarova, Montague et al. 2017; Nazarova, Montague et al. 2019).

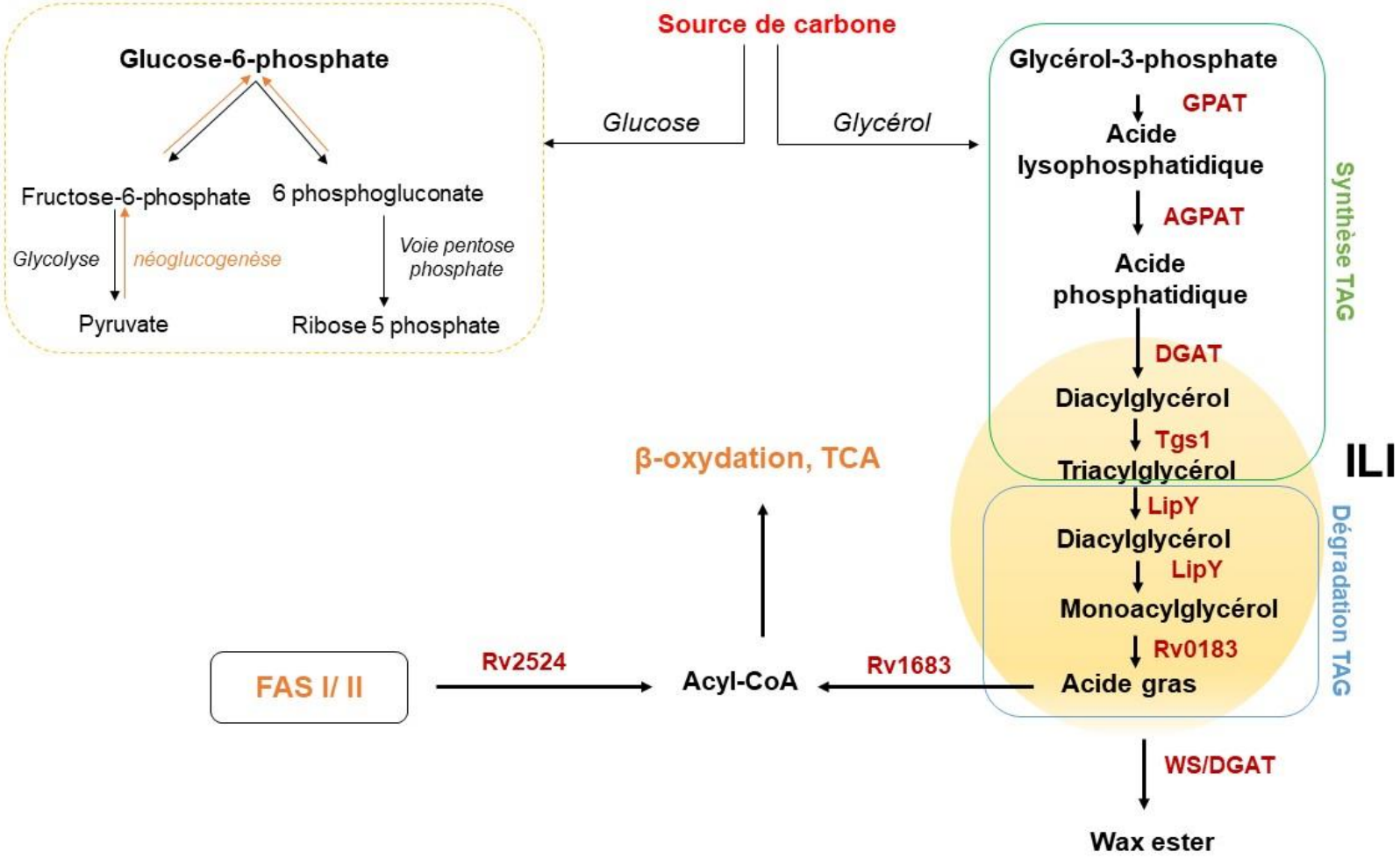

Figure 19. Représentation schématique des principales voies métaboliques impliquées dans la synthèse des TAG chez Mycobacterium. *GPAT : glycérol-3-phosphate acyltransférase, AGPAT : acylglycérophosphate acyltransférase, DGAT : diacylglycérol transférase, Tgs1 : Triglycéride synthase 1, WS/DGAT : was ester diacylglycérol transférase, TCA : cycle de l'acide tricarboxylique, FAS I/II : voie de synthèse des acides gras (fatty acid synthase I/II). Adaptée de (Stehr, Elamin et al. 2012; Bosch, Sweet et al. 2021; Dargham, Mallick et al. 2023).*

Après leur synthèse, les TAG sont incorporés soit dans la membrane externe soit des gouttelettes cytoplasmiques (Ortalo-Magné, Lemassu et al. 1996; Garton, Christensen et al. 2002). En effet, une étude réalisée chez *M. smegmatis* a démontré que la synthèse des TAG implique la présence de diglycéride transférases *via* la voie α-glycérophosphate. Grâce à l'utilisation d'acide oléique fluorescent, il a également été observé que cette source de carbone est incorporée dans la biosynthèse des phospholipides (Nakagawa, Kashiwabara et al. 1976).

Récemment un modèle pour l'export des TAG vers la membrane externe a été proposé (**Figure 20A**). Dans ce modèle, le TAG est pris en charge par deux protéines spécifiques : le transporteur facilitateur Rv1410 (**Figure 20B**), appartenant à la superfamille des transporteurs facilitants majeurs (MFS), et la lipoprotéine G « LprG » (**Figure 20C**) (Drage, Tsai et al. 2010), toutes deux localisées dans la membrane interne et codées par le même opéron. La Rv1410 présente une cavité hydrophobe orientée vers le cytoplasme grâce à des hélices transmembranaires (TM) TM5-TM8 ou TM2-TM11, permettant l'entrée des molécules de TAG. Ce processus induit un changement de conformation de la cavité, passant d'une configuration interne IF à une configuration externe OF, l'ouvrant ainsi du côté du périplasme. Par la suite, LprG peut récupérer les TAG *via* sa poche hydrophobe (**Figure 20A, D**).

Le retour à la conformation initiale de Rv1410 en IF est probablement dû à un gradient de protons (Remm, De Vecchis et al. 2023). Cependant, le trajet de la molécule de TAG au-delà de l'espace périplasmique reste mal connu.

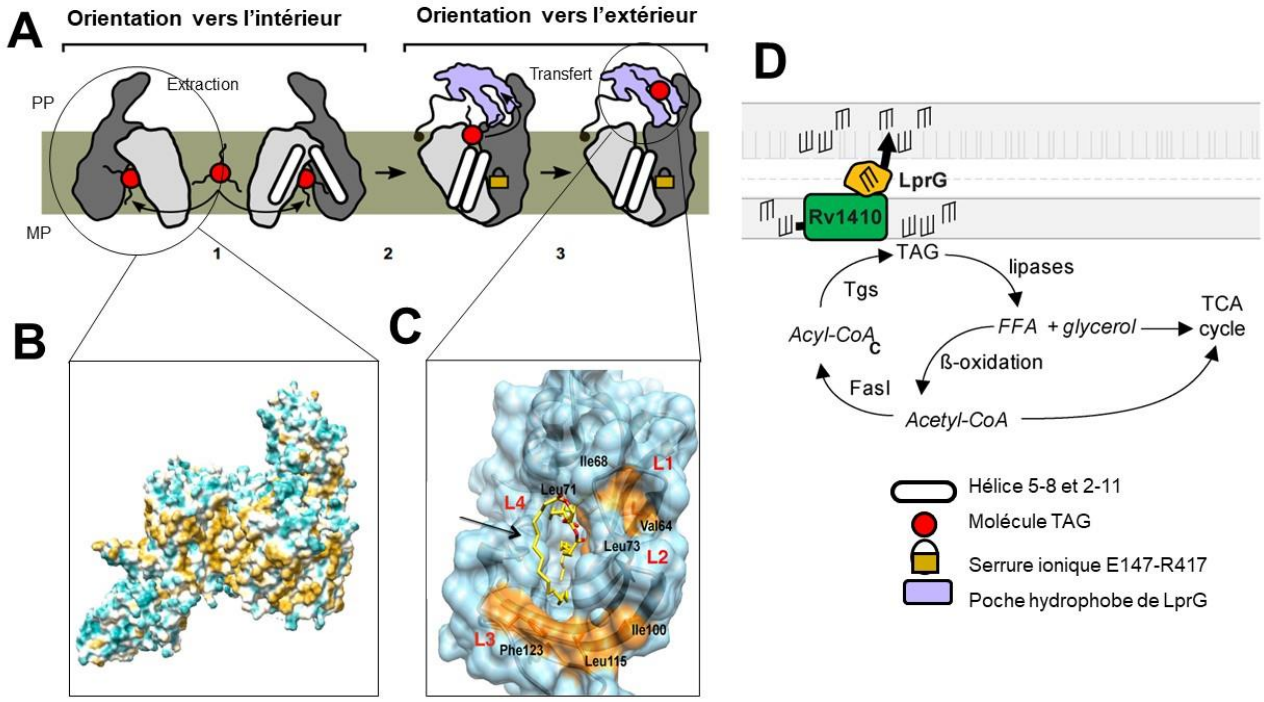

Figure 20. Mécanisme d'export du TAG par LprG et Rv1410. *A) Le domaine N-terminal du Rv1410 est représenté en gris clair et le domaine C-terminal en gris foncé. LprG est représenté en mauve. 1) La molécule de TAG entre dans la cavité centrale du transporteur par les ouvertures latérales entre les hélices transmembranaire TM5-TM8IN et TM2-TM11IN dans la conformation orientée vers l'intérieur. (2) Le transporteur passe de l'état orienté vers l'intérieur à l'état orienté vers l'extérieur tandis que la molécule de TAG reste dans la cavité centrale. La serrure ionique E147-R417 au fond de la cavité centrale se forme et le TAG est soulevé vers le feuillet périplasmique (3) Les extensions périplasmiques TM11 et TM12 protègent la molécule TAG du périplasme hydrophile tandis que la molécule TAG se déplace de la cavité du transporteur vers la poche hydrophobe de LprG. B) structure 3D de Rv1410, (PDB 8PNL), C) structure 3D du complexe LprG-TAG (PDB 4ZRA), représentant deux poches hydrophobes en orange, la molécule de TAG se trouve entre la boucle L1 et L2 à proximité du site de liaison pour la chaîne sn3-palmitoyle représentée par une flèche. D) Modèle du transport de TAG médié par LprG-Rv1410, en présence d'un LprG-Rv1410 fonctionnel, FasI fabrique de l'acyl-CoA pour la synthèse des lipides (y compris le TAG par l'intermédiaire des TAG synthases, Tgs). Le TAG peut ensuite être 1) incorporé dans la paroi cellulaire sous l'action de LprG-Rv1410 ou 2) hydrolysé par des lipases. L'acétyl-CoA du cycle TCA est généré par la ß-oxydation des acides gras libérés du TAG. hIN : orientation vers l'intérieur, MP : membrane plasmique, PP : périplasme. Adaptée de (Martinot, Farrow et al. 2016; Remm, De Vecchis et al. 2023)*

Chapitre III

Les gouttelettes lipidiques : une structure conservée

“Life is a mode of action of proteins” ~Friedrick Engels

Les lipides constituent un des éléments nutritifs primordiaux au développement de tous les organismes. Ils fournissent une source d'énergie et de carbone, ainsi qu'un rôle structural notamment dans la composition et la fluidité des membranes biologiques.

Les organismes, des plus petits aux plus complexes, ont démontré au fil de l'évolution une aptitude à stocker des lipides à l'intérieur de leurs cellules sous la forme de vésicules, communément appelées gouttelettes lipidiques (GL), corps gras ou inclusions lipidiques intrabactériennes (ILI). Outre leur rôle de stockage d'énergie, les GL peuvent, dans certains cas, fournir des acides gras servant de précurseurs d'hormones, d'agents protecteurs contre la toxicité lipidique, et agir en tant que messagers dans les voies de signalisation. Dans certaines pathologies, les cellules de mammifères se gorgent de lipides formant des GL, qui serviront, pour certains pathogènes, de facteurs augmentant leur virulence.

Ce dernier chapitre se focalisera sur la synthèse des TAG contenus dans les ILI, sur les caractéristiques générales des ILI chez les procaryotes ou des GL chez les eucaryotes, les connaissances bibliographiques actuelles sur leur composition ainsi que les techniques utilisées pour déterminer leur composition lipidique et protéique. Une grande partie de ce chapitre sera détaillée dans l'article I des résultats (page 85).

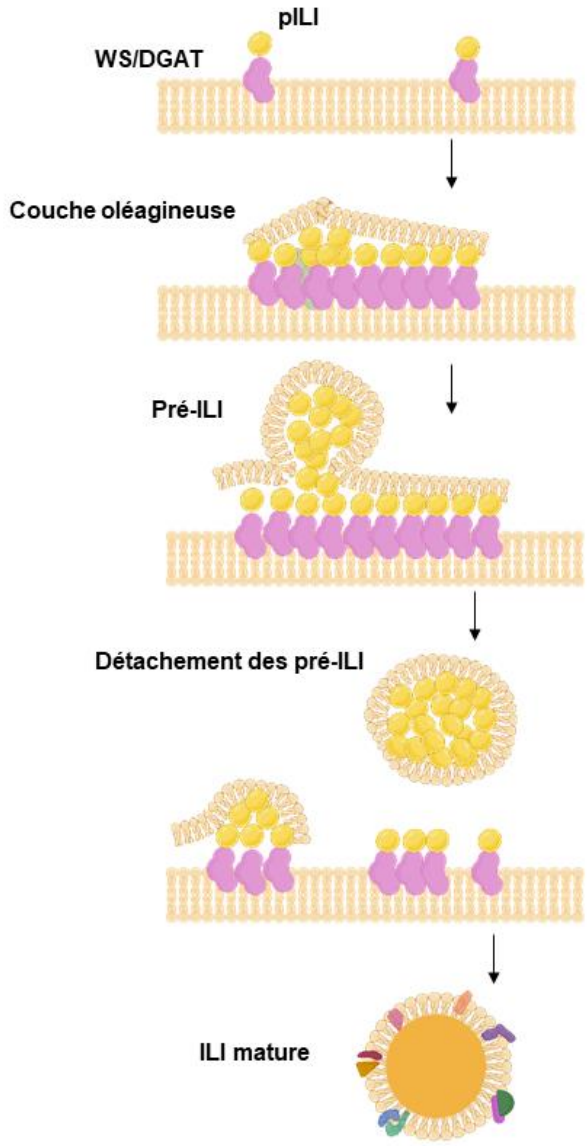

Figure 21. Formation des ILIs chez les procaryotes. *Schéma représentatif de la synthèse des ILIs. pILI : ILI de petite taille, Adaptée de (Wältermann, Hinz et al. 2005).*

3.1 Les GL chez les procaryotes : « ILI »

Les procaryotes ont la capacité d'accumuler des lipides en cas de stress nutritionnel, appelés « inclusion lipidique ». Ces dernières peuvent être formées par des TAG et des esters, ou des granules contenant des lipopolymères semi-solides appelés polyhydroxyalcanoates « PHA ». Les PHA sont des polyesters linéaires issus de la fermentation des carbohydrates ou des lipides. Ils sont divisés en 2 groupes selon le nombre de carbone et ils comprennent les poly (3-hydroxybutyrate) « PHB » et les polyhydroxyvalérates « PHV » (Możejko-Ciesielska and Kiewisz 2016). Les bactéries à Gram négatif sont capables d'accumuler 10 à 20 granules de PHB dans leur cytoplasme (Anderson and Dawes 1990). Bien que la majorité des procaryotes accumulent des granules, certains, dont les actinomycètes synthétisent en plus, des gouttelettes de TAG, notamment *Nocardia, Gordonia, Diestzia, Rhodococcus*, et *Mycobacterium.* Par microscopie de fluorescence, Waltermann *et al*. ont pu observer l'initiation de la synthèse des ILI à partir de la membrane plasmique d'*A. calcoaceticus* ADP1 et *R. opacus* PD630 (**Figure 21**) (Wältermann, Hinz et al. 2005).

Une revue intitulée « ***Intrabacterial lipid inclusions: overview of an amazing organelle*** », retraçant l'ensemble des études de la découverte des GL et des ILI, de leur formation, de leur importance physiologique ainsi que leur contribution à la virulence chez les mycobactéries pathogènes est présentée dans la première partie des résultats.

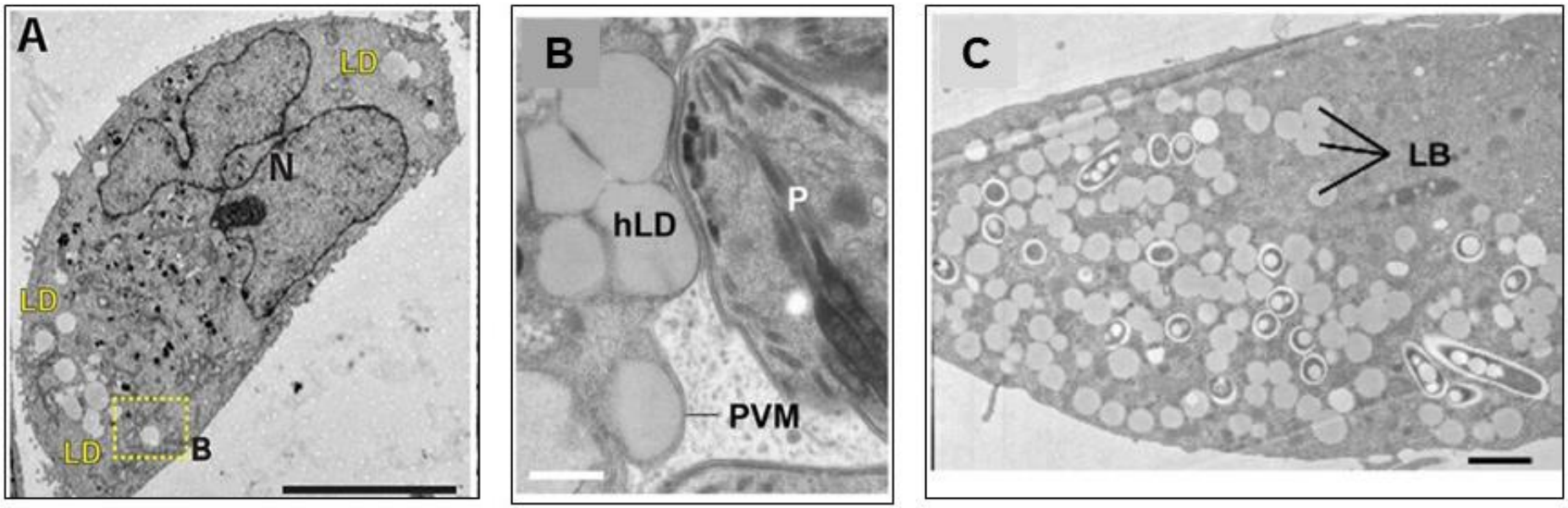

Figure 22. Accumulation des GL chez l'hôte suite à des interactions avec des pathogènes. *A) microscopie électronique des cellules HeLa infectées par le virus de l'hépatite C, N : noyau, LB : gouttelette lipidique. B) microscopie électronique des cellules HeLa infectées par Toxoplasma gondii, hLD : gouttelette lipidique de l'hôte, PVM : membrane PV P : parasite. C) microscopie électronique d'un macrophage dérivé d'une moelle épinière infecté par une mycobactérie. Adaptée de (Caire-Brändli, Papadopoulos et al. 2014; Nolan, Romano et al. 2017; Laufman, Perrino et al. 2019).*

3.2 Le rôle des GL dans l'immunité et les interactions hôte-pathogène

3.2.1 Infections et production des GL

Dans de nombreuses pathologies comme l'obésité, la lipodystrophie, mais aussi lors d'une neurodégénération, d'un cancer, de maladies cardiovasculaires, ou encore d'une stéatose pancréatique, les cellules sont capables de former des GL dans leur cytoplasme (Gao and Goodman 2015). Également, il a été démontré que des cellules de mammifères infectées par des virus, des parasites ou des bactéries accumulent des lipides. Pourtant, on ne sait toujours pas s'il y a une relation entre l'apparition des GL et l'induction ou la suppression de l'immunité (D'Avila, Maya-Monteiro et al. 2008). Cependant, les GL sont considérées maintenant comme la première ligne de défense, ayant à leur surface des protéines, comme la vipérine, capable d'activer le système immunitaire (Safi, Sánchez-Álvarez et al. 2023).

Pour cette partie, et en relation avec mes travaux de thèse, seules les interactions hôte-bactéries seront détaillées. Brièvement, les virus induisent l'accumulation des GL chez l'hôte infecté par des signaux lipogéniques afin d'utiliser les lipides tout au long de leur cycle infectieux (Ketter and Randall 2019). L'exemple le plus connu est celui du virus de l'hépatite C (Laufman, Perrino et al. 2019). L'infection chronique résultant de ce virus aboutit à une stéatose et à un métabolisme lipidique anormal ce qui stimule le réticulum endoplasmique de la cellule infectée à synthétiser des GL. Par ailleurs, Miyanari *et al.* ont montré que la capside du virus est associée aux GL, ce qui suggère que les GL sont impliquées dans la production des particules virales (Miyanari, Atsuzawa et al. 2007). De même, des GL ont été observées lors des infections par des parasites protozoaires, comme *Toxoplasma gondii* (Nolan, Romano et al. 2017) et *Leishmania major* (Rabhi, Rabhi et al. 2016), pourtant, les parasites eux-mêmes ont la capacité de synthétiser leur propre stock en lipides en détournant et utilisant ceux de l'hôte (**Figure 22**) (Charron and Sibley 2002; Vielemeyer, McIntosh et al. 2004).

Certaines bactéries intracellulaires ou extracellulaires comme les bactéries appartenant à la classe des actinomycètes ou des cyanobactéries sont capables d'induire l'accumulation des GL chez les cellules hôtes (Peyron, Vaubourgeix et al. 2008; Russell, Cardona et al. 2009; Tazi, Araujo et al. 2018).

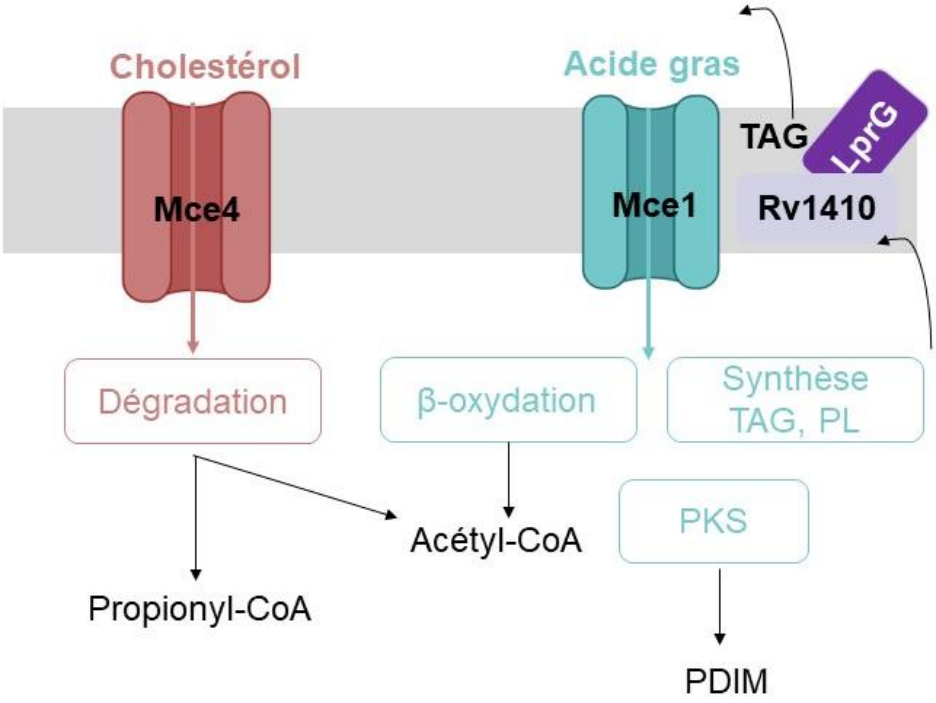

Figure 23. Import du cholestérol et des acides gras chez M. tuberculosis. *La dégradation du cholestérol et des acides gras alimente le métabolisme central. Les acides gras récupérés peuvent être utilisés dans des réactions de biosynthèse pour générer des lipides membranaires, des TAG et des lipides polykétidiques (PKS). Adaptée de (Wilburn, Fieweger et al. 2018).*

Cette présence de lipide dans le cytoplasme de l'hôte permet alors aux pathogènes présents (bactéries, virus, parasites, etc…) d'utiliser ces lipides comme nutriments, comme précurseurs de lipides de la membrane ou encore pour produire des médiateurs de l'immunité, tels que la prostaglandine, les leucotriènes, et les lipoxines (Fukuda, Lad et al. 2005; Bermúdez, Balboa et al. 2021).

Ces lipides peuvent même être dans certains cas utilisés par la bactérie pour produire ses propres inclusions lipidiques intrabactériennes. En effet Peyron *et al.,* a montré que les macrophages infectés par *M. tuberculosis* se remplissent de GL qui peuvent fusionner aux phagosomes contenant le pathogène, lui permettant à son tour de générer des ILI en dégradant les TAG et le cholestérol accumulés par l'hôte (Peyron, Vaubourgeix et al. 2008; Daniel, Maamar et al. 2011). En effet, la présence des GL dans les macrophages infectés par *M. tuberculosis* lui permet de survivre dans un environnement sévère dans le compartiment cytosolique (Knight, Braverman et al. 2018). Des études ont montré que ce pathogène exprime un système d'import de cholestérol codé par *mce* pour utiliser le carbone issu du cholestérol de l'hôte afin de persister dans les poumons de souris (Pandey and Sassetti 2008). En effet, le propionyl-CoA, élément essentiel pour le métabolisme du carbone chez les mycobactéries, est absent chez les mammifères. Cependant, il a été montré que le cholestérol de l'hôte pourrait être une source de propionyl-CoA pour les mycobactéries durant l'infection. Pour l'obtenir, le bacille utilise un complexe Mce4 renfermant deux protéines membranaires intégrales YrbE4 et YrbE4B, 6 protéines de la paroi, et 2 protéines accessoires. Les produits de la dégradation du cholestérol sont le propionyl-CoA, l'acétyl-CoA, et le pyruvate, qui seront utilisés dans le métabolisme central du bacille (**Figure 23**) (Casali and Riley 2007; Wilburn, Fieweger et al. 2018).

D'autre part, Laval *et al.* ont proposé un nouveau concept dans lequel les GL seraient plutôt une forme d'adaptation métabolique anti-mycobactérienne qui forcerait *M. tuberculosis* à changer son métabolisme afin qu'il passe vers un mode de persistance (Laval, Chaumont et al. 2021). En plus de l'utilité des GL pour la dormance chez *M. tuberculosis*, certains types d'acides gras provenant des cellules hôtes seraient des précurseurs de la synthèse des PDIM et des SL, qui sont des facteurs de virulence chez *M. tuberculosis* (Jain, Petzold et al. 2007).

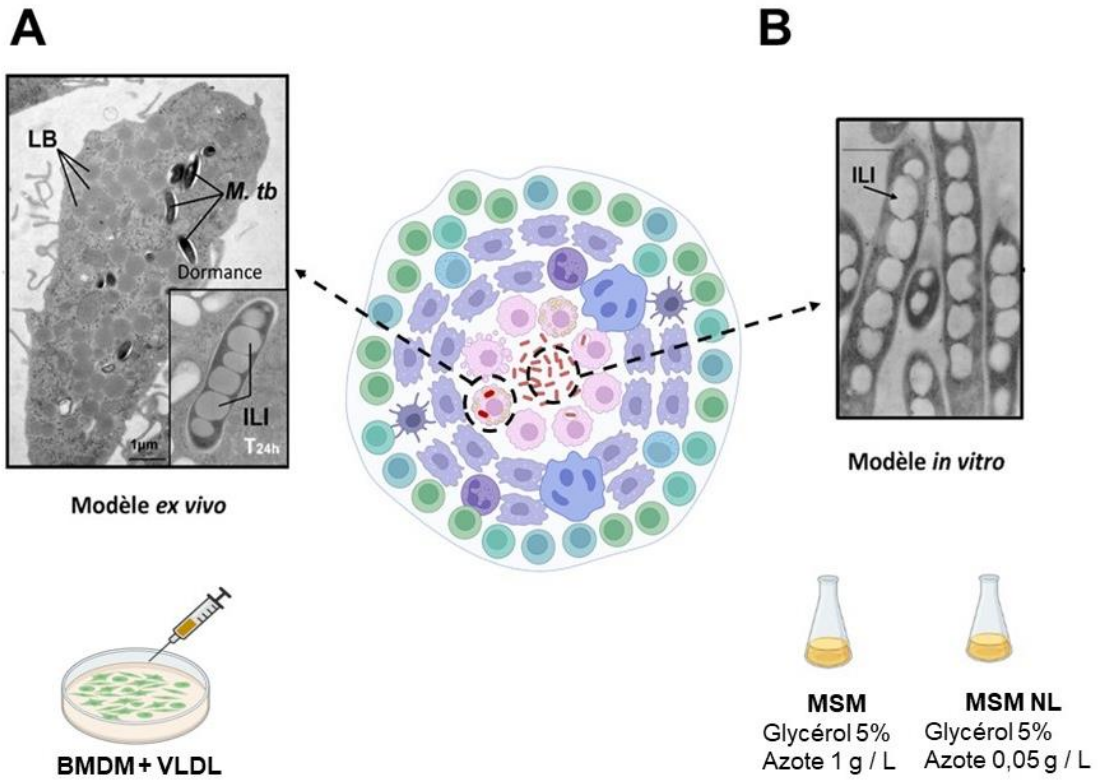

Figure 24. Représentation schématique des modèles développés au laboratoire et mimant les environnements du granulome*. A) modèle ex vivo mimant les bactéries phagocytées par des macrophages spumeux, se basant sur l'infection des macrophages murins dérivés de moelle osseuse (BMDM) et supplémentés par des lipoprotéines à faible densité (VLDL). B) modèle in vitro représentant les mycobactéries extracellulaires, se basant sur un milieu minimal en sel (MSM) et limité en azote (MSM NL). Adaptée de (Caire-Brändli, Papadopoulos et al. 2014; Santucci, Johansen et al. 2019).*

3.2.2 Modèles d'accumulation des GL et des ILI

Afin d'étudier cette accumulation de lipides à partir de la cellule hôte, un modèle basé sur la capacité des macrophages murins (Bone Marrow Derived Macrophages BMDM) infectés à accumuler des GL à partir de VLDL exogènes a été développé au laboratoire (**Figure 24**) (Caire-Brändli, Papadopoulos et al. 2014).

Quant aux mycobactéries extracellulaires, un autre modèle *in vitro* a été mis au point par Santucci *et al.* (Santucci, Johansen et al. 2019). En effet, il a été montré que les bactéries non phagocytées accumulant des ILI présentent une tolérance accrue à la rifampicine et à l'isoniazide (Sirakova, Dubey et al. 2006; Hammond, Baron et al. 2015). Dès lors, le développement de modèles pour étudier ces bacilles extracellulaires revêt une importance majeure qui permettrait de mieux comprendre la relation des ILI avec l'immunité/antibiothérapie. Dans ce contexte, le premier modèle induisant la synthèse des TAG a été généré par Wayne et Hayes (Wayne and Hayes 1996) et il se base sur les conditions de culture de *M. tuberculosis* en hypoxie. Ce modèle couplé à des analyses de protéomique a permis d'identifier pour la première fois, des protéines associées aux ILI chez les mycobactéries, plus précisément chez *M. bovis* BCG (Low, Shui et al. 2010). D'autres modèles basé sur le stress nutritif, la carence en fer ou le stress oxydatif ont permis l'induction de gènes impliqués dans le métabolisme lipidique (Rodriguez, Voskuil et al. 2002). De même, un milieu riche en glycérol a montré que cette condition favorise la synthèse des ILI chez *M. smegmatis* (Armstrong, Carter et al. 2018). Ce modèle a permis l'identification de 400 protéines probablement associées aux ILI, représentant une seconde étude réalisée chez les mycobactéries pour décrypter la composition des ILI.

Finalement, un stress lié à la carence d'azote a été utilisé chez *M. tuberculosis*, *R. opacus*, *Streptomyces*, *M. smegmatis*, et *M. abscessus* pour engendrer la synthèse des TAG (Alvarez, Mayer et al. 1996; Alvarez, Kalscheuer et al. 2000; Garton, Christensen et al. 2002; Santucci, Smichi et al. 2019). Au laboratoire, ce type de stress a été mis au point et se base sur l'utilisation d'un milieu minimal en sel (MSM), ayant le glycérol comme source unique de carbone, avec une quantité limitée d'azote (MSM-NL) (Santucci, Smichi et al. 2019).

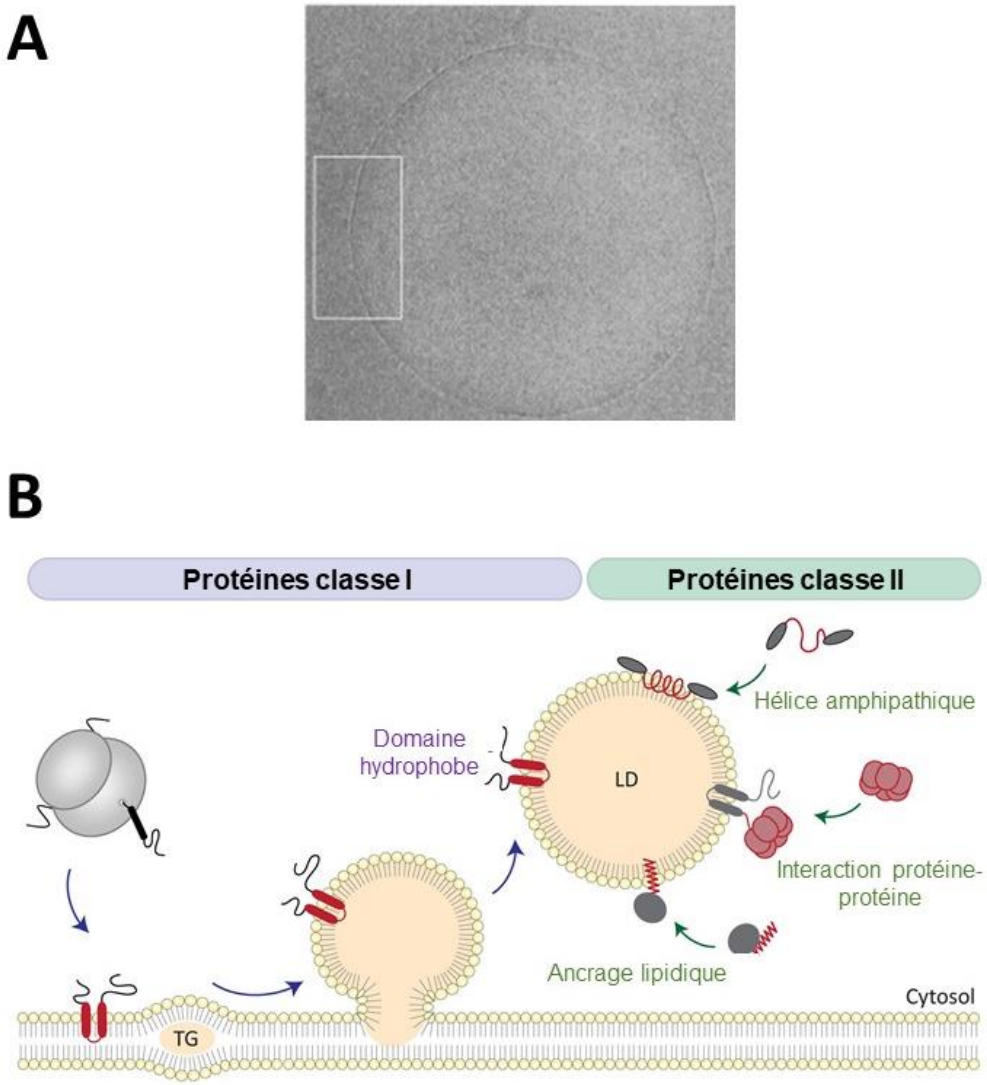

***Figure 25. Interaction protéine-GL**. A) GL observée à faible densité électronique montrant la présence d'une monocouche de phospholipides, B) Association des 2 classes de protéines sur les GL, en mauve les protéines provenant du réticulum endoplasmique (ER), en vert les protéines cytosoliques. Adaptée de (Tauchi-Sato, Ozeki et al. 2002; Dhiman, Caesar et al. 2020)*

En outre, ce modèle réversible mime de la même façon la phase de réactivation dans un granulome. En effet, en éliminant la source du carbone, les bactéries hydrolysent les TAG contenus dans les ILI et s'en servent comme source de carbone.

Ce modèle *in vitro* est le principal modèle que j'ai utilisé tout au long de mes travaux de thèse (**Figure 24**).

3.3 Interactions des protéines sur la surface

Concernant la structure des GL, la présence d'une monocouche de phospholipide entourant les TAGs a été identifiée en 2002 au cours d'une étude de cryo-microscopie électronique sur GL purifiées de cellules hépatiques cancéreuses (**Figure 25A**) (Tauchi-Sato, Ozeki et al. 2002). Comme cela a été déterminé sur les oléosomes des végétaux, des protéines interagissant à la surface des GL ont pu être identifiées (Jackson 2019; Chorlay and Thiam 2020).

Après plusieurs années de leur découverte, des protéines ont été identifiées à la surface des GL (Greenberg, Egan et al. 1991). Chez les eucaryotes ces protéines pourraient interagir avec les lipides selon deux types d'interactions : soit une interaction directe par des domaines hydrophobes (classe I) ou des hélices amphipathiques (classe II), soit une interaction indirecte par des interactions protéiques ou des ancrages lipidiques (Zhang and Liu 2019). Les protéines de la classe I proviennent du réticulum endoplasmique (RE) par diffusion latérale alors que celles de la classe II ont une origine cytosolique (**Figure 25B**) (Dhiman, Caesar et al. 2020). En revanche aucune séquence signal n'a été identifiée pour assurer l'adressage de ces protéines vers les GL.

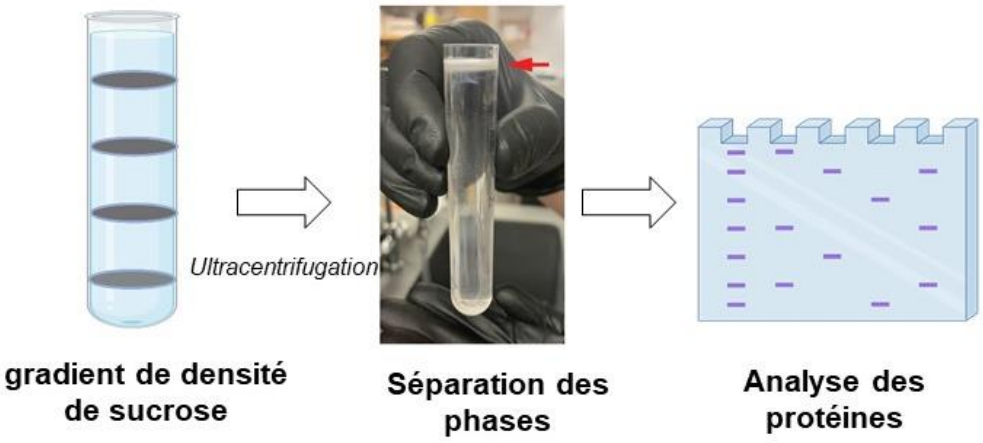

Figure 26. Schéma général de la méthode conventionnelle de purification des ILI. *Après un gradient de sucrose, suivi par des étapes d'ultracentrifugation, la phase lipidique contenant les ILI flotte à la surface grâce à sa faible densité. Cette fraction (flèche rouge) est récupérée et traitée selon le type des cellules afin que les protéines soient solubilisées. Les protéines sont analysées sur un gel de polyacrylamide et identifiées par spectrométrie de masse. Adaptée de (Kalscheuer, Wältermann et al. 2001).*

Parmi les protéines associées à la fraction lipidique, un grand nombre liées directement au métabolisme lipidique comme les lipases, les acyltransférases, et les acyl-CoA synthases, mais aussi d'autres familles de protéines comme des protéines rédox ou de signalisation ont été identifiées (Goodman 2018).

Chez les procaryotes, Armstrong *et al.* ont montré la présence d'hélices amphipathiques dans PspA, une protéine identifiée comme étant associée aux ILIs chez *M. smegmatis*. La délétion de cette hélice a montré que la protéine n'était plus capable d'interagir avec les ILI (Armstrong, Carter et al. 2018).

3.3.1 Techniques de purification des GL

Afin de déterminer le protéome des ILI chez les procaryotes, des études ont été réalisée chez différents actinomycètes, comme *Rhodoccocus* ou *M. bovis* BCG ou encore *M. smegmatis* (*Low, Shui et al. 2010; Ding, Yang et al. 2012; Armstrong, Carter et al. 2018*). Toutes ces études se sont basées sur l'extraction des ILI *via* la technique conventionnelle de centrifugation selon un gradient de densité. Après lyse mécanique et ultracentrifugation, la partie supérieure du surnageant, représentant la phase organique à faible densité contient les ILI ainsi que de nombreux contaminants, notamment des protéines hydrophobes et membranaires (**Figure 26**). En plus ces traitements invasifs, ces études n'ont pas permis de distinguer les phases de synthèse et de dégradation des ILIs. Cette partie technique sera développée dans l'article « ***Intrabacterial lipid inclusions : overview of an amazing organelle*** » (page 85).

Une approche plus pertinente basée sur le marquage de proximité (APEX2) nous a permis d'éviter ce type de contamination (détaillé dans le **§ 3.3.1.1**).

3.3.1.1 Méthodes conventionnelles *in vitro*

3.3.1.1.1 Biochimiques

Plusieurs techniques biochimiques peuvent servir pour purifier les GL comme la purification par affinité, la purification d'affinité en tandem, la co-immunoprécipitation, ou encore le « phage display ». Toutes ces techniques sont suivies par des analyses sur gels de polyacrylamide et de la spectrométrie de masse pour identifier les protéines extraites des bactéries.

3.3.1.1.2 Biophysiques

De même, des techniques biophysiques comme la spectroscopie de corrélation de fluorescence, l'interférométrie à double polarisation, et la diffusion dynamique de la lumière pourraient être utilisées pour la réalisation de ce type d'études et mieux caractériser les interactions protéiques. Cependant, comme mentionné précédemment (détaillé dans le **§ 3.3.1**), ces techniques, biochimiques ou biophysiques, qui se basent sur la lyse des cellules et la purification des GL, présentent des très nombreux faux-positifs. Ces limitations sont détaillées ultérieurement dans le premier article des résultats.

3.3.1.1 Méthodes dépendantes de marquage par proximité *in cellulo* et *in vivo*

Les méthodes de marquage par proximité fonctionnent toutes sur le même principe, l'enzyme étant soit une ligase soit une peroxydase. Elles se basent sur la présence d'un substrat qui active l'enzyme, générant ainsi des radicaux à durée de vie courte. Ces derniers se lient de façon covalente aux protéines voisines qui seront par la suite enrichies, purifiées, et identifiées par spectrométrie de masse.

APEX est une ascorbate péroxydase isolée de la plante de soja et qui a été utilisée pour la première fois sur la matrice des mitochondries dans des cellules vivantes, afin d'identifier spécifiquement les protéines de la membrane interne (Rhee, Zou et al. 2013). En présence de peroxyde d'hydrogène, elle est capable d'oxyder le biotine-phénol en un radical biotine-phénoxylé ayant une demi-vie inférieure à 1 ms. Ce radical se lie d'une façon covalente aux acides animés riches en électron des protéines endogènes dans un rayon de 20 nm. Cette réaction peut se produire dans les tous les compartiments subcellulaires des cellules vivantes aussi bien chez les eucaryotes que les procaryotes (Rhee, Zou et al. 2013; Bersuker, Peterson et al. 2018; Ganapathy, Bai et al. 2018).

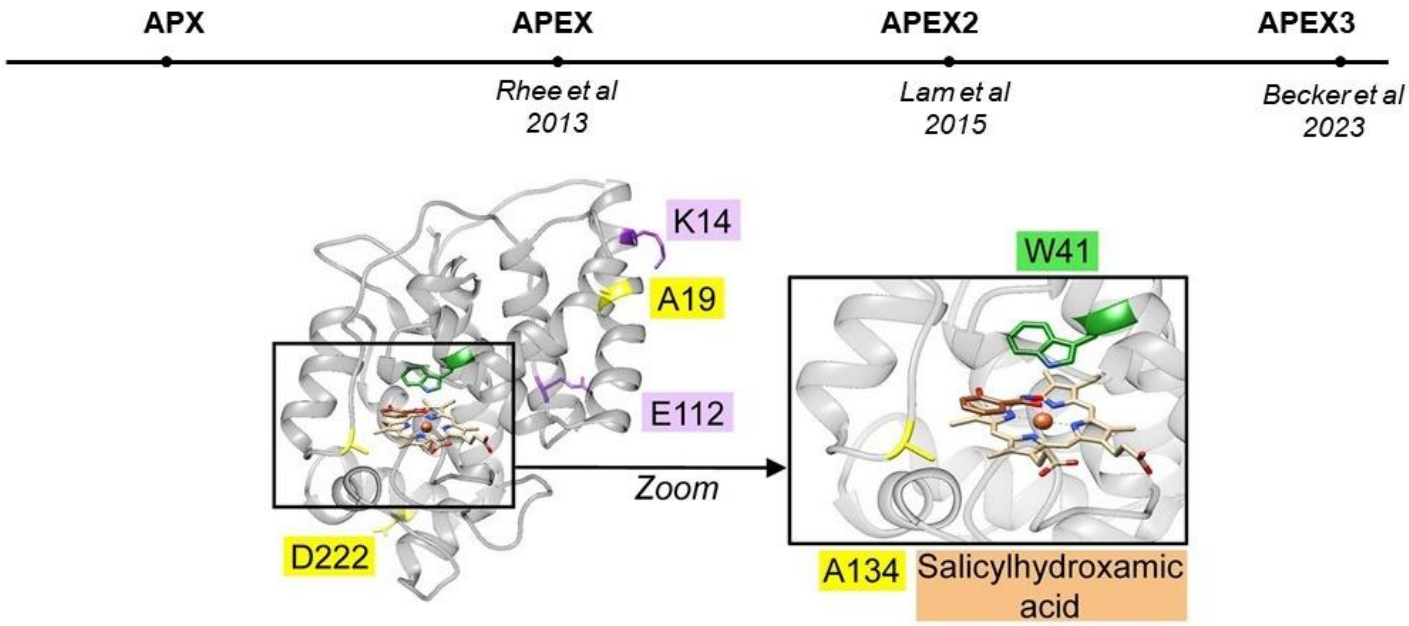

Figure 27. Evolution chronologique d'APEX. *Les couleurs représentent les mutations appliquées à la péroxydase de la plante de Soja APX pour la faire évoluer en APEX2 et APEX3. Adapté de (Neetika Jaisinghani 2023).*

En 2015, Lam *et al.* ont généré une forme plus stable d'APEX, désignée APEX2 (**Figure 27**) (Lam, Martell et al. 2015). Ce choix est basé sur une sélection d'un mutant parmi 10^6 formes d'APEX dans un modèle de levure par tri cellulaire activé par fluorescence/FACS. APEX2 a été utilisée sur plusieurs types cellulaires et compartiments différents, ainsi que pour étudier le protéome des GL (Bersuker, Peterson et al. 2018). En effet, ils ont fusionné les gènes codant pour ATGL et PLIN2, présentes pour être sur les GL, avec celui codant pour APEX2.

Cette étude a réussi à surmonter les difficultés rencontrées avec les méthodes conventionnelles en confirmant la présence de protéines dont la localisation à la surface des GL était déjà connue (Bersuker, Peterson et al. 2018). En revanche, il est important de mentionner qu'une des limitations de ce système, réside dans son incapacité à marquer certaines protéines dont les résidus Tyr, Trp, Cys et His ne sont pas accessibles. De plus, selon la taille des GL, le rayon d'action de l'enzyme pourrait cibler d'autres protéines qui n'appartiennent pas à ces organites.

Après avoir montré qu'APEX2 était produite et active chez *M. smegmatis*, ce marquage de proximité a été utilisé pour identifier les protéines du périplasme d'une façon différentielle des protéines cytoplasmiques, tout en fusionnant un signal de la voie de sécrétion Sec ou Tat au domaine N-terminal d'APEX2, cela a permis de distinguer les protéines secrétées. Plus récemment, cette technologie a également été utilisée avec succès chez *M. tuberculosis* afin d'identifier les substrats du système de sécrétion type VII ESX-1 et ESX-3 (Ganapathy, Bai et al. 2018; Neetika Jaisinghani 2023). En revanche, une autre étude récente a montré qu'APEX2 qui a une localisation cytoplasmique n'était pas adaptée pour étudier les protéines au niveau du noyau et de la membrane nucléaire. Dans ce contexte, Becker *et al* ont développé le variant APEX3 en substituant une leucine en position 242 par une alanine, générant une protéine capable de cibler préférentiellement le noyau. (**Figure 27**) (Becker, Auerbach et al. 2023).

Dans les conditions où les interactions protéiques sont transitoires, et où il y a un échange de protéines entre différents compartiments, le marquage de proximité endogène n'est pas toujours suffisant. Une étude menée par l'équipe de Ting a suggéré un marquage orthogonal en tandem sur le même échantillon, connu comme TransitID (Xu, Cheah et al. 2023).

En effet, une enzyme de marquage sera utilisée pour le compartiment de départ, et une deuxième enzyme sera utilisée sur le second compartiment. Par conséquent, le trajet de la protéine bi-marquée entre le premier et le second compartiment est facilement identifiable (Xu, Cheah et al. 2023).

Dans ce contexte, un des objectifs de mes travaux de thèse a été d'appliquer, pour la première fois, la technique de marquage par proximité en utilisant la forme APEX2 pour déterminer le protéome des ILI en utilisant un modèle *in vitro* développé chez *M. abscessus*. La première partie de ce travail a été consacrée à l'étude *in silico* des protéines identifiées sur les ILI des actinobactéries comprenant *Rhodococcus*, *M. tuberculosis*, *M. smegmatis*, *M. abscessus*, *M. leprae*, et *M. marinum*.

La caractérisation du protéome complet d'une souche sauvage de *M. abscessus* cultivée selon le modèle d'accumulation réversible des ILIs n'a pas permis d'identifier les enzymes lipolytiques intervenant dans le métabolisme des ILI. Afin de contourner ces difficultés, nous avons choisi d'utiliser une méthode de marquage de proximité médiée par la protéine APEX2, qui pourrait cibler spécifiquement les ILI. L'ensemble de ces résultats sont détaillées dans les parties suivantes.

Résultats

Article I

Intrabacterial lipid inclusions: overview of an amazing organelle

Tonia Dargham, Ivy Mallick, Dominique Raze, Laurent Kremer, Stéphane Canaan

In Biology of Mycobacterial Lipids, Chapter 12, Academic Press, 2022, Pages 253-269, *doi.org/10.1016/B978-0-323-91948-7.00003-8*

Les gouttelettes lipidiques (GL) des mammifères, décrites pour la première fois dans les années 1880, ont été pratiquement ignorées pendant plus de 100 ans. Ainsi, entre 1991 et le début des années 2000, ces GL ont été considérées comme des véhicules dynamiques du métabolisme cellulaire et non plus des globules de graisse inertes. Elles se retrouvent en très grande quantité dans les adipocytes mais plusieurs études ont montré que ces GL n'étaient pas limitées à ce seul type cellulaire et pouvaient se former dans des fibroblastes, des cellules épithéliales, des hépatocytes, des cellules immunitaires, des cellules ß du pancréas, des glandes mammaires, et même dans des muscles squelettiques. En plus des mammifères, ces structures se retrouvent également chez les levures, les plantes et de nombreuses bactéries. Dans tous ces organismes, ces organelles lipidiques sont composées essentiellement d'un cœur de triacylglycérol (TAG) entouré d'une monocouche de phospholipides, et peuvent contenir d'autres types de lipides tels que les esters de stérol, les esters de rétinol, les éthers mais aussi des stérols libres.

L'origine de la biosynthèse des GL a pu être déterminée dès 1980 grâce à des études structurales, biophysiques et des observations faites par microscopie électronique sur les pré-adipocytes. Le processus de formation de ces GL chez les eucaryotes commence au niveau du réticulum endoplasmique (RE), où la majorité des protéines de structure et du métabolisme lipidique se trouve. L'accumulation des TAG se fait entre les deux feuillets du RE, et le GL bourgeonne en formant une gouttelette recouverte d'une monocouche de phospholipides provenant de la couche externe du RE.

Chez les procaryotes et en particuliers les actinomycètes, ces GL ou inclusions lipidiques intrabactériennes (ILI), sont des organites que l'on trouve en très grande quantité, notamment chez les pathogènes intracellulaires, tels que les mycobactéries. La formation de ces ILI favoriserait l'entrée en dormance de mycobactéries, tandis que leur dégradation permettrait leur réactivation et leur propagation dans l'hôte. Au cours des deux dernières décennies, les progrès des technologies d'imagerie telles que la microscopie à fluorescence, la microscopie en temps réel ou la microscopie électronique, ainsi que les progrès de la génomique et de la protéomique ont grandement contribué à la description de la structure et de la fonction des GL et des ILI.

Il est désormais établi que les ILI et leurs protéines associées jouent divers rôles liés au métabolisme et au stockage des lipides neutres mais aussi à la biosynthèse des membranes, à la réduction de la cytotoxicité et à la transduction des signaux.

Dans ce chapitre de livre, nous présentons une rétrospective sur la découverte des GL et des ILI, leur formation, leur conservation, leur importance physiologique ainsi que leur contribution à la virulence chez les mycobactéries pathogènes. Nous discutons de l'utilisation des méthodes conventionnelles avec leurs forces et leurs limitations pour purifier des ILI/GL et des nouvelles techniques disponibles pour déterminer les protéines associées aux ILI en fonction du temps. Ces technologies permettent de déterminer en temps réel les protéines impliquées dans la synthèse et la dégradation des ILI et d'ouvrir la voie pour la découverte de nouvelles cibles thérapeutiques nécessaire pour lutter contre les mycobactéries pathogènes.

CHAPTER

12

Intrabacterial lipid inclusions: overview of an amazing organelle

Tonia Dargham[1,2], *Ivy Mallick*[1], *Dominique Raze*[3], *Laurent Kremer*[4,5] *and Stéphane Canaan*[1]

[1]Aix-Marseille University, CNRS, LISM, Institut de Microbiologie de la Méditerranée, Marseille, France; [2]IHU Méditerranée Infection, Aix-Marseille University, Marseille, France; [3]University of Lille, CNRS, INSERM, CHU Lille, Institut Pasteur de Lille, U1019-UMR 9017—CIIL—Center for Infection and Immunity of Lille, Lille, France; [4]Institut de Recherche en Infectiologie de Montpellier (IRIM), CNRS, Université de Montpellier, Montpellier, France; [5]IRIM, INSERM, Montpellier, France

Introduction

Designated as oil droplets, fat bodies, lipid bodies (LB), lipid droplets (LD) for eukaryotes and intrabacterial/intracytoplasmic lipid inclusion (ILI) for prokaryotes (Fig. 12.1) [1,2], LB appear as multifunctional structures in the cells. In addition to their primary role in energy storage, they exert pleiotropic effects by serving as a source of hormone precursors, messengers in signal transduction or as protectors against toxicity induced by other lipids. LB may also assist in membrane trafficking, metabolism, storage, and degradation of proteins, immunity, and pathogenicity [3—8]. They represent a source of lipid precursors for membrane phospholipids, thus allowing a rapid membrane expansion. In mammals, they are able to engender host defenses against intracellular pathogens as part of the innate immune response [9].

In fact, under specific conditions, eukaryotic cells have acquired the ability to accumulate lipids in their cytoplasm into the form of LD, which differ in size, state, abundance, and function [5,8]. This is distinguishable from prokaryotic cells where three different scenarios can occur. Gram-negative bacteria accumulate mostly wax ester (WE) as their main lipid reservoir. Actinobacteria belonging to the Gram-positive bacterial group and consisting of *Mycobacterium, Rhodococcus, Nocardia,* and *Streptomyces,* produce and store triacylglycerols (TAG) which are critical lipids for their physiology and lifestyle [10—13]. Other Gram-positive

Biology of Mycobacterial Lipids
https://doi.org/10.1016/B978-0-323-91948-7.00003-8

genera can synthesize and store polymeric lipids, such as poly-3-hydroxybutyrate or polyhydroxyalkanoates (PHAs) [14]. In both rapid- and slow-growing mycobacterial species, accumulation of neutral lipids in the form of ILI is thought to play a key role in the achievement of a dormant state under stressful conditions [15,16]; they are the only organelles located in mycobacterial cytosol, formed by a hydrophobic core of neutral lipid (TAG and WE) adjoining a monolayer of phospholipids associated with proteins (Fig. 12.1) [2,5,6,17–21].

Hence, knowledge on ILI formation, structure, and function has been the subject of increasing interest, especially with regard to their crucial role in the virulence of *M. tuberculosis* and other pathogenic species. In *M. tuberculosis*, ILIs are major contributors in metabolic processes, during the nonreplicating dormant state within the infected host and during the reactivation step that leads to an active TB disease. Upon infection, immune cells aggregate to form a complex structure known as the granuloma, comprising also foamy macrophages, a morphotype of lipid-loaded macrophage differentiated during infection [22]. Within the foamy macrophages, the bacilli can persist, facing multiple stresses, and accumulate ILI in the form of TAG; derived either from the lipid-rich infected cells or from de novo biosynthesis of TAG (Fig. 12.1). Once the conditions become favorable again, the bacterium consumes these lipids and reactivates its metabolism [11,13,23–27]. This implies that the bacilli are able to produce lipolytic enzymes and/or activate host hydrolytic enzymes in order to degrade the host neutral lipids into free fatty acids (FFA), absorb the released FFA, and then resynthesize complete TAG, thanks to specific set of TAG synthases [28–30]. These

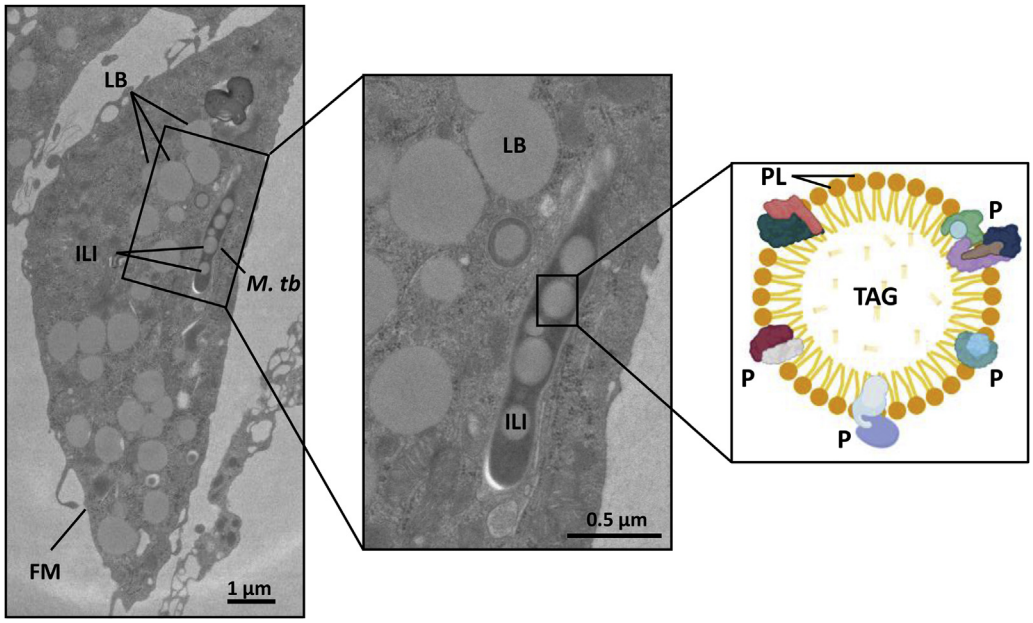

FIGURE 12.1 Electron micrograph of foamy macrophage (FM) filled with lipid bodies (LB) and infected by *M. tuberculosis* (*M. tb*) containing intrabacterial lipid inclusions (ILI). A schematic view of an ILI represents a core of neutral lipid: triacylglycerol (TAG) surrounded by a phospholipid (PL) monolayer where proteins (P) are anchored. All electron micrographs depicted are from the authors' personal collection.

observations have prompted multiple investigations to decipher the role of ILI during persistence of *M. tuberculosis* [31].

In order to better understand why and how *M. tuberculosis* accumulates de novo synthesized lipids for ILI production and subsequent entry into dormancy, studies have been conducted under different stress conditions mimicking intracellular environment, such as nutrient limitation, hypoxia, acidic pH, and NO treatment [32]. For instance, experiments based on variation in medium composition and growth conditions showed the ability of *M. smegmatis* to accumulate TAG in the form of ILI [33]. Likewise, it is now clearly established that the accumulation of TAG and ILI formation in *Rhodococcus* is linked to environmental stress [34,35]. In addition, *Rhodoccocus ruber*, *Rhodoccocus opacus* PD630, and *Rhodoccocus opacus* MR22 have been found to accumulate both PHA and TAG depending on the growth stage. In fact, the PHA-containing inclusions possess a few proteins and are accumulated mainly during exponential growth, while TAG inclusions occur mainly at the early stationary phase and comprise larger amounts of proteins [33,36]. Although lipid accumulation seems ubiquitous in all mycobacteria tested so far, a study performed on *M. tuberculosis* belonging to the Beijing lineage indicated that all these subspecies were able to accumulate TAG under conditions (NO treatment, hypoxia, nutrient starvation) where non-Beijing subspecies were unable to do so [2,37].

In this chapter, we report the discovery and importance of ILI as well as the methods used to purify these inclusions and to study the protein partners attached to the phospholipid monolayer. We also discuss the drawbacks associated with the conventional methods used for ILI/LD purification along with advantages of new techniques, such as next-generation proximity labeling technologies to overcome the limitations of the classical method.

Discovery

Over the last 2 decades, progress in imaging technologies such as fluorescence microscopy, time-lapse live microscopy or electron microscopy, and advances in genomics and proteomics study greatly helped to describe the structure and function of LD and ILI.

The discovery of LB started initially in eukaryotic cells in the nineteenth century [38], while ILIs were discovered in mycobacteria almost 200 years later. These structures were ignored for a while and so far, only few studies have been undertaken to characterize their properties and biological functions [5,17,21,39]. In 1884, Robert Koch identified, for the first time, the presence of refractile particles corresponding to lipid granules in unstained *M. tuberculosis*. Even so, due to the absence of proper staining methods, the presence of lipid remained controversial until 1941, when Grimme was able to specifically stain them with Sudan III and dimethylamidoazo-benzol [40]. Later, in 1949, Burdon et al. confirmed the presence of lipid structures in mycobacteria by using the Sudan Black B lipophilic stain and demonstrated that these lipid inclusions were more dominant in saprophytic mycobacterial species and in *Mycobacterium leprae* than in other parasitic species [2,41]. In contrast, the lipid extraction was not possible before 1952 until the use of petroleum ether, which subsequently revealed the lipid-rich content of the mycobacterial cytoplasmic compartment [42]. However, identification of the genes coding for enzymes involved in the synthesis of these lipids only

begun in 1998 when the sequencing of the complete genome of *M. tuberculosis* unraveled the bacterium's extraordinary lipid biosynthetic capacity [43].

The presence of ILI was also reported in different mycobacterial species. In fact, the first observation of lipid inclusions in *Mycobacterium avium* was done by electron microscopy in the 1950s, within a single bacterial cell [44]. Forty-seven years later, another study in the same species showed that ILI could even appear inside infected macrophage in a distorted shape [13,45]. Among nonpathogenic mycobacteria, Christensen et al. were able to detect ILI in *M. smegmatis* by electron and light microscopy [33].

To sum up, in the past years it became clearer that ILIs are not only versatile organelle depending on the genus, growth conditions, and stress factors but appear also pleiotropic in terms of biological functions and very important with respect to pathogenicity.

Occurrence and inheritance: a conserved structure

Despite differences in their lipid composition and structure, these lipidic structures are conserved organelles [46] found in all eukaryotic cells but only in a limited number of bacteria [2,4,21]. In eukaryotes, LD formed in plants represents an inert source of carbon while in fungi and protists they appear a key player in infection process. In metazoans, LD contributes to their development [47], whereas in mammals they exert various functions as mentioned above. However, only few prokaryotes have the ability to accumulate lipid, especially Gram-positive bacteria, including *Mycobacterium*, *Micromonospora*, *Dietzia*, *Nocardia, Rhodococcus, Gordonia*, *Nostoc punctiforme, Synechococcus lividus, Anabaena variabilis, Synechocystis* sp. PCC 6803, and some *streptomycetes* [47].

Although they differ in their mechanism of biogenesis, they remain inherited: the major mechanism of LD formation relies on the budding of TAG and sterol esters from the bilayer of endoplasmic reticulum (ER). In contrast, ILI biogenesis is dependent on the formation of small lipid droplets attached to the plasma membrane by a WE synthase/acyl-CoA: diacylglycerol acyltransferase (WS/DGAT), which grows progressively until it detaches from the membrane and acquires its mature form [14] (Fig. 12.2).

Alongside the shape and functional inheritance of ILI and LD, some associated proteins validate that these organelles are conserved between phyla. In fact, proteomic analysis indicated that LD and ILI contain proteins that are either resident or recruited during the biogenesis process (Fig. 12.2). Among the major resident proteins in prokaryotes, Microorganisms Lipid Droplet Small (MLDS) share similar properties and functions with the perilipins (PLN) in eukaryotes, and both belong to apolipoprotein-like protein family [4]. As an example, Hänisch et al. have reported the ability of eukaryotic resident proteins (PLN, ADRP, Tip47 known as PAT) to target droplets from other organisms. A plasmid carrying the GFP gene fused to the gene coding for PAT was expressed either in *R. opacus* or in *M. smegmatis* and the expressed proteins were located on the surface of ILI in both organisms, suggesting that these proteins have similar protein domains allowing to interact with ILIs [4,48]. To date, the LD proteome has been studied in a variety of organisms, including yeast, drosophila, hamster, human adipocyte, hepatocyte, and the majority of proteins identified were conserved in composition, presence of hydrophobic domains and function, which

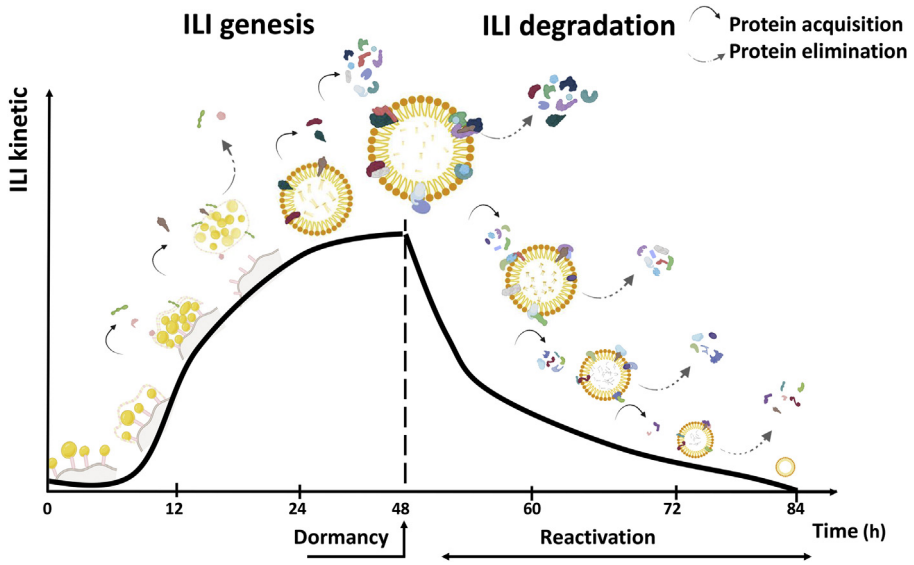

FIGURE 12.2 Dynamics of ILI formation and degradation implicating specific proteins exerting various roles in the maintenance of ILI integrity, TAG synthesis, or consumption. *ILI genesis adapted from M. Wältermann, A. Hinz, H. Robenek, D. Troyer, R. Reichelt, U. Malkus, H.-J. Galla, R. Kalscheuer, T. Stöveken, P. Von Landenberg, A. Steinbüchel, Mechanism of lipid-body formation in prokaryotes: how bacteria fatten up, Mol. Microbiol. 55 (2005) 750–763.*

suggests that these organelles are conserved among eukaryotes and are derived from a common ancestor [18,21]. However, the ILI proteome has not been convincingly studied, essentially due to the difficulty to generate highly purified preparations and because of the lack of specific biomarkers in bacteria. Nevertheless, a few ILI-associated proteins have been identified and characterized recently. The heparin-binding hemagglutinin adhesin (HbhA) is a major protein associated with ILI in *M. tuberculosis*, sharing structural features with apolipoprotein A1/A4/E [49]. When expressed in *R. opacus* PD630, HbhA from *M. tuberculosis* retains the ability to bind and interact with ILI, similarly to the original protein TadA (Triacyglycerol Accumulation Deficient), an ILI-associated protein of *R. opacus* PD630, highly similar to MLDS [50]. Following these findings, the authors proposed that based on this shared property of *Rhodococcus* and *Mycobacterium*, HbhA-like proteins were acquired from a common ancestor, while *M. tuberculosis* underwent a divergent evolution by acquiring the capacity of disseminating from the lungs, thanks to the help of the HbhA adhesin property [51]. Another interesting observation regarding the role of an Hbha-like protein (MLDS) suggests that ILI in *Rhodococcus jostii* could have a protector effect under genotoxic and other stress conditions. Under the regulation of a transcriptional regulator MLDSR, MLDS is expressed in order to protect DNA by binding it to ILI [50]. In the same way, eukaryotic proteins associated with the LB of drosophila's embryo contribute in DNA protection [52]. Additionally, a comparison between the Low et al. study on *M. bovis* BCG [53] and Athenstaedt et al. study on yeast [54], suggests the presence of conserved proteins. Interestingly, proteins from mammalian cells also share the similarities. Likewise, the similarity among ILI present in *R. ruber*, *R. opacus* PD630, and *R. opacus* MR22 with the oil bodies found in plant seeds

supports the theory of conservation of these organelles between kingdoms [36]. Moreover, the fact that some proteins involved in ILI biogenesis in mycobacteria, such as the two major triglycerides synthases Tgs1 and Tgs2, have orthologues in mammals, further supports that these organelles are conserved between eukaryotes and prokaryotes [53]. Together, structure, associated protein, and function make these organelles well conserved among the living world.

ILI-associated protein partners

Importance of ILI-associated proteins

As described above, the phospholipid monolayer of ILI comprises proteins exerting major roles required for the synthesis or degradation of ILI, budding, structure coalescence, pathogenicity, and signaling among other functions [14]. High dynamics of ILI is directly related to the presence of various proteins, suggesting an important turnover of the associated proteins at the ILI surface. Which hypothesized that the proteins involved in TAG synthesis may be removed after ILI formation and replaced by other proteins participating in their degradation. Among these proteins, two major enzymes family, which participate in ILI formation/degradation, are commonly known to play a crucial role in mycobacterial virulence since their deletion leads to an attenuated virulent phenotype. Genomic studies in *M. tb* H37Rv identified 250 genes involved in lipid metabolism mainly characterized as lipase and synthase since they hydrolyze hosts lipids in order to generate FFA useful for ILI formation and consequently for their entry in dormancy [55,56]. Subsequently, a TAG synthase 1 (Tgs1) was described as a vital protein in relation with mycobacterial persistence, one of the virulence factors of *Mycobacterium* [57]. The first characterized lipase involved in modeling host immune response was Rv0183, other lipases, belonging to lip protein family, were identified as well and play role in TAG utilization [57]. Moreover, some other proteins may remain present during the whole formation/degradation cycle to regulate the overall structure and size of ILI.

However, to date, mycobacterial lipases have not been sufficiently characterized and the dynamics of proteins during ILI formation/degradation has not been clearly established experimentally and awaits future studies (Fig. 12.2).

Purification of ILI: conventional method and limitations

The standard method used to study and characterize ILI-associated proteins relies on purified ILI preparations followed by proteomic analysis. However, the association of this structure with many organelles and the presence of abundant contaminations with cytosolic proteins generates misleading data [53].

Previously, in 1949, a failed trial of staining ILI by different solvents was used to characterize these refractile particles [41]. However, the technique has not evolved, lacking specificity, and generating false-positive results. To circumvent these difficulties and to reduce the possible artifacts, subsequent methods were developed to purify these structures and generate higher quality preparations [1].

Therefore, the classical method for ILI isolation relies on ultracentrifugation, mechanical cell lysis, and washes; but unfortunately, which lead to a substantial loss of material. In 1996, Alvarez et al. followed Preusting's method, a technique used to purify polyester(s) granules from *Pseudomonas oleovorans* and based on density gradient centrifugation after phase separation. Following the method, ILI was isolated from *Rhodococcus opacus* for the first time [58]. Elucidating the formation, the structure and the proteomics of ILI in *Rhodococcus* species allowed to draw a parallel with mycobacterial ILI formation, opening the doorway into a new research area in the mycobacterial field. A study conducted in 2001 on *R. ruber* and *R. opacus* highlighted the presence of proteins associated with ILI. In fact, the lipid inclusions were purified by centrifugation using density gradient without altering the protein pattern, and cells were broken using a French press cell. The authors were able to identify one type of granule in *R. opacus* and two types of granules (A and B) in *R. ruber*. Following granule purification, associated proteins were separated from the lipids by solubilization, using a detergent or at high ionic strength prior to their analysis by SDS-PAGE. Some proteins, which remained strongly attached to the droplets were either separated by electrophoretic homogeneity SDS-PAGE or copurified with the lipid inclusions [36]. A major drawback of this method was related to the low degree of purity of these droplets due to contaminations from other cytosolic organelles, limiting the quality of the subsequent proteomic studies.

To overcome this limitation, Ding et al. proposed a multistep technique, applied to all organisms, that includes sample homogenization in a sucrose based buffer, cell disruption using a French press cell or bubbling under nitrogen gas pressure, then ultracentrifugation and washes as previously done with *R. ruber* and *R. opacus*, followed by enriching and identifying ILI biomarkers in the fraction [1]. This protocol was applied in order to purify ILI from *Rhodococcus* RHAI. However, bacteria lack reference biomarkers like PLN, ADRP, Tip47 (PAT), which are structural proteins only found in eukaryotic cells. This prompted the authors to include additional purification steps, as quality control approach, prior to proteomic studies [1]. For eukaryotes, an additional step is performed for removing the nuclei by slow-speed centrifugation. Although the modified technique can be applied to all organisms, but is laborious and might trigger loss of data during wash or cause danger due to the toxic reagents used.

This same protocol was applied to purify ILI from *M. bovis* cultured under hypoxic stress. Furthermore, Low et al. added a delipidation step with chloroform/methanol in order to separate the lipids from associated proteins. The protein fraction was then solubilized in urea, separated by NuPAGE and stained with silver nitrate [53]. However, in this method, ILI can be broken during sample preparation, adhere to the tubes or precipitate, and be contaminated with cytosolic material. Moreover, since the amount of proteins is relatively small as compared to the amount of neutral lipids, this will strictly affect protein separation on SDS-PAGE. Therefore, optimization of bacterial lysis represents a critical step in order to avoid the presence of unbound fatty acid and keeping intact the overall structure of ILI. In addition, some washing steps using sodium carbonate can cause the loss of the less adherent proteins and/or protein denaturation. Another inconvenience of this method is the requirement of fresh samples to stimulate protein yields recovery.

Importantly, many studies did not differentiate between the formation and degradation of ILI. This appears, however, a critical factor to consider since the proteins profile is dependent on the metabolic stage of the microorganism and, consequently, on the size of ILI that varies

from budding to maturation and then degradation (Fig. 12.2). Thus, new techniques are awaited to study and compare the ILI proteomes during genesis and evolution of these lipidic inclusions.

Identified proteins

Many ILI-associated proteins were identified originally in actinobacteria, especially in *Mycobacterium* and *Rhodococcus* [20]. Two independent studies led to identify potential ILI-associated proteins: a first study identified six proteins in *M. bovis,* whereas in the second one more than 50 proteins were reported in *M. smegmatis* [20,53]. Surprisingly, no common protein candidates were found in these two studies. While the majority of proteins identified in *M. smegmatis* are likely to be involved in transcriptional and translational regulation, those identified in *M. bovis* were related to lipid metabolism. Among them, six unique ILI-associated proteins, also conserved in *M. tuberculosis* H37Rv, were identified by MALDI-MS: the putative 1-acylglycerol-3-phosphate acyltransferase BCG1489c (Rv1428c), BCG1721 (Rv1683) containing an N-terminal lipase and a C-terminal ACSL domain, BCG1169c (Rv1109c), BCG3153c (Tgs1/Rv3130c), BCG3794c (Tgs2/Rv3734c), and BCG1489c [13,53]. Armstrong et al. showed that 7% of the *M. smegmatis* proteome is associated with ILI and shares similar roles with *R. josatii* associated proteins for transcription, translation, protein folding, and metabolism [20,28].

In 2010, MacEachran and colleagues identified a gene named *tadA* in *Rhodococcus opacus* PD630, involved in TAG accumulation, which triggers the formation of large sized ILI when overexpressed [59]. Another abundant protein of the ILI proteome of *R. jostii* RHA1 is PspA, the phage shock protein A [8]. Interestingly, an ortholog of PspA is present in *M. tuberculosis* (Rv2744c) and when expressed in *M. smegmatis*, it colocalizes predominantly with ILI [60]. Because of its location on ILI, Rv2744c has a major role in regulating the size and the number of lipid inclusions. The survival of the bacilli in a model of nonreplicating persistence is impacted when *Rv2744c* is deleted or when PspA is overproduced. Moreover, a homolog to bacterial PspA is found in plants, known as Vipp1, as well as in *M. smegmatis* (MSMEG_2695) [2,20,60]. PPE15 was identified in *M. tb* as a mycobacterial PLN-like protein (MPER-1) which is overexpressed during dormancy and deletion of *ppe15* leads to defect in ILI formation [28].

Despite substantial findings, the mycobacterial ILI proteome remains largely unexplored and incomplete and the so far selected candidates have not been classified into either pro-forming or pro-degradative ILI proteins. Considering the current scenario, the advancement in technologies over the conventional one is justified but remains highly challenging.

Proximity labeling technologies: strengths and limitations

These last few years have witnessed the emergence of high throughput spatiotemporal technologies. Protein–protein interaction (PPI) is believed to be the key player in living cells and contributes to various activities including subcellular localization of the interacting proteins [61,62]. The identification of unknown protein partners in different complexes is not

only important for the characterization of the proteins but also to understand specific biological processes occurring in a living organism, which can be particularly difficult to assess when interactions are weak or transient. As compared to conventional methods [yeast two hybrid system, coimmunoprecipitation combined with mass spectrometric (MS) analysis], proximity labeling techniques represent a powerful tool for protein complex purification and proteomic mapping [61–63]. They might be particularly helpful to decipher ILI proteome avoiding contaminations and exhausting work. In this section, we summarize proximity labeling methods that may be applied to identify proteins related to ILI synthesis or consumption.

Ligase-mediated labeling

Proximity labeling is based on modifications in the presence of an engineered ligase tagged to a protein of interest, referred to as the bait protein. In presence of the specific substrate, the ligase linked to the bait protein generates short-lived active radicals, which covalently interact neighboring protein partners in living cells. Thereafter, all the labeled proteins are subjected to further enrichment by different techniques, such as streptavidin-bead enrichment or affinity chromatography followed by MS analysis for subsequent protein identification [62,64]. The advantage of this labeling method relies on the identification of the localized or compartment-specific protein population upon utilization of a fusion bait that is expressed in a specific subcellular space or structure [65]. Therefore, spatiotemporal labeling technologies not only allow enrichment and identification of abundant proteins but also insoluble membrane proteins and weak and transient PPI under native environment, proximal to the bait protein [64].

Pupylation-based interaction tagging (PUP-IT)

Various membrane proteins are involved in the interaction between cells or cellular organelles playing major roles, although they are most difficult to be identified by classical techniques. The reason behind is either the hydrophobic nature of the membrane or loss of fractions during multistep treatment processes or weak transient interaction [66]. This PUP-IT technique uses the basics of protein degradation pathway. Protein degradation is a ubiquitous mechanism for cellular detoxification that eliminates misfolded proteins and damaged organelle. Like eukaryotic cells, *M. tuberculosis* and *M. smegmatis* produce ubiquitin-like proteins available for tagging and subsequent proteolysis of other damaged proteins. Accordingly, under the activity of a small protein, named Pup ligase and encoded by *pafA*, the targeted proteins undergo posttranslational modification (i.e., pupylation) in PUP-IT labeling (Fig. 12.3A). Contrary to other ligases, which use biotin for successful tagging, the Pup ligase uses a small protein called Pup to tag the target proteins. Pup contains 64 amino acids and a Gly-Gly-Gln sequence at the C-terminus. In presence of ATP, Pup gets deaminated at its C-terminal end to form Pup (E), which is further conjugated at a lysine residue of target proteins following phosphorylation by the Pup ligase. Lysines being abundant amino-acids in cellular environment, tagging by this ligase fused to a bait protein are proved to be efficient and specific in terms of proximity-based labeling [64,66,67]. In order to improve this technique, two different smaller Pup variants, DE28 and Peptide 4.1 containing 28 and 14

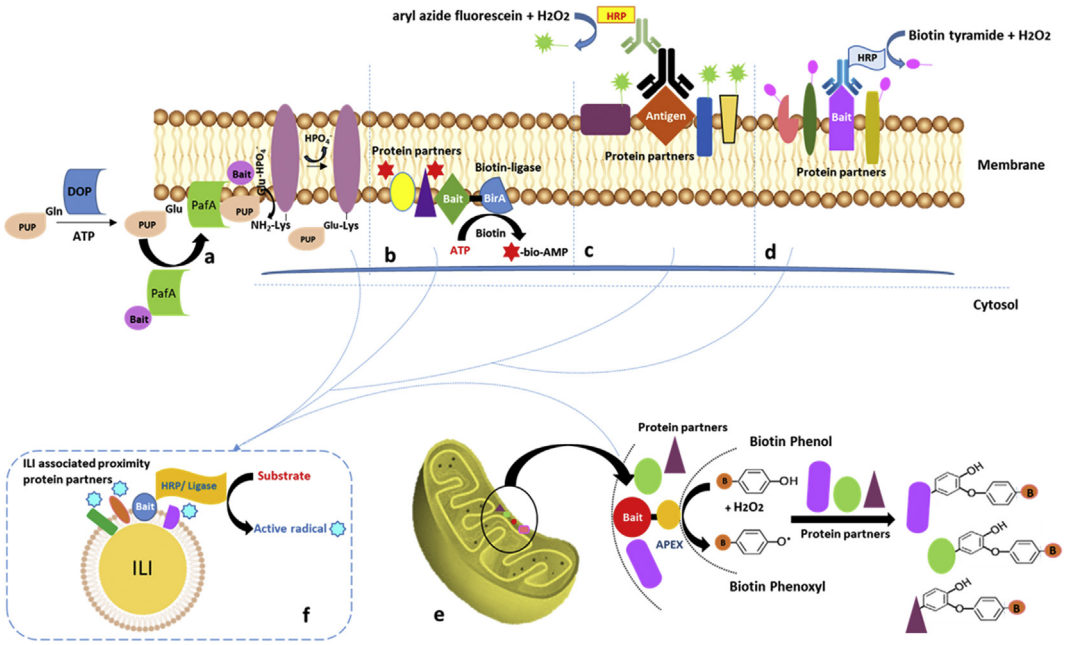

FIGURE 12.3 Schematic representation of different proximity labeling technologies in a live cell; **(A) PUPIT**, in presence of ATP, pup protein first gets deaminated from Pup-Gln to Pup-Glu at its C-terminal by the activity of deamidase Dop, which further gets attacked by the lysine residue of target proteins following a phosphorylation by Pup ligase PafA associated with bait protein; **(B) BioID**, in presence of ATP and endogenous biotin, reactive biotinoyl-5′-AMP (bio-AMP) is generated by biotin ligase BirA, which biotinylates the lysine residue of neighboring protein partners; **(C) EMARS,** this method uses HRP conjugated with antibody or a ligand that adheres to the protein targets. In the presence of aryl azide fluorescein and hydrogen peroxide (H_2O_2), the generated active fluorescent radical nonspecifically biotinylate other proximal partners at their nucleophilic groups; **(D) SPPLAT** is dependent on the activity of HRP attached to a primary or secondary antibody like in EMARS. In the presence of biotin-tyramide and H_2O_2, active free radicals are generated when a target protein or toxin or antibody interacts with the HRP antibody conjugate, which further biotinylates other proteins in the proximity; **(E) APEX,** the ascorbate peroxidase APEX can be used as a bait protein being fused with a targeted protein localized at a particular subcellular compartment, and subsequently biotinylates protein partners in the vicinity by biotin phenoxyl radical, generated in presence of biotin phenol and H_2O_2; **(F) Possible adaptation of the proximity labeling technologies on ILI in mycobacteria**.

amino acids, respectively, were identified from yeast [68]. Among these two smaller forms, peptide 4.1 is devoid of lysine residues, showing promises to reduce unwanted tags. However, none of the above-mentioned variants have been tested for further transgenic expression [69]. Although the PUP-IT labeling technology has been mainly established for revealing PPI in membrane and in host–pathogen interactions, studies remain still scanty [64].

Proximity-dependent biotin identification (BioID)

BioID (Fig. 12.3B), a biotin-based proximity labeling technique was first prospered by the Brian Burke Lab in 2012 [70]. The principle of the first-generation BioID-based technique relies on the expression of a fused mutated (R118G) form of biotin ligase, named BirA (35 kDa)

from *E. coli*. The wild-type BirA specifically biotinylates the lysine residue of neighboring acetyl-CoA carboxylase subunit in the presence of ATP and endogenous biotin as substrate. The BirA (R118G) mutant has activity that is more promiscuous since it is able to biotinylate all neighboring proteins containing lysine residues within a 10 nm diameter. The biotin is converted to reactive biotinoyl-5′-AMP (bioAMP), which retains at the active site of BirA until being transferred to the target protein [62–65,71,72]. During further improvements of the technique, another variant of BirA called BioID2 (27 kDa) was identified from the thermophilic bacterium *Aquifex aeolicus*. This variant showed potential and much more sensitivity compared to the mutated form of BirA [65]. BioID2 lacks the DNA binding domain at its N-terminal site giving rise to a shorter size, which further improved the functional aspect of the fused bait protein in terms of particular localization [63,73]. In the process of further evolution, split proximity labeling became well known for proteomic labeling of macromolecular complexes or organelle contact sites by improving spatial specificity and versatility of biotinylation process. In this split labeling system, the engineered enzyme is split into two inactive fragments, which generates a functional BioID protein upon heterodimerization [65,74,75]. Although BioID was initially developed for mammalian cells to study PPI of nuclear lamin-A peroxisome in vivo, it became widely applied to determine the protein partners involved in autophagy, cell division (mitosis), viral infection, and even interaction of proteins with RNA, playing role in the cellular functions and some diseases [64,65,76]. Despite the fact that modification of the BirA enzyme can efficiently biotinylate the neighboring proteins, it is still considered as the method to identify some known proteins already been hypothesized to be in proximity with the protein bait [65,72].

Peroxidase enzyme-mediated labeling

The use of different derivatives of biotin and amide in the presence of modified peroxidase enzymes generates active free radicals, which consecutively label neighboring partners in a limited radius and time point and is the basis of peroxidase enzyme mediated labeling under live cell environment. The principle is similar to the ligase family enzymes and the tagged proteins are subjected to further enrichment and identification by MS as mentioned earlier. This state-of-the-art method has been well adapted not only in immunoassays but also in immunohistochemistry and in situ hybridization [72].

Enzyme-mediated activation of radical sources (EMARS)

A technique named EMARS (Fig. 12.3C) uses the horseradish peroxidase (HRP) enzyme to mediate biotinylation of proteins involved in the signal transduction, trafficking, cellular adhesion, and particularly on plasma membrane microdomains which are interesting candidates and difficult to determine. This method uses HRP conjugated to antibodies or ligands that adhere to the membrane protein targets as well. A fusion between a target protein and HRP mediates localization of the bait in a particular subsurface of the membrane, thereby allowing nonspecific biotinylation of other proximal partners at their nucleophilic groups. Thereafter, the biotinylated proteins could be identified following antibody array analysis and streptavidin beads like all the other techniques. Here, the reagent used to generate active nitrene radical is aryl azide-biotin. This process is not only high throughput and can be

performed under living cell but also well recognized for the proteomic analysis of lipid rafts. However, application of this technique raised questions about its specificity, as the generated nitrene radical is thought to also cross the membrane generating background noise [49,67,72]. To increase the specificity, aryl azide fluorescein is used as alternative reagent instead, which eliminates the background and provides easy detection of labeled proteins by using fluorescence imaging technologies [77].

Selective proteomic proximity labeling assay using tyramide (SPPLAT)

Functionally correlated but weakly associated or nonassociated proteins on the surface of cell membrane are difficult to be purified by classical proteomic techniques [78,79]. SPPLAT (Fig. 12.3D) is a new biotinylation technique based also on the activity of HRP attached to a primary or secondary antibody, in the presence of tyramide-based reagent coupled to biotin and hydrogen peroxide. When a target protein or an antigen or a toxin interacts with the HRP antibody conjugate, the tyramide biotin reagent generates active free radicals and biotinylates other proteins in the proximity within a radius of 10 to <200 nm [72,79,80]. Different biotin labels and variety of linker lengths made it possible to easily identify a number of intracellular and extracellular proteins under live cell environment. SPPLAT can be adapted to quantitative differentiation of proteins, to evaluate the relative abundance of proteins over time, to identify proteins present in the whole tissue cryosection, *etc.* as well [72,80].

Ascorbate peroxidase (APEX)

Proximity-based labeling approaches allow to identify protein partners not only in an organelle or membrane microdomains but also in the subcellular compartment of the organelle. Engineered APEX (Fig. 12.3E) is a well-known compartment-specific genetic tag for electron microscopic approaches for eukaryotic system as well as for efficient proximity labeling. APEX can be used as a bait protein being fused with a targeted protein, subsequently confirming its expression at a particular subcellular compartment. This 27-kDa monomeric protein engineered from soybean catalyzes the oxidation of biotin-phenol substrate to a short-lived (half-life of <1 msec) and small distance traveling (<20 nm diameter) biotin-phenoxyl radical in presence of hydrogen peroxide (H_2O_2), which can further covalently bind to electron-rich amino acids, such as tyrosine, tryptophan, histidine, or cysteine residue of neighboring partners [81]. Then, the labeled proteins could be identified by streptavidin beads enrichment followed by MS together with other naturally biotinylated proteins. However, it shows disadvantages in terms of sensitivity and resistance to hydrogen peroxide [64,81]. Later on, and to overcome the limitation of APEX, another mutated variant was selected using yeast two-hybrid system, termed APEX2, which was more sensitive and resistant to hydrogen peroxide [82] and displaying promises for improved proteomic analysis following the same principle. To determine interaction-dependent high-resolution proximity labeling, a split-APEX technique has been used where a 200 amino acids-containing inactive N-terminal fragment and 50 amino acids-containing C-terminal inactive fragment confer peroxidase activity upon reconstitution. This technique could be used for interaction-based labeling, for example, between proteins located on the interface of two different organelles and could omit the false-negative tagging due to the overexpression of APEX2 [64,83]. Recently, a CRISPR-based genome targeted proteome mapping showed promises to analyze proteome at particular genomic locus by fusing dCas9 with APEX2, thereby limiting the

radius for high through-put proximity labeling [84]. Overall APEX proximity labeling provides a specific and powerful tool for subcellular processes occurring within a short interval. The use of APEX technology is not only advantageous in terms of reducing experimental time from hours to minutes but the half-life and diameter of the reaction increased the specificity of biotinylation.

To sum up, most of this innovative proximity labeling techniques can be possibly adapted to various subcellular compartments or organelle by targeting a specific protein localized in that compartment, for example, ILI, and subsequently tagging other proximity partners directly avoiding the chance of cross-contamination.

Perspectives and concluding remarks

It is very likely that the discovery of proteins involved in the formation and degradation of ILI as well as their maintenance will represent a major achievement for understanding *M. tuberculosis* pathogenicity and, possibly, unravel novel drug targets for future chemotherapeutic developments. ILIs are crucial for mycobacterial persistence and virulence within the host. As highly dynamic organelles, they are not structurally and morphologically stable: they can expand or decrease in size, recruit stabilizing or regulatory proteins, as well as enzymes implicated in TAG accumulation during dormancy or TAG consumption during TB reactivation. However, knowledge is finite regarding the development and degradation of those structures and the role of the ILI-associated proteins during development of the lipid inclusions. As most of the classical technologies depend on isolation of the ILI collected following cell lysis and ultracentrifugation, the outcome proteome harbors many cross-contaminating proteins or is poorly defined due to elimination of important fractions during ILI preparation. In addition, controversies has appeared from past studies regarding the number and nature of the ILI-associated proteins due to the erroneous or poor methods of ILI isolation [20,53]. The establishment of proximity-based labeling assays has opened a new avenue for proteomic analysis at a spatiotemporal level in a wide range of biological processes. These innovative techniques use a bait protein fused with engineered modification enzymes, specifically located in a particular organelle or subcellular compartment. Consequently, one can hypothesize that they are well-adapted for the establishment of the ILI-proteome (Fig. 12.3F) since they avoid traditional purification steps of ILI. Additionally, these high-throughput technologies offer the possibility to generate whole sets of proteomes at various time points (i.e., during ILI formation or degradation), to compare and decipher the role of different associated proteins during the *M. tuberculosis* lifecycle. The main advantages of these techniques rely on the fact that they can be performed in vivo under physiological conditions, thus allowing to identify protein partners even when interactions are weak or transient. The active radius and time of the labeling reaction being very short, this minimizes the chance of cross-contamination or loss of material. To date, very limited data regarding proximity labeling have been applied to ILI. A recent study identified various ILI-associated protein partners localized on the surface of ILI and involved in the cholesterol degradation pathways in *M. smegmatis* using BioID and HbhA as a bait [85]. While this substantiates the feasibility of the technique for establishing the ILI proteome, it is also

anticipated to add important insights into the involvement of protein partners in ILI in a near future. However, these novel technologies are still considered as discovery methods and should be improved by second generation of proximity labeling techniques, like split BioID, split APEX, CRISPR-Cas9-APEX, which are currently under development. Further improvements in terms of consistency and accuracy will lead to a new era of proteome mapping, where new PPI could be identified by these technologies beyond "proof of concept" and will also provide numerous details for a better global comprehension of the physiology and virulence of *M. tuberculosis*.

Acknowledgments

This work was supported by the Center National de la Recherche Scientifique (CNRS), the Université d'Aix-Marseille (AMU). I. Mallick is supported by the ANR grant (ILIome-20-CE44-0019) and T. Dargham by a PhD grant from the IHU Méditerranée Infection foundation.

References

[1] Y. Ding, S. Zhang, L. Yang, H. Na, P. Zhang, H. Zhang, Y. Wang, Y. Chen, J. Yu, C. Huo, S. Xu, M. Garaiova, Y. Cong, P. Liu, Isolating lipid droplets from multiple species, Nat. Protoc. 8 (2013) 43–51.
[2] N.J. Garton, M.R. Barer, Mycobacterial lipid bodies and the chemosensitivity and transmission of tuberculosis, in: H. Goldfine (Ed.), Health Consequences of Microbial Interactions with Hydrocarbons, Oils, and Lipids, Springer International Publishing, Cham, 2018, pp. 1–24.
[3] H.F. Hashemi, J.M. Goodman, The life cycle of lipid droplets, Curr. Opin. Cell Biol. 33 (2015) 119–124.
[4] C. Zhang, P. Liu, The lipid droplet: a conserved cellular organelle, Protein Cell 8 (2017) 796–800.
[5] T.C. Walther, R.V. Farese Jr., Lipid droplets and cellular lipid metabolism, Annu. Rev. Biochem. 81 (2012) 687–714.
[6] F. Wilfling, J.T. Haas, T.C. Walther, R.V.F. Jr, Lipid droplet biogenesis, Curr. Opin. Cell Biol. 29 (2014) 39–45.
[7] J.-X. Chen, Y.-S. Han, S.-Q. Zhang, Z.-B. Li, J. Chen, W.-J. Yi, H. Huang, T.-T. Jiang, J.-C. Li, Novel therapeutic evaluation biomarkers of lipid metabolism targets in uncomplicated pulmonary tuberculosis patients, Signal Transduct. Target.Ther. 6 (2021) 22.
[8] Y. Ding, L. Yang, S. Zhang, Y. Wang, Y. Du, J. Pu, G. Peng, Y. Chen, H. Zhang, J. Yu, H. Hang, P. Wu, F. Yang, H. Yang, A. Steinbüchel, P. Liu, Identification of the major functional proteins of prokaryotic lipid droplets, J. Lipid Res. 53 (2012) 399–411.
[9] M. Bosch, M. Sánchez-Álvarez, A. Fajardo, R. Kapetanovic, B. Steiner, F. Dutra, L. Moreira, J.A. López, R. Campo, M. Marí, F. Morales-Paytuví, O. Tort, A. Gubern, R.M. Templin, J.E.B. Curson, N. Martel, C. Català, F. Lozano, F. Tebar, C. Enrich, J. Vázquez, M.A. Del Pozo, M.J. Sweet, P.T. Bozza, S.P. Gross, R.G. Parton, A. Pol, Mammalian lipid droplets are innate immune hubs integrating cell metabolism and host defense, Science 370 (2020) eaay8085.
[10] H.M. Alvarez, Triacylglycerol and wax ester-accumulating machinery in prokaryotes, Biochimie 120 (2016) 28–39.
[11] M. Stehr, A.A. Elamin, M. Singh, Cytosolic lipid inclusions formed during infection by viral and bacterial pathogens, Microb. Infect. 14 (2012) 1227–1237.
[12] M. Wältermann, A. Steinbüchel, Neutral lipid bodies in prokaryotes: recent insights into structure, formation, and relationship to eukaryotic lipid depots, J. Bacteriol. 187 (2005) 3607–3619.
[13] I. Mallick, P. Santucci, I. Poncin, V. Point, L. Kremer, J.-F. Cavalier, S. Canaan, Intrabacterial lipid inclusions in mycobacteria: unexpected key players in survival and pathogenesis? FEMS (Fed. Eur. Microbiol. Soc.) Microbiol. Rev. 45 (6) (2021) fuab029.
[14] M. Wältermann, A. Hinz, H. Robenek, D. Troyer, R. Reichelt, U. Malkus, H.-J. Galla, R. Kalscheuer, T. Stöveken, P. Von Landenberg, A. Steinbüchel, Mechanism of lipid-body formation in prokaryotes: how bacteria fatten up, Mol. Microbiol. 55 (2005) 750–763.

[15] A.L. Mulyukin, Y.K. Kudykina, M.O. Shleeva, A.M. Anuchin, N.E. Suzina, V.N. Danilevich, V.I. Duda, A.S. Kaprelyants, G.I. El'-Registan, Intraspecies diversity of dormant forms of *Mycobacterium smegmatis*, Microbiology 79 (2010) 461–471.
[16] A. Crotta Asis, F. Savoretti, M. Cabruja, H. Gramajo, G. Gago, Characterization of key enzymes involved in triacylglycerol biosynthesis in mycobacteria, Sci. Rep. 11 (2021) 13257.
[17] M.A. Welte, Proteins under new management: lipid droplets deliver, Trends Cell Biol. 17 (2007) 363–369.
[18] B.D.M. Hodges, C.C. Wu, Proteomic insights into an expanded cellular role for cytoplasmic lipid droplets, J. Lipid Res. 51 (2010) 262–273.
[19] N.E. Wolins, D.L. Brasaemle, P.E. Bickel, A proposed model of fat packaging by exchangeable lipid droplet proteins, FEBS (Fed. Eur. Biochem. Soc.) Lett. 580 (2006) 5484–5491.
[20] R.M. Armstrong, D.C. Carter, S.N. Atkinson, S.S. Terhune, T.C. Zahrt, Association of Mycobacterium proteins with lipid droplets, J. Bacteriol. 200 (2018), 00240-00218.
[21] T. Fujimoto, Y. Ohsaki, Cytoplasmic lipid droplets: rediscovery of an old structure as a unique platform, Ann. N. Y. Acad. Sci. (2006) 010.
[22] D.G. Russell, P.J. Cardona, M.J. Kim, S. Allain, F. Altare, Foamy macrophages and the progression of the human tuberculosis granuloma, Nat. Immunol. 10 (2009) 943–948.
[23] P. Santucci, S. Canaan, Lipid droplets breakdown: adipose triglyceride lipase leads the way, Curr. Protein Pept. Sci. 19 (2018) 1131–1133.
[24] P. Santucci, F. Bouzid, N. Smichi, I. Poncin, L. Kremer, C. De Chastellier, M. Drancourt, S. Canaan, Experimental models of foamy macrophages and approaches for dissecting the mechanisms of lipid accumulation and consumption during dormancy and reactivation of tuberculosis, Front. Cell. Infect. Microbiol. 6 (2016).
[25] C. Barisch, T. Soldati, Breaking fat! How mycobacteria and other intracellular pathogens manipulate host lipid droplets, Biochimie 141 (2017) 54–61.
[26] C. Barisch, T. Soldati, Mycobacterium marinum degrades both triacylglycerols and phospholipids from its Dictyostelium host to synthesise its own triacylglycerols and generate lipid inclusions, PLoS Pathog. 13 (2017) e1006095.
[27] C. Barisch, P. Paschke, M. Hagedorn, M. Maniak, T. Soldati, Lipid droplet dynamics at early stages of *Mycobacterium marinum* infection in Dictyostelium, Cell Microbiol. 17 (2015) 1332–1349.
[28] J. Daniel, N. Kapoor, T. Sirakova, R. Sinha, P. Kolattukudy, The perilipin-like PPE15 protein in *Mycobacterium tuberculosis* is required for triacylglycerol accumulation under dormancy-inducing conditions, Mol. Microbiol. 101 (2016) 784–794.
[29] M. Stehr, A. Elamin, M. Singh, Lipid Inclusions in Mycobacterial Infections, 2013.
[30] M. Bosch, Lipid droplets and the host–pathogen dynamic:FATal attraction? JCB (J. Cell Biol.) 220 (8) (2021) e202104005.
[31] D.G. Russell, Phagosomes, fatty acids and tuberculosis, Nat. Cell Biol. 5 (2003) 776–778.
[32] C. Deb, C.M. Lee, V.S. Dubey, J. Daniel, B. Abomoelak, T.D. Sirakova, S. Pawar, L. Rogers, P.E. Kolattukudy, A novel in vitro multiple-stress dormancy model for *Mycobacterium tuberculosis* generates a lipid-loaded, drug-tolerant, dormant pathogen, PLoS One 4 (2009) 0006077.
[33] N.J. Garton, H. Christensen, D.E. Minnikin, R.A. Adegbola, M.R. Barer, Intracellular lipophilic inclusions of mycobacteria in vitro and in sputum, Microbiology 148 (2002) 2951–2958.
[34] R.A. Silva, V. Grossi, N.L. Olivera, H.M. Alvarez, Characterization of indigenous *Rhodococcus* sp. 602, a strain able to accumulate triacylglycerides from naphthyl compounds under nitrogen-starved conditions, Res. Microbiol. 161 (2010) 198–207.
[35] H.M. Alvarez, R.A. Silva, A.C. Cesari, A.L. Zamit, S.R. Peressutti, R. Reichelt, U. Keller, U. Malkus, C. Rasch, T. Maskow, F. Mayer, A. Steinbüchel, Physiological and morphological responses of the soil bacterium *Rhodococcus opacus* strain PD630 to water stress, FEMS (Fed. Eur. Microbiol. Soc.) Microbiol. Ecol. 50 (2004) 75–86.
[36] R. Kalscheuer, M. Wältermann, H. Alvarez, A. Steinbüchel, Preparative isolation of lipid inclusions from *Rhodococcus opacus* and *Rhodococcus ruber* and identification of granule-associated proteins, Arch. Microbiol. 177 (2001) 20–28.
[37] M.B. Reed, S. Gagneux, K. Deriemer, P.M. Small, C.E. Barry 3rd, The W-Beijing lineage of *Mycobacterium tuberculosis* overproduces triglycerides and has the DosR dormancy regulon constitutively upregulated, J. Bacteriol. 189 (2007) 2583–2589.

[38] R.A. Coleman, The "discovery" of lipid droplets: a brief history of organelles hidden in plain sight, Biochim. Biophys. Acta Mol. Cell Biol. Lipids 9 (2020) 1.
[39] D.J. Murphy, The biogenesis and functions of lipid bodies in animals, plants and microorganisms, Prog. Lipid Res. 40 (2001) 325–438.
[40] I.M. Lewis, The cytology of bacteria, Bacteriol. Rev. 5 (1941) 181–230.
[41] K.L. Burdon, Fatty material in bacteria and fungi revealed by staining dried, fixed slide preparations, J. Bacteriol. 52 (1946) 665–678.
[42] E.D. Chow, J.S. Cox, TB lipidomics—the final frontier, Chem. Biol. 18 (2011) 1517–1518.
[43] S.T. Cole, R. Brosch, J. Parkhill, T. Garnier, C. Churcher, D. Harris, S.V. Gordon, K. Eiglmeier, S. Gas, C.E. Barry, F. Tekaia, K. Badcock, D. Basham, D. Brown, T. Chillingworth, R. Connor, R. Davies, K. Devlin, T. Feltwell, S. Gentles, N. Hamlin, S. Holroyd, T. Hornsby, K. Jagels, A. Krogh, J. McLean, S. Moule, L. Murphy, K. Oliver, J. Osborne, M.A. Quail, M.A. Rajandream, J. Rogers, S. Rutter, K. Seeger, J. Skelton, R. Squares, S. Squares, J.E. Sulston, K. Taylor, S. Whitehead, B.G. Barrell, Deciphering the biology of *Mycobacterium tuberculosis* from the complete genome sequence, Nature 393 (1998) 537–544.
[44] G. Knaysi, J. Hillier, C. Fabricant, The cytology of an avian strain of *Mycobacterium tuberculosis* studied with the electron and light microscopes, J. Bacteriol. 60 (1950) 423–447.
[45] C. Fréhel, C. Offredo, C. de Chastellier, The phagosomal environment protects virulent *Mycobacterium avium* from killing and destruction by clarithromycin, Infect. Immun. 65 (1997) 2792–2802.
[46] K. Bersuker, J.A. Olzmann, Establishing the lipid droplet proteome: mechanisms of lipid droplet protein targeting and degradation, Biochim. Biophys. Acta Mol. Cell Biol. Lipids 1862 (2017) 1166–1177.
[47] D.J. Murphy, The dynamic roles of intracellular lipid droplets: from archaea to mammals, Protoplasma 249 (2012) 541–585.
[48] J. Hänisch, M. Wältermann, H. Robenek, A. Steinbüchel, Eukaryotic lipid body proteins in oleogenous actinomycetes and their targeting to intracellular triacylglycerol inclusions: impact on models of lipid body biogenesis, Appl. Environ. Microbiol. 72 (2006) 6743–6750.
[49] D. Raze, C. Verwaerde, G. Deloison, E. Werkmeister, B. Coupin, M. Loyens, P. Brodin, C. Rouanet, C. Locht, Heparin-binding hemagglutinin adhesin (HBHA) is involved in intracytosolic lipid inclusions formation in mycobacteria, Front. Microbiol. 9 (2018) 2258.
[50] C. Zhang, L. Yang, Y. Ding, Y. Wang, L. Lan, Q. Ma, X. Chi, P. Wei, Y. Zhao, A. Steinbüchel, H. Zhang, P. Liu, Bacterial lipid droplets bind to DNA via an intermediary protein that enhances survival under stress, Nat. Commun. 8 (2017) 15979.
[51] M.P. Lanfranconi, A. Arabolaza, H. Gramajo, H.M. Alvarez, Insights into the evolutionary history of the virulent factor HBHA of *Mycobacterium tuberculosis*, Arch. Microbiol. 203 (2021) 2171–2182.
[52] Z. Li, K. Thiel, P.J. Thul, M. Beller, R.P. Kühnlein, M.A. Welte, Lipid droplets control the maternal histone supply of *Drosophila* embryos, Curr. Biol. 22 (2012) 2104–2113.
[53] K.L. Low, G. Shui, K. Natter, W.K. Yeo, S.D. Kohlwein, T. Dick, S.P. Rao, M.R. Wenk, Lipid droplet-associated proteins are involved in the biosynthesis and hydrolysis of triacylglycerol in *Mycobacterium bovis* bacillus Calmette-Guerin, J. Biol. Chem. 285 (2010) 21662–21670.
[54] K. Athenstaedt, D. Zweytick, A. Jandrositz, S.D. Kohlwein, G. Daum, Identification and characterization of major lipid particle proteins of the yeast *Saccharomyces cerevisiae*, J. Bacteriol. 181 (1999) 6441–6448.
[55] J. Cao, G. Dang, H. Li, T. Li, Z. Yue, N. Li, Y. Liu, S. Liu, L. Chen, Identification and characterization of lipase activity and immunogenicity of LipL from *Mycobacterium tuberculosis*, PLoS One 10 (2015) e0138151.
[56] D. Yang, S. Li, J. Stabenow, L. Zalduondo, Y. Kong, *Mycobacterium tuberculosis* LipE has a lipase/esterase activity and is important for intracellular growth and in vivo infection, Infect. Immun. 88 (2019) e00750-00719.
[57] N.R. Rameshwaram, P. Singh, S. Ghosh, S. Mukhopadhyay, Lipid metabolism and intracellular bacterial virulence: key to next-generation therapeutics, Fut. Microbiol. 13 (2018) 1301–1328.
[58] H.M. Alvarez, F. Mayer, D. Fabritius, A. Steinbüchel, Formation of intracytoplasmic lipid inclusions by *Rhodococcus opacus* strain PD630, Arch. Microbiol. 165 (1996) 377–386.
[59] D.P. MacEachran, M.E. Prophete, A.J. Sinskey, The *Rhodococcus opacus* PD630 heparin-binding hemagglutinin homolog TadA mediates lipid body formation, Appl. Environ. Microbiol. 76 (2010) 7217–7225.
[60] R.M. Armstrong, K.L. Adams, J.E. Zilisch, D.J. Bretl, H. Sato, D.M. Anderson, T.C. Zahrt, Rv2744c is a PspA ortholog that regulates lipid droplet homeostasis and nonreplicating persistence in *Mycobacterium tuberculosis*, J. Bacteriol. 198 (2016) 1645–1661.

[61] X. Yang, Z. Wen, D. Zhang, Z. Li, D. Li, U. Nagalakshmi, S.P. Dinesh-Kumar, Y. Zhang, Proximity labeling: an emerging tool for probing in planta molecular interactions, Plant Commun. 2 (2021) 100137.
[62] C.-L. Chen, N. Perrimon, Proximity-dependent labeling methods for proteomic profiling in living cells, WIREs Dev. Biol. 6 (2017) e272.
[63] L. Trinkle-Mulcahy, Recent advances in proximity-based labeling methods for interactome mapping [version 1; peer review: 2 approved], F1000Research 8 (2019).
[64] Y.G. Santin, Uncovering the in vivo proxisome using proximity-tagging methods, Bioessays 41 (2019) 1900131.
[65] D.I. Kim, K.J. Roux, Filling the void: proximity-based labeling of proteins in living cells, Trends Cell Biol. 26 (2016) 804–817.
[66] Q. Liu, J. Zheng, W. Sun, Y. Huo, L. Zhang, P. Hao, H. Wang, M. Zhuang, A proximity-tagging system to identify membrane protein–protein interactions, Nat. Methods 15 (2018) 715–722.
[67] Y. Akhter, S. Thakur, Targets of ubiquitin like system in mycobacteria and related actinobacterial species, Microbiol. Res. 204 (2017) 9–29.
[68] W. Sun, Y. Huo, Y. Mei, Q. Zhou, S. Zhao, M. Zhuang, Identification of a small probe that can Be conjugated to proteins by proximity labeling, ACS Chem. Biol. 15 (2020) 39–43.
[69] J.A. Bosch, C.L. Chen, N. Perrimon, Proximity-dependent labeling methods for proteomic profiling in living cells: an update, Wiley Interdiscip. Rev. Dev. Biol. 10 (2021) 10.
[70] K.J. Roux, D.I. Kim, M. Raida, B. Burke, A promiscuous biotin ligase fusion protein identifies proximal and interacting proteins in mammalian cells, J. Cell Biol. 196 (2012) 801–810.
[71] L. Trinkle-Mulcahy, Recent advances in proximity-based labeling methods for interactome mapping, F1000Res 31 (2019).
[72] J.S. Rees, X.W. Li, S. Perrett, K.S. Lilley, A.P. Jackson, Protein neighbors and proximity proteomics, Mol. Cell. Proteomics 14 (2015) 2848–2856.
[73] X. Liu, K. Salokas, R.G. Weldatsadik, L. Gawriyski, M. Varjosalo, Combined proximity labeling and affinity purification–mass spectrometry workflow for mapping and visualizing protein interaction networks, Nat. Protoc. 15 (2020) 3182–3211.
[74] S. De Munter, J. Görnemann, R. Derua, B. Lesage, J. Qian, E. Heroes, E. Waelkens, A. Van Eynde, M. Beullens, M. Bollen, Split-BioID: a proximity biotinylation assay for dimerization-dependent protein interactions, FEBS (Fed. Eur. Biochem. Soc.) Lett. 591 (2017) 415–424.
[75] Y. Xu, X. Fan, Y. Hu, In vivo interactome profiling by enzyme-catalyzed proximity labeling, Cell Biosci. 11 (2021) 27.
[76] K. Jacquet, S.L. Banerjee, F.J.M. Chartier, S. Elowe, N. Bisson, Proteomic analysis of NCK1/2 adaptors uncovers paralog-specific interactions that reveal a new role for NCK2 in cell abscission during cytokinesis, Mol. Cell. Proteomics 17 (2018) 1979–1990.
[77] K. Honke, N. Kotani, The enzyme-mediated activation of radical source reaction: a new approach to identify partners of a given molecule in membrane microdomains, J. Neurochem. 116 (2011) 690–695.
[78] N.C. Hartman, J.T. Groves, Signaling clusters in the cell membrane, Curr. Opin. Cell Biol. 23 (2011) 370–376.
[79] J.S. Rees, X.-W. Li, S. Perrett, K.S. Lilley, A.P. Jackson, Selective proteomic proximity labeling assay using tyramide (SPPLAT): a quantitative method for the proteomic analysis of localized membrane-bound protein clusters, Curr. Protoc. Protein Sci. 88 (2017), 19.27.11-2719.27.18.
[80] X.W. Li, J.S. Rees, P. Xue, H. Zhang, S.W. Hamaia, B. Sanderson, P.E. Funk, R.W. Farndale, K.S. Lilley, S. Perrett, A.P. Jackson, New insights into the DT40 B cell receptor cluster using a proteomic proximity labeling assay, J. Biol. Chem. 289 (2014) 14434–14447.
[81] H.W. Rhee, P. Zou, N.D. Udeshi, J.D. Martell, V.K. Mootha, S.A. Carr, A.Y. Ting, Proteomic mapping of mitochondria in living cells via spatially restricted enzymatic tagging, Science 339 (2013) 1328–1331.
[82] S.S. Lam, J.D. Martell, K.J. Kamer, T.J. Deerinck, M.H. Ellisman, V.K. Mootha, A.Y. Ting, Directed evolution of APEX2 for electron microscopy and proximity labeling, Nat. Methods 12 (2015) 51–54.
[83] Y. Han, T.C. Branon, J.D. Martell, D. Boassa, D. Shechner, M.H. Ellisman, A. Ting, Directed evolution of split APEX2 peroxidase, ACS Chem. Biol. 14 (2019) 619–635.
[84] S.A. Myers, J. Wright, R. Peckner, B.T. Kalish, F. Zhang, S.A. Carr, Discovery of proteins associated with a predefined genomic locus via dCas9–APEX-mediated proximity labeling, Nat. Methods 15 (2018) 437–439.
[85] R. Veyron-Churlet, J.M. Saliou, C. Locht, Interconnection of the mycobacterial heparin-binding hemagglutinin with cholesterol degradation and heme/iron pathways identified by proximity-dependent biotin identification in *Mycobacterium smegmatis*, Environ. Microbiol. 23 (2021) 3212–3224.

Article II

Intrabacterial lipid inclusion-associated proteins: A core machinery conserved from saprophyte *Actinobacteria* to the human pathogen *Mycobacterium tuberculosis*?

Tonia Dargham, Ivy Mallick, Laurent Kremer, Pierre Santucci & Stéphane Canaan

FEBS Open Bio. 2023 Dec;13(12):2306-2323. doi: 10.1002/2211-5463.13721. Epub 2023 Nov 15.

Mycobacterium tuberculosis, l'agent étiologique de la tuberculose (TB), est capable de stocker des lipides sous forme de triacylglycérol (TAG) dans des structures appelées inclusions lipidiques intrabactériennes (ILI) pour survivre et persister chroniquement chez son hôte. Ces TAG sont des molécules hautement énergétiques qui représentent une source majeure de carbone permettant la persistance et la réactivation de la bactérie, jouant ainsi un rôle de premier plan dans la pathogenèse de la tuberculose. Similaires aux gouttelettes lipidiques eucaryotes, les ILI sont essentiellement composées de lipides neutres et de phospholipides associés à des protéines qui interagissent dynamiquement à leur surface. Cependant, la composition protéique de ces organites, le(s) rôle(s) biologique(s) et les niveaux de conservation de ces protéines à travers plusieurs espèces d'actinobactéries restent encore à déterminer. Des études récentes combinant la biochimie et la protéomique ont permis de découvrir des protéines potentiellement associées aux ILI chez les espèces *Rhodococcus*, *M. smegmatis et M. bovis* BCG. Étant donné que les ILI ont été décrits chez l'ensemble du monde mycobactérien, qu'il s'agisse de souches pathogènes (*M. abscessus*, *M. avium*, *M. ulcerans*, *M. leprae* et les membres du complexe *M. tuberculosis*), ou non pathogène (*M. smegmatis*) nous avons émis l'hypothèse que des protéines/enzymes impliquées spécifiquement dans le métabolisme de ces ILI pourraient également être conservées chez l'ensemble des mycobactéries.

Dans cette étude, nous avons effectué une analyse *in silico* de trois protéomes indépendants *R jostii RHA1* (Rjos), *R. opacus* PD630 (Rop) et *M. smegmatis* mc^2155 obtenus expérimentalement et constitués de 228, 180 et 480 protéines individuelles formant la base du protéome associé à l'ILI correspondant. Pour chaque protéome, nous avons recherché les protéines orthologues chez *M. tuberculosis*, puis chez *M. abscessus*, *M. marinum*, *M. ulcerans* et *M. leprae*. Notre étude a révélé la présence sur 168 orthologues dont 70 protéines strictement conservées, définissant ainsi un noyau minimum des protéines constitutives des ILI. Cependant, un grand nombre de protéines identifiées appartenait à 6 catégories fonctionnelles autres que le métabolisme des lipides. Ce résultat renforce le concept qui a récemment émergé et qui suggère que la composition dynamique et les rôles multiples des ILI dans le cycle de vie des mycobactéries, où finalement ces structures ne semblent pas se limiter seulement au stockage des lipides et d'énergie.

Nous avons ensuite restreint notre analyse aux protéines dont l'annotation faisait uniquement référence au métabolisme des lipides et discuté leurs fonctions biologiques, ainsi que leurs interactions moléculaires et leur dynamisme à la surface de ces organites.

Enfin, nos résultats ont permis de montrer l'existence d'un motif structural commun pour la grande majorité des protéines associées aux ILI. Ce motif formant une hélice amphipathique pourrait être essentiel pour l'interaction de la protéine avec la surface des ILI. Bien que des validations expérimentales soient nécessaires, notre analyse a révélé que de nombreuses protéines appartenant à différentes catégories fonctionnelles sont partagées par des organismes distincts produisant des TAG et appartenant à l'embranchement des Actinobactéries.

En conclusion, l'étude *in silico* présentée ici a permis de fournir un ensemble de données utiles qui constituent des ressources de connaissances intéressantes pour la communauté mycobactérienne, travaillant sur le métabolisme des lipides et des ILI chez les procaryotes, avec un intérêt tout particulier sur le rôle des ILI dans la pathogénèse de *M. tuberculosis*.

FEBS openbio

FEBS PRESS science publishing by scientists

RESEARCH ARTICLE

Intrabacterial lipid inclusion-associated proteins: a core machinery conserved from saprophyte *Actinobacteria* to the human pathogen *Mycobacterium tuberculosis*

Tonia Dargham[1,2], Ivy Mallick[1], Laurent Kremer[3,4], Pierre Santucci[1] and Stéphane Canaan[1]

1 Aix-Marseille Univ, CNRS, LISM UMR 7255, IMM FR3479, IM2B, France
2 IHU Méditerranée Infection, Aix-Marseille Univ., France
3 Centre National de la Recherche Scientifique UMR 9004, Institut de Recherche en Infectiologie de Montpellier (IRIM), Université de Montpellier, France
4 INSERM, Institut de Recherche en Infectiologie de Montpellier, France

Keywords
bacterial lipid droplets; lipid metabolism; pathogenesis; triacylglycerol

Correspondence
P. Santucci and S. Canaan, Aix-Marseille Univ, CNRS, LISM UMR 7255, IMM FR3479, IM2B, Marseille, France
E-mail: psantucci@imm.cnrs.fr; canaan@imm.cnrs.fr

Pierre Santucci and Stéphane Canaan contributed equally as co-last author

(Received 5 September 2023, revised 2 October 2023, accepted 19 October 2023)

doi:10.1002/2211-5463.13721

Mycobacterium tuberculosis (Mtb), the aetiologic agent of tuberculosis (TB), stores triacylglycerol (TAG) in the form of intrabacterial lipid inclusions (ILI) to survive and chronically persist within its host. These highly energetic molecules represent a major source of carbon to support bacterial persistence and reactivation, thus playing a leading role in TB pathogenesis. However, despite its physiological and clinical relevance, ILI metabolism in Mtb remains poorly understood. Recent discoveries have suggested that several ILI-associated proteins might be widely conserved across TAG-producing prokaryotes, but still very little is known regarding the nature and the biological functions of these proteins. Herein, we performed an *in silico* analysis of three independent ILI-associated proteomes previously reported to computationally define a potential core ILI-associated proteome, referred to as ILIome. Our investigation revealed the presence of 70 orthologous proteins that were strictly conserved, thereby defining a minimal ILIome core. We further narrowed our analysis to proteins involved in lipid metabolism and discuss here their putative biological functions, along with their molecular interactions and dynamics at the surface of these bacterial organelles. We also highlight the experimental limitations of the original proteomic investigations and of the present bioinformatic analysis, while describing new technological approaches and presenting biological perspectives in the field. The *in silico* investigation presented here aims at providing useful datasets that could constitute a scientific resource of broad interest for the mycobacterial community, with the ultimate goal of enlightening ILI metabolism in prokaryotes with a special emphasis on Mtb pathogenesis.

Abbreviations
AG, Arabinogalactan; BLASTp, Basic Local Alignment Search Tool program; BTZ, Benzothiazinones; Dgat/Tgs, Diacylglycerol acyltransferase/triacylglycerol synthases; DNB, Dinitrobenzamide; Dos, Dormancy survival regulon; FASII, Fatty acid synthase II; FC, Functional category; FFA, Free fatty acids; HC, Highly conserved; ILI, Intrabacterial lipid inclusions; KEGG, Kyoto Encyclopedia of Genes and Genomes; LAM, Lipoarabinomannan; LB, Lipid body; LD, Lipid droplet; LI, Lipid inclusion; Mabs, *Mycobacterium abscessus*; Mlep, *Mycobacterium leprae*; Mmar, *Mycobacterium marinum*; Msmeg, *Mycobacterium smegmatis*; Mtb, *Mycobacterium tuberculosis*; Mul, *Mycobacterium ulcerans*; PLIN, Perilipin; SC, Strictly conserved; TAG, Triacylglycerol; TB, Tuberculosis.

FEBS Open Bio **13** (2023) 2306–2323 © 2023 The Authors. *FEBS Open Bio* published by John Wiley & Sons Ltd on behalf of Federation of European Biochemical Societies.

Lipid droplets (LD), also referred to as lipid bodies (LBs) or lipid inclusions (LIs), are lipid-rich organelles synthesized by numerous eukaryote organisms, including plants and mammals [1–3]. These structures are also synthesized by prokaryotes, as intrabacterial lipid inclusions (ILI) [4–7], underscoring the widely conserved nature of these organelles among multiple kingdoms [1–3]. Lipid droplet and ILI are essentially composed of neutral lipids surrounded by an amphipathic monolayer of phospholipids with proteins that are dynamically interacting at their surface [6,8]. In addition to a common compositional architecture, they often share conserved proteins with multiple biological functions that are essential for their biogenesis, maintenance/integrity, and degradation [9].

Among prokaryotes, species that belong to the genus *Nocardia*, *Dietzia*, *Gordonia*, *Streptomyces*, *Rhodococcus*, and *Mycobacterium* have been reported to produce high amounts of triacylglycerol (TAG) and detectable ILI structures upon specific *in vitro* culture conditions, suggesting that all can synthesize TAG-containing ILI [4,7]. In this context, some *Rhodococcus* and *Mycobacterium* species have been widely used as model systems during the last decades to delineate the processes of ILI formation, maintenance, and consumption at both cellular and molecular levels [10–16]. Intrabacterial lipid inclusion biosynthesis was proposed to be initiated in specific and spatially distinct microdomains located at the inner leaflet of the plasma membrane [17]. In these globular microstructures, TAG keeps accumulating under the co-action of multiple enzymes, notably the diacylglycerol acyltransferase/triacylglycerol synthases (Dgat/Tgs) [17]. With the increasing level of TAG, these globules further expand to form a premature ILI that is surrounded by a phospholipid monolayer, which is later released freely in the cytosol to form a mature organelle [17]. This model, proposed almost 20 years ago, is still to date the reference biological model for ILI biosynthesis in prokaryotes [17]. Finally, upon carbon starvation or nutrient-rich favorable culture conditions, ILI are hydrolyzed by lipolytic enzymes to provide free fatty acids (FFA) and acetyl-CoA used as a major energy source for cellular homeostasis, maintenance, and regrowth, substantiating the importance of lipid metabolism in bacterial physiology [14,16,18].

In the context of tuberculosis (TB), independent studies reported that host-derived lipids and ILI metabolism are keys in the tubercle bacilli pathogenicity [19–24]. Indeed, *Mycobacterium tuberculosis* (Mtb) mutants that are unable to synthesize or hydrolyze TAG-containing ILI display important fitness defects and impaired survival *in vitro*, *in cellulo*, and in *in vivo* biological systems that recapitulate TB persistence and reactivation stages [23,25]. Moreover, the presence of ILI-positive Mtb in sputum samples from patients with active TB reinforces the idea these organelles may be essential for the Mtb physiopathological lifestyle with important clinical implications [13,26–28].

To date, while the sequential anabolic and catabolic mechanisms governing ILI metabolism start to be well-documented, the nature and function of ILI-associated proteins remain elusive. Recent investigations combining biochemical and proteomic approaches unraveled a subset of potential proteins associated with ILI in *Rhodococcus* and *Mycobacterium* species [29–32]. However, none of these studies have been directly performed with Mtb. Thus, the composition of the Mtb ILI-associated proteome remains unknown. Since ILI have been described in both pathogenic and nonpathogenic mycobacteria, including *M. smegmatis* (Msmeg) [13–15,32], *M. abscessus* (Mabs) [14,33], *M. avium* (Mav) [34], *M. marinum* (Mmar) [35], *M. ulcerans* (Mul) [36], *M. leprae* (Mlep) [37], and members of the *M. tuberculosis* complex [26,31,38–40], we speculated that proteins/enzymes involved in ILI metabolism identified in *Actinobacteria* may also be conserved in Mtb.

In this study, we capitalized from previously published proteomic investigations in *Rhodococcus* and *Mycobacterium* to identify putative ILI-associated orthologous proteins in Mtb, and computationally define and characterize a core ILI-associated proteome in the tubercle bacilli. In particular, we focus our analysis on proteins known or described as key actors in lipid metabolism and explore their putative function in ILI metabolism and mycobacterial physiology. We also discuss the plausible binding features of proteins associated with the surface of ILI. This article aims at providing new visions and insights into the biology of mycobacterial ILI to address relevant challenges and provide new scientific directions that could benefit the scientific community.

Methods

Computational prediction and conservation of the Mtb ILI-associated proteome

The ILI-associated proteomes from *Rhodococcus jostii* RHA1 (Rjos—taxid:101510), *Rhodococcus opacus* PD630 (Rop—taxid:543736) and *Mycobacterium smegmatis* mc^{2}155 (Msmeg—taxid:246196) were obtained from three independent studies [29,30,32]. Regarding the Rjos and Rop datasets, only the ILI-associated proteins found in two independent shotgun proteomic experiments were included in our analysis [29,30]. Following this specific criterion, 228

and 180 individual proteins were listed in tables to constitute the Rjos and Rop ILI-associated proteomes, respectively. Regarding the Msmeg dataset, we kept the selection criteria set up by Armstrong and colleagues [32] and further included 480 individual proteins in our analysis to constitute the Msmeg ILI-associated proteome. In both cases, each individual protein sequences were analyzed by using the Basic Local Alignment Search Tool program BLASTp (https://blast.ncbi.nlm.nih.gov/Blast.cgi) [41] to retrieve putative orthologs in the *M. tuberculosis* H37Rv proteome (Mtb—taxid:83332). Scoring parameters were set as default parameters using a BLOSUM62 matrix with gap existence costs of 11 and gap extension costs of 1. The conditional compositional score matrix adjustment option was used. The maximum alignment score was used to select the best hits and identified Mtb proteins. For each putative ortholog identified, we complemented our research using the Kyoto Encyclopedia of Genes and Genomes (KEGG) database (https://www.genome.jp/kegg/) and the MycoBrowser database (https://mycobrowser.epfl.ch/) [42,43]. We collected information regarding (a) the gene/protein id (H37Rv gene/protein number), (b) the protein sequence, (c) the corresponding annotated functional category (FC), and finally (d) the *in vitro* gene essentiality as assessed by saturating transposon mutagenesis, according to Dejesus and colleagues [44]. Then, the *in silico* Mtb ILI-associated core proteome was defined by listing putative orthologs that are conserved in multiple datasets. Finally, this putative core proteome was used to identify conserved mycobacterial ILI-associated proteins in the following species, *M. smegmatis* mc^2155 (Msmeg—taxid:246196), *M. abscessus* ATCC 19977 (Mabs—taxid:561007), *M. marinum* M (Mmar—taxid:216594), *M. leprae* TN (Mlep—taxid:272631), and *M. ulcerans* Agy99 (Mul—taxid:362242).

Structural and putative binding properties of Mtb putative ILI-associated proteins

Structural and binding properties of the conserved protein candidates across multiple datasets were analyzed by combining bioinformatic softwares. First, the primary sequence of each protein was subjected to the PSI-blast-based secondary structure PREDiction program v4.02 (PSIPred) (http://bioinf.cs.ucl.ac.uk/psipred/) [45,46] to predict the alpha helices. To screen and further identify putative ILI-targeting alpha helices, the Heliquest software (http://heliquest.ipmc.cnrs.fr) [47] was used by applying the parameters reported by Armstrong and colleagues [32]. Briefly, the hydrophobicity parameter 'H' ranged from 0.40 to 0.60, the mean hydrophobic moment 'μH' ranged from 0.40 to 0.75, and the net charge 'z' was set between − 4 and +4. The amino acid composition was set to 2 polar residues, 1 uncharged residue (Ser, Thr, Asn, Gln, and His), no glycine, 10 charged residues, no proline at i, i + 3/*n* − 3 n, and no cysteine. No geometric rules and no BlackList filters were applied. From the putative amphipathic helices identified using this screening procedure, the most interesting candidates were displayed as an helical wheel diagram. Finally, potential hydrophobic binding regions or potential electrostatic interactions were assessed manually using the experimentally determined 3D structures of the candidate proteins available from the Protein Data Bank (https://www.rcsb.org) or, alternatively, by using models generated from the AlphaFold v2.0 prediction software (https://alphafold.ebi.ac.uk/) [48] and visualized using the ChimeraX software and its in-built tools (https://www.cgl.ucsf.edu/chimerax/) [49].

Results and Discussion

Identification of Mtb orthologous ILI-associated proteins from Rjos, Rop, and Msmeg proteomic datasets

To identify mycobacterial proteins that may be commonly associated with ILI, an *in silico* analysis was initiated based on previously characterized ILI-associated proteomes. We capitalized from three available datasets established by performing proteomic analysis of ILI-enriched fractions obtained after sucrose gradient isolation [50]. *R jostii* RHA1 (Rjos), *R. opacus* PD630 (Rop), and *M. smegmatis* mc^2155 (Msmeg) original datasets [29,30,32], consisting of 228, 180, and 480 individual proteins forming the basis of their corresponding ILI-associated proteomes, respectively (Fig. 1A). Within each of these datasets, we searched for potential orthologous proteins in Mtb. BLASTp analyses identified putative candidates in the Mtb H37Rv proteome (NCBI taxid:83332). We complemented our analysis using the KEGG and the MycoBrowser database [42,43]. Our analysis unraveled 205/228 (90%), 171/180 (95%), and 449/480 (93.5%) orthologs in Mtb as compared to the previously identified ILI-associated proteins in Rjos, Rop, and Msmeg, respectively (Fig. 1A). Specific information of each of these putative targets are available in Tables S1–S3.

Since Mtb, is by far the most studied bacteria belonging to the *Actinobacteria* phylum, we took advantage of its well-documented genome and proteome to further characterize the identified orthologous proteins [51–53]. According to Cole and colleagues' initial annotation, latter updated by Camus *et al.*, the Mtb genome and its corresponding coding sequences were classified into 11 FCs based on bioinformatic comparison [51–53]. From this, the specific Mtb FC was assigned for each orthologous protein (Fig. 1B). Only nine FCs were potentially of interest since '*Stable RNAs*' and '*Insertion sequences and phages*' FC are not

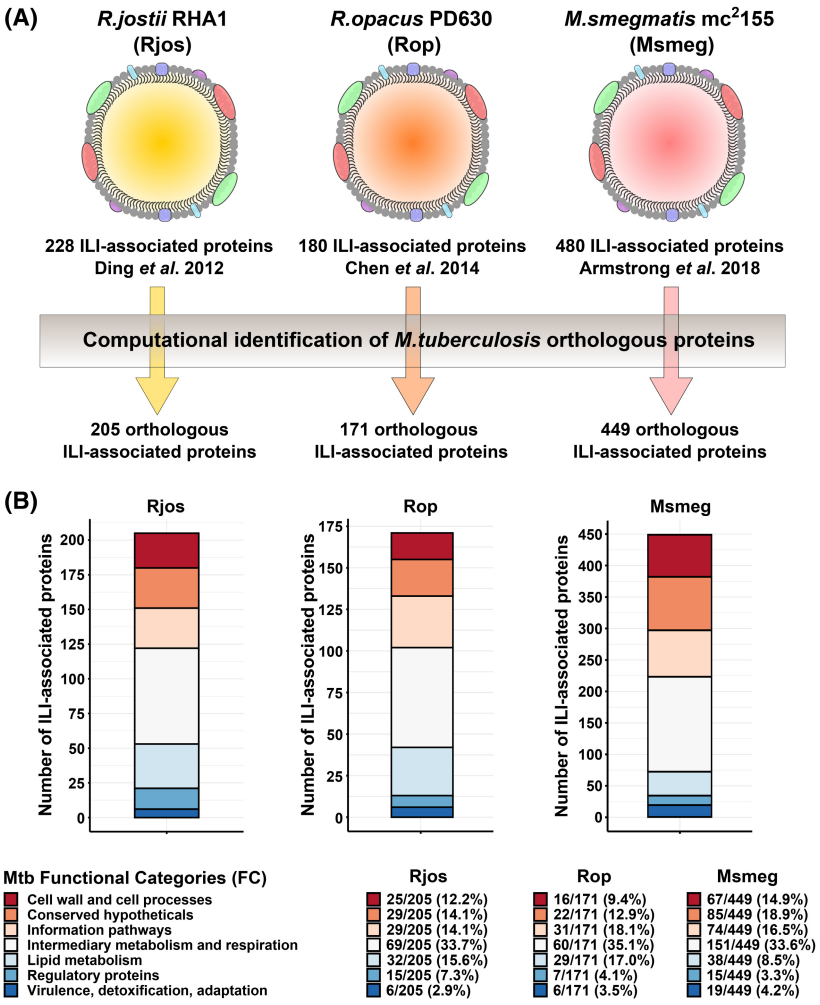

Fig. 1. Computational identification of Mtb orthologous ILI-associated proteins. (A) Schematic representation of the experimental workflow performed in this study. Previously identified ILI-associated proteins from three independent studies in Rjos, Rop, and Msmeg were selected, and their orthologous proteins in Mtb were identified by using the Basic Local Alignment Search Tool program BLASTp, KEGG, and the MycoBrowser programs. (B) Distribution of the identified ILI-associated protein orthologs from each organism based on their respective FC. FCs of each protein were obtained based on Mtb original genome annotation and include proteins of '*Cell wall and cell processes*', '*Conserved hypothetical*', '*Information pathways*', '*Intermediary metabolism and respiration*', '*Lipid metabolism*', and '*Regulation and virulence detoxification, adaptation*'.

applicable to proteins. In our analysis, only seven out of the nine FC were represented in the Rjos, Rop, and Msmeg datasets as no orthologous proteins belonging to '*Unknown*' and '*PE/PPE*' FC were identified. Overall, the partitioning of the 205, 171, and 449 identified orthologous proteins were similar in the seven FC (Fig. 1B). Surprisingly, proteins classified into the '*Intermediary metabolism and respiration*' FC represented approximately one-third of each dataset with 69/205 (33.7%), 60/171 (35.1%), and 151/449 (33.6%), respectively (Fig. 1B). On the contrary, only 32/205 (15.6%), 29/171 (17.0%), and 38/449 (8.5%) of the proteins identified belong to the '*Lipid metabolism*' FC, suggesting that proteins involved directly into lipid anabolism, catabolism, or transport are not over-represented at the surface of these organelles. We next collected information about the essentiality of each candidate in Mtb based on the seminal work of Dejesus and colleagues [44]. Results are available for each dataset in Tables S1–S3 and show that 68/205 (33.2%), 69/171 (40.4%), and 140/449 (31.2%) of the putative ILI-associated protein-encoding genes are essential for Mtb *in vitro*. This suggests that ILI shelter proteins that display critical physiological functions for cellular homeostasis and growth.

Identification of 168 ILI-associated proteins that are conserved across multiple proteomic datasets—Definition of a 'minimal' ILIome core

We postulated that some proteins might be conserved in numerous *Actinobacteria*, represented in multiple datasets, and sought to identify Mtb orthologous proteins previously listed across multiple datasets. Our investigation uncovered the presence of 168 proteins that were conserved within two or three out of three datasets (Fig. 2A). We identified 70 proteins strictly conserved (SC) across the three datasets and 98 proteins found at least in two datasets. These 98 proteins were referred to as highly conserved proteins (HC) (Fig. 2A) and

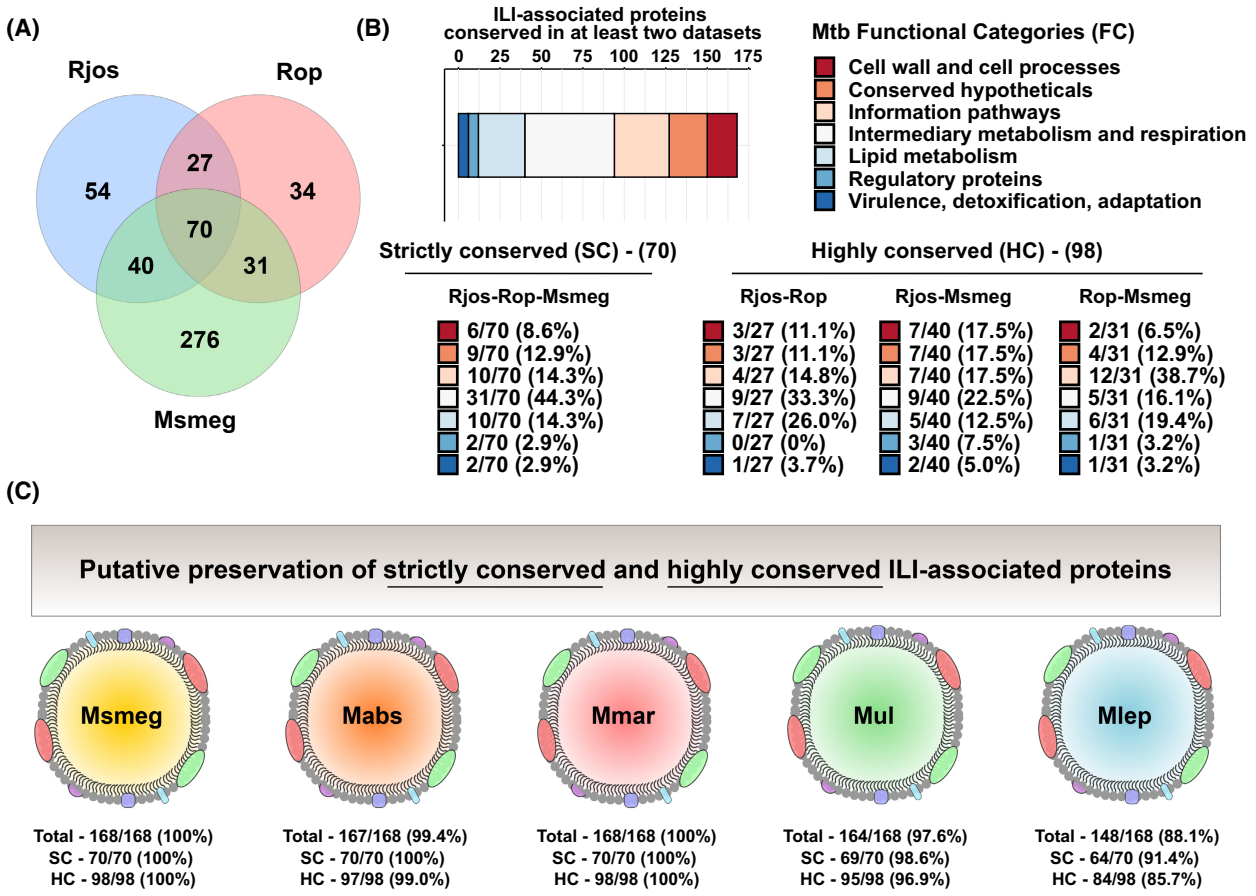

Fig. 2. Analysis of ILI-associated protein conservation across the multiple proteomic datasets. (A) Venn diagram representation of Mtb orthologous proteins repartition from the three datasets analyzed, and identification of proteins that are conserved across the three species. (B) Repartition of the 168 identified ILI-associated protein orthologs that are contained in at least 2 datasets based on their respective FC (Top panel). Repartition of the identified ILI-associated protein orthologs that are SC across Rjos, Rop, and Msmeg datasets or HC across two datasets (Bottom panels). FCs of each protein were obtained based on Mtb original genome annotation and includes proteins of '*Cell wall and cell processes*', '*Conserved hypothetical*', '*Information pathways*', '*Intermediary metabolism and respiration*', '*Lipid metabolism*', and '*Regulation and virulence detoxification, adaptation*'. (C) Schematic representation of the conservation levels of the 168 ILI-associated proteins identified in Mtb within five other mycobacterial species including Msmeg, Mabs, Mmar, Mul, and Mlep.

included 27 proteins conserved between Rjos-Rop datasets, 40 conserved between Rjos-Msmeg datasets, and the remaining 31 were conserved between Rop-Msmeg datasets (Fig. 2A). Analysis of gene essentiality in Mtb showed again a homogenous distribution with 71 essential genes, 78 nonessential genes, 18 genes involved in growth advantage/defect, and 1 gene classified as uncertain, according to Dejesus and colleagues [44].

The distribution and classification of the conserved 168 orthologous proteins in Mtb FC is as follows: '*Cell wall and cell processes*' (18/168–10.7%), '*Conserved*' '*Hypotheticals*' (23/168–13.7%), '*Information pathways*' (33/168–19.6%), '*Intermediary metabolism and respiration*' (54/168–32.1%), '*Lipid metabolism*' (28/168–16.7%), '*Regulatory proteins*' (6/168–9.5%), and '*Virulence, detoxification, adaptation*' (6/168–9.5%) (Fig. 2B). Specific analysis of Mtb FC for SC and HC proteins across the datasets is also displayed (Fig. 2B).

Next, we investigated whether the 168 candidate proteins were conserved in other mycobacterial species, positing that they may be shared with other mycobacterial species. Thus, we looked for orthologs in both nonpathogenic and pathogenic species known to produce ILI, such as Msmeg, Mabs, Mmar, Mlep, and Mul (Fig. 2C). Our results show that 168/168 (100%) of the proteins are conserved in Msmeg and Mmar, 167/168 (99.4%) in Mabs, 164/168 (97.6%) in Mul, and 148/168 (88.1%) in Mlep, the etiologic agent of leprosy (Fig. 2C). All these information are combined in Table S4.

Description of proteins involved in lipid metabolism at the ILI surface

Surprisingly, only 28 proteins were classified in the '*Lipid metabolism*' FC, therefore representing only 16.7% (28/168) of the total proteins associated with ILI and approximately 12.0% (28/233) of the total proteins that have been originally classified in this FC by Cole and colleagues [51–53]. These results are consistent with the vision that recently emerged regarding the physiological role of ILI, which are structures primarily dedicated to lipid storage but also ensuring a wide range of functions to maintain cellular homeostasis in stringent conditions [54,55].

Analysis of these 28 proteins (Table 1) showed that 20 are directly involved in phospholipids, fatty acids or mycolic acids biosynthesis, modification, or degradation processes (Fig. 2C).

The first 16 include Rv0242c (FabG4), Rv0243 (FadA2), Rv0270 (FadD2), Rv1206 (FadD6), Rv1483 (FabG1), Rv2187 (FadD15), Rv0468 (FadB2), Rv3229c (DesA3), Rv0154c (FadE2), Rv2244 (AcpM), Rv3800c (Pks13), Rv2524c (Fas), Rv0400c (FadE7), Rv0824c (DesA1), Rv2501c (AccA1), and Rv2247 (AccD6).

Three additional proteins, Rv1544, Rv3720, and Rv0437c, annotated as putative ketoacyl reductase, fatty-acyl-phospholipid synthase, and phosphatidylserine decarboxylase, respectively, were also identified. A simplified representation of the potential implication of these enzymes in Mtb lipid metabolism is shown in Fig. 3A,B.

Of note, our analysis unraveled the mycobacterial enoyl-reductase enzyme Rv1484 (InhA), target of the anti-TB drugs isoniazid and ethionamide, as potential actor at the surface of ILI. With KasAB, MabA, and HadABC, InhA forms the type II fatty acid synthase (FAS-II), which elongates short-chain fatty acids to long-chain meromycolic acids (Fig. 3A). These latter are the biosynthetic precursors of mycolic acids, which are indispensable lipids for mycobacterial growth and survival [56–58].

Although the precise molecular component(s) responsible for acid-fast staining positivity is still unknown, the common feature among all of the proposed mechanisms is the existence of an atypical lipid-rich hydrophobic barrier that can be penetrated by phenol-based stains but is impermeable to acido-alcoholic solutions used in Ziehl-Neelsen staining [59]. Seminal work on isoniazid showed that this drug inhibits mycolic biosynthesis, resulting in the loss of acid fastness in Mtb, highlighting the critical role of these lipid components in acid-fastness [59–61]. Intriguingly, several studies reported that mycobacteria harboring Nile-Red positive ILI tend to lose acid-fastness and become more tolerant to front-line drugs, including isoniazid [25,55,62]. When similar experiments were conducted in a Mtb *tgs1* deletion mutant, the bacilli failed to accumulate ILI *in vitro*, very few Nile-Red positive bacteria were detected while most remained acid-fast positive [55]. Based on these observations, it is tempting to speculate that the formation of ILI in nonreplicating bacteria is associated with alterations of the mycobacterial cell wall, which comprises the mycolic acid-containing outer membrane. In this context, the localization of InhA and its enzymatic activity at the surface of ILI could be directly linked to these global changes.

Two additional major enzymes involved in cell wall biosynthesis were identified, the decaprenylphosphoryl-β-D-ribose-2′-epimerase Rv3790 (DprE1) and the decaprenylphosphoryl-2-keto-β-D-erythro-pentose reductase Rv3791 (DprE2) (Fig. 3C). These two enzymes catalyze the formation of decaprenyl-phospho-arabinose, an essential precursor required for the synthesis of the arabinan moiety of arabinogalactan (AG) and lipoarabinomannan (LAM) (Fig. 3C). DprE enzymes are the therapeutic targets of new TB drug candidates: the benzothiazinones (BTZs) and the dinitrobenzamide derivatives (DNBs) [63,64]. However, whether this specific localization impacts on AG/LAM synthesis or Mtb susceptibility to these drugs in ILI-rich conditions remains to be investigated.

Triacylglycerol biosynthesis is subdivided into three major metabolic steps [4,7]: (i) the import or *de novo* biosynthesis of acyl-CoA molecules; (ii) the formation of various glycerol-derived intermediates, and finally (iii) the sequential esterification of acyl-CoA molecules onto these glycerol-derived intermediates. Therefore, in this metabolic model, glycerol phospholipid metabolism plays a central role in the final steps to produce TAG [4,7]. In addition to these 22 initial proteins, six additional proteins associated with fatty acids and glycerophospholipids metabolism were identified in this FC (Fig. 3D). This includes the Rv2483c and Rv2484c proteins, previously reported to participate in the conversion of lysophosphatidic acid into phosphatidic acid and TAG biosynthesis, respectively (Fig. 3D) [51,65]. Indeed, the two corresponding genes are located next to genes encoding a putative carboxylesterase LipQ (Rv2485c), a probable glycerol-3-phosphate acyltransferase (Rv2482c), and a probable enoyl-CoA hydratase (Rv2486), suggesting that they possibly be involved in TAG synthesis via the Kennedy pathway [65].

Two additional Tgs enzymes were identified in our analysis, the Rv0895 and the well-characterized

Table 1. List of the 28 proteins belonging to the lipid metabolism FC identified as part of Mtb lLIome.

Dataset	Mtb ID	Gene name	Putative function	Essentiality	Msmeg ortholog	Mabs ortholog	Mmar ortholog	Mul ortholog	Mlep ortholog
Rop-Rjos-Msmeg	Rv0242c	*fabG4*	3-ketoacyl-ACP reductase	Nonessential	MSMEG_0372	MAB_4443	MMAR_0503	MUL_1166	ML2565
Rop-Rjos-Msmeg	Rv0243	*fadA2*	Acetyl-CoA acyltransferase	Nonessential	MSMEG_0373	MAB_4442c	MMAR_0504	MUL_1167	ML2564
Rop-Rjos-Msmeg	Rv0270	*fadD2*	Fatty-acid-CoA ligase	Nonessential	MSMEG_0599	MAB_4340c	MMAR_0528	MUL_1191	ML2546
Rop-Rjos-Msmeg	Rv1206	*fadD6*	Fatty-acid-CoA ligase	Nonessential	MSMEG_5086	MAB_1342	MMAR_4232	MUL_0957	ML1346
Rop-Rjos-Msmeg	Rv1483	*fabG1*	3-ketoacyl-ACP reductase	Essential	MSMEG_3150	MAB_2723c	MMAR_2289	MUL_1491	ML1807c
Rop-Rjos-Msmeg	Rv1484	*inhA*	NADH-dependent enoyl-ACP reductase	Essential	MSMEG_3151	MAB_2722c	MMAR_2290	MUL_1492	ML1806c
Rop-Rjos-Msmeg	Rv1683	–	Long-chain acyl-CoA synthase and lipase	Nonessential	MSMEG_3767	MAB_2348	MMAR_2478	MUL_1660	ML1346
Rop-Rjos-Msmeg	Rv2187	*fadD15*	Long-chain-fatty-acid-CoA ligase	Nonessential	MSMEG_4254	MAB_1978c	MMAR_3231	MUL_3542	ML0887
Rop-Rjos-Msmeg	Rv3720	–	FAS	Nonessential	MSMEG_6284	MAB_0310c	MMAR_5236	–	ML2334
Rop-Rjos-Msmeg	Rv3791	*dprE2*	Decaprenylphosphoryl-keto erythro pentose reductase	Essential	MSMEG_6385	MAB_0191c	MMAR_5353	MUL_4970	ML0108c
Rop-Msmeg	Rv0468	*fadB2*	3-hydroxybutyryl-CoA dehydrogenase	Nonessential	MSMEG_0912	MAB_4094c	MMAR_0793	MUL_4537	ML2461c
Rop-Msmeg	Rv2244	*acpM*	Meromycolate extension acyl carrier protein	Essential	MSMEG_4326	MAB_1878c	MMAR_3337	MUL_1305	ML1654
Rop-Msmeg	Rv3800c	*pks13*	Polyketide synthase	Essential	MSMEG_6392	MAB_0180	MMAR_5364	MUL_4983	ML0101
Rop-Msmeg	Rv2524c	*fas*	FAS	Essential	MSMEG_4757	MAB_1512	MMAR_3962	MUL_3818	ML1191
Rop-Msmeg	Rv3790	*dprE1*	Decaprenylphosphoryl-beta-D-ribose 2′-oxidase	Essential	MSMEG_6382	MAB_0192c	MMAR_5352	MUL_4969	ML0109c
Rop-Msmeg	Rv2483c	*plsC*	Transmembrane phospholipid biosynthesis bifunctional enzyme	Nonessential	MSMEG_4704	MAB_2455c	MMAR_3834	MUL_3764	ML1245
Rjos-Msmeg	Rv2484c	–	Triacylglycerol synthase	Nonessential	MSMEG_4705	MAB_4544c	MMAR_3835	MUL_3765	ML1244
Rjos-Msmeg	Rv1544	–	Ketoacyl reductase	Nonessential	MSMEG_0737	MAB_1537c	MMAR_2367	MUL_1543	ML0429c
Rjos-Msmeg	Rv0437c	*psd*	Phosphatidylserine decarboxylase	Nonessential	MSMEG_0861	MAB_0639c	MMAR_0754	MUL_1386	ML0311c
Rjos-Msmeg	Rv3229c	*desA3*	Linoleoyl-CoA desaturase	Nonessential	MSMEG_1743	MAB_2148	MMAR_1315	MUL_2565	–
Rjos-Msmeg	Rv0154c	*fadE2*	Acyl-CoA dehydrogenase	Nonessential	MSMEG_0102	MAB_0255	MMAR_0374	MUL_4790	ML0737
Rop-Rjos	Rv0895	–	Triacylglycerol synthase	Nonessential	MSMEG_6322	MAB_4544c	MMAR_5271	MUL_2057	ML1244
Rop-Rjos	Rv3391	*acrA1*	Multi-functional enzyme with acyl-CoA-reductase activity	Nonessential	MSMEG_1623	MAB_3710	MMAR_1153	MUL_0918	ML0862
Rop-Rjos	Rv0400c	*fadE7*	Acyl-CoA dehydrogenase	Nonessential	MSMEG_2466	MAB_0822	MMAR_0698	MUL_2825	ML0737
Rop-Rjos	Rv2501c	*accA1*	Acetyl−/propionyl-coenzyme A carboxylase alpha chain	Nonessential	MSMEG_4716	MAB_4539c	MMAR_3848	MUL_3779	ML0726c
Rop-Rjos	Rv0824c	*desA1*	Acyl-ACP desaturase	Essential	MSMEG_5773	MAB_0754c	MMAR_4856	MUL_0445	ML2185

Table 1. (Continued).

Dataset	Mtb ID	Gene name	Putative function	Essentiality	Msmeg ortholog	Mabs ortholog	Mmar ortholog	Mul ortholog	Mlep ortholog
Rop-Rjos	Rv3130c	*tgs1*	Triacylglycerol synthase	Nonessential	MSMEG_5242	MAB_3551c	MMAR_1519	MUL_2420	ML1244
Rop-Rjos	Rv2247	*accD6*	Acetyl/propionyl-CoA carboxylase	Growth defect	MSMEG_4329	MAB_1876c	MMAR_3340	MUL_1302	ML1657

Rv3130c (Tgs1), consisting of the major TAG synthase in Mtb (Fig. 3D) [65]. The Mtb H37Rv genome possesses 15 *tgs*-like genes, identified on their homology with the bifunctional wax synthase-*tgs* gene of *A. calcoaceticus* [65]. Among these 15 proteins, Tgs1 has been identified as the final and primary enzyme involved in TAG synthesis *in vitro*, since deletion of the *tgs1* was associated with a severe defect in TAG production and reduced Nile-Red positivity in under hypoxic conditions as well as in granuloma-like models [55,62,65,66].

Since ILI-positive Mtb have been described in sputum from patients with active TB [13,26], it is now commonly accepted that these organelles play a key role in the adaptation to pathophysiological environments such as the one encountered within granulomatous lesions. Indeed, upon stringent conditions, Mtb realigns its metabolism to produce TAG, which seem to be required for adaptation and overcoming multiple stresses [7,18,25,55,62]. One of the most characterized pathways involved in such adaptation is the upregulation of the dormancy survival regulon (Dos), which is coordinated by its two sensor histidine kinases, DosS and DosT, and its response regulator DosR [67]. This regulon comprises 48 genes (including *tgs1*) involved in lipid metabolism and anaerobic respiration [65,68]. Among Mtb lineages, the Beijing lineage strains (L2 strains) show a constitutive overexpression of *dosR* compared with the non-Beijing strains [69], where *tgs1* is always upregulated. As a result, *tgs1* is overexpressed by approximately 10-fold, which leads to greater TAG accumulation. In addition, clinical isolates from this lineage also upregulate *tgs2*, independently of Dos, which has also been reported to increase TAG levels [70]. Such lipid-rich phenotype has been proposed to be one of the phenotypic traits explaining the hypervirulence among these strains and their epidemiological effects [69,70].

More recently, Mtb *tgs1* orthologs were identified in other mycobacterial species, including the emerging opportunistic pathogen Mabs. Among the seven *tgs* genes present within Mabs genome, one enzyme annotated *MAB_3551* was identified as the closest homolog to Tgs1 sharing 40% of sequence identity [33]. Molecular characterization of MAB_3551c indicated that this protein was essential for TAG production and the formation of ILI *in vitro* as well as in the foamy macrophage infection model [33].

One can hypothesize that the spatial distribution of Tgs enzymes within bacterial cells is bimodal. Indeed, time-dependent analysis of TAG-rich *Rhodococcus* cells by sophisticated electron microscopy approaches combined with immunolabelling experiments allowed us to

establish that Dgat/Tgs enzymes were mainly localized at the plasma membrane level within specific microdomains [17]. This was recently confirmed in Mabs where the 7 Tgs were localized within the membrane fraction by cell-fractionation and immunoblotting [33]. In contrast, Tgs1 has also been identified on the surface of mature ILI in *Mycobacterium bovis* BCG [31], suggesting that this critical enzyme might be either continuously associated with membrane-derived premature ILI and remains associated upon releasing of cytosolic mature ILI, or displays a dynamic spatial distribution within the cells that fluctuates between these subbacterial compartments.

Our analysis suggests also the presence of the acyl-CoA reductase Rv3391 (*fcr1* or *acrA1*) [71], which is involved in the generation of fatty alcohol from acyl-CoA to generate wax ester molecules (Fig. 3D). In Mtb, wax esters molecules have been observed to be involved in response to iron starvation [72], and described for being required to undergo into a nonreplicating persistent state when subjected to *in vitro* dormancy-inducing conditions [71]. However, their direct contribution to Mtb pathogenesis remains unknown.

Finally, our analysis identified as well the conservation of the Rv1683 protein, a putative bifunctional long-chain acyl-CoA synthase/lipase (Fig. 3D), reported as an important regulator of TAG levels in *M. bovis* BCG [31]. Indeed, the Rv1683 and the BCG1721 protein are 100% identical, with the N-terminal domain that is thought to express acyl-CoA synthase/ligase activity whereas the putative C-terminal harbors a lipase domain, typified by the consensus GXSXG motif and is homologous to the catalytic domain of the human gastric lipase [31]. Overexpression of *M. bovis* BCG *BCG1721* gene had a dual impact on TAG levels and ILI formation/consumption processes when assessed under nonreplicating or resuscitating conditions in the Wayne model [31]. The authors demonstrate that long-chain TAG levels significantly increased under the nonreplicating states when the *BCG1721* gene was overexpressed [31]. However, overexpression of *BCG1721* during the reactivation phase was associated with an increase in TAG lipolysis; this process was impaired when the inactive $BCG1721^{S150A}$ gene in which the catalytic serine replaced by an alanine residue in the lipase domain was overexpressed [31]. Thus, many questions regarding the physiological function of this bifunctional enzyme remain to be discovered.

Importantly, these 28 proteins were also found in other mycobacterial species with the exception of Rv3720 and Rv3229 orthologs in Mul and in Mlep, respectively (Table 1). This suggests that the few enzymes that belong to the '*Lipid metabolism*' FC are likely to play a key role in the formation, maintenance, and degradation of ILI in various mycobacteria.

Since the presence of ILI is associated with a nonreplicating persistent-like phenotype, antibiotic tolerance, and some hypervirulent features, targeting ILI metabolism may be viewed as a potent antivirulence strategy and/or a potential therapeutic option in the context of mycobacterial-related diseases. Therefore, dissecting the fundamental contribution of each of these proteins at the molecular and cellular level should be considered as a top priority.

Identification of structural motifs and molecular binding features of ILI-associated proteins—Amphipathic helices and the case of Tgs1

Understanding how ILI-associated proteins bind to the lipid surface of these organelles represents a real challenge. However, pioneering studies have proposed several mechanisms by which these proteins interact with ILI.

Since the phospholipid monolayer constitutes the main biological interface, LD- or ILI-associated proteins must display well-defined physico-chemical and/or structural properties to interact with such surface. Indeed, electrostatic interactions, hydrophobic binding regions, β-hairpins, and amphipathic helices are, until today, the known patterns for LD-associated protein localization [73]. While β-hairpins have been extensively studied for protein targeting on LD [74], little is known about their role in prokaryotes, especially in mycobacteria. However, it was proposed that ILI-associated proteins found in mycobacteria heavily rely on amphipathic helices for ILI binding [32]. The presence of multiple amphipathic patterns using the Heliquest Prediction algorithm suggests that this structural motif may govern protein targeting to ILI in Msmeg [32]. This prompted us to further test this model in our dataset according to their experimental strategy and search for amphipathic motifs that could be conserved in the 168 HC ILI-associated candidate proteins. Through our analysis, we identify that approximately 56% (95/168) of the candidate proteins displayed a putative amphipathic helix. Information about each individual protein is available in the Table S4. Interestingly, these results are in accordance with previously published observations, suggesting that the presence of such motif could be important but not essential for targeting proteins to the ILI surface [32].

Among the 28 '*Lipid metabolism*' FC proteins identified as potential core components of Mtb ILIome, 20

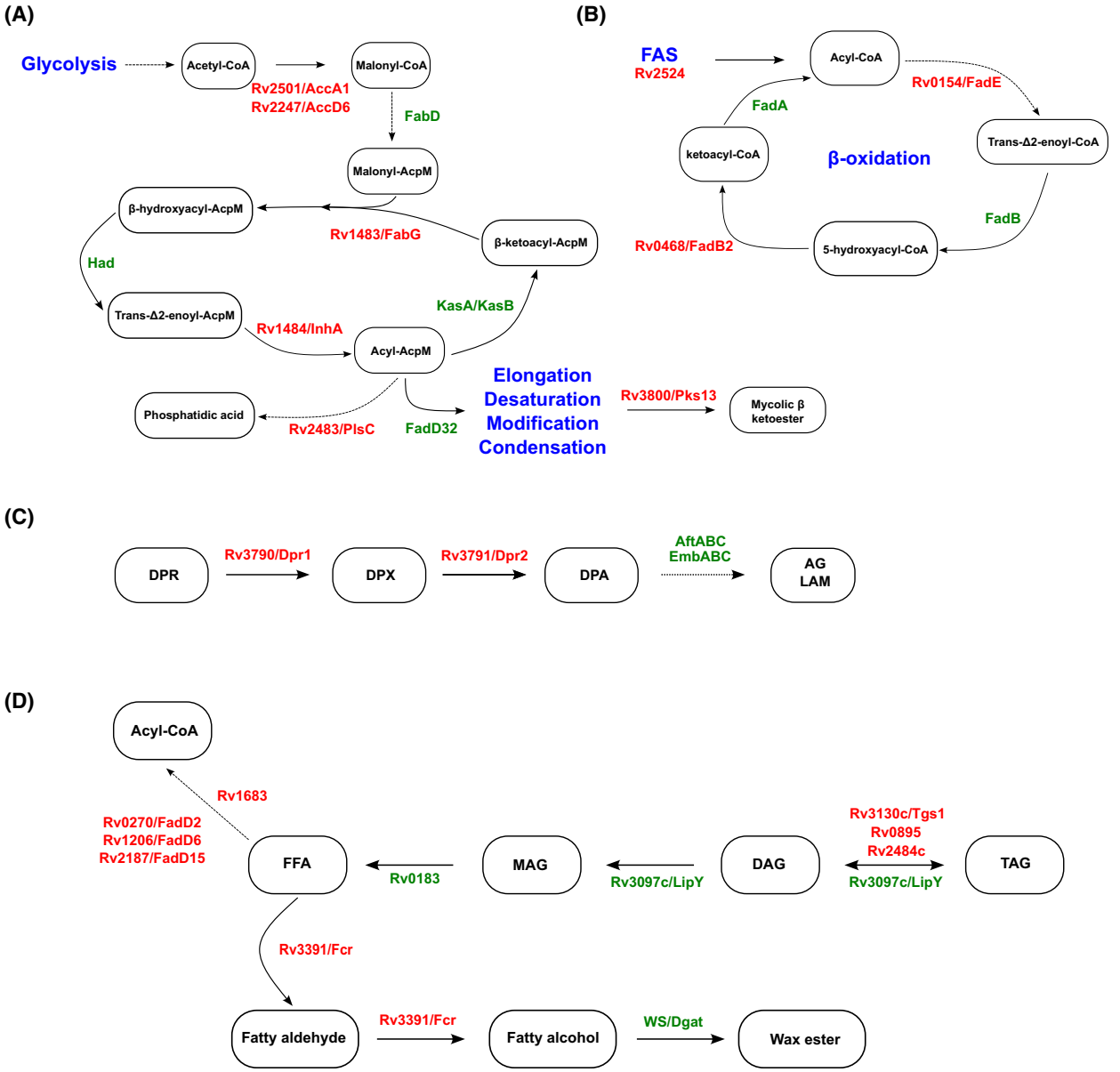

Fig. 3. Schematic representation of the major pathways containing ILI-associated proteins that belong in the '*Lipid Metabolism*' FC. Schematic representation of (A) the biosynthesis of phosphatidic acid and mycolic acids from glycolysis-derived acetyl-CoA molecules; (B) FAS and β-oxidation steps that are achieved through the action of identified ILI-associated proteins; (C) ILI-associated proteins Dpr1 and Dpr2-mediated reactions involved in arabinogalactan and lipoarabinomannan biosynthesis. (D) FFAs, glycerolipids, and wax ester metabolism mediated by ILI-associated proteins. All the proteins identified as ILI-associated are highlighted in red in the scheme, whereas other proteins are displayed in green. FAS system, decaprenylphosphoryl ribose (DPR), decaprenylphosphoryl-X (DPX), decaprenylphosphoryl-D-Araf (DPA), arabinogalactan (AG), lipoarabinomannan (LAM), FFA, monoacylglycerol (MAG), diacylglycerol (DAG), TAG, and wax ester synthase/diacylglycerol acyltransferase (WS/Dgat).

show putative amphipathic helices, possibly constituting strong binding motifs. Of note, Tgs1, the major TAG synthase in multiple mycobacterial species, possesses such a motif [31,33,35,75,76].

Since previous reports have proposed that Tgs proteins, and more particularly Tgs1, could localize and interact with the ILI surface through these conserved binding motifs involving amphipathic helices [32], we investigated whether we could identify putative ILI-binding motifs contained within the mycobacterial Tgs1 proteins. We first started with the most characterized Tgs, and confirmed the presence of a putative

amphipathic helix motif in the Tgs1 of Mtb by using Heliquest-based predictions combined with structural analysis. Results predicted an alpha-helix fold in the C-terminal region that displays putative amphipathic properties (Fig. 4A). Structural investigations using AlphaFold2 predictions confirmed that these 18 consecutive residues, formed an amphipathic patch located within an alpha-helix at the C terminus position 429–446/463 of Tgs1, which agrees with previous observations (Fig. 4B,C) [32]. Interestingly, according to the AlphaFold2 model, this C-terminal helix is predicted to be surface exposed, therefore fully accessible to bind the lipid interface without major structural rearrangements. Analysis of this C-terminal patch revealed two interfaces with well-defined biochemical properties (Fig. 4C). The first one is essentially composed of hydrophilic charged residues (ERDQ residues), which might facilitate the interaction of the protein with negatively charged phospholipid heads, other proteins, or the cytosolic environment. On the contrary, the second side is mainly composed by hydrophobic amino acids (AVIL residues) that form the putative ILI-binding motif (Fig. 4C).

Overall, this analysis suggests that these two sides may constitute a strong binding motif that facilitates the insertion of the helix into the phospholipid monolayer, enabling the enzyme's activity onto the ILI surface.

We next investigated the conservation of the amphipathic helix in other mycobacterial Tgs1 proteins. By combining PSIPred and Heliquest analysis, we identified one or two amphipathic helices, ranging from 14 to 25 residues, as putative lipid-binding sites for each of the tested Tgs1. Results from Msmeg (Fig. 4D), Mmar (Fig. 4F), and Mlep (Fig. 4H) showed that two putative motifs were detectable, with one motif that was very similar to the one identified at the C-terminal of Mtb Tgs1. Regarding Mabs and Mul, only one amphipathic motif was identified, which was not located at the C-terminal, but rather in the middle of the protein sequence (positions 273-290/476 and 196-213/463 for Mabs and Mul, respectively) (Fig. 4E,G). Using AlphaFold2 predictions, we checked that all the identified amphipathic helices were surface exposed (data not shown) and not buried within the structure or the catalytic site of the proteins. All of them were surface-exposed and, therefore, could be clearly involved in these interfacial interactions. Next, we investigated whether these candidates harbor strong hydrophobic binding regions or patches with high electrostatic potential [77,78], as observed for peripheral proteins interacting with phospholipids membrane [79]. However, we could not detect these features, suggesting that the amphipathic motifs are likely to represent the primary motif responsible for ILI targeting.

ILI-associated proteins from other functional categories—A cornerstone for metabolic adaptation?

Herein, we have listed 168 proteins that might be associated with ILI in the tubercule bacilli but also in other mycobacterial species, constituting a potential ILIome core. Unexpectedly, only 28 proteins were classified into the '*Lipid metabolism*' FC and the remaining 140 proteins (84%) belonged to 6 other FC: '*Information pathways*', '*Cell wall and cell processes*', '*Intermediary metabolism and respiration*', '*Regulatory proteins*', '*Conserved hypotheticals*', and '*Virulence, detoxification and adaptation*'. These findings clearly support the concept that has recently emerged regarding the dynamic composition and multi-faceted roles of ILI in the mycobacterial lifecycle where these structures are not just limited to lipid and energy storage [7].

Among LD-associated proteins, the first identified proteins were the perilipins (PLINs), which were described as scaffolding proteins responsible for the LD structure integrity [80–82]. These proteins play a crucial role in LD formation, maintenance, and degradation, highlighting that some key actors that are not directly involved or referenced as '*Lipid metabolism*' proteins may constitute a corner stone for TAG accumulation under the form of LD. Interestingly, structural proteins that might have a role similar to PLINs have been also identified in prokaryotes. The regulator protein TadA (named for '*triacylglycerol accumulation deficient*') was identified as essential for TAG accumulation and ILI formation in *R. opacus* PD630 [83]. Studies showed that this protein belongs to the heparin-binding family and contributes to regulating the size and shape of ILI [83]. The TadA ortholog HbhA was later identified in Msmeg [84,85]. In *R. jostii* RHA1, Ding *et al.* identified another ILI-associated protein PspA responsible for the regulation of ILI size and homeostasis [30]. A PspA ortholog was also found and recently characterized in mycobacteria where it localizes to the ILI surface, regulates their number and size, and impacts survival upon hypoxia-induced dormancy [86]. Additionally, the PLIN-like protein Rv1039c (PPE15 or MPER1) was identified in Mtb as required for optimal TAG accumulation and the display of key nonreplicating features within *in vitro* models of dormancy, including a three-dimensional human granuloma model [87].

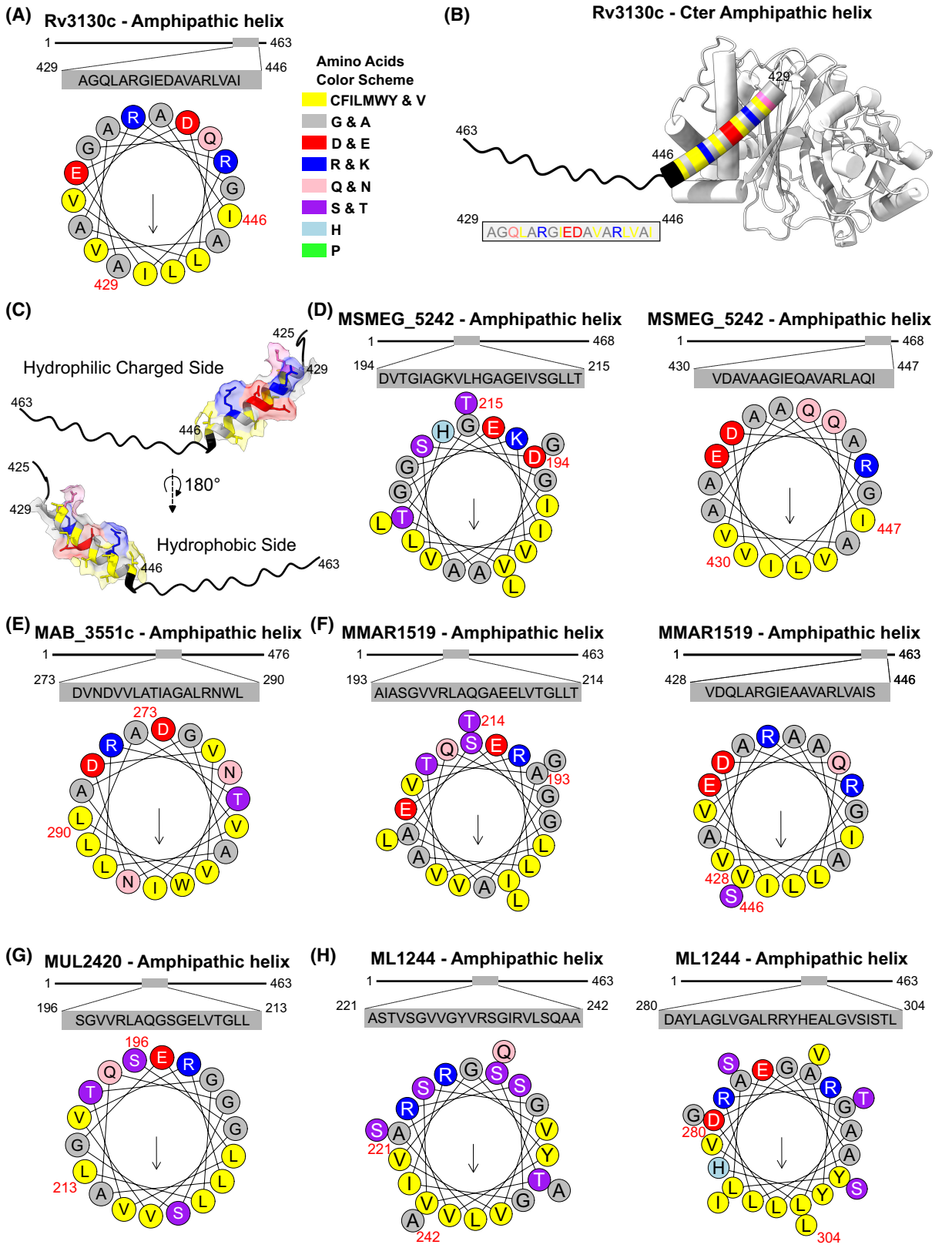
(A)
Rv3130c - Amphipathic helix
1
463
429
446
AGQLARGIEDAVARLVAI
Amino Acids
Color Scheme
CFILMWY & V
G & A
D & E
R & K
Q & N
S & T
H
P
(B)
Rv3130c - Cter Amphipathic helix
429
463
446
429
446
AGQLARGIEDAVARLVAI
(C)
Hydrophilic Charged Side
425
429
463
446
180°
425
429
Hydrophobic Side
446
463
(D)
MSMEG_5242 - Amphipathic helix
1
468
194
215
DVTGIAGKVLHGAGEIVSGLLT
MSMEG_5242 - Amphipathic helix
1
468
430
447
VDAVAAGIEQAVARLAQI
(E)
MAB_3551c - Amphipathic helix
1
476
273
290
DVNDVVLATIAGALRNWL
(F)
MMAR1519 - Amphipathic helix
1
463
193
214
AIASGVVRLAQGAEELVTGLLT
MMAR1519 - Amphipathic helix
1
463
428
446
VDQLARGIEAAVARLVAIS
(G)
MUL2420 - Amphipathic helix
1
463
196
213
SGVVRLAQGSGELVTGLL
(H)
ML1244 - Amphipathic helix
1
463
221
242
ASTVSGVVGYVRSGIRVLSQAA
ML1244 - Amphipathic helix
1
463
280
304
DAYLAGLVGALRRYHEALGVSISTL

Fig. 4. Amphipathic helices from Tgs proteins as putative ILI-binding motifs. (A) Representation of Mtb Tgs1 C-terminal amphipathic helix as a helical wheel diagram. The helix comprises residues 429 to 446/463 of the protein. The arrow indicates the angle of the mean hydrophobic moment toward the hydrophobic face of the amphipathic helix. The amino acids color code is summarized on the right part of the panel. (B) Overall view of the AlphaFold2 prediction of Mtb Tgs1 3D structural model. The protein is displayed in white with the extreme C-terminal end that is highlighted in black and the amphipathic helix (429–446) is shown as multi-colored cylinder according to the amino acids color code displayed in (A). (C) A zoomed version of the C-terminal end of Mtb Tgs1 and the amphipathic motif is displayed from two distinct views, highlighting the hydrophilic/hydrophobic sides of the helix. (D–H) Representation of Tgs1 putative amphipathic helices as helical wheel diagrams from multiple mycobacterial strains. The arrow indicates the angle of the mean hydrophobic moment toward the hydrophobic face of the amphipathic helix. The amino acids color code is summarized on the right part of the panel (A).

These observations highlight that some proteins which do not belong the '*Lipid metabolism*' FC, can have very important role in the formation, maintenance, or degradation of ILI. This idea is also supported by the recent discovery of an unconventional DNA binding feature of these membrane-less organelles. Indeed, it was established in different eukaryote organisms that LD binds to the nucleus, histones, or nucleic acids to help nuclear lipid homeostasis or even act as an antibacterial defense system [88–91]. Likewise, Zhang and collaborators demonstrated that such peculiar feature was conserved in prokaryotes, and they observed that ILI from *R. jostii* binds to DNA to prevent genotoxic stress [92]. In addition, ILI has been proposed to serve as anchor which contributes to the detoxification process upon excessive lipid or ROS levels [93]. In multiple organisms, TAG production protects against FFA and reductive stress, therefore limiting lipotoxicity [18,94,95]. Thus, it is not surprising to find that most of these proteins belong to '*Virulence, detoxification and adaptation*' and the '*Intermediary metabolism and respiration*' FC.

In summary, our analysis revealed that numerous proteins from different FCs are shared among distinct TAG-producing organisms that belong to the *Actinobacteria* phylum. These proteins are HC in Mtb, suggesting that a core of specific proteins might form a dedicated ILI-associated proteome that localizes at the surface of this particular organelle. The presence of this ILIome core reinforces the idea that ILI are not just energy storage organelles, but are more complex structures with multiple physiological functions in prokaryotes, and specifically in the mycobacterial lifestyle. Moreover, our study uncovered the presence of amphipathic helix in numerous ILI-associated proteins, prompting us and others to propose that such motif could be essential for binding and targeting ILI [32]. While these investigations and the proposed amphipathic patches-mediated binding model by which these proteins interact with the ILI surface remain hypothetic, requiring further experimental validations [32].

Finally, since conventional ILI purification strategies rely on mechanical disruption of bacterial cells followed by ultracentrifugation separation, it is very likely that the isolated ILI-associated proteomes harbor cross-contaminating proteins. This raises questions about the accuracy of these subcellular localization studies. To overcome these limitations, the development of new technological modalities that allow to noninvasively investigate ILI-associated proteome is urgently needed [8]. The recent emergence of proximity labelling technologies has the potential to circumvent these limitations and offer further insights into the exact composition of the ILIomes [31]. Furthermore, these approaches have not only the potential to prevail over some of the spatial limitations, but they should open new avenues regarding the temporal dynamics of ILI-associated protein recruitment. In that context, we believe that such proximity labelling techniques should be implemented at different stages of organelle formation and consumption, to finely dissect the dynamics interactions that occur at the ILI surface.

We hope that this study will provide relevant information and concepts in order to further delineate and investigate the nature and function of ILI-associated proteins in Mtb and other mycobacterial species, and will contribute to a better understanding of the cellular and molecular mechanisms underlying ILI biology.

Acknowledgments

We would like to acknowledge all members of the Lipolysis and Bacterial Pathogenicity group and the LISM unit for continuous support and insightful discussions. Work performed in the Lipolysis and Bacterial Pathogenicity group is supported by the Centre National de la Recherche Scientifique (CNRS) and the Université d'Aix-Marseille (AMU). SC and LK received financial support from the Agence Nationale de la Recherche (ANR) (ILIome—20-CE44-0019). PS received financial support from the Institut des Sciences Biologiques (INSB), the Agence Nationale de Recherches sur le Sida et les Hépatites virales (ANRS) (project no. ANRS0358). PS also received support from the French government under the France 2030 investment plan, as part of the Initiative d'Excellence

d'Aix-Marseille Université—A*MIDEX and is part of the Institute of Microbiology, Bioenergies and Biotechnology—IM2B (AMX-19-IET-006). TD PhD fellowship was funded by the foundation IHU Méditerranée Infection.

Conflict of interest

The authors declare no conflict of interest.

Peer review

The peer review history for this article is available at https://www.webofscience.com/api/gateway/wos/peer-review/10.1002/2211-5463.13721.

Data accessibility

Any additional data that support the findings of this study are available upon reasonable request from the corresponding authors at canaan@imm.cnrs.fr or psantucci@imm.cnrs.fr.

Authors contributions

PS proposed conceived and led the study. SC secured funding and co-advised this work with LK. TD and IM performed most of the *in silico* analysis with the guidance of PS and SC. PS and TD edited the figures. All authors provided intellectual input by organizing, analyzing, and/or discussing data. PS wrote the manuscript with input from TD, LK, and SC. All authors read the manuscript and provided critical feedback before its submission.

References

1 Murphy DJ and Vance J (1999) Mechanisms of lipid-body formation. *Trends Biochem Sci* **24**, 109–115.
2 Lundquist PK, Shivaiah KK and Espinoza-Corral R (2020) Lipid droplets throughout the evolutionary tree. *Prog Lipid Res* **78**, 101029.
3 Murphy DJ (2001) The biogenesis and functions of lipid bodies in animals, plants and microorganisms. *Prog Lipid Res* **40**, 325–438.
4 Alvarez HM and Steinbuchel A (2002) Triacylglycerols in prokaryotic microorganisms. *Appl Microbiol Biotechnol* **60**, 367–376.
5 Alvarez HM (2016) Triacylglycerol and wax ester-accumulating machinery in prokaryotes. *Biochimie* **120**, 28–39.
6 Waltermann M and Steinbuchel A (2005) Neutral lipid bodies in prokaryotes: recent insights into structure, formation, and relationship to eukaryotic lipid depots. *J Bacteriol* **187**, 3607–3619.
7 Mallick I, Santucci P, Poncin I, Point V, Kremer L, Cavalier JF and Canaan S (2021) Intrabacterial lipid inclusions in mycobacteria: unexpected key players in survival and pathogenesis? *FEMS Microbiol Rev* **45**, fuab029
8 Dargham T, Mallick I, Raze D, Kremer L and Canaan SJ (2022) Intrabacterial lipid inclusions: overview of an amazing organelle, 253–269.
9 Zhang C and Liu P (2017) The lipid droplet: a conserved cellular organelle. *Protein Cell* **8**, 796–800.
10 Kremer L, de Chastellier C, Dobson G, Gibson KJ, Bifani P, Balor S, Gorvel JP, Locht C, Minnikin DE and Besra GS (2005) Identification and structural characterization of an unusual mycobacterial monomeromycolyl-diacylglycerol. *Mol Microbiol* **57**, 1113–1126.
11 Alvarez HM, Mayer F, Fabritius D and Steinbuchel A (1996) Formation of intracytoplasmic lipid inclusions by *Rhodococcus opacus* strain PD630. *Arch Microbiol* **165**, 377–386.
12 Alvarez HM, Kalscheuer R and Steinbuchel A (2000) Accumulation and mobilization of storage lipids by *Rhodococcus opacus* PD630 and *Rhodococcus ruber* NCIMB 40126. *Appl Microbiol Biotechnol* **54**, 218–223.
13 Garton NJ, Christensen H, Minnikin DE, Adegbola RA and Barer MR (2002) Intracellular lipophilic inclusions of mycobacteria in vitro and in sputum. *Microbiology* **148**, 2951–2958.
14 Santucci P, Johansen MD, Point V, Poncin I, Viljoen A, Cavalier JF, Kremer L and Canaan S (2019) Nitrogen deprivation induces triacylglycerol accumulation, drug tolerance and hypervirulence in mycobacteria. *Sci Rep* **9**, 8667.
15 Dhouib R, Ducret A, Hubert P, Carriere F, Dukan S and Canaan S (2011) Watching intracellular lipolysis in mycobacteria using time lapse fluorescence microscopy. *Biochim Biophys Acta* **1811**, 234–241.
16 Low KL, Rao PS, Shui G, Bendt AK, Pethe K, Dick T and Wenk MR (2009) Triacylglycerol utilization is required for regrowth of in vitro hypoxic nonreplicating *Mycobacterium bovis* bacillus Calmette-Guerin. *J Bacteriol* **191**, 5037–5043.
17 Waltermann M, Hinz A, Robenek H, Troyer D, Reichelt R, Malkus U, Galla HJ, Kalscheuer R, Stoveken T, von Landenberg P *et al.* (2005) Mechanism of lipid-body formation in prokaryotes: how bacteria fatten up. *Mol Microbiol* **55**, 750–763.
18 Rodriguez JG, Hernandez AC, Helguera-Repetto C, Aguilar Ayala D, Guadarrama-Medina R, Anzola JM, Bustos JR, Zambrano MM, Gonzalez YMJ, Garcia MJ *et al.* (2014) Global adaptation to a lipid environment triggers the dormancy-related phenotype of *Mycobacterium tuberculosis*. *MBio* **5**, e01125–14.

19 McKinney JD, Honer zu Bentrup K, Munoz-Elias EJ, Miczak A, Chen B, Chan WT, Swenson D, Sacchettini JC, Jacobs WR Jr and Russell DG (2000) Persistence of *Mycobacterium tuberculosis* in macrophages and mice requires the glyoxylate shunt enzyme isocitrate lyase. *Nature* **406**, 735–738.
20 Schnappinger D, Ehrt S, Voskuil MI, Liu Y, Mangan JA, Monahan IM, Dolganov G, Efron B, Butcher PD, Nathan C *et al*. (2003) Transcriptional adaptation of *Mycobacterium tuberculosis* within macrophages: insights into the phagosomal environment. *J Exp Med* **198**, 693–704.
21 Timm J, Post FA, Bekker LG, Walther GB, Wainwright HC, Manganelli R, Chan WT, Tsenova L, Gold B, Smith I *et al*. (2003) Differential expression of iron-, carbon-, and oxygen-responsive mycobacterial genes in the lungs of chronically infected mice and tuberculosis patients. *Proc Natl Acad Sci U S A* **100**, 14321–14326.
22 Lee W, VanderVen BC, Fahey RJ and Russell DG (2013) Intracellular *Mycobacterium tuberculosis* exploits host-derived fatty acids to limit metabolic stress. *J Biol Chem* **288**, 6788–6800.
23 Nazarova EV, Montague CR, La T, Wilburn KM, Sukumar N, Lee W, Caldwell S, Russell DG and VanderVen BC (2017) Rv3723/LucA coordinates fatty acid and cholesterol uptake in *Mycobacterium tuberculosis*. *Elife* **6**, e26969.
24 Bloch H and Segal W (1956) Biochemical differentiation of *Mycobacterium tuberculosis* grown in vivo and in vitro. *J Bacteriol* **72**, 132–141.
25 Daniel J, Maamar H, Deb C, Sirakova TD and Kolattukudy PE (2011) *Mycobacterium tuberculosis* uses host triacylglycerol to accumulate lipid droplets and acquires a dormancy-like phenotype in lipid-loaded macrophages. *PLoS Pathog* **7**, e1002093.
26 Garton NJ, Waddell SJ, Sherratt AL, Lee SM, Smith RJ, Senner C, Hinds J, Rajakumar K, Adegbola RA, Besra GS *et al*. (2008) Cytological and transcript analyses reveal fat and lazy persister-like bacilli in tuberculous sputum. *PLoS Med* **5**, e75.
27 Sloan DJ, Mwandumba HC, Garton NJ, Khoo SH, Butterworth AE, Allain TJ, Heyderman RS, Corbett EL, Barer MR and Davies GR (2015) Pharmacodynamic modeling of bacillary elimination rates and detection of bacterial lipid bodies in sputum to predict and understand outcomes in treatment of pulmonary tuberculosis. *Clin Infect Dis* **61**, 1–8.
28 Mekonnen D, Derbie A, Mihret A, Yimer SA, Tonjum T, Gelaw B, Nibret E, Munshae A, Waddell SJ and Aseffa A (2021) Lipid droplets and the transcriptome of *Mycobacterium tuberculosis* from direct sputa: a literature review. *Lipids Health Dis* **20**, 129.
29 Chen Y, Ding Y, Yang L, Yu J, Liu G, Wang X, Zhang S, Yu D, Song L, Zhang H *et al*. (2014) Integrated omics study delineates the dynamics of lipid droplets in *Rhodococcus opacus* PD630. *Nucleic Acids Res* **42**, 1052–1064.
30 Ding Y, Yang L, Zhang S, Wang Y, Du Y, Pu J, Peng G, Chen Y, Zhang H, Yu J *et al*. (2012) Identification of the major functional proteins of prokaryotic lipid droplets. *J Lipid Res* **53**, 399–411.
31 Low KL, Shui G, Natter K, Yeo WK, Kohlwein SD, Dick T, Rao SP and Wenk MR (2010) Lipid droplet-associated proteins are involved in the biosynthesis and hydrolysis of triacylglycerol in *Mycobacterium bovis* bacillus Calmette-Guerin. *J Biol Chem* **285**, 21662–21670.
32 Armstrong RM, Carter DC, Atkinson SN, Terhune SS and Zahrt TC (2018) Association of Mycobacterium proteins with lipid droplets. *J Bacteriol* **200**, e00240–18.
33 Viljoen A, Blaise M, de Chastellier C and Kremer L (2016) MAB_3551c encodes the primary triacylglycerol synthase involved in lipid accumulation in *Mycobacterium abscessus*. *Mol Microbiol* **102**, 611–627.
34 Caire-Brandli I, Papadopoulos A, Malaga W, Marais D, Canaan S, Thilo L and de Chastellier C (2014) Reversible lipid accumulation and associated division arrest of *Mycobacterium avium* in lipoprotein-induced foamy macrophages may resemble key events during latency and reactivation of tuberculosis. *Infect Immun* **82**, 476–490.
35 Barisch C and Soldati T (2017) *Mycobacterium marinum* degrades both triacylglycerols and phospholipids from its dictyostelium host to synthesise its own triacylglycerols and generate lipid inclusions. *PLoS Pathog* **13**, e1006095.
36 Robbe-Saule M, Foulon M, Poncin I, Esnault L, Varet H, Legendre R, Besnard A, Grzegorzewicz AE, Jackson M, Canaan S *et al*. (2021) Transcriptional adaptation of *Mycobacterium ulcerans* in an original mouse model: new insights into the regulation of mycolactone. *Virulence* **12**, 1438–1451.
37 Mattos KA, Oliveira VG, D'Avila H, Rodrigues LS, Pinheiro RO, Sarno EN, Pessolani MC and Bozza PT (2011) TLR6-driven lipid droplets in *Mycobacterium leprae*-infected Schwann cells: immunoinflammatory platforms associated with bacterial persistence. *J Immunol* **187**, 2548–2558.
38 Bouzid F, Bregeon F, Poncin I, Weber P, Drancourt M and Canaan S (2017) *Mycobacterium canettii* infection of adipose tissues. *Front Cell Infect Microbiol* **7**, 189.
39 Santucci P, Diomande S, Poncin I, Alibaud L, Viljoen A, Kremer L, de Chastellier C and Canaan S (2018) Delineating the physiological roles of the PE and catalytic domains of LipY in lipid consumption in Mycobacterium-infected foamy macrophages. *Infect Immun* **86**, e00394–18.
40 Sheehan HL and Whitwell F (1949) The staining of tubercle bacilli with Sudan black B. *J Pathol Bacteriol* **61**, 269–271, pl.

41 Altschul SF, Gish W, Miller W, Myers EW and Lipman DJ (1990) Basic local alignment search tool. *J Mol Biol* **215**, 403–410.
42 Kanehisa M and Goto S (2000) KEGG: Kyoto encyclopedia of genes and genomes. *Nucleic Acids Res* **28**, 27–30.
43 Kapopoulou A, Lew JM and Cole ST (2011) The MycoBrowser portal: a comprehensive and manually annotated resource for mycobacterial genomes. *Tuberculosis (Edinb)* **91**, 8–13.
44 DeJesus MA, Gerrick ER, Xu W, Park SW, Long JE, Boutte CC, Rubin EJ, Schnappinger D, Ehrt S, Fortune SM *et al.* (2017) Comprehensive essentiality analysis of the *Mycobacterium tuberculosis* genome via saturating transposon mutagenesis. *MBio* **8**, e02133–16.
45 Jones DT (1999) Protein secondary structure prediction based on position-specific scoring matrices. *J Mol Biol* **292**, 195–202.
46 Buchan DWA and Jones DT (2019) The PSIPRED protein analysis workbench: 20 years on. *Nucleic Acids Res* **47**, W402–W407.
47 Gautier R, Douguet D, Antonny B and Drin G (2008) HELIQUEST: a web server to screen sequences with specific alpha-helical properties. *Bioinformatics* **24**, 2101–2102.
48 Jumper J, Evans R, Pritzel A, Green T, Figurnov M, Ronneberger O, Tunyasuvunakool K, Bates R, Zidek A, Potapenko A *et al.* (2021) Highly accurate protein structure prediction with AlphaFold. *Nature* **596**, 583–589.
49 Pettersen EF, Goddard TD, Huang CC, Meng EC, Couch GS, Croll TI, Morris JH and Ferrin TE (2021) UCSF ChimeraX: structure visualization for researchers, educators, and developers. *Protein Sci* **30**, 70–82.
50 Ding Y, Zhang S, Yang L, Na H, Zhang P, Zhang H, Wang Y, Chen Y, Yu J, Huo C *et al.* (2013) Isolating lipid droplets from multiple species. *Nat Protoc* **8**, 43–51.
51 Cole ST, Brosch R, Parkhill J, Garnier T, Churcher C, Harris D, Gordon SV, Eiglmeier K, Gas S, Barry CE 3rd *et al.* (1998) Deciphering the biology of *Mycobacterium tuberculosis* from the complete genome sequence. *Nature* **393**, 537–544.
52 Cole ST (1999) Learning from the genome sequence of *Mycobacterium tuberculosis* H37Rv. *FEBS Lett* **452**, 7–10.
53 Camus JC, Pryor MJ, Medigue C and Cole ST (2002) Re-annotation of the genome sequence of *Mycobacterium tuberculosis* H37Rv. *Microbiology* **148**, 2967–2973.
54 Cabruja M, Mondino S, Tsai YT, Lara J, Gramajo H and Gago G (2017) A conditional mutant of the fatty acid synthase unveils unexpected cross talks in mycobacterial lipid metabolism. *Open Biol* **7**, 160277.
55 Deb C, Lee CM, Dubey VS, Daniel J, Abomoelak B, Sirakova TD, Pawar S, Rogers L and Kolattukudy PE (2009) A novel in vitro multiple-stress dormancy model for *Mycobacterium tuberculosis* generates a lipid-loaded, drug-tolerant, dormant pathogen. *PLoS One* **4**, e6077.
56 Takayama K, Wang C and Besra GS (2005) Pathway to synthesis and processing of mycolic acids in *Mycobacterium tuberculosis*. *Clin Microbiol Rev* **18**, 81–101.
57 Marrakchi H, Laneelle MA and Daffe M (2014) Mycolic acids: structures, biosynthesis, and beyond. *Chem Biol* **21**, 67–85.
58 Bhatt A, Molle V, Besra GS, Jacobs WR Jr and Kremer L (2007) The *Mycobacterium tuberculosis* FAS-II condensing enzymes: their role in mycolic acid biosynthesis, acid-fastness, pathogenesis and in future drug development. *Mol Microbiol* **64**, 1442–1454.
59 Vilcheze C and Kremer L (2017) Acid-fast positive and acid-fast negative *Mycobacterium tuberculosis*: the Koch Paradox. *Microbiol Spectr* **5**, doi: 10.1128/microbiolspec.TBTB2-0003-2015
60 Rist N, Grumbach F, Cals S and Riebel J (1952) Isonicotinic acid hydrazide (INH); antituberculous activity in mice; creation of resistant strains in vitro. *Ann Inst Pasteur* **82**, 757–760.
61 Takayama K, Wang L and David HL (1972) Effect of isoniazid on the in vivo mycolic acid synthesis, cell growth, and viability of *Mycobacterium tuberculosis*. *Antimicrob Agents Chemother* **2**, 29–35.
62 Kapoor N, Pawar S, Sirakova TD, Deb C, Warren WL and Kolattukudy PE (2013) Human granuloma in vitro model, for TB dormancy and resuscitation. *PLoS One* **8**, e53657.
63 Makarov V, Manina G, Mikusova K, Mollmann U, Ryabova O, Saint-Joanis B, Dhar N, Pasca MR, Buroni S, Lucarelli AP *et al.* (2009) Benzothiazinones kill *Mycobacterium tuberculosis* by blocking arabinan synthesis. *Science* **324**, 801–804.
64 Christophe T, Jackson M, Jeon HK, Fenistein D, Contreras-Dominguez M, Kim J, Genovesio A, Carralot JP, Ewann F, Kim EH *et al.* (2009) High content screening identifies decaprenyl-phosphoribose 2′ epimerase as a target for intracellular antimycobacterial inhibitors. *PLoS Pathog* **5**, e1000645.
65 Daniel J, Deb C, Dubey VS, Sirakova TD, Abomoelak B, Morbidoni HR and Kolattukudy PE (2004) Induction of a novel class of diacylglycerol acyltransferases and triacylglycerol accumulation in *Mycobacterium tuberculosis* as it goes into a dormancy-like state in culture. *J Bacteriol* **186**, 5017–5030.
66 Sirakova TD, Dubey VS, Deb C, Daniel J, Korotkova TA, Abomoelak B and Kolattukudy PE (2006) Identification of a diacylglycerol acyltransferase gene involved in accumulation of triacylglycerol in *Mycobacterium tuberculosis* under stress. *Microbiology* **152**, 2717–2725.
67 Park HD, Guinn KM, Harrell MI, Liao R, Voskuil MI, Tompa M, Schoolnik GK and Sherman DR (2003)

Rv3133c/dosR is a transcription factor that mediates the hypoxic response of *Mycobacterium tuberculosis*. *Mol Microbiol* **48**, 833–843.
68 Boon C and Dick T (2002) *Mycobacterium bovis* BCG response regulator essential for hypoxic dormancy. *J Bacteriol* **184**, 6760–6767.
69 Reed MB, Gagneux S, Deriemer K, Small PM and Barry CE 3rd (2007) The W-Beijing lineage of *Mycobacterium tuberculosis* overproduces triglycerides and has the DosR dormancy regulon constitutively upregulated. *J Bacteriol* **189**, 2583–2589.
70 Tong J, Liu Q, Wu J, Jiang Y, Takiff HE and Gao Q (2020) *Mycobacterium tuberculosis* strains of the modern Beijing sublineage excessively accumulate triacylglycerols in vitro. *Tuberculosis* **120**, 101892.
71 Sirakova TD, Deb C, Daniel J, Singh HD, Maamar H, Dubey VS and Kolattukudy PE (2012) Wax ester synthesis is required for *Mycobacterium tuberculosis* to enter in vitro dormancy. *PLoS One* **7**, e51641.
72 Bacon J, Dover LG, Hatch KA, Zhang Y, Gomes JM, Kendall S, Wernisch L, Stoker NG, Butcher PD, Besra GS *et al*. (2007) Lipid composition and transcriptional response of *Mycobacterium tuberculosis* grown under iron-limitation in continuous culture: identification of a novel wax ester. *Microbiology* **153**, 1435–1444.
73 Dhiman R, Caesar S, Thiam AR and Schrul B (2020) Mechanisms of protein targeting to lipid droplets: a unified cell biological and biophysical perspective. *Semin Cell Dev Biol* **108**, 4–13.
74 Abell BM, Holbrook LA, Abenes M, Murphy DJ, Hills MJ and Moloney MM (1997) Role of the proline knot motif in oleosin endoplasmic reticulum topology and oil body targeting. *Plant Cell* **9**, 1481–1493.
75 Elamin AA, Stehr M and Singh M (2012) Lipid droplets and *Mycobacterium leprae* infection. *J Pathog* **2012**, 361374.
76 Liu DQ, Zhang JL, Pan ZF, Mai JT, Mei HJ, Dai Y, Zhang L and Wang QZ (2020) Over-expression of Tgs1 in *Mycobacterium marinum* enhances virulence in adult zebrafish. *Int J Med Microbiol* **310**, 151378.
77 Whited AM and Johs A (2015) The interactions of peripheral membrane proteins with biological membranes. *Chem Phys Lipids* **192**, 51–59.
78 Murray D, Arbuzova A, Honig B, McLaughlint SJC and t. i. m. (2002) The role of electrostatic and nonpolar interactions in the association of peripheral proteins with membranes. *Curr Top Membr* **52**, 277–307.
79 Santucci P, Point V, Poncin I, Guy A, Crauste C, Serveau-Avesque C, Galano JM, Spilling CD, Cavalier JF and Canaan S (2018) LipG a bifunctional phospholipase/thioesterase involved in mycobacterial envelope remodeling. *Biosci Rep* **38**, BSR20181953.
80 Kimmel AR and Sztalryd C (2016) The perilipins: major cytosolic lipid droplet-associated proteins and their roles in cellular lipid storage, mobilization, and systemic homeostasis. *Annu Rev Nutr* **36**, 471–509.
81 Greenberg AS, Egan JJ, Wek SA, Garty NB, Blanchette-Mackie EJ and Londos C (1991) Perilipin, a major hormonally regulated adipocyte-specific phosphoprotein associated with the periphery of lipid storage droplets. *J Biol Chem* **266**, 11341–11346.
82 Bickel PE, Tansey JT and Welte MA (2009) PAT proteins, an ancient family of lipid droplet proteins that regulate cellular lipid stores. *Biochim Biophys Acta* **1791**, 419–440.
83 MacEachran DP, Prophete ME and Sinskey AJ (2010) The Rhodococcus opacus PD630 heparin-binding hemagglutinin homolog TadA mediates lipid body formation. *Appl Environ Microbiol* **76**, 7217–7225.
84 Raze D, Verwaerde C, Deloison G, Werkmeister E, Coupin B, Loyens M, Brodin P, Rouanet C and Locht C (2018) Heparin-binding hemagglutinin adhesin (HBHA) is involved in intracytosolic lipid inclusions formation in mycobacteria. *Front Microbiol* **9**, 2258.
85 Lanfranconi MP and Alvarez HM (2016) Functional divergence of HBHA from *Mycobacterium tuberculosis* and its evolutionary relationship with TadA from *Rhodococcus opacus*. *Biochimie* **127**, 241–248.
86 Armstrong RM, Adams KL, Zilisch JE, Bretl DJ, Sato H, Anderson DM and Zahrt TC (2016) Rv2744c is a PspA ortholog that regulates lipid droplet homeostasis and nonreplicating persistence in *Mycobacterium tuberculosis*. *J Bacteriol* **198**, 1645–1661.
87 Daniel J, Kapoor N, Sirakova T, Sinha R and Kolattukudy P (2016) The perilipin-like PPE15 protein in *Mycobacterium tuberculosis* is required for triacylglycerol accumulation under dormancy-inducing conditions. *Mol Microbiol* **101**, 784–794.
88 Uzbekov R and Roingeard P (2013) Nuclear lipid droplets identified by electron microscopy of serial sections. *BMC Res Notes* **6**, 386.
89 Layerenza JP, Gonzalez P, Garcia de Bravo MM, Polo MP, Sisti MS and Ves-Losada A (2013) Nuclear lipid droplets: a novel nuclear domain. *Biochim Biophys Acta* **1831**, 327–340.
90 Anand P, Cermelli S, Li Z, Kassan A, Bosch M, Sigua R, Huang L, Ouellette AJ, Pol A, Welte MA *et al*. (2012) A novel role for lipid droplets in the organismal antibacterial response. *Elife* **1**, e00003.
91 Bosch M, Sanchez-Alvarez M, Fajardo A, Kapetanovic R, Steiner B, Dutra F, Moreira L, Lopez JA, Campo R, Mari M *et al*. (2020) Mammalian lipid droplets are innate immune hubs integrating cell metabolism and host defense. *Science* **370**, eaay8085.
92 Zhang C, Yang L, Ding Y, Wang Y, Lan L, Ma Q, Chi X, Wei P, Zhao Y, Steinbuchel A *et al*. (2017) Bacterial lipid droplets bind to DNA via an intermediary protein that enhances survival under stress. *Nat Commun* **8**, 15979.

93 Listenberger LL, Han X, Lewis SE, Cases S, Farese RV Jr, Ory DS and Schaffer JE (2003) Triglyceride accumulation protects against fatty acid-induced lipotoxicity. *Proc Natl Acad Sci U S A* **100**, 3077–3082.
94 Garbarino J, Padamsee M, Wilcox L, Oelkers PM, D'Ambrosio D, Ruggles KV, Ramsey N, Jabado O, Turkish A and Sturley SL (2009) Sterol and diacylglycerol acyltransferase deficiency triggers fatty acid-mediated cell death. *J Biol Chem* **284**, 30994–31005.
95 Petschnigg J, Wolinski H, Kolb D, Zellnig G, Kurat CF, Natter K and Kohlwein SD (2009) Good fat, essential cellular requirements for triacylglycerol synthesis to maintain membrane homeostasis in yeast. *J Biol Chem* **284**, 30981–30993.

Supporting information

Additional supporting information may be found online in the Supporting Information section at the end of the article.

Table S1. Computational identification of Mtb orthologous ILI-associated proteins from Rjos RHA1.

Table S2. Computational identification of Mtb orthologous ILI-associated proteins from Rop PD630.

Table S3. Computational identification of Mtb orthologous ILI-associated proteins from Msmeg mc^2 155.

Table S4. List of the 168 Mtb orthologous ILI-associated proteins that are shared in at least two or three datasets analyzed and form Mtb ILIome.

Article III

Deciphering the ILI proteome dynamics during the synthesis phase: unveiling novel therapeutic targets against mycobacteria

Tonia Dargham, John-Jairo Aguilera-Correa, Romain Avellan, Ivy Mallick, Léa Celik, Gael Brasseur, Isabelle Poncin, Vanessa Point, Stéphane Audebert, Luc Camoin, Wassim Daher, Jean-François Cavalier, Laurent Kremer, Stéphane Canaan

En préparation

Les résultats supplémentaires sont téléchargeables en cliquant ici.

Depuis maintenant quelques années, de nombreuses études sur le métabolisme des lipides intracellulaires chez les mycobactéries ont été réalisé et il a été montré que présence de ces ILI revêt d'une importance majeure pour la physiologie bactérienne. De manière générale, les GL, leurs rôles et leurs caractéristiques ont malgré tout été mieux décrits et étudiés chez les eucaryotes que chez les procaryotes,

Cependant, un certain nombre d'études ont été menées sur les actinomycètes. Une première étude en 2001 a permis de déterminer la présence des protéines associées aux ILI chez *Rhodococcus ruber* et *Rhodococcus opacus* et quelques années plus tard deux autres études ont été menées chez les mycobactéries. En 2010, Low *et al*. ont purifié les ILI formés dans le cytoplasme de *M. bovis* BCG préalablement cultivé dans des conditions hypoxiques. Les auteurs ont pu identifier 6 protéines présentes à la surface de ces ILI, dont 4 sont connues pour être impliquées dans la synthèse des TAG (tgs1, tgs2, BCG1169c, et BCG1489c) et une enzyme bifonctionnelle (BCG1721) probablement impliqué à la fois dans leur synthèse et leur dégradation. Plus récemment, une autre étude visant à identifier le protéome des ILI a été réalisée sur l'espèce saprophyte *M. smegmatis* dans des conditions riches en glycérol. Contrairement à la précédente étude, cette dernière a identifié la présence de plus de 400 protéines dans la fraction lipidique mais d'après les annotations 7% seulement s'avèreraient être potentiellement impliquées dans la synthèse des lipides. Ces différences entre les deux études pourraient s'expliquer par la méthodologie employée pour isoler les GL. En effet, la technique utilisée était basée sur une lyse mécanique des cellules par la Presse de French, suivie de plusieurs centrifugations et ultracentrifugations qui ont permis de séparer la fraction lipidique de la fraction cytosolique. Cependant, au cours de ces traitements invasifs, les protéines membranaires ainsi que les protéines hydrophobes du cytoplasme peuvent interagir de façon non covalente avec la fraction lipidique, conduisant à l'identification de nombreux faux-positifs. De plus, dans ces expériences aucune étude cinétique n'a permis de distinguer les protéines impliquées dans les phases de synthèse de celles impliquées dans les phases de dégradation des ILI.

A la vue de la quantité de lipides produit au moment de la formation des ILI, nous avons pensé que la simple analyse du le protéome total à 24 h et 48 h d'accumulation en utilisant notre modèle MSM NL nous permettrait d'identifier facilement par spectrométrie de masse les protéines associées aux ILI.

Malheureusement, il s'est avéré que ce modèle crée un remodelage du métabolisme du bacille et que les conditions nutritives imposées à la bactérie pour synthétiser les ILI se traduisent préférentiellement par une augmentation de l'expression de facteurs de transcription, des transporteurs de l'azote, et des enzymes qui métabolisent le glycérol. Par conséquent, toutes les enzymes annotées dans le métabolisme lipidique se retrouvaient masquées par les enzymes impliquées dans le métabolisme du glycérol et de l'azote.

Par conséquent l'utilisation d'une technique non invasive applicable à des cellules vivantes qui prendrait en compte la synthèse et la dégradation, permettrait une étude plus complète du protéome de ces structures lipidiques.

Parmi les techniques disponibles présentées dans la première partie des résultats (Article I, page 85), celle du marquage de proximité qui a été mis au point pour la détermination du protéome des GL chez les eucaryotes semble être un outil de choix pour déterminer le protéome de ces ILI chez les mycobactéries.

Comme indiqué précédemment, Low *et al*. ont identifiés à la surface des ILI de *M. bovis* BCG la triglycéride synthase 1 annotée BCG_3153c qui permet la conversion de DAG en TAG qui sont les composants essentiels des ILI. Cette dernière se trouve conservée chez *M. tuberculosis* (Rv3130c), *M. bovis* (BCG_3153c) et chez *M. abscessus* (MAB_3551c). De plus la construction de souches délétion chez *M. abscessus*, *M. tuberculosis* ou *M. bovis* pour le gène de *tsg1* a montré une absence quasi-totale d'ILI au niveau du cytoplasme bactérien suggérant que parmi les 7 triglycérides synthases identifiées chez *M. abscessus*, Tgs1 serait la plus importante pour la formation des ILI. Dans ce contexte, la Tgs1 est donc un candidat de choix pour étudier les phases de la synthèse des ILI et déterminer par la technique de marquage par proximité, l'ensemble des protéines présentent simultanément avec Tgs1 à la surface des ILI.

Par conséquent, en utilisant le modèle réversible développé au laboratoire pour induire l'accumulation des ILI chez *M. abscessus* ainsi que le marquage par proximité *in vivo*, nous avons pu mettre en place une cinétique d'accumulation de lipides sous un stress nutritif et identifier les protéines potentiellement associées aux ILI.

Après avoir vérifié l'homogénéité des échantillons contenant des ILI par cytométrie de flux et microscopie de fluorescence, la co-localisation de Tgs1 avec les ILI formés, puis la fonctionnalité du vecteur d'expression permettant de produire la protéine de fusion Tgs1-APEX2, des analyses de protéomique par quantification « label-free » basée sur l'intensité relative ont été réalisées. Mes résultats ont permis de montrer qu'après 24 h et 48 h d'accumulation de lipide, 123 et 143 protéines, respectivement, ont pu être identifiées. Durant cette phase de synthèse des ILI, 38 protéines sont présentes aux deux temps choisis. Ces premières données montrent que la formation des ILI est un phénomène dynamique au cours duquel de nombreux échanges protéiques ont lieu à la surface des ILI.

En utilisant les bases de données Mycobrowser et KEGG, nous avons réalisé une analyse bioinformatique qui nous a permis d'identifier les catégories fonctionnelles de ces 228 protéines.

Cependant afin de valider notre approche et déterminé leur importance dans la physiologie des ILI, nous avons sélectionnées 10 protéines ayant des annotations fonctionnelles en lien avec les voies du métabolisme des lipides.

Les 10 gènes codant ses protéines ont été fusionnés au gène de la GFP et une analyse par microscopie de fluorescence à montrer que toutes les protéines sans exception étaient co-localisées avec les ILI. La localisation de ces protéines à la surface des ILI ont permis de valider les résultats de bioinformatiques obtenus dans le second article de ma thèse.

Enfin, le rôle physiologique de chacun de ces gènes a été étudié en générant des mutants de délétions obtenus par une double recombinaison homologue. Leur capacité à former des ILI a été analysée par chromatographie sur couche mince et par microscopie de fluorescence.

Cette étude représente le premier « proxysome » des ILI chez les mycobactéries.

Deciphering the ILI proteome dynamics during the synthesis phase: unveiling novel therapeutic targets against mycobacteria

Tonia Dargham[1,2,*], John-Jairo Aguilera-Correa[3,*], Romain Avellan[1,*], Ivy Mallick[1], Léa Celik[1], Gael Brasseur[4], Isabelle Poncin[1], Vanessa Point[1], Stéphane Audebert[5], Luc Camoin[5], Wassim Daher[3], Jean-François Cavalier[1], Laurent Kremer[3] & Stéphane Canaan[1§]

[1] Aix-Marseille Univ., CNRS, LISM UMR 7255, IMM FR3479, IM2B, Marseille, France

[2] IHU Méditerranée Infection, Aix-Marseille Univ., Marseille, France

[3] Université de Montpellier, INSERM, CNRS, IRIM UMR 9004, Montpellier, France

[4] Aix-Marseille Univ., CNRS, LCB UMR 7283, IMM FR3479, IM2B, Marseille, France

[5] Aix-Marseille Univ., INSERM, CNRS, Institut Paoli-Calmettes, CRCM, Marseille, France

[*] Authors contributed equally to this work, and should be considered as first co-authors

[§] Correspondence address to Stéphane Canaan, canaan@imm.cnrs.fr.

Keywords: ILI, lipid metabolism, persistence, mycobacteria, ILI-associated proteins, proteomic, proximity labelling, APEX2.

Abstract

During infection and granuloma formation, *M. tuberculosis*, the etiological agent of tuberculosis, accumulates lipids in the form of Intrabacterial Lipid Inclusions (ILI). These ILI, facilitating bacterial evasion from the immune system, serve as essential carbon sources for their persistence. Similarly, most mycobacteria, including *M. abscessus*, a rapidly-growing non-tuberculous opportunistic pathogen prevalent in cystic fibrosis patients, can generate these lipid structures throughout their infectious cycle. In this context, identifying proteins crucial for ILI formation could unveil novel therapeutic targets for attenuating pathogenic mycobacteria.

Employing the genetic tool APEX2 and an *in vitro* model of lipid accumulation, we pinpointed 228 proteins potentially implicated in ILI synthesis. Following validation of over 10 identified targets, our investigation honed in on MAB_4532c and MAB_3486 proteins, distinct enzymes exerting significant influence on TAG accumulation. This study paves the way for enhanced comprehension of lipid metabolism and the exploration of new therapeutic targets applicable in forthcoming treatments.

Introduction

Actinobacteria accumulate neutral lipids as intrabacterial lipid inclusions (ILI) under specific environmental conditions. Unlike many microorganisms that preferentially store glycogen, polyphosphates, and polyhydroxyalkanoate, mycobacterial species, part of Actinomycetes, store triacylglycerol (TAG) in their cytoplasm during particular stress conditions [1, 2-4]. During granuloma formation in *M. tuberculosis*-infected macrophages, lipid bodies accumulate, which the bacilli exploit to synthesize ILI, enabling the pathogen to persist in a dormant state for decades within foamy macrophages (FM) [5].

ILI appear to play a crucial role in the virulence and induction of dormancy of *M. tuberculosis* [3,6]. Moreover, Deb *et al.* demonstrated increased antibiotic resistance when mycobacteria accumulate these lipids [6]. This trait extends beyond the *M. tuberculosis* complex, as all mycobacterial species tend to accumulate ILI in their cytoplasm. *M. abscessus* [7], *M. ulcerans* [8] and *M. leprae* [9] also accumulate lipids and form ILI, serving as an energy reservoir. Zebrafish infected with lipid- rich *M. abscessus* exhibit higher mortality, indicating a role for ILI in mycobacterial virulence [3,7]. Similarly, during tissue repair following *M. ulcerans* infection, the bacilli adapt by modifying their metabolic activity and nutrient sources to ensure survival in healing tissues [8]. Infected cells by *M. leprae* highlight the importance of ILI in the pathogenesis process, using host lipids for survival and inducing an inflammatory response conducive to bacilli proliferation [9]. ILI observation extends beyond pathogenic mycobacteria, as it has been described in saprophytic *M. smegmatis* since the 1970s [10,11]. Recently, ILI from *M. brumae* have been studied, indicating that numerous large ILI may confer significant advantages to the life cycle of this bacterium, serving as lipid reserves and essential metabolites [12].

The role of proteins in ILI formation, function, maintenance, and degradation, as well as their number and identification, remains poorly understood. Proteomic experiments on lipid droplets from *Rhodococcus opacus* [13] and *R. jostii* [14] identified approximately 200 distinct proteins. In mycobacteria, only two studies have been conducted: one on *M. bovis* bacillus Calmette and Guerin [15], where seven proteins related to ILI formation were identified, and a second on *M. smegmatis* [10], where the authors identified around 400 potential targets associated with ILI. A major difference between these two studies is the duration of ILI purification, leading to variations in ILI size and the number of

interacting proteins. Among these proteins, a bifunctional enzyme with a synthase domain (ACSL) in its C-terminal and a lipase domain in its N-terminal was identified among the 50 abundant proteins in *M. smegmatis* (MSMEG_3637), as well as in *M. bovis* BCG (BCG1721), increasing TAG production and degradation when overexpressed [15]. Furthermore, triglyceride synthase 1 (Tgs1) has been shown to be involved in TAG accumulation in *M. bovis* BCG [15], *M. tuberculosis* [16], and *M. abscessus* [7], as mutation drastically decreases TAG synthesis. These studies suggested a link between ILI accumulation/degradation and the action of Tgs1 and the bifunctional enzyme.

To gain insights into ILI-protein interactions and the significance of this organelle in bacteria, an *in-silico* analysis was conducted to identify a conserved ILIome in Actinobacteria, using three independent ILI-associated proteomes [17]. These bioinformatics findings revealed the presence of a conserved amphipathic helix in Tgs1 structure, potentially interacting with ILI [17]. From these observations, we inferred that Tgs1 and the bifunctional enzyme are highly conserved across all mycobacterial species and could serve as probes to elucidate the neighbouring partners involved in ILI synthesis and degradation. To pursue this, an *in-vitro* model using *M. abscessus* was employed to discern the ILI composition [3], focusing on the ILI synthesis phase and utilizing Tgs1 as a probe.

This study aimed to precisely determine the ILI proteome involved in each stage of ILI formation, comprehending the dynamics of this process and its impact on mycobacterial virulence. Unlike prior studies on *M. bovis* BCG [15] and *M. smegmatis* [10], this approach employed a non-invasive method on living mycobacteria, engaging a proximity labelling technique to identify the ILI proteome and minimize false positive hits. Compared to conventional methods like the two-hybrid system or co-immunoprecipitation coupled with mass spectrometry analysis, proximity labelling techniques offer a robust approach for proteomic mapping [18-20], aiding in deciphering the kinetics of the ILI proteome by reducing contaminations or artefacts. Using ascorbate peroxidase (APEX2) [19,21,22] fused with Tgs1, the kinetics of ILI synthesis were monitored, identifying 228 protein partners involved in lipid biosynthesis pathways. Although further studies are warranted to confirm the function and contribution of all identified targets in ILI biogenesis, we validated our approach and results on 10 selected targets. In summary, our data represents the first ILI proxisome

and provides insight into the dynamics of ILI formation, potentially paving the way for the discovery of new therapeutic targets.

Material and Methods

Bacterial strains and growth conditions

Escherichia coli DH10B cells used for cloning were grown in Luria-Bertani agar plates at 37 °C. Culture media were supplemented with 50 µg/mL Kanamycin when necessary.

M. abscessus CIP104536^T with a smooth (S) morphotype was cultivated in Middlebrook 7H9 liquid medium (BD Difco, Le Pont de Claix, France) supplemented with 0.05% Tween 80 (Sigma-Aldrich, Saint-Quentin Fallavier, France), 0.2% glycerol (Euromedex, France), and 10% oleic albumin dextrose catalase (OADC enrichment, BD Difco, France) (7H9-S^{OADC}) at 37 °C with agitation at 200 rpm.

ILI accumulation in *M. abscessus* S liquid culture was performed as previously described [3]. Briefly, from a logarithmic growth stage culture (OD_{600} ~1-1.5), *M. abscessus* S cells were harvested by centrifugation at 3,500 *g* for 10 min. Pellets were washed twice with sterile phosphate-buffered saline (PBS) (pH 7.4) containing 0.05% (*v/v*) Tween-20, then once with PBS, and finally re-suspended in PBS at a final theoretical OD_{600} of 10. This bacterial solution was used to inoculate at an initial OD_{600} of 0.1, either fresh Mineral Salt Medium (MSM) (2 g/L Na_2HPO_4, 1 g/L KH_2PO_4, 0.5 g/L NaCl, 0.2 g/L $MgSO_4$, 20 mg/L $CaCl_2$, 1 g/L NH_4Cl, and 5% glycerol) or Mineral Salt Medium Nitrogen Limited (MSM NL) containing only 0.15 g/L NH_4Cl. To prevent bacterial clumping, Tyloxapol (Sigma-Aldrich) was added at a final concentration of 0.02% (*v/v*). The MSM and MSM NL culture media were then incubated for 24 and 48 h at 37 °C under agitation (200 rpm).

Plasmid construction and cloning

Primers used in this study are described in (**Table S1**) and were synthetized by IDT (Integrated DNA Technologies). The *MAB_3551c* (*tgs1*) gene was amplified by PCR using Phusion High-Fidelity Enzyme (Thermo Fisher Scientific, Waltham, MA) and fused with *apex* or *gfp* gene, and cloned using the SLIC method [23] into the pMV306 vector containing a kanamycin resistance cassette under the endogenous promotor. The sequence of each clone was validated by GATC Eurofins, Germany.

The deletion of each selected target from the *M. abscessus* genome was performed as described previously [24]. Briefly, electrocompetent cells were transformed with pUX1-*katG-target.* Red kanamycin-resistant colonies were selected in the first round.

Positive strains underwent a second selection based on isoniazid resistance and absence of red fluorescence. Screening by PCR and sequencing validated each deletion mutant strain (**Fig S1, Table S1**).

Bacterial fixation and Nile Red staining

Bacterial cells cultured in MSM or MSM NL medium were collected by centrifugation at 3,500 *g* for 10 min at 20 °C, then fixed with 2% paraformaldehyde in PBS for 1 h at room temperature. The pellets were washed twice with PBS-Tween 80 (0.05%, *v/v*) and re-suspended in PBS to a theoretical OD_{600nm} of 10.

Detection of ILI formation in mycobacterial culture was achieved using Nile Red staining. Fixed bacterial cells (300 µL - OD_{600nm} = 10) were incubated for 20 min at 37 °C in the dark with Nile Red (15 µL - 0.5 mg/mL in ethanol, Interchim). The stained bacteria were then centrifuged for 5 min at 5,000 *g*, washed twice with 500 µL PBS-Tween 80 (0.05%, *v/v*), and re-suspended in 300 µL of PBS. The bacterial suspension was visualized at a 540 nm wavelength using an Olympus IX81 confocal microscope equipped with an UPlanSApo 100× 1.40 NA objective and operated with the FV1000 software.

Flow cytometry

Bacterial populations studied by flow cytometer were at OD_{600nm} = 0.1. Fixed cells were stained with Nile Red as described above. Density plots obtained (forward scattering FSC versus side scattering SSC signals) were gated on the population of interest, filtered to remove multiple events, and then analysed for fluorescence intensity (FL3 615/25 nm) using 488 and 561 nm lasers excitation. For each biological sample, 300,000 events were measured. Data were acquired with a S3E cell sorter (Bio-Rad), and analysed and plotted using FlowJo v10.8. Data represent at least 3 biological replicates, and statistical analyses were performed with Prism v8.2 software using two-way ANOVA.

SDS PAGE and western blot

Total lysates, at 24 h and 48 h culture in MSM or MSM NL medium, were denatured by incubating with 1× SDS loading dye for 10 min at 95 °C and subjected to dodecyl sulfate-polyacrylamide gel electrophoresis SDS-PAGE. Proteins were transferred onto 0.2 µm polyvinylidene difluoride (PVDF) using the Trans-Blot Turbo transfer system at 25 V, 1 A for 7 min (Bio-Rad, Hercules, CA). The membrane was then blocked in TBS-

T (0.3% BSA) and incubated with a primary antibody anti-APEX2 (1 µg/ml, Thermo Fisher Scientific, Waltham, MA) overnight at 4°C. After three quick washes with TBST for 10 min each, the membrane was incubated for 1 h with the secondary anti-llama antibody. Detection was achieved using the Pierce ECL Western blotting substrate solution (Thermo Fisher Scientific, Waltham, MA) and visualized using the ChemiDoc MP imaging system (Bio-Rad).

Whole cell protein extract

At each time point, cells were centrifuged, washed twice in PBS, and re-suspended in PBS-urea 8 M (Euromedex) at pH 8, then sonicated to lyse completely. The lysate was recovered after centrifugation at 4°C for 5 min at 1,300 *g*. The concentration of the supernatant was measured by Bradford technique. An SDS PAGE (any kDa) was performed for 100 µg of each lysate, and 50 µg were analyzed by mass spectrometry.

Biotinylation reaction

M. abscessus S strains harboring pMV306 plasmid were cultured in MSM and MSM NL at 37 °C under agitation at 200 rpm as previously described. Cells were harvested by centrifugation for 10 min at 3,500 *g* at 20 °C, and the pellets were washed twice with PBS and re-suspended in PBS to an OD_{600nm} of 40. One hundred millimolar of biotin phenol (Iris Biotech) was added to each vial and incubated at 37 °C, 200 rpm, in the dark for 30 min. Subsequently, 100 mM of hydrogen peroxide was added under the same conditions for exactly 2 min. The reaction was stopped by 1 mL of 2× quenching solution composed of PBS, 1 M sodium ascorbate (Sigma), and 1 M sodium azide (Sigma), followed by centrifugation at 3,500 *g* for 10 min at 20 °C. Pellets were washed twice with 1 mL of 1× quenching solution and 1 mL of PBS-Tween 80 (0.05%, *v/v*) each, and re-suspended in 2 mL ice-cold PBS-protease inhibitor cocktail (c*O*mplete Mini, EDTA-free, Sigma Aldrich) [25]. Cells were lysed using Mini-Beadbeater-96 (BioSpec) for 3×4 min with 250 µL of glass beads (0.1 mm-diameter glass beads, Biospec). The lysates were centrifuged for 5 min at 1,300 *g* at 4 °C, and the supernatant was collected. Protein concentration in each sample was measured using the Bradford technique (Bio-Rad).

Streptavidin enrichment

Twenty microliters of 10 mg/mL Streptavidin agarose resin (Thermo Fisher Scientific, Waltham, MA) were washed twice with 500 µL of PBS and centrifuged for 5 min at

5,000 *g*. In parallel, 1 µg of each lysate was heated at 95°C for 5 min. Then, washed streptavidin was mixed with each lysate and incubated under gentle rotative agitation (15 rpm) for 3 h. The beads were washed with 200 µL PBS-20% SDS and incubated for 20 min on the orbital shaker (15 rpm/min) at room temperature. The mixture was washed twice with PBS and centrifuged at 5,000 *g* for 5 min. SDS loading dye 1× was added, and the sample was boiled for 10 min at 95 °C.

Silver Staining

After electrophoresis, gels were fixed in 30% ethanol and 10% acetic acid solution for 30 min, then washed twice in 10% ethanol for 5 min each as described in the kit (Pierce, Thermo Fisher Scientific, Waltham, MA). Gels were then impregnated in silver nitrate solution for 30 min, washed, and immersed in the developer solution until bands appeared. The reaction was stopped by adding 3% acetic acid solution.

Mass spectrometry

1-Whole proteome analysis: For relative proteomic analysis, 15 µg of proteins were solubilized in LDS sample buffer (2× concentrated), (Invitrogen, Life Technologies), before loading on NuPAGE™ 4–12% Bis–tris acrylamide gels according to the manufacturer's instructions (Invitrogen, Life Technologies). Running of samples was stopped as soon as proteins stacked as a single band, and following imperial blue staining (Life Technologies), the upper part of the gel containing the proteins was cut and processed for classical in-gel digestion (washes, thiols reduction with 10 mM DTT, and cysteine alkylation with 55 mM iodoacetamide). Each band was further digested as previously described with trypsin and analyzed by liquid chromatography (LC)-tandem MS (MS/MS) using an Orbitrap Fusion Lumos Tribrid Mass Spectrometer (ThermoFisher Scientific, San Jose, CA) online with a nanoRSLC Ultimate 3000 chromatography system (ThermoFisher Scientific, Sunnyvale, CA). First, peptides were concentrated and purified on a pre-column PepMap100 C18, 2 cm × 100 µm I.D, 100 Å pore size, 5-µm particle size in solvent A (0.1% formic acid in 2% acetonitrile). In the second step, peptides were separated on a reverse phase LC EASY-Spray C18 column PepMap RSLC C18, 50cm × 75 µm I.D, 100 Å pore size, 2-µm particle size (ThermoFisher) at 300 nL/min flow rate and 40°C. After column equilibration using 4% of solvent B (20% water - 80% acetonitrile - 0.1% formic acid), peptides were eluted from the analytical column by a two-step linear gradient (2-20% acetonitrile/H_2O; 0.1% formic acid for 90 min and 20-45% acetonitrile/H_2O; 0.1% formic acid for 20 min). For

peptide ionization in the EASY-Spray nanosource in front of mass spectrometer, spray voltage was set at 2.2 kV and the capillary temperature at 275°C. The Orbitrap Lumos was used in data-independent mode with the following parameters. First, MS spectra were acquired in the Orbitrap in the range of m/z 375-1,500 at a FWHM resolution of 120,000 measured at 400 m/z. AGC target was set at standard parameters with an automatic Maximum Injection Time. MS2 spectra were acquired in the Orbitrap with a resolution of 30,000, in the mass range of 200-1,800 m/z after isolation of parent ion in the quadrupole and fragmentation in the HCD cell under collision Energy of 30%. DIA parent ion range was from 400 to 1,000 m/z divided into 40 windows 16 Da wide and from 1,000 to 1,500 m/z divided into 10 windows 50 Da wide.

Relative intensity-based label-free quantification (LFQ) was processed using the DIA-NN 1.8 algorithm. Initially, the acquired raw LC Orbitrap MS data underwent processing using the integrated Andromeda search engine. Spectra were searched against the *M. abcessus* database (UP000007137) extracted from UniProt on March 10, 2021, containing 4940 entries, with the addition of a protein contaminant bank [26]. The search parameters included: *(i)* trypsin allowing cleavage before proline; *(ii)* one missed cleavages were allowed; *(iii)* cysteine carbamidomethylation (+57.02146) as a fixed modification, and methionine oxidation (+15.99491) and N-terminal acetylation (+42.0106) as variable modifications; *(iv)* a maximum of 1 variable modification per peptide was allowed; and *(v)* a minimum peptide length was 7 amino acids and a maximum of 30 amino acids. The match between runs option was enabled to transfer identifications across different LC-MS/MS replicates based on their masses and retention time. The precursor false discovery rate was set to 1%. DIA-NN parameters were configured on Single-pass mode for Neural Network classifier, Robust LC High precision for quantification strategy, and RT-dependent mode for Cross-run normalization. A library was generated using Smart profiling set up. The primary output file from DIA-NN was further filtered at 1% FDR, and LFQ intensity was calculated using the iq package at 1% q-value [27].

Statistical analysis was conducted using the Perseus program (version 1.6.15.0) from the MaxQuant environment (http://www.maxquant.org). Quantifiable proteins were defined as those detected in above 70% of samples in one condition or more. Missing values were replaced using data imputation by randomly selecting from a normal distribution centered on the lower edge of the intensity values that simulates signals of

low abundant proteins using default parameters (a downshift of 1.8 standard deviation and a width of 0.3 of the original distribution). To determine whether a given detected protein was specifically differential, a two-sample t-test was performed using permutation-based FDR control at 0.05 and employing 250 permutations. The *p*-value was adjusted using a scaling factor s0 with a value of 1. Analysis was performed on biological triplicates, each injected twice on mass spectrometers.

2-Biotinylated proteome: Protein isolates were loaded onto NuPAGE™ 4–12% Bis–tris acrylamide gels according to the manufacturer's instructions (Invitrogen, Life Technologies). Running of samples was stopped after a short time, as soon as proteins stacked as a single band. Protein containing bands were stained with Thermo Scientific Imperial Blue, cut from the gel, and subjected to reduction and iodoacetamide alkylation, followed by digestion with high sequencing grade trypsin (Promega, Madison, WI, USA). Extracted peptides were concentrated before mass spectrometry analysis under speed-vacuum. Samples were reconstituted with 0.1% trifluoroacetic acid in 2% acetonitrile and analyzed by liquid chromatography (LC)-tandem MS (MS/MS) using a Q Exactive Plus Hybrid Quadrupole-Orbitrap online with a nanoLC Ultimate 3,000 chromatography system (Thermo Fisher Scientific™, San Jose, CA). For each biological sample, 5 microliters corresponding to 33% of the digested sample were injected in duplicate into the system. After pre-concentration and washing of the sample on an Acclaim PepMap 100 column (C18, 2 cm × 100 µm i.d. 100 Å pore size, 5 µm particle size), peptides were separated on a LC EASY-Spray column (C18, 50 cm × 75 µm i.d., 100 Å, 2 µm, 100 Å particle size) at a flow rate of 300 nL/min with a two-step linear gradient (2-22% acetonitrile/H_20; 0.1% formic acid for 100 min and 22-32% acetonitrile/H_20; 0.1% formic acid for 20 min). Peptides were ionized in the EASYSpray source, with a spray voltage set at 1.9 kV and the capillary temperature at 250°C. All samples were measured in a data-dependent acquisition mode. Each run was preceded by a blank MS run to monitor system background. Peptide masses were measured in a survey full scan (scan range 375-1,500 m/z, with 70 K FWHM resolution at m/z=400, target AGC value of 3.00×10^6 and maximum injection time of 100 ms), and the 10 most intense data-dependent precursor ions were successively fragmented in the HCD cell and measured in Orbitrap (normalized collision energy of 25%, activation time of 10 ms, target AGC value of 1.00×10^5, intensity threshold 1.00×10^4 maximum injection time 100 ms, isolation window 2 m/z, 17.5 K FWHM resolution,

scan range 200 to 2000 m/z). Dynamic exclusion was implemented with a repeat count of 1 and exclusion duration of 20 s.

Relative intensity-based label-free quantification (LFQ) was processed using the MaxLFQ algorithm available on the MaxQuant computational proteomics platform, version 1.6.3.4. Analysis was performed on three biological replicates, each injected twice into mass spectrometers. The acquired raw LC Orbitrap MS data underwent initial processing using the integrated Andromeda search engine. Spectra were searched against the *M. abcessus* database (UP000007137) extracted from UniProt on March 10, 2021, containing 4,940 entries. The false discovery rate (FDR) at the peptide and protein levels was set to 1% and determined by searching a reverse database. For protein grouping, all proteins that could not be distinguished based on their identified peptides were assembled into a single entry according to the MaxQuant rules. Statistical analysis was performed using the Perseus program (version 1.6.15) within the MaxQuant environment (http://www.maxquant.org). Quantifiable proteins were defined as those detected in above 70% of samples in one condition or more. Protein LFQ normalized intensities were base 2 logarithmized to achieve a normal distribution. Missing values were replaced using data imputation by randomly selecting from a normal distribution centered on the lower edge of the intensity values, simulating signals of low abundant proteins using default parameters (a downshift of 1.8 standard deviations and a width of 0.3 of the original distribution). To determine whether a given detected protein was specifically differential, a two-sample t-test was conducted using permutation-based FDR-control at 5 and employing 250 permutations. The p value was adjusted using a scaling factor s0 with a value of 1.

The mass spectrometry proteomics data have been deposited to the ProteomeXchange Consortium (www.proteomexchange.org) (ref: https://doi.org/10.1093/nar/gkz984) *via* the PRIDE partner repository (ref: https://doi.org/10.1093/nar/gkab1038) with the dataset identifier PXDxxxxx (Reviewer account details: **username**: xxxx / **password**: xxxx).

Lipid extraction and TLC analysis.

Mycobacterial strains were grown in MSM NL until reaching an OD_{600nm} of 1, then collected after either 24 or 48 h of culture. Cultures underwent centrifugation for 15 min at 4,000 *g* and were washed twice with water. Pellets were boiled at 95 °C for 10 min, lyophilized overnight, and weighted to determine the exact dry weight of mycobacterial

cells. Apolar lipids were extracted according to a previously described method [3]. Briefly, 2 mL of MeOH-0.3% NaCl (10:1, *v/v*) was added per 10 mg of dry extract. This saline-MeOH solution containing the bacterial dry extract was mixed for 15 min with 1 mL petroleum ether in Pyrex® tubes at room temperature using a tube rotator. After centrifugation at 3,000 *g* for 5 min, the upper organic layer was transferred to a fresh tube. This step was repeated twice. The combined organic layers containing apolar lipids were transferred to a pre-weighed vial, and the solvent was evaporated to dryness under a nitrogen stream. Finally, the resulting dry apolar lipid residue was re-suspended in dichloromethane.

The extracted lipids were analyzed by thin-layer chromatography (TLC) using glass TLC plates (TLC Silica Gel 60 F_{254}, Merck). Following eluent migration (*i.e.*, petroleum ether (40-60 °C fraction)/diethyl ether 90:10, *v*/*v*), the plates were dried at room temperature for 10 min, and then sprayed with a cupric acetate-orthophosphoric acid solution. This solution was prepared by mixing a saturated aqueous solution of cupric acetate with 85% phosphoric acid in a 1-to-1 volume ratio, followed by heating at 140 °C in an oven for 5-10 min.

Results & Discussion

1- Whole proteome analysis alone is insufficient to fully decipher the ILI proteome

In our quest to identify proteins involved in ILI synthesis, we employed an *in vitro* model established in our laboratory based on a nitrogen-limiting minimal salt medium (MSM NL) (**Fig. 1A**) [3]. Before delving into the study of ILI synthesis, our initial focus was to assess population homogeneity over time within this medium. To achieve this, we used flow cytometry analysis with Nile red staining to quantify ILI-positive bacteria *versus* ILI-negative bacteria (**Fig. 1A**). To ensure the use of a system generating a homogeneous population of lipid-rich *M. abscessus* cells, flow cytometry was leveraged to analyze bacterial populations at different time points in the two distinct media. Interestingly, the MSM NL medium induced a peculiar and highly homogeneous population characterized by a singular, well-defined Gaussian distribution at the two time points, indicating the presence of lipid-rich ILI-positive bacteria. In contrast, the control MSM consistently displayed two asymmetric Gaussian distributions, reflecting a low and heterogeneous population of lipid-poor and lipid-rich bacteria (**Fig. 1B**). Having confirmed population homogeneity in the MSM NL, we adapted the same culture workflow, culminating in bacterial lysis at 24 and 48 h of the ILI synthesis phase. This enabled us to analyze the entire proteome during TAG accumulation in the form of ILI (**Fig. 1B**). This approach allows for the investigation of the proteomic landscape during different stages of ILI synthesis in a controlled and homogeneous bacterial population.

Due to the significant lipid accumulation observed at 24 and 48 h in our MSM NL, we initially conducted a full proteome analysis, anticipating abundant presence of mycobacterial enzymes involved in ILI biosynthesis under these specific conditions. At 24 h, label-free proteomic analysis of bacteria cultured in MSM NL revealed 21 differentially expressed proteins compared to MSM, with a *p*-value threshold of ≤0.05 and a fold change (Log_2) ≥1 (**Fig. 1C**, **Table S2**). Among these proteins, only three (MAB_1066, MAB_1774, and MAB_1704c) lack orthologs in *M. tuberculosis*. Surprisingly, only two identified proteins (MAB_4455c, MAB_2258) belong to the lipid metabolism functional category.

The remaining proteins are associated with cell wall and cell processes (MAB_2448, MAB_1432, MAB_4615, MAB_1262, MAB_0356c), intermediary metabolism

(MAB_1273, MAB_0451c, MAB_0459c), virulence and detoxification processes (MAB_3904), information pathways (MAB_3100), or regulatory proteins (MAB_3099c).

At 48 h, a greater number of proteins were overproduced (**Fig. 1C**, **Table S3**). Fifty-five proteins were more abundant in MSM NL (red dots), while 22 were significantly produced in MSM (blue dots). Of particular interest, the most abundantly produced protein at 48 h is MAB_3100, an L-alanine dehydrogenase (ALD), involved in the information pathway and detected at 24 h. It has been demonstrated that during the non-replicating state, *M. tuberculosis* expresses the alanine dehydrogenase Rv2780, which shares 77.8% sequence identity with MAB_3100, and is involved in metabolic remodeling and bacterial reactivation [28]. The observed increase in MAB_3100 overproduction in *M. abscessus* suggests that, in our model, *M. abscessus* may have entered a physiological state like the persistence observed in *M. tuberculosis*. This aligns with the understanding that bacterial persistence involves adaptations to environmental stress, alterations in metabolic pathways, and a transition to a non-replicative state, often characterized by the upregulation of specific genes like *ald* [28]. The identification of other highly abundant proteins in MSM NL, including ABC transporter MAB_2262c, hypothetical protein MAB_0131c, possible siderophore-interacting protein MAB_2235, and putative polyketide synthase MAB_2119c involved in mycobactin siderophore synthesis [29], also suggests a response to iron limitation. The presence of iron-related enzymes in this context may be explained by the need for iron, which is absent in the medium. This observation aligns with the well-known strategy of bacteria to modulate the expression of iron-related proteins in response to varying iron availability in their environment. The upregulation of these proteins may be part of the bacterial adaptation to optimize iron acquisition under nitrogen-limiting conditions. Five proteins were present at both time points (MAB_3100, MAB_1704, MAB_3099, MAB_0459 and KdpB MAB_3256c). These common proteins are mainly involved in secondary metabolism or are classified as regulatory proteins. We noticed that the six proteins previously identified by Low *et al* [15] were present in our model at 48 h but not at 24 h, coinciding with the complete formation of ILI. Intriguingly, these proteins did not exhibit significant differential expression. In contrast, among the 50 highly abundant proteins identified by Armstrong *et al*. in *M. smegmatis* [10], two proteins do not have an ortholog in *M. abscessus* (MSMEG_6291, MSMEG_6049), 12 proteins were not detected at 24 and 48 h (MSMEG_1030, MSMEG_1442, MSMEG_0098,

MSMEG_4936, MSMEG_1445, MSMEG_2776, MSMEG_0023, MSMEG_1399, MSMEG_5430, MSMEG_1401, MSMEG_1368, MSMEG_4938), and all the remaining proteins were detected in our model at 24 h and 48 h. The undetected proteins are mainly involved in genetic information processing, including elongation factors or ribosomal subunits (MSMEG_1442, MSMEG_1445, MSMEG_1399, MSMEG_1368, and MSMEG_1401). Some other proteins are related to cofactors metabolism and ATP synthesis (MSMEG_4936, MSMEG_4938, MSMEG_2227, and MSMEG_5430), with one monooxygenase (MSMEG_1030), one methyltransferase (MSMEG_0098), and one uncharacterized protein (MSMEG_0023).

The identification of a significant number of ribosomal proteins (rplP, rplO, rplO, rpsL, rpsK, rpsN, rpsR, rpmG1) in MSM suggests an increased need for protein translation and synthesis. The upregulation of these ribosomal proteins may indicate an adaptive response by mycobacteria in MSM, suggesting an enhanced requirement for protein synthesis, potentially to meet specific metabolic demands or environmental challenges present in this medium. Indeed, as the nutritional content undergoes alterations, the proportions of ribosomal proteins in the proteome typically exhibit a positive correlation with growth rates[30]. The 11 remaining proteins are mainly conserved hypothetical with unknown function.

Proteins annotated with lipid metabolism orthologs from *M. tuberculosis* are found in the background of our data with a fold change (Log_2) between -0.5 and 0.5 and a *p*-value of $-Log_{10}$ (*p-value*) less than 2 (**Fig. 1C**). Furthermore, the absence of significantly produced enzymes involved in the lipid metabolism pathway suggests that TAG biosynthesis might not be the major metabolic pathway occurring in our model under the given conditions. It is plausible that other metabolic pathways take precedence, potentially aiding mycobacteria in adapting and remodeling their metabolism to persist in the nitrogen-limiting environment. This observation underscores the complexity of bacterial metabolic responses and their ability to shift priorities based on environmental cues.

Our findings revealed an enrichment of proteins attributable to the characteristics of our experimental model and the corresponding metabolic shifts. These results may lend support to the proposition that ILI serves a role beyond mere energy storage. The identification of diverse protein families in our model implies that enzymes associated

with lipid metabolism may not be the primary actors on the surface of ILI. These findings prompt us to use a more sensitive and specific technique focusing on the proximity labelling of ILI core-structure using the APEX2 technology [25], rather than a whole proteome analysis. Enriching proteins in the vicinity of the ILI would indeed provide a more targeted view, potentially revealing specific key players and pathways directly associated with lipid metabolism within this organelle. The choice of this experimental model can significantly impact the observed metabolic processes, and focusing on the ILI core-structure allows for a more nuanced exploration of the relevant proteins in this context. This approach may lead to better understand the dynamics and intricacies of lipid metabolism within the mycobacterial cells *in vivo*, offering a more accurate representation of the metabolic landscape during the ILI synthesis phase.

2- Validation of the APEX2 system for *in vitro/in vivo* biotinylation of ILI-associated proteins in *M. abscessus* using Tgs1 as bait.

To specifically identify ILI-associated proteins, we adapted the APEX2 approach in our *in vitro* model of lipid accumulation [3,21]. Having a pre-identified bait located at the ILI surface was crucial since APEX2 is mainly found in the cytoplasm [22]. To confirm Tgs1 as a genuine ILI-associated protein in *M. abscessus*, as observed in *M. bovis* BCG [15], the protein was fused with an *sf*GFP tag to facilitate colocalization investigation within ILI (**Fig. 2A**). As expected, Tgs1 was identified by western blot at both 24 and 48 h during the synthesis phase (**Fig S2**), aligning seamlessly with the selected kinetic parameters. To direct APEX2 to the ILI, we constructed an integrative plasmid containing the endogenous promotor of *tgs1* fused to *apex2* through a linker (**Fig. 2B**). Subsequent quantification of the fluorescence emitted by the Nile Red fluorophore through flow cytometry revealed higher fluorescence levels in the MSM NL at 48 h (700 a.u) compared to 24 h (150 a.u) and to MSM at 48 h (270 a.u), consistent with prior investigations (**Fig. 2B**). This ensures that the APEX2 fusion does not affect the activity of Tgs1.

In the presence of biotin phenol (BP), APEX2 generates a short-lived phenoxyl radical (15 ms) that biotinylates high-electron amino acids within a 20-nm radius **(Fig. 2C**). To reduce false-positive hits, all endogenous biotinylated proteins identified in the control group (MSM NL without BP) were removed from the analysis. Furthermore, a silver stain was conducted after streptavidin enrichment for all lysates, both with and without

biotin-phenol, to confirm that ILI-targeted APEX2 biotinylates proteins exclusively under conditions of biotin-phenol addition.

APEX2 was fused at the C-terminus domain of the bait Tgs1, expressed in *M. abscessus* strains, and grown in culture in MSM NL, pulsed with biotin-phenol and H_2O_2. Biotinylated products were enriched with streptavidin beads from cell lysates, and proteins were stripped from the beads and analyzed by LC-MS/MS. Despite alternatives to biotin for APEX2 functionalization, biotin-phenol was chosen for its robustness with our chosen proteomic analysis. Using this assay, we found 228 highly enriched proteins, with 85 proteins at 24 h, 105 at 48 h and 38 proteins present at both time points. Our results established APEX2-mediated protein tagging as a highly accurate method for localizing proteins to the ILI surface. However, some limitations can be associated with this technique. The target proteins should possess tyrosine, cysteine, histidine, or tryptophan residues at their surface to be efficiently biotinylated by BP. Furthermore, mycobacteria inherently possess biotinylated proteins, excluded from our study, which may play a role in ILI biosynthesis. A recent investigation addressed the constraints of APEX2 localization by introducing an optimized construct of a novel ascorbate peroxidase, designated APEX3 [22]. However, in our investigation, the selection of APEX2 is appropriate for probing protein-protein interactions within the cytoplasm, aligning with established methodologies employed in the examination of eukaryotic lipid droplet proteomes [18,20].

3- Using Tgs1-APEX2 to identify ILI-associated proteins

Using a recombinant *M. abscessus* strain producing Tgs1-APEX2, we subjected the prepared samples to mass spectrometry analysis following the enrichment of biotinylated proteins. Lists of identified proteins derived from the whole-cell lysates experiments are provided in **Table S4 and S5**. Using an enrichment technique allows for specificity, targeting a unique condition of proteins.

A total of 463 proteins were identified at 24 h of ILI accumulation in MSM NL. However, applying a *p*-value ≤0.05 (*i.e.*, -log (*p*-value) >1.3) and a fold change (Log_2) ≥1, we identified 123 proteins significantly more abundant in MSM NL compared to MSM. At the 48-h time point, 624 proteins were identified, with only 143 meeting the specified cut-off criteria. Of these, 123 proteins were identified at 24 and 143 at 48 h, with 38 of them present at both time points, resulting in a set of 228 distinct proteins enriched at the two time points compared to the un-induced control (**Fig. 3A**).

Among the subset of proteins, most (7/85 at 24 h, 28/105 at 48 h, and 4/38 at 24 and 48 h) were uncharacterized with unknown functions according to their orthologs in *M. tuberculosis* (**Fig. 3B**). Proteins associated with lipid metabolism were equally represented in abundance at 24 h (22/85) and 48 h (16/105), while those engaged in amino acid and carbohydrate metabolism represented 24/85, 17/105, and 10/38 respectively, of the 228 distinct proteins. (**Fig. 3B**). These findings align with our *in silico* analysis [12], where only 17% of identified proteins were classified in the lipid metabolism functional category. Therefore, these data corroborate with the newly established understanding of the physiological function of ILI, primarily designed for lipid storage but also crucial in maintaining cellular homeostasis under challenging conditions [6,31].

From the pool of 228 proteins identified during the ILI synthesis phase, we chose 10 targets for validation. These proteins were encoded by non-essential genes, shared orthologs with *M. tuberculosis* with a sequence identity of ≥ 25%, belonged to a known functional category (FC), and were annotated in the lipid metabolism category (**Table.1**). We excluded genes encoding transcription factors.

Among the selected targets, four acyl-CoA dehydrogenases (MAB_4437, MAB_3040, MAB_3481, and MAB_3486) were identified at 24 h or 48 h, along with Tgs2 (MAB_1917) (detected at 48 h) and an acyl-CoA acetyltransferase (MAB_1463). A probable enoyl-CoA hydratase (MAB_1187c) was also identified at 24 h. Two proteins with diverse functions (MAB_4532c, and MAB_2737) were common at both 24 and 48 h. Furthermore, the lipoprotein LprG (MAB_2806) was identified at 48 h, consistent with its role in TAG transportation throughout the membrane [32]. Knowing that LprG is located in the inner membrane [32], its identification with APEX2 is not surprising. We think that at 48 h, with the maximal size of ILI, the radius of action of APEX2 may biotinylate this LprG du to the tight distance between the mature ILI and the inner membrane. Only 38 proteins exhibited persistent presence throughout the entirety of the ILI biosynthesis phase, highlighting the dynamic nature of ILI synthesis [33,34]. Disparities in ILI size, composition, hydrophobicity, and surface tension between the 24 and 48 h time points suggest that certain proteins may display differential affinities for distinct lipid molecules or necessitate specific lipid anchors, beta hairpins, or helices [35,36]. Thus, employing a kinetic approach and selecting diverse time points is crucial to comprehensively unravel the entire proteome during the ILI accumulation

phase. The discussion regarding the relationship between resident proteins on the lipid droplet and the presence of an amphipathic helix responsible for their interaction aligns with previous findings [37]. It has been established that the primary mode of interaction within prokaryotes often involves these amphipathic helices [10]. Considering structural motifs, such as amphipathic helices, is essential for understanding the molecular basis of protein-lipid droplet interactions, particularly within prokaryotic systems.

To assess the potential presence of amphipathic helices in our selected candidate targets [10,17], we employed the Heliquest software. Remarkably, 7 out of 10 candidates exhibited at least one amphipathic helix, utilizing the same cut-off criteria as in our previous analyses (**Fig S3**). Notably, MAB_4532c, MAB_2806, and MAB_1917 did not manifest any amphipathic helix structures in their protein architecture. We propose that an alternative pattern could play a role in the interaction between the protein and ILI, indicating that the helix may not be a crucial component for this interaction. However, MAB_2806 does not show colocalization with ILI (**Fig S5**). Despite the conservation of an amphipathic helix in Tgs1 across various mycobacterial species [17], Tgs2 appears to deviate from this pattern (**Fig S3**). Nonetheless, a secondary structure prediction using PSI-blast based secondary structure PREDiction (PSIPRed) revealed the presence of 11 alpha-helices, 13 beta-sheets, and numerous coils in Tgs2 (**Fig S4**). However, it is still unclear what pattern is involved in the Tgs2-ILI interaction. Contrary to previous studies indicating upregulation of Tgs2 in the presence of ILI, suggesting its involvement in TAG biosynthesis [15,16,38], there is a paucity of evidence regarding its direct localization on the ILI surface. In this study, we present a qualitative colocalization of Tgs2-GFP with the ILI (**Fig S5**), albeit acknowledging the need for further investigations to validate and quantify this observation.

4- <u>What is the impact of these selected targets on ILI synthesis?</u>

In this context, the 10 selected proteins underwent overexpression and subsequent fusion with superfolder Green Fluorescent Protein (*sf*GFP) under the control of each gene's native promoter. This methodology facilitated the qualitative confirmation of their intracellular localization. In the MSM, a diffuse low fluorescence was observed, suggesting a lipid poor bacterium with a homogenous distribution of the protein (**Fig. 4A**). Conversely, in MSM NL, well-defined regions were marked by Nile Red, indicating ILI^+ bacteria with a clear colocalization of the *sf*GFP signal (**Fig. 4A, Fig S5**). Among them, 8 demonstrated successful colocalization with ILI, independently of the presence

of the amphipathic helix (MAB_3481, MAB_3486, MAB_1917, MAB_4437, MAB_1187, MAB_2737c, MAB_4532c, and MAB_3040), thereby affirming the effectiveness of APEX2 technology in investigating the formation of ILI (**Fig S5**).

To assess the impact of each designated target on the formation of ILI, homologous recombination was employed to excise the corresponding genes using the pUX1-*katG* vector as described previously [24].

Further validation was implemented to confirm that the gene deletions of these 8 selected proteins (**Fig S1**) did not significantly affect bacterial growth in all mutants (**Fig S6**). TAG accumulation was subsequently examined through thin-layer chromatography. We noticed that at 24 h of accumulation, *MAB_3040* and *MAB_4437* mutants both displayed a significant reduction in TAG levels of 40% and 32%, respectively, compared to the WT strain. Moreover, in each case, the TAG accumulation phenotype was restored with the complemented strains (**Fig. 4B**). We further thought that a double knock-out mutant (Δ2) of these two genes belonging to the same protein family and expressed at 24 h may completely abolish TAG accumulation. Interestingly, Δ2 showed a similar phenotype as the WT and the complemented strains. We also noticed that the TAG reduction observed at 24 h (**Fig. 4B**) is compensated at 48 h for each single mutant (**Fig. 4C**). We hypothesize that these proteins are not essential for TAG accumulation or present redundancy, which emphasizes the dynamism of ILI biogenesis. Three different phenotypes are present at 48 h (**Fig. 4C**). Intriguingly, some genes appeared to act as inhibitors of lipid accumulation, as their deletion led to an increase in TAG proportions, such as the acyl-CoA dehydrogenase (MAB_4437) and Tgs2 (MAB_1917), compared to the WT. Two other deletion mutants presented a significant decrease in TAG level compared to the WT and Δ*tgs1*, with a significant reduction of 57% for Δ*MAB_3486* and 49% in the Δ*MAB_4532c* mutant. The remaining mutants showed a small reduction in TAG level ranging from 25 to 40%. Taken together, these results confirm the important role of both MAB_4532c and MAB_3486 in ILI biosynthesis. Unfortunately, unlike the other 8 proteins, these two proteins are not identified in the core ILIome previously described [17]. Their absence may be related to differences in metabolism between the two genera, *Rhodococcus* and *Mycobacterium*.

In contrast, the structure of MAB_4532c, also known as Eis2 in *M. abscessus*, has been resolved, revealing its affiliation with the GNAT (GCN5-related N-

acetyltransferase) family [37]. A knock-out of this gene in *M. abscessus* showed attenuation in bacterial survival within murine macrophages [39]. Notably, Eis2 is recognized for conferring resistance to aminoglycoside antibiotics, and numerous inhibitors targeting this protein have been developed, emphasizing its potential significance as a therapeutic target against mycobacteria. Despite these advancements, the specific mechanism by which Eis2 binds to the ILI remains elusive and has yet to be elucidated. However, Willby *et al.* developed inhibitors to overcome the resistance of *M. tuberculosis* to antibiotics [40]. The use of these molecules in *M. abscessus* and in our model may yield insightful progresses. The orthologue of MAB_3486 in the *M. tuberculosis* genome is FadE24 (Rv3139), belonging to the FadE23-FadE24 complex. This protein is known to be repressed by cholesterol and to be involved in fatty acid recycling [41,42]. However, it was shown that this complex has a different catalytic activity than dehydrogenating the acyl-CoA, and it is upregulated in the presence of isoniazid [43]. Indeed, FadE23-FadE24 is under the control of SigE, required to face environmental stresses.

The recent identification of two major phosphatidic acid phosphatases (PAPs), PAP-α and PAP-β, playing a role in *de novo* TAG biosynthesis in *M. smegmatis* is noteworthy [44]. However, in our experimental conditions, these enzymes did not exhibit high abundance at any time point. This discrepancy could be attributed to the metabolic shift induced by the presence of glycerol and nitrogen in our medium, possibly diverting the pathway towards an alternative route for TAG synthesis. The interplay of medium composition and metabolic pathways highlights the complexity of lipid biosynthesis and underscores the need for nuanced interpretation in different experimental contexts.

The significance of two acyltransferases, PlsB (MAB_1984) and PlsM (MAB_0165), in the phosphatidic acid biosynthetic pathway, leading to TAG accumulation, has been highlighted in a study by Angala *et al.* [45]. The deletion of PlsM in *M. smegmatis* led to a decrease in glycerolipids esterified with saturated acyl chains. Interestingly, in our model, these two enzymes, one of which is essential, were identified at the 48 h mark of the ILI biosynthesis phase. While they did not meet the initial selection criteria for further characterization, their presence underscores their potential importance, warranting future investigation to elucidate their specific roles in the context of ILI biosynthesis.

Conclusion

Lipid droplet-associated proteins encompass a diverse array of families, including structural proteins, signaling proteins, membrane trafficking components, metabolism enzymes, proteins implicated in protein degradation, DNA-binding proteins, and several other yet-to-be-categorized families [46-48]. Although the proteins associated with ILI have not been extensively investigated, their significance is progressively gaining elucidation. Existing evidence underscores the pivotal role of mycobacterial ILI in virulence. Despite two studies on *M. smegmatis* and *M. bovis* BCG exploring ILI-associated proteins [10,15], the direct identification of proteins crucial to ILI synthesis remains incomplete. It is hypothesized that the identification of these interacting enzymes would constitute an initial stride in unraveling ILI metabolism within pathogenic mycobacteria, offering novel perspectives for the management of mycobacterial-related diseases.

In summary, by using a proximity labelling method in a model lacking nutrient/nitrogen sources and inducing ILI accumulation, we identified 228 proteins seeming to play a role in ILI biogenesis, through direct or indirect pathways. We validated that this process is dynamic and complicated, involving different protein families and redundant proteins. Based on our defined criteria, and following a TAG quantification screen, we showed that MAB_3486 and MAB_4532c may be the most important proteins in our model for ILI metabolism. This is the first complementary study on mycobacterial ILI, revealing a refined proteome that is dynamic over time. Some recent techniques can be applied to narrow down the ILI peroxisome by combining APEX2 with TurboID. This labelling method, known as TransitID could allow us to follow a specific proteome from the very beginning of biogenesis until ILI maturation.

Although there is still a lot of work missing to have a complete study and to characterize and validate the other proteins, our study opens the way for a better understanding of this process, especially mycobacterial lipid metabolism, and the discovery of new therapeutic targets that can be exploited in future treatment.

Legends

Figure 1

Whole proteome analysis. (A) Representative image of the whole proteome analysis workflow, flow cytometry workflow, and mass spectrometry workflow. **(B**) Nile red accumulation in *M. abscessus* measured by Flow cytometry: Bacterial cells were harvested at 24, 48, 56 and 66 h from MSM, fixed and stained by Nile red, washed, and diluted in PBS. A total of 300,000 events were measured for each biological sample, and Nile Red fluorescence was collected at 615/25 nm. **(C)** Volcano map of differentially expressed proteins. The blue dots represent up-regulated differentially expressed proteins in MSM, the red dots represent up-regulated differentially expressed proteins in MSM NL, and the gray dots represent non-significantly differentially expressed proteins, at 24 and 48 h of lysate analysis. Both red circles represent the location of lipid metabolism proteins. Volcano plots were generated using Volcanoser.

Figure 2

Setting up the APEX2 system. (A) Diagram of the construct encoding the endogenous promoter and full genomic sequence of *tgs1* fused to *sfGFP* in C-terminal. *M. abscessus* cells fixed in paraformaldehyde and grown in MSM and MSM NL. Fluorescence microscopy with Nile red (559/635 nm), *sf*GFP (488/510 nm), and Merge channels of Cells contain ILI colocalizing with Tgs1 are represented with scale bars of 2 µm. **(B)** Diagram of the construct encoding the native promoter and full genomic sequence of *tgs1* fused to *APEX2* by a linker. Data represent the mean of Nile Red fluorescence accumulation in three biological replicates. Statistical analyses were carried using a two ways ANOVA using a Šidák test. * *p-value* <0.05, ** *p-value* <0.01, *** *p-value* <0.001, **** *p-value* <0.0001. **(C)** A representative workflow of APEX2 action with the chosen bait (Tgs1) in green and APEX2 molecule in purple. The main amino acids interacting with Biotin-phenol are show by their chemical formula. “His” for histidine, “Cys” for cysteine, “Trp” for tryptophan, and “Tyr” for tyrosine. Silver staining of SDS-PAGE gel: representative silver-stained SDS-PAGE gel of treated (+BP) and untreated (-BP) lysate following streptavidin enrichment, at 24 and 48 h respectively. 35 ng of BSA was loaded as control. Images were taken using Chemidoc™ MP Imaging System (Bio-Rad). Color information was preserved to show the different hues

produced by the stain. No other digital manipulation was done. All blemishes, scratches and dust particles were left untouched.

Figure 3

Targets selection by APEX2. (A) ILI biosynthesis kinetic adapted from [34], followed by a Venn diagram representing selected targets at 24 h and 48 h based on a p-value threshold of 1.3 and a fold change of 1. **(B)** Distribution of the selected ILI-associated protein based on their respective KEGG pathway at each time point.

Figure 4

Validation of mutants. A) *M. abscessus* strains harboring gene overexpression fused to *sf*GFP showing colocalization with ILI. Bacteria were grown in MSM and MSM NL, fixed with 2% paraformaldehyde, colored with Nile Red, and visualized by fluorescent microscopy. Scale bars represent 2 µm. Deleted and complemented *M. abscessus* strains were grown in MSM NL and cultures were collected at 24 h **(B)** and 48 h **(C)**. After lyophilization, equal amounts of dry cells are used for apolar lipids extraction. TAG levels from each culture were analyzed by TLC. Each TLC plate is representative of individual experiments performed in triplicate. TLC densitometry analysis of relative TAG levels (%) in each strain (Y axis), with cultures from *M. abscessus* S WT used as a reference, are reported using the TAG levels of *M. abscessus* S WT in the MSM NL as 100%. Densitometry analysis is represented for samples at 48 h. black represents 100% of TAG accumulation, blue represents the strains accumulating TAG more than the WT, orange represents the higher TAG reduction, and the blue represents the reduction of TAG ranging from 25 to 40%.

Table 1

List of *M. abscessus* selected proteins enriched at the ILI in the proximity of Tgs1. The relative abundance of each protein was determined across all samples, and the Log2 fold change (Log2 FC) was determined for various sample ratios. The proteins were filtered by a minimum Log2 FC of 1 and log (p) of 1.3. Displayed here are all the *M. absce*ssus selected proteins (identified by unique peptides, protein score, and with protein) which passed the above thresholds. The time of their detection can be found

743 in the column 24 or 48h, their proteins ID and corresponding genes are listed in the
744 subsequent columns, their protein names according to Mycobrowser
745 (https://mycobrowser.epfl.ch/), and their orthologs based on the KEGG database
746 (https://www.genome.jp/kegg/) are also provided. The percentage of homology is
747 indicated in the seq-identity % column. Essentiality, as indicated by Dejesus *et al.*, and
748 the functional category according to Camus *et al.* are also annotated in the table[49,50].

749

750 **Figure 1**

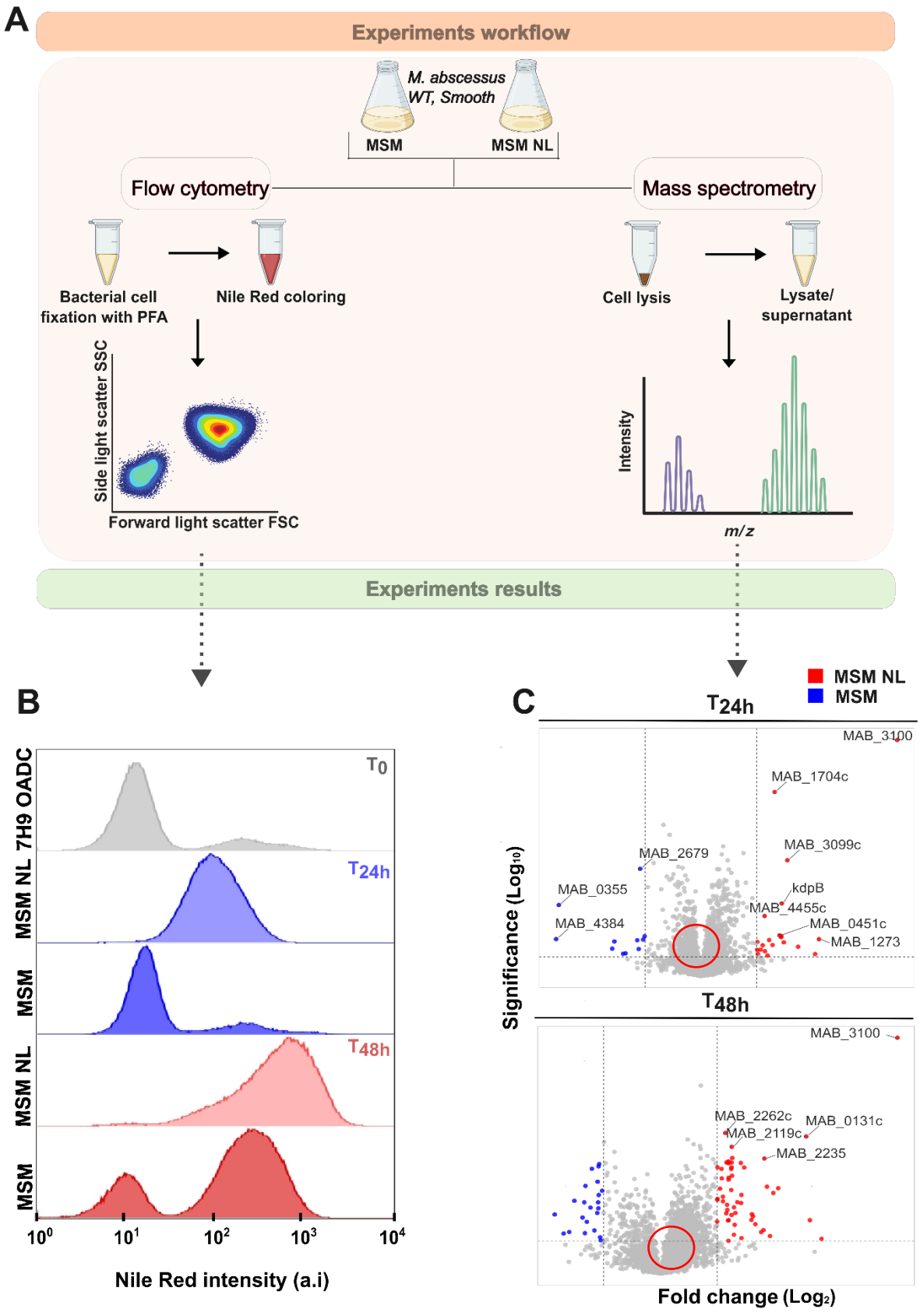

751

752

753 **Figure 2**

754

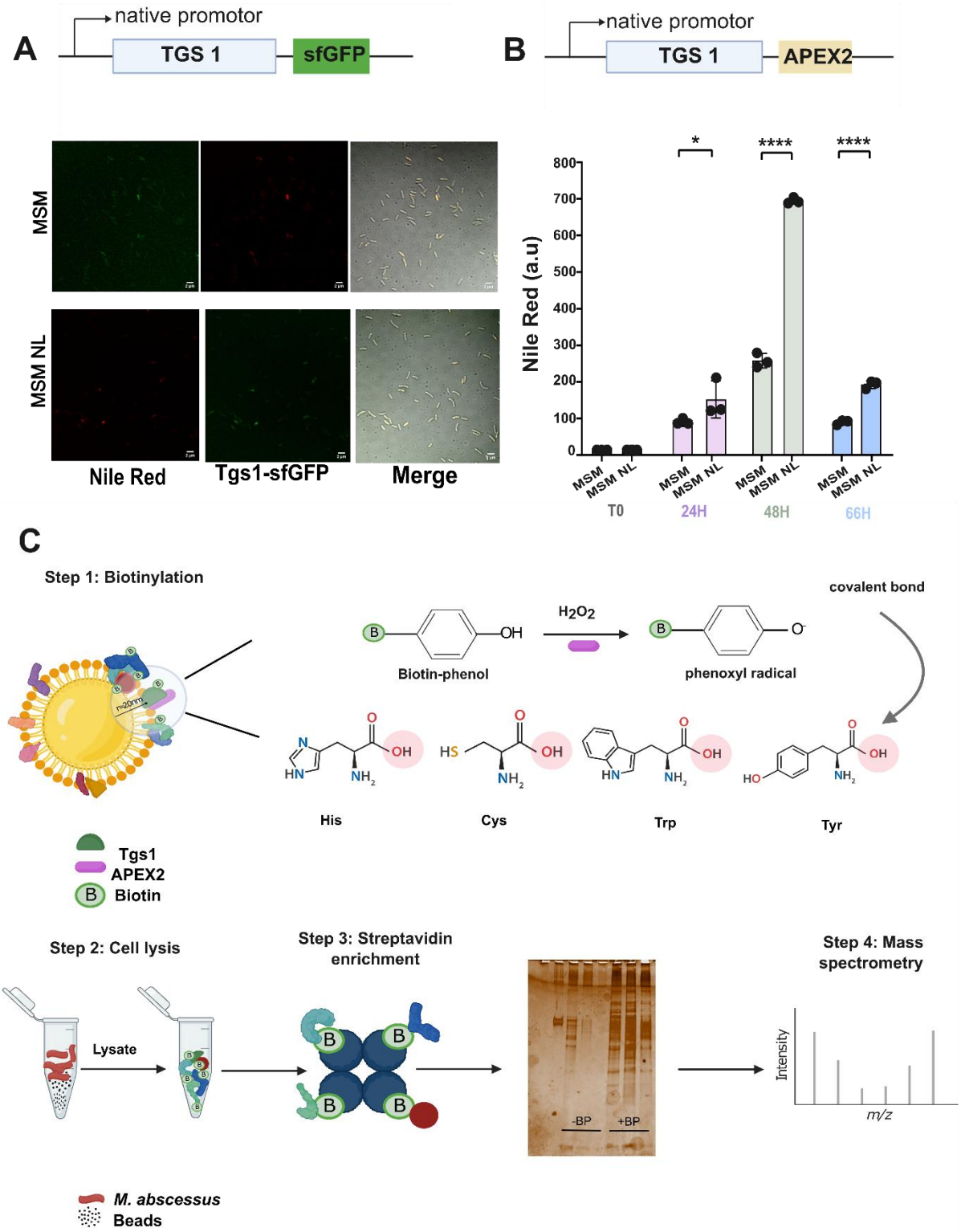

755

Table 1

24 h	48 h	Genes	Protein names	Mtb ortholog	Sequence identity%	Essentiality	Functional category
	+	*MAB_2806*	Lipoprotein LprG	Rv1411c	42.2	Non-Essential	Cell wall and cell processes
+	+	*MAB_2737C*	Probable enoyl-CoA hydratase/isomerase	Rv1472	75.7	Non-Essential	Lipid metabolism
+		*MAB_3040C*	Probable acyl-CoA dehydrogenase	Rv2724c	77.3	Non-Essential	Lipid metabolism
+		*MAB_1187C*	Probable enoyl-CoA hydratase	Rv1071c	70.5	Non-Essential	Lipid metabolism
+		*MAB_4437*	Probable acyl-CoA dehydrogenase FadE5	Rv0244c	79.1	Non-Essential	Lipid metabolism
	+	*MAB_1463*	Probable acetyl-CoA acetyltransferase FadA4	Rv1323	76.5	Non-Essential	Lipid metabolism
	+	*MAB_3148C*	Probable polyketide synthase Pks5	Rv1527c	62.4	Non-Essential	Lipid metabolism
	+	*MAB_3486*	Probable acyl-CoA dehydrogenase	Rv3139	69.4	Non-Essential	Lipid metabolism
	+	*MAB_1917*	Diacylglycerol O-acyltransferase	Rv1760	56.2	Non-Essential	Lipid metabolism
+	+	*MAB_4532C*	Uncharacterized N-acetyltransferase	Rv2416c	28.7	Non-Essential	Virulence, detoxification, adaptation

758 **Figure 3**

759

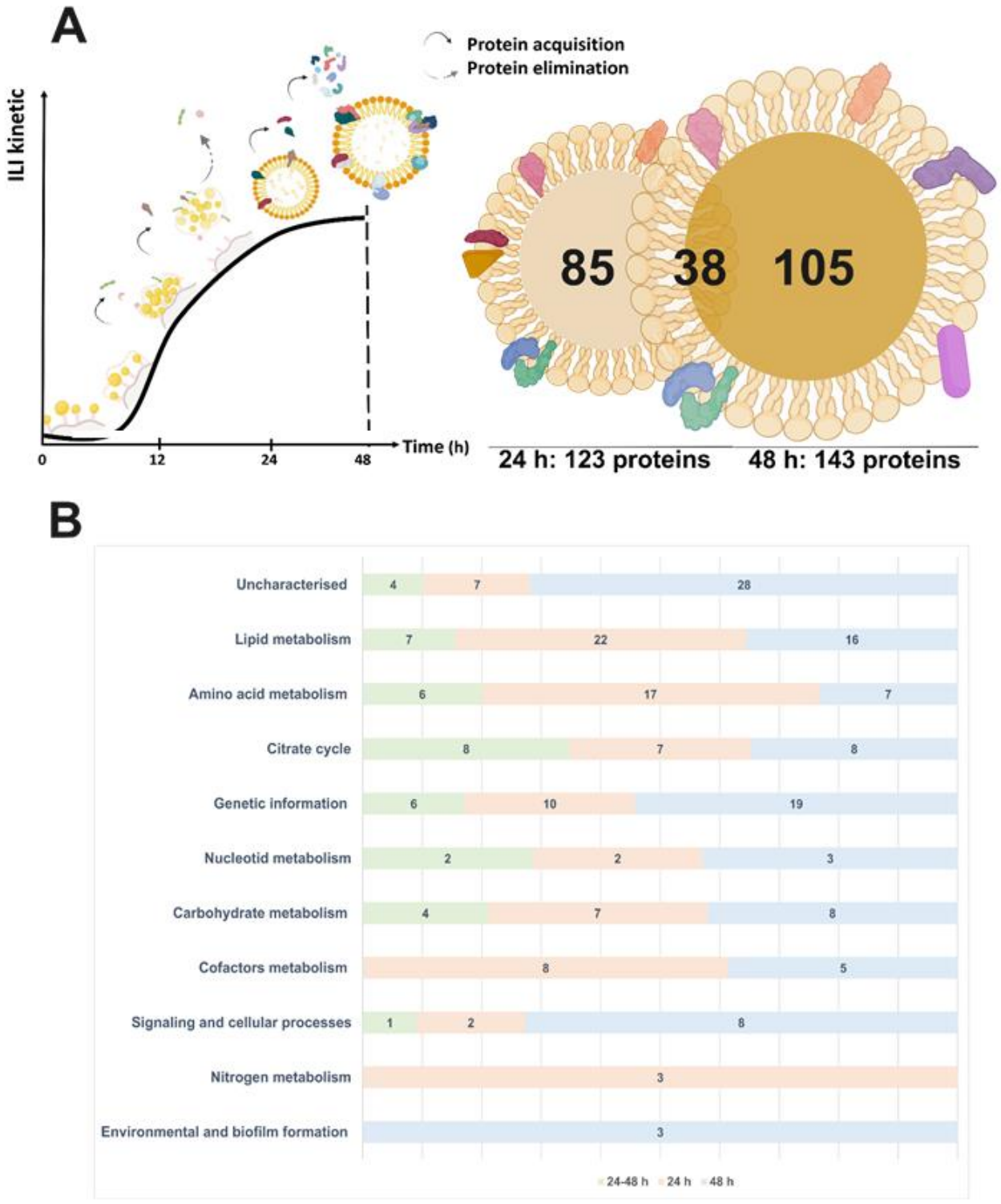

760

761 **Figure 4**

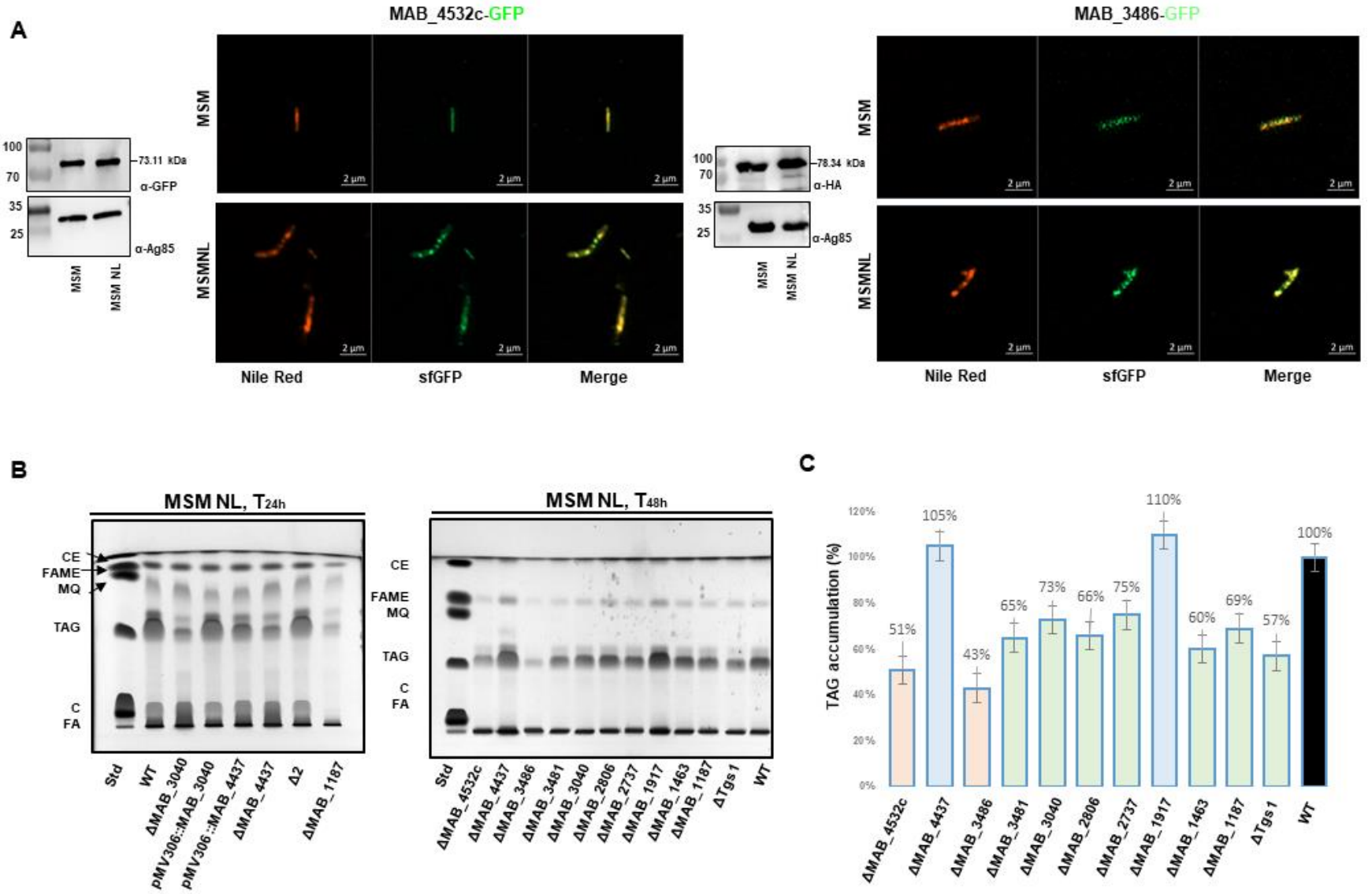

762

Acknowledgements

This work was supported by the CNRS, Aix Marseille University, and the Agence Nationale de la Recherche (LipInTB project N°ANR-19-CE44-0011, and ILIome project N°ANR-20-CE44-0019). Proteomics analyses were done using the mass spectrometry facility of Marseille Proteomics (marseille-proteomique.univ-amu.fr) supported by IBISA, the Cancéropôle PACA, the Provence-Alpes-Côte d'Azur Region, the Institut Paoli-Calmettes, and Fonds Européen de Développement Regional (FEDER). T.D. PhD fellowship was funded by the foundation IHU Méditerranée Infection. JC post doctorate fellowship was supported by the Agence Nationale de la Recherche (ILIome project N°ANR-20-CE44-0019). R.A. was supported by a PhD fellowship from the Agence Nationale de la Recherche (LipInTB project N°ANR-19-CE44-0011).

Authors' contribution

SC secured funding and supervised the study. TD and IM performed most of the analysis with the help of LC1, JJAC, IP and RA. VP help in lipidomic analysis. GB performed all the flow cytometry analysis. LC2 and SA performed all proteomic analysis with the help of JFC in the data analysis. JJAC and WD performed most of deletion mutants' construction. TD and SC edited the figures. All authors provided intellectual input by analysing and/or discussing data. TD, LK and SC wrote the initial version of the manuscript with input from all authors. All authors read the manuscript and provided critical feedback before submission.

Declaration of interests

The authors declare no competing interests.

References

1 Murphy, D. J. The biogenesis and functions of lipid bodies in animals, plants and microorganisms. *Prog Lipid Res* **40**, 325-438 (2001).

2 Wayne, L. G. & Hayes, L. G. An in vitro model for sequential study of shiftdown of Mycobacterium tuberculosis through two stages of nonreplicating persistence. *Infect Immun* **64**, 2062-2069 (1996).

3 Santucci, P. *et al.* Nitrogen deprivation induces triacylglycerol accumulation, drug tolerance and hypervirulence in mycobacteria. *Sci Rep* **9**, 019-45164 (2019).

4 Rodriguez, G. M., Voskuil, M. I., Gold, B., Schoolnik, G. K. & Smith, I. ideR, An essential gene in mycobacterium tuberculosis: role of IdeR in iron-dependent gene expression, iron metabolism, and oxidative stress response. *Infect Immun* **70**, 3371-3381 (2002).

5 Mallick, I. *et al.* Intrabacterial lipid inclusions in mycobacteria: unexpected key players in survival and pathogenesis? *FEMS Microbiol Rev* **45**, fuab029, doi:10.1093/femsre/fuab029 (2021).

6 Deb, C. *et al.* A novel in vitro multiple-stress dormancy model for Mycobacterium tuberculosis generates a lipid-loaded, drug-tolerant, dormant pathogen. *PLoS One* **4**, 0006077 (2009).

7 Viljoen, A., Blaise, M., de Chastellier, C. & Kremer, L. MAB_3551c encodes the primary triacylglycerol synthase involved in lipid accumulation in Mycobacterium abscessus. *Mol Microbiol* **102**, 611-627 (2016).

8 Robbe-Saule, M. *et al.* Transcriptional adaptation of Mycobacterium ulcerans in an original mouse model: New insights into the regulation of mycolactone. *Virulence* **12**, 1438-1451 (2021).

9 Mattos, K. A. *et al.* TLR6-driven lipid droplets in Mycobacterium leprae-infected Schwann cells: immunoinflammatory platforms associated with bacterial persistence. *J Immunol* **187**, 2548-2558 (2011).

10 Armstrong, R. M., Carter, D. C., Atkinson, S. N., Terhune, S. S. & Zahrt, T. C. Association of Mycobacterium Proteins with Lipid Droplets. *J Bacteriol* **200**, 00240-00218 (2018).

11 Barksdale, L. & Kim, K. S. Mycobacterium. *Bacteriol Rev* **41**, 217-372 (1977).

12 Campo-Pérez, V., Guallar-Garrido, S., Luquin, M., Sánchez-Chardi, A. & Julián, E. The High Plasticity of Nonpathogenic Mycobacterium brumae Induces Rapid Changes in Its Lipid Profile during Pellicle Maturation: The Potential of This Bacterium as a Versatile Cell Factory for Lipid Compounds of Therapeutic Interest. *Int J Mol Sci* **23** (2022).

13 Chen, Y. *et al.* Integrated omics study delineates the dynamics of lipid droplets in Rhodococcus opacus PD630. *Nucleic Acids Res* **42**, 1052-1064 (2014).

14 Ding, Y. *et al.* Identification of the major functional proteins of prokaryotic lipid droplets. *J Lipid Res* **53**, 399-411 (2012).

15 Low, K. L. *et al.* Lipid droplet-associated proteins are involved in the biosynthesis and hydrolysis of triacylglycerol in Mycobacterium bovis bacillus Calmette-Guerin. *J Biol Chem* **285**, 21662-21670 (2010).

16 Sirakova, T. D. *et al.* Identification of a diacylglycerol acyltransferase gene involved in accumulation of triacylglycerol in Mycobacterium tuberculosis under stress. *Microbiology* **152**, 2717-2725 (2006).

17 Dargham, T., Mallick, I., Kremer, L., Santucci, P. & Canaan, S. Intrabacterial lipid inclusion-associated proteins: a core machinery conserved from saprophyte Actinobacteria to the human pathogen Mycobacterium tuberculosis. *FEBS Open Bio* **23**, 2211-5463 (2023).

18 Bersuker, K. *et al.* A Proximity Labeling Strategy Provides Insights into the Composition and Dynamics of Lipid Droplet Proteomes. *Dev Cell* **44**, 97-112 (2018).

19 Lam, S. S. *et al.* Directed evolution of APEX2 for electron microscopy and proximity labeling. *Nat Methods* **12**, 51-54 (2015).

20 Peterson, C. W. H., Deol, K. K., To, M. & Olzmann, J. A. Optimized protocol for the identification of lipid droplet proteomes using proximity labeling proteomics in cultured human cells. *STAR Protoc* **2**, 18 (2021).

21 Ahamed, M. *et al.* in *Methods in Enzymology* Vol. 664 (ed Erin E. Carlson) 267-289 (Academic Press, 2022).

22 Becker, J. T., Auerbach, A. A. & Harris, R. S. APEX3 - An Optimized Tool for Rapid and Unbiased Proximity Labeling. *J Mol Biol* **435**, 13 (2023).

23 Li, M. Z. & Elledge, S. J. SLIC: a method for sequence- and ligation-independent cloning. *Methods Mol Biol* **852**, 51-59 (2012).

24 Richard, M. *et al.* Mutations in the MAB_2299c TetR Regulator Confer Cross-Resistance to Clofazimine and Bedaquiline in Mycobacterium abscessus. *Antimicrob Agents Chemother* **63**, 01316-01318 (2018).

25 Ganapathy, U. S. *et al.* Correction to Compartment-Specific Labeling of Bacterial Periplasmic Proteins by Peroxidase-Mediated Biotinylation. *ACS Infect Dis* **4**, 25 (2018).

26 Frankenfield, A. M., Ni, J., Ahmed, M. & Hao, L. Protein Contaminants Matter: Building Universal Protein Contaminant Libraries for DDA and DIA Proteomics. *J Proteome Res* **21**, 2104-2113 (2022).

27 Pham, T. V., Henneman, A. A. & Jimenez, C. R. iq: an R package to estimate relative protein abundances from ion quantification in DIA-MS-based proteomics. *Bioinformatics* **36**, 2611-2613 (2020).

28 Giffin, M. M., Shi, L., Gennaro, M. L. & Sohaskey, C. D. Role of Alanine Dehydrogenase of Mycobacterium tuberculosis during Recovery from Hypoxic Nonreplicating Persistence. *PLoS One* **11** (2016).

29 Etienne, G. *et al.* Identification of the polyketide synthase involved in the biosynthesis of the surface-exposed lipooligosaccharides in mycobacteria. *J Bacteriol* **191**, 2613-2621 (2009).

30 Wang, Q. & Lin, J. Environment-specificity and universality of the microbial growth law. *Commun Biol* **5**, 022-03815 (2022).

31 Cabruja, M. *et al.* A conditional mutant of the fatty acid synthase unveils unexpected cross talks in mycobacterial lipid metabolism. *Open Biol* **7**, 160277 (2017).

32 Drage, M. G. *et al.* Mycobacterium tuberculosis lipoprotein LprG (Rv1411c) binds triacylated glycolipid agonists of Toll-like receptor 2. *Nat Struct Mol Biol* **17**, 1088-1095 (2010).

33 Wältermann, M. *et al.* Mechanism of lipid-body formation in prokaryotes: how bacteria fatten up. *Mol Microbiol* **55**, 750-763 (2005).

34 Dargham, T., Mallick, I., Raze, D., Kremer, L. & Canaan, S. in *Biology of Mycobacterial Lipids* (eds Zeeshan Fatima & Stéphane Canaan) 253-269 (Academic Press, 2022).

35 Skinner, J. R. *et al.* Diacylglycerol enrichment of endoplasmic reticulum or lipid droplets recruits perilipin 3/TIP47 during lipid storage and mobilization. *J Biol Chem* **284**, 30941-30948 (2009).

36 Zhang, C. & Liu, P. The New Face of the Lipid Droplet: Lipid Droplet Proteins. *Proteomics* **19**, 8 (2019).

37 Ung, K. L., Alsarraf, H., Olieric, V., Kremer, L. & Blaise, M. Crystal structure of the aminoglycosides N-acetyltransferase Eis2 from Mycobacterium abscessus. *Febs J* **286**, 4342-4355 (2019).

38 Rastogi, S., Agarwal, P. & Krishnan, M. Y. Use of an adipocyte model to study the transcriptional adaptation of Mycobacterium tuberculosis to store and degrade host fat. *Int J Mycobacteriol* **5**, 92-98 (2016).

39 Dubois, V. *et al.* Mycobacterium abscessus virulence traits unraveled by transcriptomic profiling in amoeba and macrophages. *PLoS Pathog* **15** (2019).

40 Willby, M. J. *et al.* Potent Inhibitors of Acetyltransferase Eis Overcome Kanamycin Resistance in Mycobacterium tuberculosis. *ACS Chem Biol* **11**, 1639-1646 (2016).

41 Voskuil, M. I. Mycobacterium tuberculosis cholesterol catabolism requires a new class of acyl coenzyme A dehydrogenase. *J Bacteriol* **195**, 4319-4321 (2013).

42 Wipperman, M. F., Yang, M., Thomas, S. T. & Sampson, N. S. Shrinking the FadE proteome of Mycobacterium tuberculosis: insights into cholesterol metabolism through identification of an α2β2 heterotetrameric acyl coenzyme A dehydrogenase family. *J Bacteriol* **195**, 4331-4341 (2013).

43 Ansong, C. *et al.* Identification of widespread adenosine nucleotide binding in Mycobacterium tuberculosis. *Chem Biol* **20**, 123-133 (2013).

44 Crotta Asis, A., Savoretti, F., Cabruja, M., Gramajo, H. & Gago, G. Characterization of key enzymes involved in triacylglycerol biosynthesis in mycobacteria. *Sci Rep* **11**, 021-92721 (2021).

45 Angala, S. K. *et al.* Acylation of glycerolipids in mycobacteria. *Nat Commun* **14**, 023-42478 (2023).

46 Kimmel, A. R. & Sztalryd, C. The Perilipins: Major Cytosolic Lipid Droplet-Associated Proteins and Their Roles in Cellular Lipid Storage, Mobilization, and Systemic Homeostasis. *Annu Rev Nutr* **36**, 471-509 (2016).

47 Greenberg, A. S. *et al.* Perilipin, a major hormonally regulated adipocyte-specific phosphoprotein associated with the periphery of lipid storage droplets. *J Biol Chem* **266**, 11341-11346 (1991).

48 Bickel, P. E., Tansey, J. T. & Welte, M. A. PAT proteins, an ancient family of lipid droplet proteins that regulate cellular lipid stores. *Biochim Biophys Acta* **6**, 419-440 (2009).

49 DeJesus, M. A. *et al.* Comprehensive Essentiality Analysis of the Mycobacterium tuberculosis Genome via Saturating Transposon Mutagenesis. *mBio* **8**, 02133-02116 (2017).

50 Camus, J. C., Pryor, M. J., Médigue, C. & Cole, S. T. Re-annotation of the genome sequence of Mycobacterium tuberculosis H37Rv. *Microbiology* **148**, 2967-2973 (2002).

Article IV

Mapping of lipolytic enzymes involved in triacylglycerol accumulation as intrabacterial lipid inclusions using multi-target inhibitor-like affinity-based probes.

Romain Avellan[#], Jordan Lehoux[#], **Tonia Dargham[#]**, Léa Celik, Alexandre Guy, Isabelle Poncin, Vanessa Point, Laurent Kremer, Thierry Durand, Stéphane Audebert, Luc Camoin, Christopher D. Spilling, Céline Crauste, Stéphane Canaan, Jean-François Cavalier*.

En préparation

Les résultats supplémentaires sont téléchargeables en cliquant ici.

En plus de l'utilisation des marquages de proximité, le développement d'inhibiteurs de la formation ou la dégradation des ILI, est une autre voie que nous avons prospectée pour étudier le métabolisme des lipides. En effet, au laboratoire nous avons découvert des inhibiteurs spécifiques d'enzyme à sérine ou cystéine qui avaient la capacité de bloquer la synthèse des TAG ainsi que leur dégradation. Ces composés qui sont des analogues d'Oxadiazolones (OX) et de Cyclophostines/Cyclipostins (CyC) sont des inhibiteurs multi-cibles qui forment une liaison covalente avec la sérine ou la cystéine catalytique de leurs enzymes cibles. Des études bioinformatiques ont montré que la plupart de ces enzymes présentent un repliement α/β-hydrolase, et possèdent diverses activités : hydrolases, isomérases, lyases, ligases, oxydoréductases et transférases.

En utilisant l'approche d'« Activity Based Protein Profiling », 18 et 23 cibles respectivement pour le CyC_{17} et l'HPOX ont été identifiées chez *M. tuberculosis* et 39 et 21 cibles respectivement pour le CyC_{17} et l'iB*p*PPOX chez *M. abscessus*. Parmi les protéines identifiées, plusieurs ont été validées comme cibles de nos inhibiteurs par des approches biochimiques et structurales. C'est le cas de la thioésterase-phospholipase LipG (Rv0646c), de la mycolyltransférase Ag85C (Rv0129c et MAB_0175), de la thioésterase TesA (Rv2928), et de l'hydrolase HsaD (Rv3569c). Dès lors, ces composés étant capables d'agir sur le métabolisme de lipides, ils représentent des sondes de choix pour étudier les mécanismes moléculaires utilisés par les mycobactéries dans l'acquisition des lipides de l'hôte, la synthèse, et la dégradation des ILI. C'est donc dans ce contexte que nous avons synthétisé et caractérisé, des sondes CyC et OX porteuses d'un alcyne terminal (CyC_{31yne}/$HPOX_{yne}$) de façon à effectuer la capture directe des cibles de ces composés par chimie click.

Après avoir montré que ces dérivés de CyC et d'OX avaient les mêmes activités que les molécules mères et étaient capables d'inhiber partiellement la synthèse des TAG dans notre modèle MSM-NL, nous les avons utilisés pour capturer les enzymes lipolytiques qui pourraient intervenir dans d'accumulation et la dégradation des ILI.

Des expériences de protéomique ont permis d'identifier, par le biais des deux sondes, 65 enzymes potentiellement impliquées dans la biosynthèse (24 et 48 h) des ILI chez *Mycobacterium abscessus*.

Seulement 15 protéines étaient présentes tout au long de cette phase. Ces données confortent les résultats précédents (article I et III) et démontrent, une fois de plus, que la synthèse des ILI est un processus dynamique. En effet, 30% des protéines capturées par au moins une de ces sondes et potentiellement impliquées dans le métabolisme des lipides, ont été identifiées par APEX2, dont la « long-chain-fatty-acid-CoA ligase » (FadD15 annotéeMAB_1978).

La construction de souches de délétion, de complémentation et de surexpression de cette dernière a ensuite été utilisée pour valider son implication dans ce processus. En effet, la souche de délétion a présenté une réduction de 50 % des TAG, tandis que la complémentation permet de restaurer le phénotype d'accumulation de TAG. De plus, la construction d'une souche reportrice de fusion MAB_1978c-sfGFP a permis de confirmer la colocalisation de cette enzyme sur les ILI.

Ce travail a permis d'une part, de synthétiser des nouvelles molécules de CyC-yne et HPOX-yne représentant ainsi des outils performants pour identifier des cibles potentielles chez les mycobactéries. D'autre part, on a pu valider l'implication de FadD15 dans la biosynthèse des ILI chez *M. abscessus*. Des travaux complémentaires sont nécessaires pour caractériser et valider l'ensemble des protéines identifiées par ABPP. Ces investigations permettront alors de mieux comprendre le métabolisme des ILI.

Ma contribution dans ce travail a concerné la « validation des cibles », ma participation aux analyses de protéomiques, à la construction des vecteurs de complémentation et de surexpression de cibles, à la microscopie de fluorescence, ainsi qu'aux analyses des lipides par chromatographie sur couche mince. Enfin j'ai activement participé à la rédaction et la mise en forme du manuscrit.

Mapping of mycobacterial lipolytic enzymes involved in triacylglycerol accumulation as intrabacterial lipid inclusions using activity-based multi-target inhibitor probes

Romain Avellan[1,#], Jordan Lehoux[2,#], Tonia Dargham[1,3,#], Thomas Francis[1], Léa Celik[1], Alexandre Guy[2], Isabelle Poncin[1], Vanessa Point[1], Laurent Kremer[4,5], Thierry Durand[2], Stéphane Audebert[6], Luc Camoin[6], Christopher D. Spilling[7], Céline Crauste[2], Stéphane Canaan[1], Jean-François Cavalier[1]*

[1] Aix-Marseille Univ., CNRS, LISM UMR7255, IMM FR3479, Marseille, France

[2] IBMM, Univ Montpellier, CNRS, ENSCM, Montpellier, France

[3] IHU Méditerranée Infection, Aix-Marseille Univ., Marseille, France

[4] Centre National de la Recherche Scientifique UMR 9004, Institut de Recherche en Infectiologie de Montpellier (IRIM), Université de Montpellier, 1919 route de Mende, 34293, Montpellier, France

[5] INSERM, IRIM, 34293 Montpellier, France

[6] INSERM, CNRS, Institut Paoli-Calmettes, CRCM, Marseille Protéomique, Aix-Marseille Univ., France

[7] Department of Chemistry and Biochemistry, University of Missouri-St. Louis, MO, USA

[#] These authors contributed equally to this work, and should be considered as first co-authors

[*] Corresponding author: Jean-François Cavalier (jfcavalier@imm.cnrs.fr).

ABSTRACT

Mycobacterial lipids play a critical role in the physiology, life cycle and pathogenicity of mycobacteria-related diseases. They participate in host-pathogen interactions and fulfill important functions, related to virulence (reactivation and replication), adaptation to a non-replicating dormant form, cell wall biosynthesis, bacterial growth, lipid storage and degradation as intrabacterial lipid inclusions (ILI). They play also a major role in lipid metabolism for long-term survival and persistence but the enzymes involved in these processes remain largely undefined. Herein, we report the direct capture of target proteins in *Mycobacterimu abscessus* growing under carbon excess and nitrogen-deprived *in vitro* conditions that promote TAG production and ILI formation. The method developed relies on bio-orthogonal click-chemistry activity-based protein profiling (CC-ABPP) of newly synthetized Oxadiazolone (**OX**), Cyclophostin and Cyclipostins (**CyC**) probes. This approach led to the identification of a set of 65 enzymes, potentially involved in the global processes related to ILI anabolism. Among these, the long-chain-fatty-acid-CoA ligase MAB_1978c/FadD15 has been validated as a pivotal enzyme that co-localizes on ILI and as a major contributor in ILI formation in *M. abscessus*.

KEYWORDS

Activity-based protein profiling; multitarget inhibitor-like affinity-based probes; lipid metabolism; Cyclipostins and Cyclophostin; Oxadiazolone; *M. abscessus*; triacylglycerol.

INTRODUCTION

Mycobacteria are known for their unique and complex cell wall architecture [1], characterized by distinct lipid-rich outer layers, making lipid metabolism a central point of their physiological processes. One crucial aspect of all mycobacteria is their ability to metabolize host lipids and to accumulate the resulting neutral lipids in their own cytoplasm in the form of intrabacterial lipid inclusions (ILI) [2-4]. These lipid-rich organelles consist of a hydrophobic core containing neutral lipids, essentially triacylglycerol (TAG), surrounded by a phospholipid monolayer, associated with numerous proteins [5-9]. These ILI not only serve as reservoirs for energy storage and provide a platform for the synthesis and maintenance of lipids, which are essential for the adaptability and survival of mycobacteria under various environmental stresses [3, 10-11]. This is particularly true in the case of *M. tuberculosis*, the causative agent of tuberculosis (TB), where ILI play a critical role in pathogenesis of the disease by contributing to the ability of the bacillus to establish and maintain infection [10, 12-15] and to induce increased tolerance to first-line anti-TB drugs [13, 16-17].

ILI have been reported in all mycobacterial species; including pathogenic (*i.e.*, *M. canettii* [18], *M. leprae* [19], *M. avium* [11], *M. marinum* [20], *M. ulcerans* [21], and *M. tuberculosis* [7, 10, 13, 22-23]), non-tuberculous (*i.e.*, *M. abscessus* [24-25]), as well as saprophytic mycobacteria (*i.e.*, *M. smegmatis* [22, 24, 26-27]); suggests a conserved function of these organelles in the mycobacterial lifecycle and physiology [28]. Furthermore, zebrafish embryos infected with lipid-rich *M. abscessus* showed higher mortality, consistent with a role of ILI and host infection [24-25]. How these mycobacteria acquire host lipids and how ILI are formed remain largely unanswered questions. While these issues have been tackled, mostly by studying pure recombinant lipolytic enzymes secreted by mycobacteria [23, 25, 29-30], studies dedicated to the identification and characterization of proteins involved in ILI accumulation and consumption remain scarce [7, 26].

Stimulated by these observations, we developed two robust experimental models to report ILI formation and degradation, in order to mimic lipid metabolism during the dormancy and reactivation stages [31]. The first model is based on infected murine bone-marrow-derived macrophages (mBMDM) fed with Very Low-Density Lipoproteins (VLDL) to trigger the differentiation of the macrophages into foamy macrophages [11, 23]. In this specific environment, mycobacteria are able to accumulate host lipids to form ILI, and further hydrolyze these stored ILI upon removal of VLDL from the culture medium, thus mimicking reactivation and propagation of the disease. The second one is an *in vitro* and reversible model based on carbon excess and nitrogen starvation allowing *in vitro* ILI biosynthesis and hydrolysis [24]. Interestingly, we demonstrated in both models that the presence of serine-hydrolase inhibitors impaired TAG accumulation in the form of ILI as well as their further hydrolysis, confirming the involvement of lipolytic enzymes in the ILI accumulation and consumption processes. [23-24]. Most enzymes participating in ILI metabolism are members of the α/β-hydrolase fold superfamily [32-33], consisting in hydrolases, isomerases, lyases, ligases, oxidoreductases and transferases. Moreover, the hydrolase class includes esterases, dienelactone hydrolases, epoxide hydrolases, haloalkane dehalogenases, lipases, thioesterases, and peptidases [32]; all possessing a catalytic serine or cysteine residue in their active site, *i.e.*, (Ser/Cys)-based enzymes.

We have previously reported the potent antimycobacterial activity of two families of enzyme inhibitors, namely the Oxadiazolone compounds (**OX**) and the Cyclophostin & Cyclipostins analogs (**CyC**) [29]. These molecules form a covalent bond with the catalytic serine or cysteine, thereby inhibiting the activity of the corresponding (Ser/Cys)-based enzyme [29]. Non-toxic to host cell macrophages (CC_{50}>100 µM), both **OX** and **CyC** efficiently inhibited the growth of *M. tuberculosis* and *M. abscessus* in broth medium and/or within infected macrophages [29, 34-39]. A competitive activity-based protein profiling (ABPP) approach using either **CyC$_{17}$**- or **HPOX**-pre-treated *M. tuberculosis* cell culture, after enrichment with the ActivX^{TM} Desthiobiotin-FP

probe, allowed the identification of 18 and 23 distinct target proteins, respectively [36-37]. A similar competitive ABPP strategy was further applied to *M. abscessus*, resulting in 39 and 21 potential target enzymes for **CyC$_{17}$** and **iB*p*PPOX**, respectively [34, 36]. Most of the identified proteins are (Ser/Cys)-based enzymes related to global lipid metabolism (cholesterol and free fatty acid) and cell wall biosynthesis. Among them, the bifunctional thioesterase-phospholipase LipG (Rv0646c) [40], the mycolyltransferase Ag85C (Rv0129c & MAB_0175) [34, 41], the thioesterase TesA (Rv2928) [42], and the carbon-carbon hydrolase HsaD (Rv3569c) [43] have been validated as effective targets and subsequently confirmed by resolving their crystal structures in complex with **CyC$_{17}$**. Consequently, the use of these inhibitors as efficient activity-based probes (ABP) to decipher the metabolic pathways used by the mycobacteria to catabolize host derived lipids (cholesterol and fatty acids), notably by identifying key enzymes involved in the accumulation and consumption of ILI, will provide highly valuable data related to cellular and molecular mechanisms crucial for mycobacteria survival, persistence and virulence [3]. In addition, we have recently validated the use of new efficient **CyC** ABPs, obtained by direct introduction of either a Dansyl fluorescent moiety (*i.e.*, **CyC$_{31\text{-Dansyl}}$** [39]) or a terminal alkyne function (*i.e.*, **CyC$_{31\text{yne}}$** [43]), as a means to ***i)*** specifically label living mycobacterial species through the covalent binding to (Ser/Cys)-based enzymes, and ***ii)*** capture target proteins in live mycobacteria through direct click-chemistry ABPP (CC-ABPP) [39].

In the present study, we report the synthesis of two novel **OX** ABPs derived from the **HPOX** inhibitor [34, 36], and containing either a terminal alkyne function (*i.e.*, **HPOX$_{\text{yne}}$**) or a fluorescent NBD tag (*i.e.*, **HP$_{\text{-NBD-}}$OX**). The **HPOX** derivative was selected based on its moderate antibacterial activity (MIC_{50} / MIC_{90} = 92.9 / 99.9 µM) against *M. abscessus* S growth. These four **OX** & **CyC** ABPs have been further exploited to decipher ILI formation in *M. abscessus* using the nitrogen-deprived (MSM-NL) *in vitro* model. Strikingly, the two alkyne-containing

inhibitors, **HPOX$_{yne}$** and **CyC$_{31yne}$**, allowed the direct fishing of (Ser/Cys)-based target enzymes involved in these lipidic processes *via* bio-orthogonal CC-ABPP.

RESULTS AND DISCUSSION

Synthesis of New OX Affinity Probes. The Cyclipostins analog **CyC$_{31}$**, as well as the corresponding **CyC$_{31yne}$** and **CyC$_{31\text{-}Dansyl}$** affinity probes were synthesized, as described previously [39, 43]. The new **HPOX$_{yne}$** click-ready derivative was synthesized in a one-pot two-steps reaction using the methodology reported earlier to access the **HPOX** compound [36] (**Scheme 1A**).

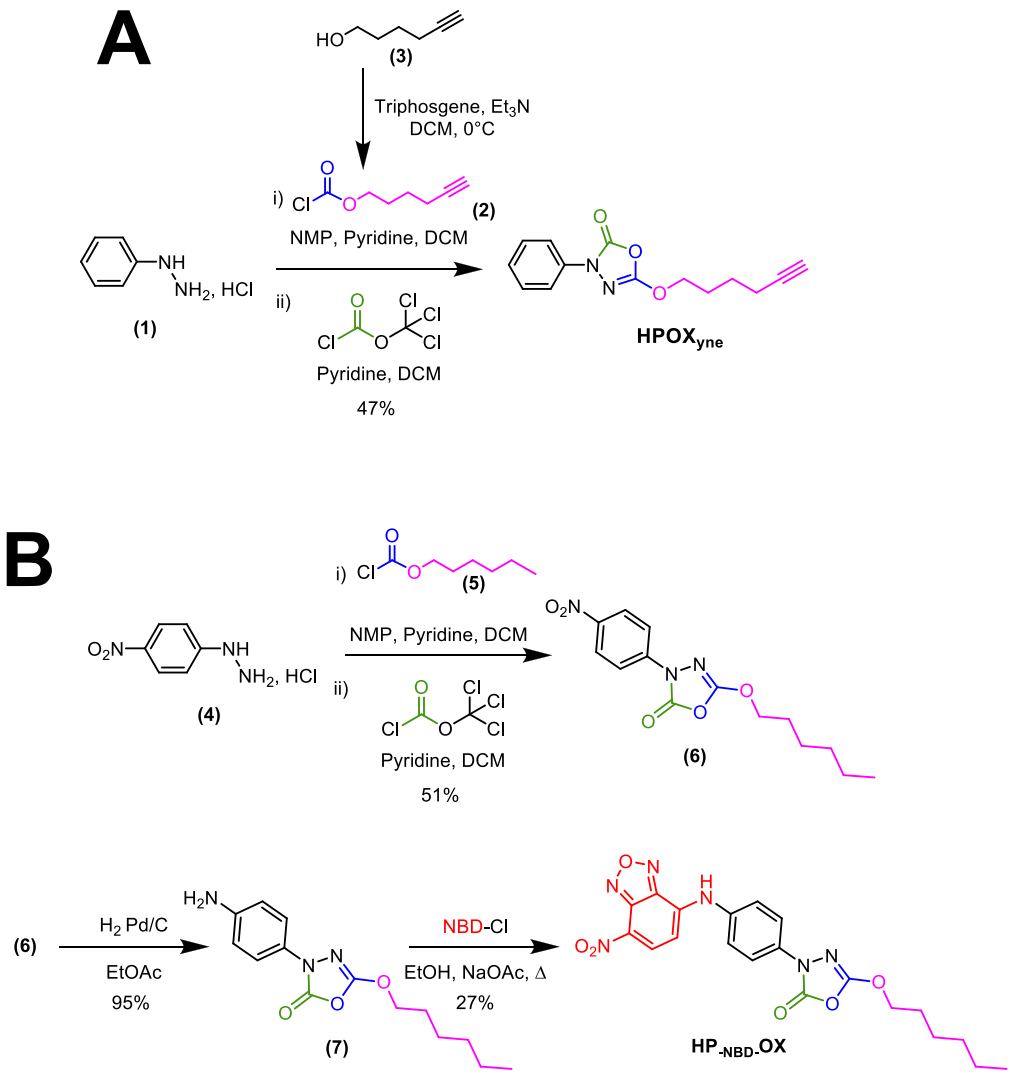

Scheme 1. General procedure for the synthesis of (**A**) **HPOX$_{yne}$** and (**B**) **HP$_{\text{-NBD-}}$OX**.

Briefly, commercially available phenylhydrazine hydrochloride (**1**) and hexyne chloroformate (**2**) formed *in situ* from 5-hexyn-1-ol (**3**) were used in basic conditions to produce a carbamate intermediate (*step i*) that was directly involved in the cyclization reaction in presence of diphosgene (*step ii*) to obtain the desired **HPOX$_{yne}$** derivative in 47% yields [36, 44]. Incorporation of a fluorescent tag on the aromatic phenyl ring of the **HPOX** chemical structure was further achieved in 3 consecutive steps with introduction of the fluorescent NBD group after oxadiazolone ring formation (**Scheme 1B**). The synthesis started from commercially *p*-nitrophenyl hydrazine (**4**) that was engaged into the one-pot two-steps cyclisation process in presence of hexyl chloroformate (**5**). Catalytic hydrogenation of the nitro-oxadiazolone (**6**) over palladium led to the aniline derivative (**7**), which was further coupled through a nucleophilic substitution using NBD-chloride to afford the desire fluorescent **HP$_{-NBD-}$OX** in 13% overall yields.

The CyC and OX Affinity Probes Retain Antibacterial Activity comparable to The Parent Molecules. The antimicrobial potency of the selected **CyC** probes [**CyC$_{31yne}$** and **CyC$_{31-Dansyl}$**] as well as the new **OX** ABPs [**HPOX$_{yne}$** and **HP$_{-NBD-}$OX**] was next evaluated against the two variants S and R of *M. abscessus* and compared to that of their parent molecules, *i.e.*, **CyC$_{31}$** and **HPOX** (**Figure 1A**), respectively. The minimal inhibitory concentrations (MIC) leading to 50% and 90% bacterial growth inhibition (*i.e.*, MIC_{50}/MIC_{90}) were determined by the resazurin microtiter assay (REMA) and are reported in **Figure 1B** [34-35, 39, 45]. Importantly, **HPOX$_{yne}$** and **HP$_{-NBD-}$OX**, retained the same moderate antibacterial activity as the unmarked parent **HPOX** molecule against *M. abscessus*, with fold changes in MIC_{50} / MIC_{90} ranging from ×0.7-1.0 / ×1.3-2.0. Regarding the **CyC** probes, **CyC$_{31-Dansyl}$**, we had previously reported [39] that this fluorescent analog exhibited extracellular activity comparable to the parent unlabeled **CyC$_{31}$** compound, with very good (MIC_{50} = 1.4 µM / MIC_{90} = 6.1 µM) to moderate (MIC_{50} =

24.1 µM / MIC_{90} = 63.4 µM) anti-mycobacterial activity against *M. abscessus* S and R, respectively (**Figure 1B**). In addition, and as expected from our previous work on *M. tuberculosis* [43], **CyC_{31yne}** showed similar antibacterial activities against *M. abscessus* S (MIC_{50} = 0.84 µM / MIC_{90} = 2.1 µM) and R (MIC_{50} = 10.3 µM / MIC_{90} = 18.5 µM) variants compared to unmodified **CyC_{31}**, with a fold change in MICs of ×0.7 to ×1.75 (**Figure 1B**).

Overall, these results indicate that incorporation of a fluorescent group or an alkyne bond does not alter the activity of the **OX** & **CyC** affinity-based probes. In addition to determining their MICs values, a prerequisite for using these ABPs to identify mycobacterial enzymes involved in ILI accumulation was to verify their ability to ***i)*** colocalize with ILI and ***ii)*** limit the total TAG content in *M. abscessus* S grown in nitrogen-limited MSM-NL.

Fluorescent OX and CyC Affinity probes colocalizes with ILI inside *M. abscessus*. In order to confirm the localization of **OX** & **CyC** ABPs inside lipid-rich bacteria, *M. abscessus* S cells were grown in MSM or MSM-NL for 24 h, harvested and resuspended in fresh medium in the presence of each fluorescent probe at a 100 µM final concentration for an additional 24 h. The **HP_{-NBD}-OX** / **$CyC_{31-Dansyl}$**-treated bacteria were stained with Nile Red for ILI labeling, as previously described [24] and further processed for fluorescent microscopy. As expected, [24] *M. abscessus* cultured in MSM-NL medium harbored clear, intense and compact cytoplasmic signal in the form of foci due to ILI staining. In both cases, a clear co-localization of the Dansyl and NBD fluorescent signal with Nile Red ILI' positive regions was observed (**Figure 1C**). Subsequent statistical analysis of the data resulted in Pearson's correlation coefficients and Manders' colocalization coefficients (overlap of green and red pixel) of 0.788-0.808 as well as 0.845-1, respectively; together with a Costes *p*-value of 1 and Li's ICQ value of 0.280-0.324 (See **Methods** for parameters' detail).

In contrast, when cells were grown in MSM, the absence of ILI resulted in only low and mainly peripheral Nile Red staining corresponding to cell wall-associated lipids labeling (**Figure S1**). Consequently, as previously reported in the case of labeled **CyC-$_{\text{Dansyl}}$**-mycobacteria [39], the diffuse fluorescence (*i.e.*, pale green and orange resulting colors) observed with the **HP-$_{\text{NBD}}$-OX** & **CyC$_{\text{31-Dansyl}}$**-treated *M. abscessus* strains grown in MSM is likely to results from a homogeneous distribution of the probes in the cell wall and/or the cytoplasm of the bacteria.

ILI accumulation is partially blocked by (Ser/Cys)-based enzyme inhibitors. (Ser/Cys)-based enzyme inhibitors can interfere with lipid metabolism by impairing the activity of lipolytic enzymes [24, 27, 46-51]. To confirm that such mycobacterial (Ser/Cys)-based enzyme are involved in ILI mobilization after a 24-hour culture of *M. abscessus* S in MSM-NL to induce ILI accumulation, lipid-rich mycobacteria were harvested, resuspended in fresh MSM-NL, and treated with either **HPOX$_{\text{yne}}$** or **CyC$_{\text{31yne}}$**. Apolar lipids were further extracted and the TAG content was analyzed by thin layer chromatography (TLC) (**Figure 1D**). Following 24 h incubation with **HPOX$_{\text{yne}}$** or **CyC$_{\text{31yne}}$**, a significant reduction in TAG levels of 28.6% and 22.6% (p-value < 0.01), respectively, was reached compared to the untreated bacteria.

These findings suggest that the two click-ready ABPs impair TAG production, presumably through the inhibition of (Ser/Cys)-based enzymes. As a consequence, they can be exploited as affinity probes in a click-chemistry activity-based protein profiling (CC-ABPP) strategy.

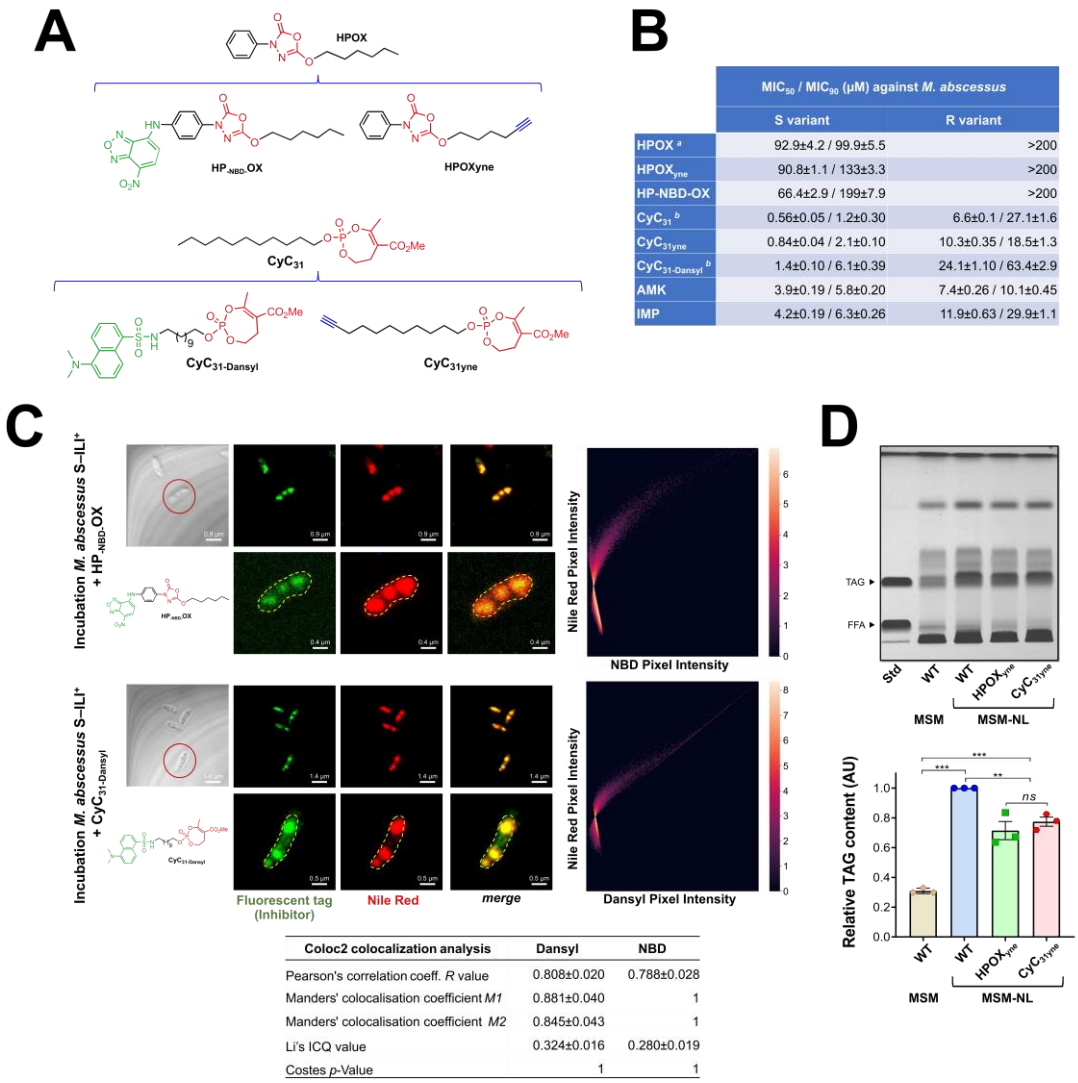

	MIC50 / MIC90 (µM) against *M. abscessus*	
	S variant	R variant
HPOX [a]	92.9±4.2 / 99.9±5.5	>200
HPOXyne	90.8±1.1 / 133±3.3	>200
HP-NBD-OX	66.4±2.9 / 199±7.9	>200
CyC31 [b]	0.56±0.05 / 1.2±0.30	6.6±0.1 / 27.1±1.6
CyC31yne	0.84±0.04 / 2.1±0.10	10.3±0.35 / 18.5±1.3
CyC31-Dansyl [b]	1.4±0.10 / 6.1±0.39	24.1±1.10 / 63.4±2.9
AMK	3.9±0.19 / 5.8±0.20	7.4±0.26 / 10.1±0.45
IMP	4.2±0.19 / 6.3±0.26	11.9±0.63 / 29.9±1.1

Coloc2 colocalization analysis	Dansyl	NBD
Pearson's correlation coeff. *R* value	0.808±0.020	0.788±0.028
Manders' colocalisation coefficient *M1*	0.881±0.040	1
Manders' colocalisation coefficient *M2*	0.845±0.043	1
Li's ICQ value	0.324±0.016	0.280±0.019
Costes *p*-Value	1	1

Figure 1. OX & CyC inhibitors efficiently co-localize with ILI inside bacteria and partially block TAG accumulation. **(A)** Chemical structure of the fluorescent and click-ready **OX** & **CyC** activity-based probes as well as their respective parent molecules. **(B)** Antibacterial activity of the three **OX** and **CyC** derivatives against the two variants of *M. abscessus* in broth medium, expressed as the minimal concentration leading to 50% (MIC_{50}) or 90% (MIC_{90}) of growth inhibition, as determined by the REMA assay. [a] Data from [34]. [b] Data from [39]. Values are mean of at least two independent assays performed in triplicate. INH, isoniazid; AMK, amikacin, used as control drugs. **(C)** The fluorescent **HP$_{\text{-NBD-}}$OX** and **CyC$_{\text{31-Dansyl}}$** specifically colocalized with ILI on *M. abscessus* S in nitrogen-limiting medium. Following a 24 h-culture of *M. abscessus* S in MSM-NL to induce ILI accumulation, lipid rich mycobacteria were harvested, re-suspended in fresh MSM-NL in presence of **HP$_{\text{-NBD-}}$OX** or **CyC$_{\text{31-Dansyl}}$** fluorescent probe for additional 24 h before chemical fixation, neutral lipids staining with Nile Red fluorescent dye, and confocal fluorescence imaging. The Coloc2 plugin of ImageJ/Fiji was used to assess the colocalization

between NBD or Dansyl fluorescent tag (*i.e.*, green channel) and Nile Red (*i.e.*, red channel), with the corresponding pixel intensity scatterplots shown on the right. Summary of the correlation coefficients, including Pearson's correlation coefficient, Manders' coefficients (*M1* and *M2*), the intensity correlation quotient (ICQ) value as suggested by Li, and Costes' *p*-value are shown underneath. Micrographs are representative of 3 independent experiments with ten acquisitions per sample. **(D)** TAG accumulation is partially blocked by the click-ready **HPOX$_{yne}$** and **CyC$_{31yne}$** (Ser/Cys)-based enzyme inhibitors. Following a 24 h-culture in MSM-NL, lipid rich mycobacteria were harvested, re-suspended in fresh MSM-NL at $OD_{600\ nm}$ of 20 and incubated with **HPOX$_{yne}$** or **CyC$_{31yne}$** for additional 24 h. Cells were collected and their lipids were extracted and analyzed by TLC. Each TLC plate is representative of three independent experiments. TAG levels from each *M. abscessus* S culture were analyzed by TLC with triolein as standard. Results from densitometry are expressed as mean values ± SD of three biologically independent experiments, and reported as relative percentages using the TAG levels of *M. abscessus* WT in the MSM-NL as 100%. Statistical significance was assessed with one-way ANOVA followed by Tukey's multiple comparisons post-hoc test using Prism 8.0 (GraphPad, Inc): ** *p*-value <0.01; *** *p*-value <0.001; *ns*, not significant (*p*-value >0.05).

OX and CyC click-ready probes allow identifying potential enzymes involved in TAG accumulation. As recently reported in the case of *M. tuberculosis* [43], to gain access to putative enzymes involved in ILI metabolism, lipid-rich (*i.e.*, MSM-NL) and lipid-poor (*i.e.*, MSM) *M. abscessus* S cultures were subjected to the chemoproteomic CC-ABPP approach using the two alkyne-containing inhibitors (**Figure 2A**). After either 24 h or 48 h of culture in MSM or MSM-NL, the bacteria were centrifuged and the pellets resuspended in fresh medium in presence of **HPOX$_{yne}$**, **CyC$_{31yne}$**, or DMSO (control) for additional 24 h incubation at 37 °C. Following cell lysis, click-chemistry reaction between the obtained **HPOX$_{yne}$**- or **CyC$_{31yne}$**-enzyme complexes and the Desthiobiotin-N_3 *via* copper(I)-catalyzed Huisgen's 1,3-dipolar cycloaddition reaction afforded a stable triazole ring [33]. Enrichment on streptavidin agarose-beads followed by subsequent digestion with trypsin, the resulting peptides were analyzed by liquid chromatography-tandem mass spectrometry (LC-MS/MS), and quantified by label-free quantitative analysis (**Figure 2A**).

A first comparative proteomic analysis between each control sample (*i.e.*, DMSO-treated *M. abscessus* for non-specific binding to streptavidin agarose-beads) at the two time-points and the APB-treated samples led to a first set of target enzymes with **HPOX$_{yne}$** and **CyC$_{31yne}$**, respectively, when applying *p*-value ≤0.01 and Fold change (Log_2) ≥1.0 thresholds on the proteomic analysis results (**Tables S1-S4**).

Each of these first data sets, *i.e.*, the target proteins of **HPOX$_{yne}$** and **CyC$_{31yne}$** identified in MSM-NL culture of *M. abscessus* at 24 h and 48 h incubation, was further refined by means of a second comparative proteomic analysis using the data obtained from the same fishing experiments carried out in MSM (**Tables S1-S4**). The resulting mycobacterial targets of **HPOX$_{yne}$** and **CyC$_{31yne}$**, displayed as volcano plots (**Figure 2B**), highlight the proteins captured by the two ABPs that were significantly more abundant in MSM-NL *vs*. MSM (*p*-value ≤0.05 and Fold change (Log_2) ≥1.0), and thus involved in physiological processes directly related to nitrogen-deprived condition and ILI-rich phenotype. As shown in the Venn diagram (**Figure 2C, upper panel**), using **HPOX$_{yne}$** as a probe, 26 and 236 enzymes were found to be differentially expressed after 24 and 48 h of incubation in MSM-NL, respectively, with 14 proteins conserved over time. Most of the identified proteins belonged to the categories of conserved hypothetical proteins (4 / 26 and 35 / 236), cell wall/cell processes (2 / 26 and 14 / 236), intermediary metabolism/respiration (7 / 26 and 129 / 236), and global lipid metabolism (12 / 26 and 43 / 236). Interestingly, among the 14 conserved identified enzymes, 10 belonged to the global lipid metabolism functional category and 4 to the intermediary metabolism/respiration (**Table S5** and **Figure 2C, upper panel**).

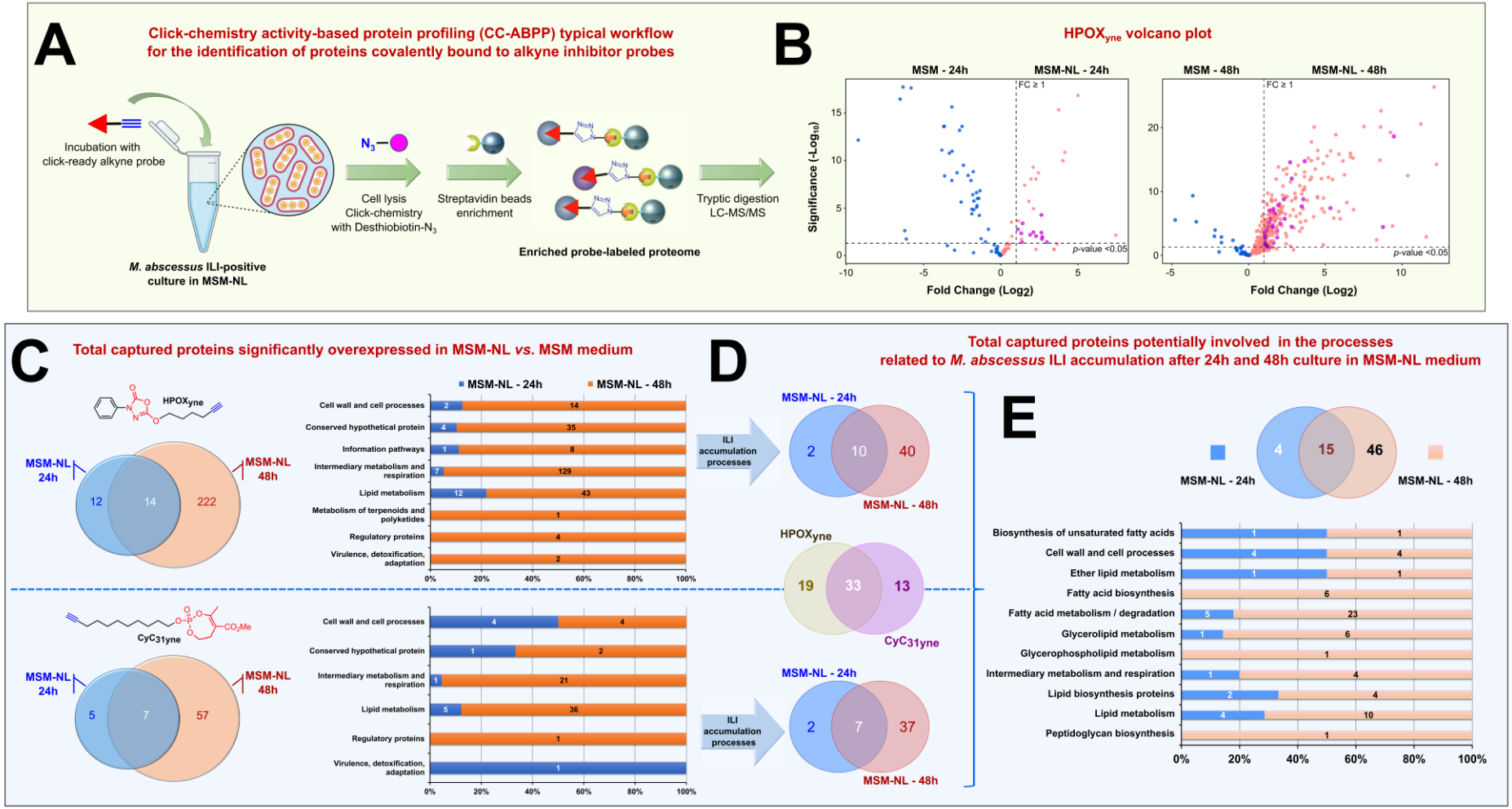

Figure 2. Click chemistry activity-based protein profiling in living *M. abscessus* in MSM-NL. (A) Click chemistry activity-based protein profiling (CC-ABPP) typical workflow for the identification of proteins covalently bound to the **HPOX$_{yne}$** or **CyC$_{31yne}$** inhibitors. A 24 h or 48 h growth phase culture of *M.*

abscessus S was pre-treated with either **HPOX$_{yne}$** or **CyC$_{31yne}$** prior to cell lysis and subsequent click-reaction with Azide-PEG$_3$-Desthiobiotin reporter. Samples were then treated with streptavidin-agarose beads for the capture and enrichment of labeled proteins, followed by tryptic digestion. Tandem mass spectrometry analyses and subsequent differential peptides analysis allowed the identification of the target enzymes captured by the two inhibitors. **(B)** Volcano plot of the differential proteomic analysis between MSM-NL and MSM captured enzymes by **HPOX$_{yne}$** and showing the significance of two sample *t*-test (-Log(*p*-value)) *versus* fold-change (Log$_2$(LFQ normalized intensity in NSN-NL *vs*. MSM condition)) on the *y* and *x* axes, respectively. The dashed lines indicate the threshold of *p-value* ≤ 0.05 and a fold-change ≥ 1.0. Purple dots represent proteins potentially involved in mycobacterial lipid metabolism. **(C)** Venn diagrams showing the total number of proteins that were differentially captured by **HPOX$_{yne}$** or **CyC$_{31yne}$**, respectively, from a 24 h or 48 h culture in MSM-NL; and corresponding Functional categories of *M. abscessus* proteins identified with the two probes, according to the functional classification system of the KEGG [52-53] and Mycobrowser [54] databases. The numbers correspond to the total number of identified proteins in each category. Proteins without functional annotation are denoted as uncharacterized proteins. **(D)** Venn diagrams showing the total number of proteins potentially involved in lipid metabolism that were differentially captured by **HPOX$_{yne}$** or **CyC$_{31yne}$** from a 24 h or 48 h culture in MSM-NL, and total merged captured enzymes from each probe (medium panel). **(E)** Venn diagram showing the total number of *M. abscessus* proteins potentially involved in lipid metabolism that were differentially captured from a 24 h or 48 h culture in MSM-NL and their corresponding Functional categories according to the functional classification system of the KEGG [52-53] and Mycobrowser [54] databases.

A comparable distribution profile of differentially expressed proteins at 24 h and 48 h incubation in MSM-NL was obtained using **CyC$_{31yne}$** as a probe (**Figure 2C, lower panel**), with 12 and 64 enzymes differentially expressed after 24 and 48 h of incubation in MSM-NL, respectively (**Table S6**). As observed above, these identified proteins mainly belonged to the functional categories of conserved hypothetical proteins (1 / 12 and 2 / 64), cell wall/cell processes (4 / 12 and 4 / 64), intermediary metabolism/respiration (1 / 12 and 21 / 64), and global lipid metabolism (5 / 12 and 36 / 64). Seven proteins were conserved over time, 4 of which belonging to the cell wall/cell processes and 3 to the global lipid metabolism functional categories (**Table S6**). Such distribution profiles agree with previous competitive ABPP experiments conducted with **OX** and **CyC** on *M. tuberculosis* and *M. abscessus* cultures [34-37].

To further focus on enzymes potentially involved in ILI metabolism, and considering that orthologs usually perform equivalent functions in the respective organisms [28, 55], the corresponding orthologs in the *M. tuberculosis* H37Rv genome of all identified proteins were reported using the KEGG database [52-53]. These data, cross-referenced with the Uniprot [56] and Mycobrowser [54] databases, provide reliable predictions of gene function in terms of essentiality, genomic location and activity.

The results of this differential pathway analysis led to the selection of 52 and 46 enzymes, captured by **HPOX$_{yne}$** and **CyC$_{31yne}$**, respectively, that may potentially be involved in the total lipid metabolism associated with ILI accumulation (**Figure 2D** and **Tables S7-S10**). In view of the similarity of their mechanisms of action [29], a comparable distribution of the captured "lipolytic" enzymes was obtained at 24 h and 48 h in MSM-NL, as reported for each inhibitor probe in the Venn diagrams (**Figure 2D**). Interestingly, while both inhibitors share 33 common targets, 19 and 13 additional specific target enzymes were obtained with **HPOX$_{yne}$** (**Tables S7-S8**) and **CyC$_{31yne}$** (**Tables S9-S10**), respectively (**Figure 2D**).

The full list of these target enzymes is shown in **Table 1**, confirming the complementary selectivity of these two families of inhibitors with respect to the enzymes they capture. Of these 65 enzymes, 4 were captured only at 24 h, 46 only at 48 h, and 15 were fully conserved at both time points (**Figure 2E**), implying a dynamic process of ILI biosynthesis [3-4] with mostly different protein partners recruited over time.

Table 1. Target proteins potentially involved in ILI accumulation after 24/48 h culture of *M. abscessus* S in MSM-NL, through CC-ABPP by LC-ESI-MS/MS analysis [a]

$HPOX_{yne}$		CyC_{31yne}		Protein Ids	*M. tuberculosis* Ortholog	Essentiality	Protein names	Pathways
24h	48h	24h	48h					
	+		+	MAB_2891c	Rv2605c		Probable acyl-CoA thioesterase II TesB2	Biosynthesis of unsaturated fatty acids
		+		MAB_3588 *	Rv2500c		Putative acyl-CoA oxidase	Biosynthesis of unsaturated fatty acids
	+	+	+	MAB_3765 *	Rv3451 *		Probable Cutinase Cut3	Cell wall / cell processes
	+	+	+	MAB_3763 *	Rv2301 *		Probable Cutinase Cut2	Cell wall / cell processes
		+	+	MAB_3766 *	Rv3451/Rv3452 *		Probable Cutinase precursor Cut3/Cut4	Cell wall / cell processes
	+	+	+	MAB_3809c *	Rv3452 *	GA	Probable Cutinase Cut4	Cell wall / cell processes
+	+		+	MAB_3884 *	Rv2251		Possible flavoprotein	Ether lipid metabolism
	+		+	MAB_0952	Rv1928c		3-oxoacyl-[acyl-carrier protein] reductase	Fatty acid biosynthesis
			+	MAB_0949c	Rv2589		Hypothetical aminotransferase	Fatty acid biosynthesis
	+		+	MAB_1512	Rv2524c †	ES	Probable fatty acid synthase Fas-I	Fatty acid biosynthesis
	+		+	MAB_3592c	Rv3089		Putative medium-chain acyl-CoA ligase FadD13	Fatty acid biosynthesis
	+			MAB_0598 *	Rv3559c		Short-chain dehydrogenase/reductase	Fatty acid biosynthesis
	+			MAB_1978c *	Rv2187 †		Probable long-chain-fatty-acid--CoA ligase FadD15	Fatty acid biosynthesis
	+		+	MAB_0850 *	Rv0859		Probable acyl-CoA thiolase FadA	Fatty acid degradation
	+		+	MAB_1187c *	Rv1071c		Probable enoyl-CoA hydratase	Fatty acid degradation
+	+		+	MAB_0612c #	Rv3546		Probable acetyl-CoA acetyltransferase FadA5	Fatty acid degradation
	+		+	MAB_1192c *	Rv1074c		Probable acyl-CoA thiolase FadA3	Fatty acid degradation
	+		+	MAB_0981c *	Rv0860		Possible enoyl-CoA hydratase/isomerase	Fatty acid degradation
+	+		+	MAB_0983c *	Rv0162c		Probable alcohol dehydrogenase, zinc-containing	Fatty acid degradation
	+			MAB_1069c	Rv0971c		Probable enoyl-CoA hydratase EchA7	Fatty acid degradation
+	+			MAB_2085	Rv0975c	GA	Probable acyl CoA dehydrogenase	Fatty acid degradation
+	+			MAB_3636c	Rv2500c		Probable acyl-CoA dehydrogenase	Fatty acid degradation
	+			MAB_0900c	Rv0223c *		Bifunctional aldehyde dehydrogenase/enoyl-CoA hydratase	Fatty acid degradation
	+			MAB_3350 *	Rv3774		Putative enoyl-CoA hydratase/isomerase	Fatty acid degradation
	+			MAB_3649	Rv3293		Probable aldehyde dehydrogenase	Fatty acid degradation
	+			MAB_3481	Rv0231		Probable acyl-CoA dehydrogenase FadE4	Fatty acid degradation
	+			MAB_0851 *	Rv0860		3-hydroxyacyl-CoA dehydrogenase FadB	Fatty acid degradation
+	+		+	MAB_4437 #	Rv0244c		Probable acyl-CoA dehydrogenase FadE5	Fatty acid metabolism
			+	MAB_4780 *	Rv0636		MaoC-like dehydratase component of FasII	Fatty acid metabolism
			+	MAB_0902	Rv1074c *		Probable beta-ketoadipyl-CoA thiolase	Fatty acid metabolism/degradation
	+		+	MAB_4609c	Rv0400c †		Putative acyl-CoA dehydrogenase FadE7	Fatty acid metabolism/degradation
	+		+	MAB_3455c #	Rv3556c		Acetyl-CoA acetyltransferase FadA6	Fatty acid metabolism/degradation
	+		+	MAB_2042c *	Rv1867	GA	Acetyl-CoA C-acetyltransferase FadA	Fatty acid metabolism/degradation

	+		+	MAB_0255	Rv0154c †		Putative acyl-CoA dehydrogenase FadE2	Fatty acid metabolism/degradation
	+		+	MAB_1463 *	Rv1323	GA	Probable acetyl-CoA acetyltransferase FadA4	Fatty acid metabolism/degradation
	+			MAB_3040c *	Rv2724c		Probable acyl-CoA dehydrogenase FadE20	Fatty acid metabolism/degradation
	+		+	MAB_0328 *	Rv0154c		Putative acyl-CoA dehydrogenase	Fatty acid metabolism/degradation
+	+	+	+	MAB_0175 *	Rv0129c *		Antigen 85-C FbpC	Glycerolipid metabolism
			+	MAB_0177 *	Rv3804c *	GA	Antigen 85-A/B/C	Glycerolipid metabolism
			+	MAB_0176 *	Rv3804c *		Antigen 85-A	Glycerolipid metabolism
	+		+	MAB_3400 *	Rv3045 *		NADP-dependent alcohol dehydrogenase C	Glycerolipid metabolism
	+		+	MAB_0382 *	Rv3696c	GD	Glycerol kinase GlpK	Glycerolipid metabolism
			+	MAB_2357	Rv1692 *	GA	HAD superfamily hydrolase (Glycerol-1-phosphatase)	Glycerolipid metabolism
	+		+	MAB_3655c	Rv3302c	ES	Glycerol-3-phosphate dehydrogenase GlpD2	Glycerophospholipid metabolism
+	+		+	MAB_2814 *	Rv1399c		Probable lipase LipH	Intermediary metabolism and respiration
	+		+	MAB_3447c *	Rv0220		Putative lipase/esterase LipC	Intermediary metabolism and respiration
	+		+	MAB_2818c	Rv0480c		Putative hydrolase	Intermediary metabolism and respiration
	+		+	MAB_3810	Rv3569c *	GA	Putative hydrolase, alpha/beta fold	Intermediary metabolism and respiration
			+	MAB_2348	Rv1683 †		Possible long-chain acyl-CoA synthase	Lipid biosynthesis proteins
	+		+	MAB_0425c *	Rv3667		Acetyl-coenzyme A synthetase	Lipid biosynthesis proteins
			+	MAB_1141c *	Rv0533c *		3-oxoacyl-[acyl-carrier-protein] synthase 3 FabH	Lipid biosynthesis proteins
	+			MAB_2212	Rv1527c *		Probable polyketide synthase Pks5	Lipid biosynthesis proteins
+				MAB_0179	Rv3801c	ES	Probable fatty-acid-CoA ligase FadD32	Lipid biosynthesis proteins
+				MAB_1140	Rv1013		Putative polyketide synthase Pks16	Lipid biosynthesis proteins
		+	+	MAB_0178	Rv3802c *	ES	Probable Cutinase Cut6	Lipid metabolism
		+		MAB_4587c *	Rv3767c		Putative S-adenosyl-L-methionine-dependent methyltransferase	Lipid metabolism
+	+	+	+	MAB_4328c	Rv0281 *		Putative S-adenosyl-L-methionine-dependent methyltransferase	Lipid metabolism
	+		+	MAB_3860c	Rv0672 *		Probable acyl-CoA dehydrogenase FadE8	Lipid metabolism
+	+		+	MAB_4336 *	Rv0271c		Probable acyl-CoA dehydrogenase FadE6	Lipid metabolism
			+	MAB_2619	Rv1627c		Probable lipid-transfer protein Ltp1 (Thiolase?)	Lipid metabolism
	+			MAB_0310c *	Rv3720 †		Putative cyclopropane-fatty-acyl-phospholipid synthase	Lipid metabolism
	+			MAB_4055c #	Rv3561		Putative acyl-CoA synthetase/ligase FadD3	Lipid metabolism
	+			MAB_0065c *	Rv2724c	GA	Probable acyl-CoA dehydrogenase FadE20	Lipid metabolism
	+			MAB_1188c	Rv0752c		Probable acyl-CoA dehydrogenase FadE9	Lipid metabolism
	+			MAB_3234 *	Rv2911	GA	Probable D-alanyl-D-alanine carboxypeptidase DacB	Peptidoglycan biosynthesis

[a] *M. tuberculosis* orthologs were retrieved using the KEGG database [52-53] and then cross-referenced with the Uniprot [56] and Mycobrowser [54] databases for accurate **Protein names** and **Pathways**. The **Essentiality** of each *mab* gene was checked using the *Data Set S1B* (xls file) from [57]: ES, essential gene; GA, causing growth advantage; GD, causing a growth defect. *, proteins previously identified from ABPP experiments on culture or total lysate of *M. abscessus* [34-35] or *M. tuberculosis* [36-37, 43] with the **OX** and **CyC**. † proteins involved in lipid metabolism and identified as part of *M. tuberculosis* ILIome [28]. #, genes predicted to encode enzymes necessary for the biochemical activation and β-oxidation of fatty acids that were up-regulated in both *M. abscessus*-infected amoebae and murine macrophages [58].

All these identified proteins covered nearly all functional categories listed under the pathways related to *M. abscessus* total lipid metabolism, ranging from biosynthesis of unsaturated fatty acids (2 proteins), cell wall/cell processes (4 proteins), ether lipid metabolism (1 protein), fatty acid biosynthesis (6 proteins), fatty acid metabolism/degradation (23 proteins), glycerolipid metabolism (6 proteins), glycerophospholipid metabolism (1 protein), lipid biosynthesis proteins (6 proteins), and peptidoglycan biosynthesis (1 protein). An additional 10 proteins classified as being involved in lipid metabolism, and 4 proteins belonging to intermediary metabolism and respiration have also been added (**Table 1**).

In agreement with previous work, 41 / 65 (63%) proteins had already been identified *via* ABPP with **OX** and **CyC** molecules either on culture and/or total lysate of *M. abscessus* [34-35] and *M. tuberculosis* [36-37, 43]. These included five Cutinase-like proteins (MAB_3763 – Cut2; Mab_3765 – Cut3; MAB_3766 – Cut2/Cut3 precursor; MAB_3809c – Cut4; MAB_0178 – Cut6); two Lip-family members (MAB_2814 – LipH; MAB_3447c - LipC); a possible α/β-fold hydrolase (MAB_3810); two putative methyltransferases (MAB_4587c; MAB_4328c); the probable D-alanyl-D-alanine carboxypeptidase DacB (MAB_3234); the β-ketoacyl-ACP synthase III (MAB_1141c - FabH); and members of the antigen 85 complex (MAB_177 – Ag85A/B/C; MAB_0176 – Ag85A; MAB_0175 – Ag85C) (**Table 1**).

Given our *in vitro* model of ILI accumulation based on nitrogen starvation in presence of glycerol as the sole carbon source, glycerolipid and glycerophospholipid metabolism thus plays a central role in TAG production [2-3]. Accordingly, key enzymes in the regulation of glycerol uptake and metabolism were identified. This included the glycerol kinase (MAB_0382 - Glpk) and the HAD superfamily hydrolase (MAB_2357) which participated in the conversion of glycerol to glycerol-3-phosphate; and the glycerol-3-phosphate dehydrogenase GlpD2 (MAB_3655c) involved in the reduction of glycerol-3-phosphate to generate glycerone phosphate.

In addition to these proteins, 38 / 65 (58.5%) enzymes were found directly associated with fatty acid biosynthesis, metabolism and degradation. Among these, the essential fatty-acid synthase (MAB_1512 – Fas-I), four putative acyl-CoA synthetase/ligase (MAB_3592c – FadD13; MAB_1978c – FadD15; MAB_0179 – FadD32; MAB_4055c – FadD3), two probable acyl-CoA thiolase (MAB_0850 – FadA; MAB_1192c – FadA3), four probable acetyl-CoA acetyltransferase (MAB_0612c – FadA5; MAB_3455c – FadA6; MAB_2042c – FadA; MAB_1463 – FadA4), four probable enoyl-CoA hydratase/isomerase (MAB_1187c; MAB_0981c; MAB_1069c – AchA7; MAB_3350), twelve probable acyl-CoA dehydrogenase (MAB_2085; MAB_3636c; MAB_3481 – FadE4; MAB_4437 – FadE5; MAB_4609c – FadE7;MAB_0255 – FadE2; MAB_0328; MAB_3040c – FadE20; MAB_3860c – FadE8; MAB_4336 – FadE6; MAB_0065c – FadE; MAB_1188c – FadE9), and two dehydrogenases (MAB_0598; MAB_0983c) were identified (**Table 1**). Four additional proteins annotated as the acetyl-coenzyme A synthetase (MAB_0425c), two polyketide synthases (MAB_2212 - Pks5; MAB_1140 – Pks16), and the putative cyclopropane-fatty-acyl-phospholipid synthase (MAB_0310c) were also identified. Finally, our differential proteomic analysis has highlighted the presence of the putative long-chain acyl-CoA synthase MAB_2348. This protein is indeed homologous to the bifunctional long-chain acyl-CoA synthase/lipase BCG_1721 (65% sequence identity) which has been reported as an important regulator of TAG levels and so in ILI formation in *M. bovis* BCG [7].

Recently, Dubois et al. reported the complete description and analysis of the *M. abscessus* transcriptome both in an amoebic environmental host and in infected murine macrophages [58]. Interestingly, the genes encoding the fatty acid-CoA synthase *fadD3*, the acyl-CoA dehydrogenase *fadE5*, and the two acetyl-CoA transferases *fadA5* and *fadA6* were among the 15 genes up-regulated in both *M. abscessus*-infected amoebae and murine macrophages, demonstrating their potential role in the biochemical activation and β-oxidation of fatty acids upon infection (**Table 1**). In addition, 6 of our captured proteins, namely MAB_1512 (Rv2524c - Fas-I), MAB_1978c (Rv2187 - FadD15), MAB_4609c (Rv0400c - FadE7), MAB_0255 (Rv0154c - FadE2), MAB_2348 (Rv1683) and

MAB_0310c (Rv3720), were also among the 28 proteins belonging to the lipid metabolism functional category recently reported as potential core components of the *M. tuberculosis* ILI-associated proteome [28].

Overall, the diversity of proteins captured under these nitrogen-limiting conditions suggests that TAG accumulation in the form of ILI may not be limited to energy storage, but may also provide a source of lipids dedicated to maintaining overall cellular homeostasis of mycobacteria under stringent conditions [3]. Most importantly, these results underscore the power and combined value of using both **OX** and **CyC** probes to identify key mycobacterial enzymes involved in ILI accumulation through activity-based profiling approaches, enlightening our understanding of the metabolic pathways used by pathogenic mycobacteria to catabolize host-derived lipids for survival.

The long chain-fatty-acid--CoA ligase MAB_1978c (FadD15) is involved in TAG production and ILI accumulation. To further investigate the impact of these identified enzymes on TAG accumulation, the MAB_1978c (FadD15) was further selected to investigate its involvement in ILI accumulation.

FadD15 is a putative long-chain-fatty-acid--CoA ligase that is functionally categorized as being involved in lipid metabolism. Its *M. tuberculosis* ortholog Rv2187 [59], is predicted to act at the termination of the fatty acid biosynthesis pathway [KEGG PATH:mab00061] and to catalyze the activation of long-chain fatty acids as acyl-CoA that would be further processed for elongation, glycerolipid and/or glycerophospholipid biosynthesis. In addition, Rv2187 is core component of the *M. tuberculosis* ILI-associated proteome [28], thus reinforcing the potential involvement of this protein in ILI biosynthesis.

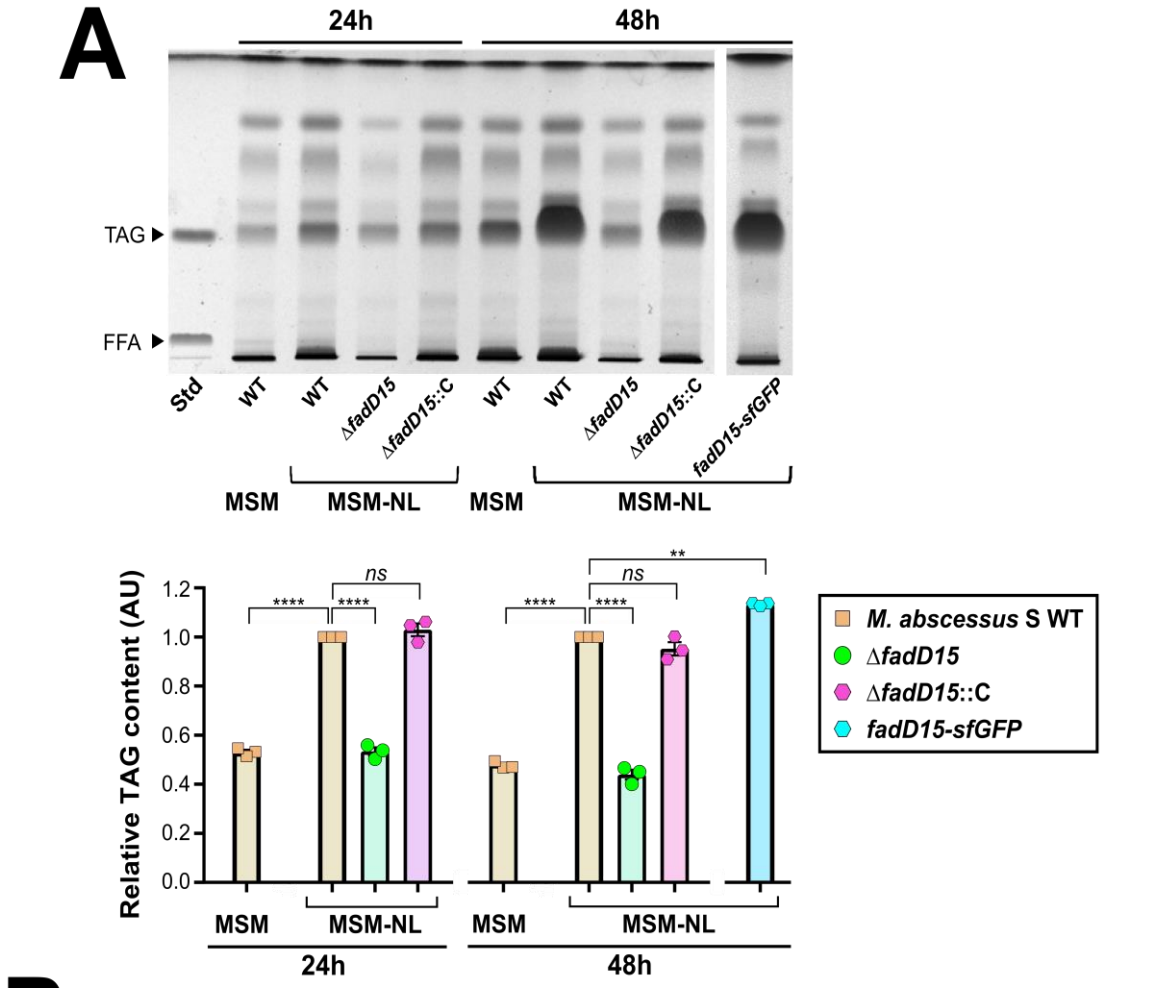

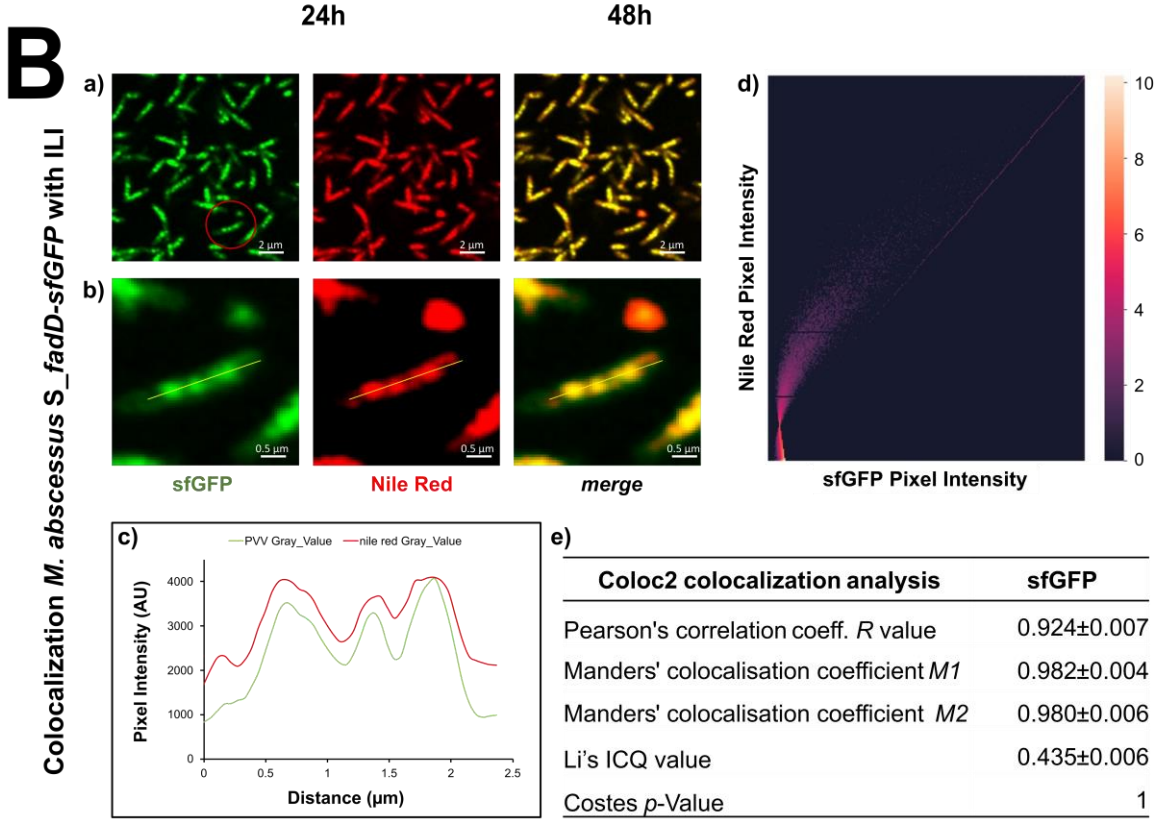

e)

Coloc2 colocalization analysis	sfGFP
Pearson's correlation coeff. *R* value	0.924±0.007
Manders' colocalisation coefficient *M1*	0.982±0.004
Manders' colocalisation coefficient *M2*	0.980±0.006
Li's ICQ value	0.435±0.006
Costes *p*-Value	1

Figure 3. **MAB_1978c (FadD15) is essential for TAG production and accumulation in the form of ILI in *M. abscessus*. (A)** TAG levels from *M. abscessus* cultures in MSM-NL. Cultures were collected after a 24 h or 48 h incubation period, lyophilized and equal weights of dry cells were used for apolar lipid extraction. TAG levels from *M. abscessus* WT, Δ*fadD15*, and its complemented strain Δ*fadD15*::C as well as the *fadD15*-*sf*GFP overexpressing strain were analyzed by TLC with triolein as standard. TLC densitometry analysis of relative TAG levels in each strain, with cultures from *M. abscessus* WT used as a reference, are reported. Results from densitometry are expressed as mean values ± SD of three biologically independent experiments, and reported as relative percentages using the TAG levels of *M. abscessus* WT in the MSM-NL as 100%. Statistical significance was assessed with one-way ANOVA followed by Tukey's multiple comparisons post-hoc test using Prism 8.0 (GraphPad, Inc): ** *p*-value <0.01; **** *p*-value <0.0001; *ns*, not significant (*p*-value >0.05). **(B)** The FadD15-*sf*GFP protein specifically co-localized with ILI in *M. abscessus*. Following a 48 h-culture in MSM-NL to induce ILI accumulation, lipid-rich mycobacteria were harvested, chemically fixed, stained with Nile Red fluorescent dye, and processed for confocal fluorescence imaging. **Panel (a)**: Large filed image representative of the dataset acquired. **Panel (b)**: zoom on a single bacterium to demonstrate *sf*GFP fluorescent colocalization with ILI when cultured in MSM-NL. **Panel (c)**: plot of fluorescence intensity of *sf*GFP channel and Nile Red channel as a function of the distance of each pixel from the yellow line depicted in **panel (b)**. The Coloc2 plugin of ImageJ/Fiji was used to assess the colocalization between *sf*GFP fluorescent tag (*i.e.*, green channel) and the Nile Red (*i.e.*, red channel), the corresponding pixel intensity scatterplots being shown on the right **panel (d)**. Summary of the correlation coefficients, including Pearson's correlation coefficient, Manders' coefficients (*M1* and *M2*), the intensity correlation quotient (ICQ) value as suggested by Li, and Costes' *p*-value are shown underneath. Micrographs are representative of 3 independent experiments with ten acquisitions per sample.

Thus, a deletion mutant, designated Δ*fadD15*, was generated by using a two-step homologous recombination procedure using the pUX1-*katG* vector [60]. Its complemented counterpart Δ*fadD15*::C was obtained using the pVV16::*fadD15* that allows the constitutive production of MAB_1978c under the control of the *hsp60* promoter. In parallel, *MAB_1978c* was cloned and overexpressed in *M. abscessus* using the same *pVV16::fadD15-sfGFP* vector fused to a *sf*GFP protein for subsequent fluorescence microscopy experiments. First, when grown in 7H9TG^{OADC}, MSM or MSM-NL for 72 h at 37 °C, no significant differences in growth rate were observed between the *M. abscessus* wild-type and Δ*fadD15*(**Figure S2**), in agreement with the non-essentiality of the *fadD15* gene in *M. abscessus* [57].

Then, each strain was grown in MSM-NL for 24 h and 48 h, and then processed for apolar lipids TLC analysis (**Figure 3A**). At the two time points, quantitative densitometry revealed that TAG production was impaired by 46.7 ± 1.4% and 56.1 ± 2.5% (p-value < 0.0001) in Δ*fadD15* after 24 and 48 h of incubation in MSM-NL, respectively, as compared to the WT strain (**Figure 3A**). In contrast, complete restoration of TAG levels, *i.e.*, 102.9 ± 2.6% and 95.2 ± 2.7%, at 24 and 48 h, respectively, was achieved upon complementation in Δ*fadD15*::C. Moreover, the *fadD15-sfGFP* overexpressing strain induced a slight but significant increase in TAG levels by 1.13-fold (p-value < 0.01) as compared to the WT strain. Most importantly, comparable TAG levels were reached with Δ*fadD15* and a triacylglycerol synthase 1 deletion mutant (Δ*tgs1*) in *M. abscessus* using the MSM-NL [24]. Indeed, it has been clearly demonstrated that TAG accumulation in the form of ILI was *tgs1* dependent, in *M. tuberculosis* (*rv3130c*) [13, 61-63], *M. marinum* (*mmar_1519*) [20, 64] and in *M. abscessus* (*mab_3551c*) [24-25]. Moreover, this major TAG synthase has also been identified on the surface of mature ILI in *M. bovis* BCG [7], confirming its major contribution in ILI formation.

The *fadD15-sfGFP* overexpressing strain was grown in MSM-NL or MSM for 48 h, harvested, fixed with 4% paraformaldehyde, then stained with Nile Red and processed for fluorescent microscopy. As observed previously with the fluorescent inhibitor probes, in MSM a diffuse and mainly peripheral fluorescence signal was observed, suggesting a homogeneous distribution of the labelled FadD15-*sf*GFP protein in the lipid-poor bacteria (**Figure S3**). Conversely, *fadD15-sfGFP* cultured in MSM-NL displayed clear, intense and compact Nile Red ILI' positive regions, which co-localized with the *sf*GFP fluorescent signal (**Figure 3B**). Statistical analysis confirmed the overlap between green (*sf*GFP) and red pixel (Nile Red) with Pearson's correlation coefficients and Manders' co-localization coefficients of 0.924 and 0.982, respectively; a Costes p-value of 1 and Li's ICQ value of 0.435.

All these results demonstrated the clear role of MAB_1978c/FadD15 in TAG production and subsequent ILI formation *in vitro*.

More globally, the fact that glycerol is the sole carbon source available in our MSM-NL model implies the use of well conserved pathways to synthesize TAG [65]. Consequently, from the set of the

65 captured proteins with both **HPOX$_{yne}$** and **CyC$_{31yne}$**, and literature data on *M. tuberculosis* [66-68] and *M. abscessus* [58] transcriptomic studies, it is possible to map some enzymes involved in *M. abscessus* lipid metabolism related to TAG formation and accumulation through ILI (**Figure 4**).

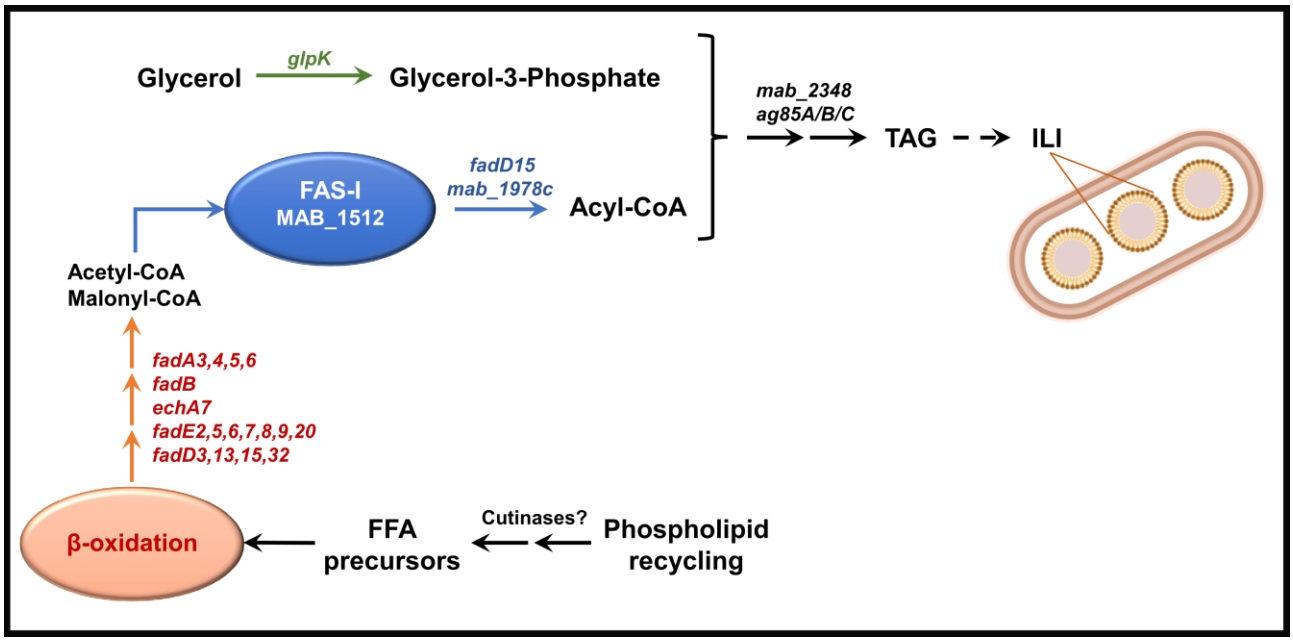

Figure 4. **Schematic diagram of the biosynthetic pathways involved in TAG accumulation in the form of ILI in in *M. abscessus*.** This pathway provides a brief overview of the main findings and illustrates the involvement of proteins belonging to the lipid metabolism's functional category in TAG formations and storage as ILI following *M. abscessus* growth in MSM-NL.

The initial step would consist in the *de novo* biosynthesis of fatty acyl-compounds in the form of acyl-CoA molecules through the action of the type I fatty acid synthase (Fas-I) as well as all enzymes necessary for the biochemical activation and β-oxidation of fatty acids: fatty acid-CoA synthase/ligase (FadD3,13,15,32), acyl-CoA dehydrogenase (FadE2,5,6,7,8,9,20), enoyl-CoA hydratase (EchA7), hydroxybutyryl-CoA dehydrogenase (FadB), and acetyl-CoA transferase (FadA3,4,5,6). However, given the energetic costs associated with such *de novo* fatty acid biosynthesis in MSM-NL, where glycerol is the sole carbon source, it is likely that other rearrangements of lipid metabolism, such as phospholipid recycling through the action of some Cutinase-like proteins (*e.g.*, MAB_3809c/Cut4) [69-70], may led to fatty acid precursors that could be incorporated into biosynthetic pathways *via* the β-oxidation pathway. The second step is the

formation of glycerol-3-phosphate (G3P) substrates generated by the action of the glycerol kinase (MAB_0382/GlpK). Finally, the sequential acylation of the G3P substrates with the latter fatty acyl-CoA residues is mediated by the enzymes from the Kennedy pathway. These may include the bifunctional long-chain acyl-CoA synthase/lipase (MAB_2348) which *M. bovis* BCG ortholog [7] has been demonstrated to be involved in long-chain TAG and ILI formation processes when assessed under non-replicating conditions; as well as the Ag85A/B/C complex proteins which were found to express diacylglycerol acyltransferase (DGAT) activity and to mediate the transesterification of diacylglycerol using long-chain acyl-CoA, making thus an important contribution in TAG synthesis [41].

CONCLUSION

Using an *in vitro* model based on nitrogen deprivation to promote TAG accumulation and subsequent production of lipid-loaded *M. abscessus* cells, together with two selective multitarget inhibitors belonging to the **OX** and **CyC** distinct families, we identified a set of 65 enzymes that may directly or indirectly participate in these processes. We have validated this approach by demonstrating that the long-chain-fatty-acid-CoA ligase MAB_1978c/FadD15 co-localizes with ILI and acts as a major contributor in ILI formation. More work remains to be done to fully characterize and validate the other proteins identified *via* ABPP to generate a clear picture regarding their specific role(s) in ILI metabolism.

Overall, our data confirm the importance of fatty acid and lipid metabolism in *M. abscessus* under nutritional stress and highlight the importance of proteins involved in TAG mobilization as potential therapeutic targets. Nevertheless, it is true that the nutrients available *in vivo* differ from the *in vitro* conditions described here, as mycobacteria can be found in different cellular compartments (*e.g.* phagosome, macrophage, etc.) during infection. In particular, mycobacteria reside in different lipidic environments, such as foamy macrophages, giving them access to host lipids to metabolize their own TAGs, which are subsequently stored into ILI [4].

In summary, the multi-targeted **OX** & **CyC** inhibitors represent powerful probes for monitoring mycobacterial infection and identifying key specific targets within infected macrophages. In particular, their use as specific activity-based probes to identify the mycobacterial lipolytic enzymes involved in host lipid bodies degradation, lipid accumulation in ILI, as well as in the consumption of these intrabacterial lipids using the model of infected foamy and non-foamy macrophages [11, 23, 31], will open exciting opportunities. By working on living infected cells, such knowledge will also provide crucial information on the life cycle of intracellular mycobacteria, inspiring new therapeutic strategies to counter latent/persistent bacilli in infected individuals. Such studies are currently under progress and will be reported in due course.

METHODS

Chemistry

Synthesis of OX and CyC activity-based probes. The Cycliphostin analogs **CyC$_{31}$**, **CyC$_{31yne}$** and **CyC$_{31\text{-}Dansyl}$**, as well as the Oxadiazolone derivative **HPOX**, were synthesized as described previously [36, 39, 43]. Stock solutions (10 mM) in which the **OX** & **CyC** molecules (purity of ≥95%) were found to be completely soluble in dimethyl sulfoxide (DMSO) were prepared and stored at 4 °C. See **Supporting Information** for NMR spectra of the new **OX** probes.

General Methods. All solvents were anhydrous reagents from commercial sources. Unless otherwise noted, all chemicals and reagents were obtained commercially and used without purification. The reactions were monitored using TLC on plates that were pre-coated with silica gel 60 (Merck, Kenilworth, New Jersey, USA). The reaction components were visualized using a 254 nm UV lamp, stained with phosphomolybdic acid solution followed by gentle heating. Purifications of the synthesized compounds were performed by column chromatography on silica gel 40–63 µm. Melting points (Mp) were determined on a Stuart capillary apparatus and are uncorrected. High resolution mass spectrometry (HRMS) was recorded using electrospray ionization (ESI) techniques on Q-TOF mass spectrometer. NMR spectra were recorded at 300 or 500 MHz (^{1}H) and 75 or 126 MHz (^{13}C) using Bruker spectrometers. Chemical shifts are reported in parts per million (ppm, δ) relative to residual deuterated solvent peaks. The NMR spectra were assigned with the help of 2D NMR analyses. The multiplicities reported are as follows: br = broad singlet, m = multiplet, s = singlet, d = doublet, t = triplet, q = quadruplet, quint = quintuplet, h = hexuplet, or combinations thereof.

5-(hex-5-ynyloxy)-3-phenyl-1,3,4-oxadiazol-2(3H)-one (HPOX$_{yne}$).

Commercial 5-hexyn-1-ol (**3**) (720 µL, 6.44 mmol, 2.5 equiv.) was dissolved in dry CH_2Cl_2 (25 mL) in presence of dry distilled Et_3N (1 mL, 7.50 mmol, 2.9 equiv.) and stirred at 0 °C. Then, a solution of triphosgene (760 mg, 2.60 mmol, 1 equiv.) in CH_2Cl_2 (10 mL) was added dropwise. The resulting

mixture was stirred at 0 °C for 30 min, then 1.5 h at room temperature. The mixture was then degassed with N_2 in order to evacuate remaining phosgene and poured into pentane (100 mL). The resulting suspension was filtered on celite and solvents evaporated cautiously to afford crude chloroformate directly engaged in the next step without further purification (Rf = 0.3 (cyclohexane/EtOAc 80:20)). The crude hex-5-yn-1 chloroformate (**2**) was dissolved in CH_2Cl_2 (12 mL), and slowly added dropwise over a period of 5 min at 0-5 °C to a solution of phenylhydrazine hydrochloride (**1**) (800 mg, 5.53 mmol, 1 equiv.) and 1-methyl pyrrolidone (480 µL, 4.98 mmol, 0.9 equiv.) in dry pyridine (11 mL). The reaction was stirred for 1 h at 0 °C and 1h at room temperature. The reaction mixture was diluted by addition of CH_2Cl_2 (50 mL) and dry pyridine (11 mL) and cooled at -10 °C using an ice-salt bath. A solution of diphosgene (1 mL, 8.3 mmol, 1.5 equiv.) in CH_2Cl_2 (5 mL) was added dropwise over a period of 10 min while maintaining -10 °C with an ice-salt bath. After the addition is complete, the reaction mixture was stirred 2 h at -10 °C, then 2 h at room temperature. The mixture was then degassed with N_2 to eliminate the remaining phosgene. The reaction mixture was diluted with water (100 mL) and extracted with diethyl ether (3×50 mL). The combined organic layers were washed with water (2×50 mL) and brine (3×50 mL), dried over $MgSO_4$, and filtered. Purification by column chromatography using cyclohexane/ethyl acetate (99:1 to 90:10, *v/v*) as eluent, followed by recrystallization with hexane gave the title compound as a white solid (680 mg, 47%).

Analytical data for **HPOX$_{yne}$**. Mp: 61.0-63.2° C. R*f* (AcOEt/Cyclohexane 1:3, *v/v*) 0.50. IR (neat) *v* 3283 (C≡C-H), 2974 (C-H), 1787 (C=O), 1661, 1646 (C=C) cm^{-1}. HRMS (ESI) *m/z* $[M+H]^+$ calcd. for $C_{14}H_{14}N_2O_3$: 259.1080 Da; found: 259.1083 Da. ^1H NMR (300 MHz, $CDCl_3$) δ 7.80-7.77 (m, 2H, H_{Ar}), 7.45-7.38 (m, 2H, H_{Ar}), 7.26-7.19 (m, 1H, H_{Ar}), 4.44 (t, $^3J_{H,H}$ = 6.3 Hz, 2H, CH_2-O), 2.29 (td, $^3J_{H,H}$ = 6.9, $^4J_{H,H}$ = 2.6 Hz, 2H, CH_2-C≡CH), 2.04-1.94 (m, 3H, CH_2-CH_2 + C≡C*H*), 1.76-1.66 (m, 2H, CH_2-CH_2). ^{13}C NMR (75 MHz, $CDCl_3$) δ 155.4, 148.4, 136.3, 129.2 (2C), 125.6, 118.0 (2C), 83.5, 71.2, 69.3, 27.5, 24.5, 18.0.

5-(hexyloxy)-3-(4-nitrophenyl)-1,3,4-oxadiazol-2(3H)-one (6)

A solution of *p*-nitrophenylhydrazine (**4**) (3 g, 15.82 mmol, 1 equiv.) in dry pyridine (28 mL) was stirred at room temperature. After 15 min, the mixture was cooled to 0 °C and a solution of hexylchloroformate (**5**) (2.59 mL, 15.82 mmol, 1 equiv.) in dry CH_2Cl_2 (12 mL) was slowly added dropwise over a period of 5 min at 0-5 °C. The mixture was stirred at 0 °C for 30 min followed by 2 h at room temperature. Additional hexylchloroformate (**5**) (1.30 mL, 7.94 mmol, 1 equiv.) in dry CH_2Cl_2 (6 mL) was slowly added to increase full conversion of starting material. After 40 min, the mixture was diluted with dry CH_2Cl_2 (45 mL), dry pyridine (12.5 mL) and cooled to 0 °C. A solution of diphosgene (1.91 mL, 15.82 mmol, 1 equiv.) in dry CH_2Cl_2 (12 mL) was added dropwise. The mixture was stirred at 0 °C for 30 min followed by 2 h at room temperature. The mixture was then degassed with N_2 to eliminate the remaining phosgene, treated with 1M HCl (50 mL) and extracted with Et_2O (2×100 mL). The organic layers were washed with brine (100 mL), dried over $MgSO_4$ and solvents were removed under reduced pressure. The crude product was then adsorbed on silica and purified through gel chromatography in isocratic pentane/Et_2O (90:10, *v/v*) to give the titled compound (**6**) (2.476 g, 8.05 mmol, 51% over 2 steps) as a yellow solid.

Analytical data for compound (**6**). Mp: 43.3-44.6° C. R*f* (AcOEt/Cyclohexane 20:80, *v/v*) 0.50. IR (neat) *v* 3125, 2920 (C-H), 1780 (C=O), 1660, 1596, 1521 (C=C), 1353 (NO_2), 734 (C-H aromatic) cm^{-1}. HRMS (ESI) *m/z* $[M+H]^+$ calcd. for $C_{14}H_{18}N_3O_5$: 308.1241 Da; found: 308.1243 Da. ^1H NMR (300 MHz, $CDCl_3$) δ 8.30 (d, $^3J_{H,H}$ = 9.3 Hz, 2H, H_{Ar}), 8.00 (d, $^3J_{H,H}$ = 9.3 Hz, 2H, H_{Ar}), 4.44 (t, $^3J_{H,H}$ = 6.7 Hz, 2H, CH_2-O), 1.86 (quint, $^3J_{H,H}$ = 7.0 Hz, 2H, CH_2-CH_3), 1.49-1.43 (m, 2H, CH_2), 1.38-1.33 (m, 4H, 2xCH_2), 0.92 (t, 3H, $^3J_{H,H}$ = 7 Hz, CH_2-CH_3). ^{13}C NMR (75 MHz, $CDCl_3$) δ 155.9, 148.0, 144.6, 141.2, 125.1 (2C), 117.6 (2C), 72.5, 31.3, 28.4, 25.2, 22.6, 14.0.

3-(4-aminophenyl)-5-(hexyloxy)-1,3,4-oxadiazol-2(3H)-one (7)

A solution of the nitro-oxadiazolone (**6**) (500 mg, 1.60 mmol, 1 equiv.) in EtOAc (7.5 mL) was prepared at room temperature. Then, Pd/C (10% *w/w*, 50 mg) was added. The resulting suspension was stirred for 1 h under H_2 atmosphere. After elimination of the remaining H_2, the mixture was

filtered on celite and the solvent was removed under reduced pressure. The crude compound was adsorbed on silica and purified through gel chromatography in isocratic pentane/EtOAc (70:30, *v/v*) to give the titled compound (**7**) (420 mg, 1.50 mmol, 95%) as a yellow solid.

Analytical data for compound (**7**). Mp: 69.1-71.1° C. R*f* (AcOEt/Hexane 30:70, *v/v*) 0.29. IR (neat) *v* 3470, 3373 (N-H), 2961, 2926 (C-H), 1772 (C=O), 1648 (δ N-H), 1630, 1516 (C=C), 718 (C-H aromatic) cm^{-1}. HRMS (ESI) *m/z* $[M+H]^+$ calcd. for $C_{14}H_{20}N_3O_3$: 278.1499 Da; found: 278.1503 Da. ^1H NMR (300 MHz, $CDCl_3$) δ 7.51 (d, $^3J_{H,H}$ = 8.9 Hz, 2H, *H*$_{Ar}$), 6.71 (d, $^3J_{H,H}$ = 8.9 Hz, 2H, *H*$_{Ar}$), 4.36 (t, $^3J_{H,H}$ = 6.6 Hz, 2H, C*H*$_2$-O), 3.69 (br, 2H, N*H*$_2$), 1.82 (quint, $^3J_{H,H}$ = 7.0 Hz, 2H, C*H*$_2$-CH_3), 1.48-1.41 (m, 2H, C*H*$_2$), 1.35-1.32 (m, 4H, 2xC*H*$_2$), 0.91 (t, $^3J_{H,H}$ = 7.0 Hz, 3H, CH_2-C*H*$_3$). ^{13}C NMR (75 MHz, $CDCl_3$) δ 155.3, 148.7, 144.6, 127.8, 120.4 (2*C*), 115.3 (2*C*), 71.7, 31.3, 28.5, 25.2, 22.6, 14.1.

5-(hexyloxy)-3-(4-((7-nitrobenzo[c][1,2,5]oxadiazol-4-yl)amino)phenyl)-1,3,4-oxadiazol-2(3H)-one (HP-NBD-OX)

A solution 4-chloro-7-nitro-2,1,3-benzoxadiazole (NBD-Cl, 296 mg, 1.35 mmol, 1.5 equiv.) in absolute EtOH (25 mL) was prepared. To this solution, the aniline-oxadiazolone (**7**) (250 mg, 0.90 mmol, 1 equiv.) was added. Then, NaOAc (4 mg, 0.05 mmol, 0.05 equiv.) was added and the mixture was stirred at reflux for 2 h. The resulting suspension was cooled to room temperature and diluted with Et_2O (50 mL). The precipitate was filtered and washed with Et_2O (10×10 mL) to afford a crude residue which was purified by recrystallization in CH_2Cl_2 to give the titled compound (106 mg, 0.24 mmol, 27%) as a red solid.

Analytical data for **HP-NBD-OX**. Mp: 225-226° C. R*f* (AcOEt/Hexane 20:80, *v/v*) 0.39. IR (neat) *v* 3345, 3110 (N-H), 2927 (C-H), 1768 (C=O), 1655 (δ N-H), 1597, 1567, 1503 (C=C), 897, 830 (C-H aromatic) cm^{-1}. HRMS (ESI) *m/z* $[M+H]^+$ calcd. for $C_{20}H_{21}N_6O_6$: 441.1517 Da; found: 441.1516 Da. ^1H NMR (300 MHz, $CDCl_3$) δ 11.08 (s, 1H, N*H*), 8.52 (d, $^3J_{H,H}$ = 8.8 Hz, 1H, *H*$_{Ar}$), 7.79 (d, $^3J_{H,H}$ = 8.8 Hz, 2H, *H*$_{Ar}$), 7.59 (d, $^3J_{H,H}$ = 8.75 Hz, 2H, *H*$_{Ar}$), 6.73 (d, $^3J_{H,H}$ = 8.82 Hz, 1H, *H*$_{Ar}$), 4.41 (t, $^3J_{H,H}$

= 6 Hz, 2H, CH_2-O), 1.79 (quint, $^3J_{H,H}$ = 6.0 Hz, 2H, CH_2-CH_3), 1.41-1.37 (m, 2H, CH_2), 1.32-1.31 (m, 4H, 2xCH_2), 0.89 (t, $^3J_{H,H}$ = 6.0 Hz, 3H, CH_2-CH_3). ^{13}C NMR (75 MHz, $CDCl_3$) δ 154.8, 147.9, 145.0, 144.1, 142.1, 137.5, 134.8, 133.8, 124.7 (2C), 123.2, 118.6 (2C), 101.8, 71.7, 30.7, 27.7, 24.6, 21.9, 13.8.

Biological evaluation

Bacterial strains and growth conditions. *M. abscessus* CIP104536^T with either a smooth (S) or a rough (R) morphotype, was classically grown in Middlebrook 7H9 liquid medium (BD Difco, Le Pont de Claix, France) supplemented with 0.05% Tween 80 (Sigma-Aldrich, Saint-Quentin Fallavier, France), 0.2% glycerol (Euromedex, France) and 10% oleic albumin dextrose catalase (OADC enrichment, BD Difco, France) (7H9-S^{OADC}) at 37 °C and 200 rpm.

Generation of lipid-loaded cells. ILI accumulation in *M. abscessus* S liquid culture was performed as previously reported [24]. Briefly, from a culture at the logarithmic growth stage (OD_{600} ~1-1.5), *M. abscessus* S cells were harvested by centrifugation at 5,000 rpm for 15 min. Pellets were washed once with sterile PBS buffer (pH 7.4) containing 0.05% (*v*/*v*) Tween-20, then once with PBS buffer, and finally re-suspended in PBS at a final theoretical OD_{600} of 10. This bacterial solution was used to inoculate at an initial OD_{600} of 0.1, either fresh Mineral Salt Medium (MSM) (2 g/L Na_2HPO_4, 1 g/L KH_2PO_4, 0.5 g/L NaCl, 0.2 g/L $MgSO_4$, 20 mg/L $CaCl_2$, 1 g/L NH_4Cl, and 5% glycerol) or Mineral Salt Medium Nitrogen Limiting (MSM-NL) containing only 0.15 g/L NH_4Cl. To avoid bacterial clumping, Tyloxapol (Sigma-Aldrich) was added at a final concentration of 0.02% (*v*/*v*). The MSM and MSM-NL culture media were next incubated for 24 and 48 h at 37 °C under agitation (200 rpm). Alternatively, after 24 h incubation period at 37 °C and 200 rpm, the latter cultures were centrifuged and the pellets resuspended in respective fresh MSM or MSM-NL at a final theoretical OD_{600} of 20. One mL sample of these homogeneous bacterial suspensions was further incubated with **CyC$_{31yne}$** (200 µM final concentration), **HPOX$_{yne}$** (500 µM final concentration) or DMSO (control), as well as

with the fluorescent **CyC$_{31\text{-}Dansyl}$** or **HP$_{\text{-}NBD\text{-}}$OX** probes (100 µM final concentration) for additional 24 h at 37 °C under shaking at 200 rpm.

Normalization, lipid extraction and thin layer chromatography (TLC) analysis – adapted from [24]. *M. abscessus* S cells were grown in MSM or MSM-NL in presence or absence of inhibitor as described above. At 24 and 48 h incubation period, cultures were centrifuged at 3,500 rpm for 10 min at 4 °C. Cells were washed three times with distilled water, heated at 95 °C for 15 min and removed. Pellets were next lyophilized overnight and weighed to obtain the exact dry weight of the mycobacterial residue. Apolar lipids were extracted as previously reported [24]. Briefly, 2 mL of MeOH-0.3% NaCl (10:1, *v/v*) was added per 10 mg dry extract. The saline-MeOH solution containing the bacterial dry extract was mixed for 15 min with 1 mL petroleum ether in Pyrex® tubes at room temperature using a tube rotator. After centrifugation at 3,000 rpm for 5 min, the upper organic layer was transferred to a fresh tube. This step was repeated two times. The combined organic layers containing apolar lipids were transferred to a fresh pre-weighed vial, and the solvent was evaporated to dryness under nitrogen stream. Finally, the obtained dry apolar lipid residue was re-suspended in 200 µL dichloromethane.

The obtained extracted lipids were analyzed using glass TLC plates (TLC Silica Gel 60 F_{254}, Merck). Petroleum ether (40-60 °C fraction)/diethyl ether (90:10, *v*/*v*) was used as eluent for the TLC analysis of TAG. Following eluent migration, the plates were dried at room temperature for 10 min, and then sprayed with a cupric acetate-orthophosphoric acid solution prepared by mixing a saturated aqueous solution of cupric acetate with 85% phosphoric acid in a 1-to-1 volume ratio, followed by heating at 140 °C in an oven for 5-10 min. Each resolved plate was scanned using a Chemidoc™ MP Imaging System (Bio-Rad), and densitometric analyses were performed using the open-source program ImageJ/Fiji 1.53f51 (NIH, USA) to determine relative TAG content per sample.

MIC determination. The antibacterial activity of the fluorescent **CyC$_{31\text{-Dansyl}}$** and **HP$_{\text{-NBD-}}$OX**, as well as the **CyC$_{31yne}$** and **HPOX$_{yne}$** probes as compared to the parent **CyC$_{31}$** and **HPOX** against *M. abscessus* S & R growth, was assessed by determining their MICs in 96-well flat-bottom Nunclon Delta Surface microplates with lid (Thermo-Fisher Scientific, Illkirch, France) using the REMA assay [34-35, 39, 45]. Briefly, a log-phase *M. abscessus* culture was diluted to a cell density of 5×10^6 cells/mL in 7H9-S^{OADC}. Then 100 µL of the above inoculum (*i.e.*, 5×10^5 cells per well) were added to 100 µL of a serial two-fold dilutions of each compound (or DMSO as control) in 7H9-S^{OADC} medium, to a final volume of 200 µL per well of the 96-well plate [34-35, 39]. Plates were incubated at 37 °C for 3-5 days. Then, 20 µL of a 0.025% (*w/v*) resazurin solution was added to each well, and the plates were incubated at 37 °C for color change from blue to pink or violet and for a reading of fluorescence units (FU). Fluorescence corresponding to the resazurin reduction to its metabolite resorufin ($\lambda_{ex}/\lambda_{em}$ = 530/590 nm) was quantified using a Tecan Spark 10M multimode microplate reader (Tecan Group Ltd, France). MIC values were determined by fitting the relative fluorescence unit (RFU%) sigmoidal dose-response curves in Kaleidagraph 4.2 software (Synergy Software). The lowest compound concentration leading to 50% and 90% growth inhibition was defined as the MIC_{50} and MIC_{90}, respectively. Amikacin (AMK) and Imipenem (IMP) were used as reference drugs.

Activity-based protein profiling (ABPP) experiments – adapted from [43].

Capture of M. abscessus S potential target enzymes from HPOX$_{yne}$ and CyC$_{31yne}$-treated MSM and MSM-NL culture. A pre-culture in 7H9-S^{OADC} was grown to the logarithmic growth stage (OD_{600} ~1-1.5), then *M. abscessus* S cells were harvested by centrifugation at 5,000 rpm for 15 min, washed with PBS-Tween 20 (0.05%, *v/v*) and PBS, resuspended in PBS at an $OD_{600\ nm}$ of 10, and inoculated to either fresh MSM or MSM-NL at an initial $OD_{600\ nm}$ of 0.1. After 24 h or 48 h incubation period at 37 °C and 200 rpm, the culture was centrifuged and the pellets were resuspended in fresh MSM or MSM-NL at a final theoretical $OD_{600\ nm}$ of 20. One mL sample of these homogeneous bacterial suspensions was incubated with **CyC$_{31yne}$** (200 µM final concentration), **HPOX$_{yne}$** (500 µM final

concentration) or DMSO (control) at 37 °C for additional 24 h under shaking at 200 rpm. Bacteria were harvested (13,000 rpm, 4 °C, 2 min) and washed with 3× 500 µL PBS. Pellets were resuspended in 750 µL PBS supplemented with EDTA-free protease inhibitors (cOmplete Mini, EDTA-free, Roche) at a 1:1 (*w/v*) ratio. The bacterial cells were then mixed with 200 µL of 0.1 mm diameter glass beads (BioSpec) in a 1.5-mL Eppendorf tube and disrupted during 2×4 min of violent shaking, with ice cooling between each run, using Mini-Beadbeater-96 (BioSpec). The lysate was cooled down in ice for 5 min and then centrifuged at 4 °C and at 1300 rpm for 10 min to remove the cell debris and unbroken cells. The concentration of total proteins in the supernatants was determined *via* the Bradford method, adjusted to a concentration of 1 mg/mL, snap frozen in liquid nitrogen and stored at –80 °C until further use.

Both **CyC$_{31yne}$**- and **HPOX$_{yne}$**-treated *M. abscessus* and DMSO-control lysate samples (500 µL – 0.5 mg total proteins) were subjected to click-chemistry reaction by successive addition of Desthiobiotin-PEG$_3$-N$_3$ (Jena Bioscience, CLK-AZ104P4-100), TBTA ligand and fresh TCEP solution (Sigma-Aldrich) to the cells (see table below for added volumes).

Reagents	**Stock solution**	**Volume of reagent (µL) depending on the probe concentration 200 µM / 500 µM**
Desthiobiotin-Peg$_3$-N$_3$	40 mM DMSO	3.2 / 8.0
TCEP	50 mM H_2O	6.3 / 16.0
TBTA	1.667 mM *t*BuOH/DMSO (80:20, *v/v*)	19.0 / 48.1
$CuSO_4$	50 mM H_2O	6.3 / 16.0

After gently vortexing of the samples, the cycloaddition reaction was initiated by addition of fresh $CuSO_4$ solution (50 mM in H_2O). The lysates were mixed by vortexing again and incubated for 2 h under gentle rotative agitation (15 rpm) at room temperature in the dark. The proteins were further precipitated overnight at -20 °C by adding 1.2 mL ice-cold acetone, and pelletized by centrifugation (13,000 rpm, 4 °C, 15 min). The supernatant was discarded and the proteins were washed with 2×500 µL cold MeOH (resuspension by sonication, 3×1 min, 10% max. intensity). After centrifugation (13,000 rpm, 4 °C, 10 min), the pellets were resuspended in 0.2% (*w/v*) SDS in PBS (250 µL) at room

temperature by mild sonication (4×1 min, 10% max. intensity). Affinity enrichment was performed with 25 µL Pierce™ High-Capacity Streptavidin Agarose Resin (Thermo Scientific ref. 20359; pre-washed 3×500 µL 0.4% (*w/v*) SDS in PBS, then 3×500 µL PBS, centrifugation was performed at 5,000 rpm for 2 min). Each *M. abscessus* S treated-lysate was enriched for labelled proteins by transfer to the previously washed beads (around 250 µg) and incubated under gentle rotative agitation (15 rpm) at room temperature for 3 h. Beads were stringently washed following pull-down (1 mL each time): 2× 0.4% (*w/v*) SDS in PBS, and 1× 10 M urea in PBS. All centrifugation steps were conducted at 5000 rpm for 2 min at room temperature. The beads containing bound, biotinylated proteins were resuspended in 40 µL PBS buffer pH 7.4 containing 50 mM free D-biotin. The resulting solution was mixed with 5X Laemmli reducing sample buffer, and heated at 95°C for 5 min. This step allowed the recovery of the captured labelled proteins by exchanging the initially captured Desthiobiotin/streptavidin complex to the greater affinity biotin/streptavidin complex. Each sample was snap frozen in liquid nitrogen and stored at –80°C before mass spectrometry experiments. To check for unspecific binding, the DMSO-treated lysate sample was also incubated with the streptavidin-agarose beads, and processed as described above.

***Mass spectrometry analysis*.** The protein isolates were loaded on NuPAGE™ 4-12% Bis–tris acrylamide gels according to the manufacturer's instructions (Invitrogen, Life Technologies). Running of samples was stopped as soon as proteins stacked as a single band. Protein containing bands were stained with Thermo Scientific Imperial Blue, cut from the gel, and following reduction and iodoacetamide alkylation, digested with high sequencing grade trypsin (Promega, Madison, WI, USA) [35, 43]. Extracted peptides were concentrated before mass spectrometry analysis under speed-vacuum. Samples were reconstituted with 0.1% trifluoroacetic acid in 2% acetonitrile and analyzed by liquid chromatography (LC)-tandem MS (MS/MS) using a Q Exactive Plus Hybrid Quadrupole-Orbitrap online with a nanoLC Ultimate 3000 chromatography system (Thermo Fisher Scientific™, San Jose, CA). For each biological sample, 3 µL corresponding to 16.6% of digested sample were injected in duplicate on the system. After pre-concentration and washing of the sample on a Acclaim

PepMap 100 column (C18, 2 cm × 100 µm i.d. 100 Å pore size, 5 µm particle size), peptides were separated on a LC EASY-Spray column (C18, 50 cm × 75 µm i.d., 100 Å, 2 µm, 100 Å particle size) at a flow rate of 300 nL/min with a two-step linear gradient (2-22% acetonitrile/H_20; 0.1% formic acid for 100 min and 22-32% acetonitrile/H_20; 0.1% formic acid for 20 min). For peptides ionization in the EASY-Spray source, spray voltage was set at 1.9 kV and the capillary temperature at 250 °C. All samples were measured in a data dependent acquisition mode. Each run was preceded by a blank MS run in order to monitor system background. The peptide masses were measured in a survey full scan (scan range 375-1500 *m/z*, with 70 K FWHM resolution at *m/z*=400, target AGC value of 3.00×10^6 and maximum injection time of 100 ms). Following the high-resolution full scan in the Orbitrap, the 10 most intense data-dependent precursor ions were successively fragmented in HCD cell and measured in Orbitrap (normalized collision energy of 25%, activation time of 10 ms, target AGC value of 1.00×10^5, intensity threshold 1.00×10^4 maximum injection time 100 ms, isolation window 2 *m/z*, 17.5 K FWHM resolution, scan range 200 to 2000 *m/z*). Dynamic exclusion was implemented with a repeat count of 1 and exclusion duration of 20 s.

***Protein identification and quantification*.** Relative intensity-based label-free quantification (LFQ) was processed using the MaxLFQ algorithm [71] from the freely available MaxQuant computational proteomics platform, version 1.6.3.4 [72]. Analysis was done on three biological duplicates, each injected two times on mass spectrometers. The acquired raw LC Orbitrap MS data were first processed using the integrated Andromeda search engine [73]. Spectra were searched against the *Mycobacterium abscessus* (UP000007137) database extracted from UniProt (date 2021-03-10; 4,940 entries) [74]. The false discovery rate (FDR) at the peptide and protein levels were set to 1% and determined by searching a reverse database. For protein grouping, all proteins that could not be distinguished based on their identified peptides were assembled into a single entry according to the MaxQuant rules. The statistical analysis was done with Perseus program (version 1.6.15) from the MaxQuant environment (www.maxquant.org). Quantifiable proteins were defined as those detected in above 70% of samples in one condition or more. Protein LFQ normalized intensities were base 2

logarithmized to obtain a normal distribution. Missing values were replaced using data imputation by randomly selecting from a normal distribution centered on the lower edge of the intensity values that simulates signals of low abundant proteins using default parameters (a downshift of 1.8 standard deviation and a width of 0.3 of the original distribution). To determine whether a given detected protein was specifically differential in **CyC$_{31yne}$** pulldown, a two-sample t-test was done using permutation-based FDR-controlled at 5 and employing 250 permutations. The *p*-value was adjusted using a scaling factor s0 with a value of 0.1. In case of **HPOX$_{yne}$**, the permutation-based FDR was controlled at 1 and the scaling factor s0 with a value of 1 [75].

The mass spectrometry proteomics data have been deposited to the ProteomeXchange Consortium (www.proteomexchange.org) [76] *via* the PRIDE partner repository [77] with the dataset identifier PXD048770 (Reviewer account details: **username**: reviewer_pxd048770@ebi.ac.uk / **password**: UTx078nj).

Fluorescence imaging of lipid-loaded *M. abscessus* cells

Nile Red staining. After 24 h and 48 h incubation period either in MSM or MSM-NL, and in presence/absence of inhibitors, *M. abscessus* S cultures were centrifuged at 3,500 rpm for 10 min, washed with 2× 1 mL of PBS, and then fixed with 4% paraformaldehyde in PBS for 20 min at room temperature. The pellets were washed three times with PBS-Tween 80 (0.05%, *v/v*) and resuspended in PBS at a theoretical OD_{600} of 10. The above fixed bacterial suspension (300 µL) was further incubated for 20-30 min at 37 °C in the dark with 15 µL (0.5 mg/mL in absolute ethanol) of Nile Red fluorescent dye (Interchim, Montluçon, France) for ILI staining as previously described [24]. Stained bacteria were harvested for 5 min at 5,000 rpm, then washed with 2× 500 µL of PBS-Tween 80 (0.05%, *v/v*), and re-suspended in 300 µL of PBS.

Fluorescent Microscopy. Fixed stained samples (5 µL bacterial suspension, *i.e.*, 7.5×10^6 cells, spotted between a coverslip of 170 µm thickness and a 1.5% agarose-PBS pad) were analyzed by snapshot fluorescence imaging at room temperature using an Olympus IX81 confocal microscope

equipped with a UPlanSApo 100× 1.40 NA objective and operated with the FV1000 software. Acquisitions were taken using a 2-line Kalman integration with sequential channels acquisition. Exposure time was 10 µs/pixel for both laser transmission and fluorescence images with conserved settings (HV, Gain and offset). The Dansyl was detected by excitation with a 405 nm laser with 39-50% intensity, and emission was collected using a semi-transparent mirror collecting all wavelength below 560 nm. The NBD was detected by excitation with a 405 nm laser with 40% intensity, and emission was collected using a semi-transparent mirror collecting all wavelength below 560 nm. The GFP signal was detected by excitation with a 443 nm laser with 33% intensity, and emission was collected using a semi-transparent mirror collecting all wavelength below 560 nm. The Nile Red was detected by excitation with a 543 nm laser with 39-50% intensity, and emission was collected using a semitransparent mirror collecting all wavelength over 640 nm.

Images recorded (126.98 µm × 126.98 µm; 512 × 512 pixels) were processed using the open-source program ImageJ/Fiji 1.53f51 (NIH, USA). In all cases, three biological replicates were made; and for each sample, 10 different images were taken per frame in order to get more than 200 bacteria in total. In addition, all corresponding control images were taken/checked prior to any fluorescence imaging and quantification.

Colocalization analysis between the Dansyl, NBD or GFP and Nile Red fluorescence using coloc2 plugin of ImageJ/Fiji (adapted from [78]). Colocalization between the Nile Red and Dansyl, NBD or GFP fluorescence intensity was assessed by evaluating the pixel intensity correlation over space using the Coloc2 plugin of ImageJ/Fiji, through the computed colocalization parameters: the Manders' correlation coefficients, the Pearson coefficient, and the intensity correlation quotient (ICQ) value as suggested by Li [79]. Manders' coefficients (*M1* and *M2*) estimate the co-occurrence fraction of a fluorescent signal on one channel (*i.e.*, red color) with a fluorescent signal of another channel (*i.e.*, green color). Pearson's coefficient (*R*) evaluate the correlation between two signals by measuring the relationship between the signal intensities in one image (*i.e.*, channel red) and the corresponding values in another (*i.e.*, channel green) [80]. The statistical significance of these computed correlation

coefficients has been assessed by the Costes randomization test [81], resulting in a Costes' *p*-value which should be ≥95%.

The Manders' coefficients vary from 0 to 1, the former corresponding to non-overlapping images and the latter reflecting 100% co-localization between two images. A calculated Pearson coefficient value ranges from 1 to -1, with 1 standing for complete positive correlation and -1 for a negative one, while a 0 value indicates no correlation. The ICQ value varies from 0.5 (co-localisation) to -0.5 (exclusion) while random staining and images impeded by noise will give a value close to 0. The table below depicts the values of the different colocalization coefficients and their meanings with respect to the colocalization results.

Colocalization coefficients, their values and meanings

Coefficients	Values	Meanings
Manders' coefficients *M1* & *M2*	0	Co-occurrence
	1	No co-occurrence
Pearson coefficient *R*	-1	Negative correlation
	0	No correlation
	1	Positive correlation
	±0.5-±1	Strong correlation
	±0.3-±0.49	Moderate correlation
	±0.1-±0.29	Weak correlation
ICQ value	-0.5	Exclusion
	0	Random
	0.5	Co-localization

First, 32-bit images were transformed into 8-bit single channels images, and a background noise was calculated by taking the mean fluorescence intensity of 10 different areas free of any cells for each channel (*i.e.*, Dansyl, NBD, GFP or Nile red frames, respectively), and was subtracted to each frame before running the Coloc2 analyses plugin.

Plasmid construction and cloning. All specific primers and plasmids used in this study are listed in **Tables S11-S12** (see **Supporting Information**). All cloned fragments were amplified using purified *M. abscessus* genomic DNA.

Construction of MAB_1978c mutant strains. Deletion mutant Δ*mab_1978c* (= Δ*fadD15*) was obtained by a simple and rapid gene disruption strategy in *M. abscessus* developed by Richard *et al*. [60]. First, the *pUX1-katG::*Δ*fadD15_outer* and *pUX1-katG::*Δ*fadD15_inner* primers were PCR amplified using their respective forward and reverse oligonucleotides. These two amplicons were fused together through PCR with *pUX1-katG::*Δ*fadD15-inner_Fw* and *pUX1-katG::*Δ*fadD15-outer_Rev* primers thanks to their overlapping extension. The resulting product was gel purified (Macherey Nagel #740609) and cloned into pUX1-*katG* vector using NheI and HpaI restriction sites by classical cloning.

For complementation strain, the *fadD15* gene was amplified using the primer pairs *pVV16::fadD15-F* and *pVV16::fadD15-R*, then fused with *sfGfp* gene, and cloned into pVV16 plasmid downstream of the *hsp60* promoter also containing a kanamycin resistance cassette, using BamHI and NdeI restriction sites by classical cloning to generate *pVV16::fadD15-sfGFP*. Sequence integrity of each construct was confirmed by DNA sequencing (Eurofins Genomics). All the constructs were further transformed in electrocompetent *M. abscessus* S_Δ*fadD15* strains and selected on respective antibiotic agar plates as described previously [82].

Alternatively, overexpressing mutant strain was built using the same *pVV16::fadD15-sfGFP* vector and transformation in electrocompetent *M. abscessus* S wild-type strain.

The *M. abscessus* S_Δ*fadD15*::C complementation strain as well as the overexpressing *M. abscessus* S*_fadD15-sfGFP* were checked PCR amplification and sequencing strategy. Regarding the deletion strain, the selection was made based on red fluorescent colonies followed by PCR amplification and sequencing strategy as described in [82].

***Functional validation of mab_1978c in ILI accumulation*.** The abovementioned transformed bacteria; *i.e*., the *M. abscessus* S_Δ*fadD15* deletion strain and its complemented counterpart *M. abscessus* S_Δ*fadD15*::C, as well as the overexpressing *M. abscessus* S*_fadD15-sfGFP* strain were cultured in MSM and MSM-NL, supplemented with 250 µg/mL kanamycin when needed, for their

ability to accumulate ILI. After 48 h incubation, all bacterial cultures were processed for TAG content analysis through TLC as described above.

Statistical analysis. GraphPad Prism 8 (GraphPad Inc.) was used to perform all statistical analyses, which details are given in each figure legend. Differences were considered significant when the calculated *p*-values were smaller than 0.05.

ASSOCIATED CONTENT

* Supporting Information

Supporting Information for this article is available online

Tables S1-S10. Target proteins identified after a 24 h or 48 h culture of *M. abscessus* S in MSM-NL, through CC-ABPP by LC-ESI-MS/MS analysis, using **HPOX$_{yne}$** or **CyC$_{31yne}$** probes (XLSX).

S1 Appendix. List of primers and plasmids used in this study (**Tables S11-S12**); **Figure S1**, the **HP-$_{NBD}$-OX** and **the CyC$_{31-Dansyl}$** colocalized with ILI on *M. abscessus* S culture in MSM-NL; **Figure S2**, growth curves of *M. abscessus* S wild-type and Δ*fadD15* deletion mutant in 7H9TG^{OADC}, MSM and MSM-NL, respectively; **Figures S3**, *fadD15-sfGFP* overexpressing strain displays a diffuse fluorescence when grown in MSM; **Figure S4**, NMR spectra of the new **HPOX$_{yne}$** and **HP-$_{NBD}$-OX** compounds (PDF).

AUTHOR INFORMATION

Corresponding Author

Jean-François Cavalier - Aix-Marseille Univ, CNRS, LISM, IMM FR3479, Marseille, France.

Email: jfcavalier@imm.cnrs.fr. ORCID: https://orcid.org/0000-0003-0864-8314

Authors

Romain Avellan - Aix-Marseille Univ, CNRS, LISM, IMM FR3479, Marseille, France.

Jordan Lehoux - IBMM, Univ Montpellier, CNRS, ENSCM, Montpellier, France.

Tonia Dargham - Aix-Marseille Univ, CNRS, LISM, IMM FR3479, Marseille, France; and IHU Méditerranée Infection, Aix-Marseille Univ., Marseille, France

Thomas Francis - Aix-Marseille Univ, CNRS, LISM, IMM FR3479, Marseille, France.

Léa Celik - Aix-Marseille Univ, CNRS, LISM, IMM FR3479, Marseille, France.

Alexandre Guy - IBMM, Univ Montpellier, CNRS, ENSCM, Montpellier, France

Isabelle Poncin - Aix-Marseille Univ, CNRS, LISM, IMM FR3479, Marseille, France

Vanessa Point - Aix-Marseille Univ, CNRS, LISM, IMM FR3479, Marseille, France

Laurent Kremer - Centre National de la Recherche Scientifique UMR 9004, Institut de Recherche en Infectiologie de Montpellier (IRIM), Université de Montpellier, 1919 route de Mende, 34293, Montpellier, France; and INSERM, IRIM, 34293 Montpellier, France

Thierry Durand - IBMM, Univ Montpellier, CNRS, ENSCM, Montpellier, France

Stéphane Audebert - INSERM, CNRS, Institut Paoli-Calmettes, CRCM, Marseille Prot´eomique, Aix-Marseille University, France

Luc Camoin - INSERM, CNRS, Institut Paoli-Calmettes, CRCM, Marseille Prot´eomique, Aix-Marseille University, France

Christopher D. Spilling - Department of Chemistry and Biochemistry, University of Missouri-St. Louis, MO, USA

Céline Crauste - IBMM, Univ Montpellier, CNRS, ENSCM, Montpellier, France

Stéphane Canaan - Aix-Marseille Univ., CNRS, LISM UMR7255, IMM FR3479, Marseille, France

Author Contributions

Conceptualization: S.C. and J.-F.C. Data curation: S.A. and L.C. Resources: J.L., A.G., T.D., C.C. and C.D.S. Investigations: R.A., T.D., T.F., S.A., L.C., I.P. and V.P. Formal analysis: R.A., T.D., T.F., S.A., L.C., S.C. and J.-F.C. Visualization: R.A., T.D. and J.-F.C. Writing-original draft: J.-F.C. Writing-review & editing: R.A., T.D., L.K., T.D., S.A., L.C., C.D.S., C.C., S.C. and J.-F.C. Supervision: S.C. and J.-F.C. Funding acquisition: S.C. and J.-F.C. Validation: J.-F.C. Project administration: J.-F.C.

R.A., J.L. and T.D. contributed equally and should be considered as first coauthors. All authors have given approval to the final version of the manuscript.

Declaration of interests

The authors declare no competing interests.

ACKNOWLEDGEMENTS

This work was supported by the CNRS, Aix Marseille University, and the Agence Nationale de la Recherche (LipInTB project N°ANR-19-CE44-0011, and ILIome project N°ANR-20-CE44-0019). Proteomics analyses were done using the mass spectrometry facility of Marseille Proteomics (marseille-proteomique.univ-amu.fr) supported by IBISA, the Cancéropôle PACA, the Provence-Alpes-Côte d'Azur Region, the Institut Paoli-Calmettes, and Fonds Européen de Développement Regional (FEDER). R.A. was supported by a PhD fellowship from the Agence Nationale de la Recherche (LipInTB project N°ANR-19-CE44-0011). T.D. PhD fellowship was funded by the foundation IHU Méditerranée Infection. T.F. PhD fellowship is supported by the Ministère de l'Enseignement Supérieur et de la Recherche. J-F.C. is particularly grateful to Deezer and Carte Noire coffee for their invaluable help and support during the writing of this manuscript. The authors wish also to thank Dr Wassim Daher (IRIM, Montpellier, France) for his valuable input and discussions.

REFERENCES

(1) Brennan, P. J., Structure, function, and biogenesis of the cell wall of *Mycobacterium tuberculosis*. *Tuberculosis* **2003**, *83* (1), 91-97.

(2) Alvarez, H. M.; Steinbuchel, A., Triacylglycerols in prokaryotic microorganisms. *Appl Microbiol Biotechnol* **2002**, *60* (4), 367-76.

(3) Mallick, I.; Santucci, P.; Poncin, I.; Point, V.; Kremer, L.; Cavalier, J.-F.; Canaan, S., Intrabacterial lipid inclusions in mycobacteria: unexpected key players in survival and pathogenesis? *FEMS Microbiol Rev* **2021**, *45* (6), fuab029.

(4) Dargham, T.; Mallick, I.; Raze, D.; Kremer, L.; Canaan, S., Chapter 12 - Intrabacterial lipid inclusions: overview of an amazing organelle. In *Biology of Mycobacterial Lipids*, Fatima, Z.; Canaan, S., Eds. Academic Press: 2022; pp 253-269. DOI: https://doi.org/10.1016/B978-0-323-91948-7.00003-8.

(5) Fujimoto, T.; Ohsaki, Y., Cytoplasmic lipid droplets: rediscovery of an old structure as a unique platform. *Ann N Y Acad Sci* **2006**, *1086*, 104-15.

(6) Garton, N. J.; Barer, M. R., Mycobacterial Lipid Bodies and the Chemosensitivity and Transmission of Tuberculosis. In *Health Consequences of Microbial Interactions with Hydrocarbons, Oils, and Lipids*, 2020; pp 109-132. DOI: http://doi.org/10.1007/978-3-030-15147-8_6.

(7) Low, K. L.; Shui, G.; Natter, K.; Yeo, W. K.; Kohlwein, S. D.; Dick, T.; Rao, S. P.; Wenk, M. R., Lipid droplet-associated proteins are involved in the biosynthesis and hydrolysis of triacylglycerol in *Mycobacterium bovis* bacillus Calmette-Guerin. *J Biol Chem* **2010**, *285* (28), 21662-70.

(8) Walther, T. C.; Farese, R. V., Jr., Lipid droplets and cellular lipid metabolism. *Annu Rev Biochem* **2012**, *81*, 687-714.

(9) Wilfling, F.; Haas, J. T.; Walther, T. C.; Farese, R. V., Jr., Lipid droplet biogenesis. *Curr Opin Cell Biol* **2014**, *29*, 39-45.

(10) Daniel, J.; Maamar, H.; Deb, C.; Sirakova, T. D.; Kolattukudy, P. E., *Mycobacterium tuberculosis* Uses Host Triacylglycerol to Accumulate Lipid Droplets and Acquires a Dormancy-Like Phenotype in Lipid-Loaded Macrophages. *PLOS Pathogens* **2011**, *7* (6), e1002093.

(11) Caire-Brändli, I.; Papadopoulos, A.; Malaga, W.; Marais, D.; Canaan, S.; Thilo, L.; de Chastellier, C.; Flynn, J. L., Reversible Lipid Accumulation and Associated Division Arrest of *Mycobacterium avium* in Lipoprotein-Induced Foamy Macrophages May Resemble Key Events during Latency and Reactivation of Tuberculosis. *Infect Immun.* **2014**, *82* (2), 476-490.

(12) Neyrolles, O.; Hernández-Pando, R.; Pietri-Rouxel, F.; Fornès, P.; Tailleux, L.; Payán, J. A. B.; Pivert, E.; Bordat, Y.; Aguilar, D.; Prévost, M.-C.; Petit, C.; Gicquel, B., Is Adipose Tissue a Place for *Mycobacterium tuberculosis* Persistence? *PLoS ONE* **2006**, *1* (1), e43.

(13) Deb, C.; Lee, C.-M.; Dubey, V. S.; Daniel, J.; Abomoelak, B.; Sirakova, T. D.; Pawar, S.; Rogers, L.; Kolattukudy, P. E., A Novel In Vitro Multiple-Stress Dormancy Model for *Mycobacterium tuberculosis* Generates a Lipid-Loaded, Drug-Tolerant, Dormant Pathogen. *PLOS ONE* **2009**, *4* (6), e6077.

(14) Garton, N. J.; Waddell, S. J.; Sherratt, A. L.; Lee, S.-M.; Smith, R. J.; Senner, C.; Hinds, J.; Rajakumar, K.; Adegbola, R. A.; Besra, G. S.; Butcher, P. D.; Barer, M. R., Cytological and Transcript Analyses Reveal Fat and Lazy Persister-Like Bacilli in Tuberculous Sputum. *PLOS Medicine* **2008**, *5* (4), e75.

(15) Sloan, D. J.; Mwandumba, H. C.; Garton, N. J.; Khoo, S. H.; Butterworth, A. E.; Allain, T. J.; Heyderman, R. S.; Corbett, E. L.; Barer, M. R.; Davies, G. R., Pharmacodynamic Modeling of Bacillary Elimination Rates and Detection of Bacterial Lipid Bodies in Sputum to Predict and Understand Outcomes in Treatment of Pulmonary Tuberculosis. *Clin Infect Dis.* **2015**, *61* (1), 1-8.

(16) Hammond, R. J.; Baron, V. O.; Oravcova, K.; Lipworth, S.; Gillespie, S. H., Phenotypic resistance in mycobacteria: is it because I am old or fat that I resist you? *J Antimicrob Chemother* **2015**, *70* (10), 2823-7.

(17) Iona, E.; Giannoni, F.; Pardini, M.; Brunori, L.; Orefici, G.; Fattorini, L., Metronidazole plus rifampin sterilizes long-term dormant *Mycobacterium tuberculosis*. *Antimicrob Agents Chemother* **2007**, *51* (4), 1537-40.

(18) Bouzid, F.; Bregeon, F.; Poncin, I.; Weber, P.; Drancourt, M.; Canaan, S., *Mycobacterium canettii* Infection of Adipose Tissues. *Front Cell Infect Microbiol* **2017**, *7*, 189.

(19) Mattos, K. A.; Oliveira, V. G.; D'Avila, H.; Rodrigues, L. S.; Pinheiro, R. O.; Sarno, E. N.; Pessolani, M. C.; Bozza, P. T., TLR6-driven lipid droplets in *Mycobacterium leprae*-infected Schwann cells: immunoinflammatory platforms associated with bacterial persistence. *J Immunol* **2011**, *187* (5), 2548-58.

(20) Barisch, C.; Soldati, T., *Mycobacterium marinum* Degrades Both Triacylglycerols and Phospholipids from Its Dictyostelium Host to Synthesise Its Own Triacylglycerols and Generate Lipid Inclusions. *PLoS Pathog* **2017**, *13* (1), e1006095.

(21) Robbe-Saule, M.; Foulon, M.; Poncin, I.; Esnault, L.; Varet, H.; Legendre, R.; Besnard, A.; Grzegorzewicz, A. E.; Jackson, M.; Canaan, S.; Marsollier, L.; Marion, E., Transcriptional adaptation of *Mycobacterium ulcerans* in an original mouse model: New insights into the regulation of mycolactone. *Virulence* **2021**, *12* (1), 1438-1451.

(22) Garton, N. J.; Christensen, H.; Minnikin, D. E.; Adegbola, R. A.; Barer, M. R., Intracellular lipophilic inclusions of mycobacteria *in vitro* and *in sputum*. *Microbiology (Reading)* **2002**, *148* (Pt 10), 2951-8.

(23) Santucci, P.; Diomande, S.; Poncin, I.; Alibaud, L.; Viljoen, A.; Kremer, L.; de Chastellier, C.; Canaan, S., Delineating the Physiological Roles of the PE and Catalytic Domains of LipY in Lipid Consumption in Mycobacterium-Infected Foamy Macrophages. *Infect Immun* **2018**, *86* (9).

(24) Santucci, P.; Johansen, M. D.; Point, V.; Poncin, I.; Viljoen, A.; Cavalier, J. F.; Kremer, L.; Canaan, S., Nitrogen deprivation induces triacylglycerol accumulation, drug tolerance and hypervirulence in mycobacteria. *Sci Rep* **2019**, *9* (1), 8667.

(25) Viljoen, A.; Blaise, M.; de Chastellier, C.; Kremer, L., MAB_3551c encodes the primary triacylglycerol synthase involved in lipid accumulation in *Mycobacterium abscessus*. *Molecular microbiology* **2016**.

(26) Armstrong, R. M.; Carter, D. C.; Atkinson, S. N.; Terhune, S. S.; Zahrt, T. C., Association of Mycobacterium Proteins with Lipid Droplets. *J Bacteriol* **2018**, *200* (16).

(27) Dhouib, R.; Ducret, A.; Hubert, P.; Carriere, F.; Dukan, S.; Canaan, S., Watching intracellular lipolysis in mycobacteria using time lapse fluorescence microscopy. *Biochim Biophys Acta* **2011**, *1811* (4), 234-241.

(28) Dargham, T.; Mallick, I.; Kremer, L.; Santucci, P.; Canaan, S., Intrabacterial lipid inclusion-associated proteins: A core machinery conserved from saprophyte Actinobacteria to the human pathogen *Mycobacterium tuberculosis*. *FEBS Open Bio* **2023**.

(29) Cavalier, J. F.; Spilling, C. D.; Durand, T.; Camoin, L.; Canaan, S., Lipolytic enzymes inhibitors: A new way for antibacterial drugs discovery. *Eur J Med Chem* **2021**, *209*, 112908.

(30) Daniel, J.; Kapoor, N.; Sirakova, T.; Sinha, R.; Kolattukudy, P., The perilipin-like PPE15 protein in *Mycobacterium tuberculosis* is required for triacylglycerol accumulation under dormancy-inducing conditions. *Mol Microbiol* **2016**, *101* (5), 784-794.

(31) Santucci, P.; Bouzid, F.; Smichi, N.; Poncin, I.; Kremer, L.; De Chastellier, C.; Drancourt, M.; Canaan, S., Experimental Models of Foamy Macrophages and Approaches for Dissecting the Mechanisms of Lipid Accumulation and Consumption during Dormancy and Reactivation of Tuberculosis. *Front Cell Infect Microbiol* **2016**, *6*, 122.

(32) Johnson, G., The alpha/beta Hydrolase Fold Proteins of *Mycobacterium tuberculosis*, with Reference to their Contribution to Virulence. *Curr Protein Pept Sci* **2017**, *18* (3), 190-210.

(33) Avellan, R.; Sarrazin, M.; Spilling, C. D.; Crauste, C.; Canaan, S.; Cavalier, J.-F., Chapter 11 - Deciphering the physiological role of serine enzymes involved in mycobacterial lipid metabolism using activity-based protein profiling. In *Biology of Mycobacterial Lipids*, Fatima, Z.; Canaan, S., Eds. Academic Press: 2022; pp 235-251. DOI: https://doi.org/10.1016/B978-0-323-91948-7.00001-4.

(34) Madani, A.; Mallick, I.; Guy, A.; Crauste, C.; Durand, T.; Fourquet, P.; Audebert, S.; Camoin, L.; Canaan, S.; Cavalier, J. F., Dissecting the antibacterial activity of oxadiazolone-core derivatives against *Mycobacterium abscessus*. *PLoS One* **2020**, *15* (9), e0238178.

(35) Madani, A.; Ridenour, J. N.; Martin, B. P.; Paudel, R. R.; Abdul Basir, A.; Le Moigne, V.; Herrmann, J. L.; Audebert, S.; Camoin, L.; Kremer, L.; Spilling, C. D.; Canaan, S.; Cavalier, J. F., Cyclipostins and Cyclophostin Analogues as Multitarget Inhibitors That Impair Growth of *Mycobacterium abscessus*. *ACS Infect Dis* **2019**, *5* (9), 1597-1608.

(36) Nguyen, P. C.; Delorme, V.; Benarouche, A.; Guy, A.; Landry, V.; Audebert, S.; Pophillat, M.; Camoin, L.; Crauste, C.; Galano, J. M.; Durand, T.; Brodin, P.; Canaan, S.; Cavalier, J. F., Oxadiazolone derivatives, new promising multi-target inhibitors against *M. tuberculosis*. *Bioorg Chem* **2018**, *81*, 414-424.

(37) Nguyen, P. C.; Delorme, V.; Bénarouche, A.; Martin, B. P.; Paudel, R.; Gnawali, G. R.; Madani, A.; Puppo, R.; Landry, V.; Kremer, L.; Brodin, P.; Spilling, C. D.; Cavalier, J.-F.; Canaan, S., Cyclipostins and Cyclophostin analogs as promising compounds in the fight against tuberculosis. *Sci Rep* **2017**, *7* (1), 11751.

(38) Nguyen, P. C.; Madani, A.; Santucci, P.; Martin, B. P.; Paudel, R. R.; Delattre, S.; Herrmann, J.-L.; Spilling, C. D.; Kremer, L.; Canaan, S.; Cavalier, J.-F., Cyclophostin and Cyclipostins analogs, new promising molecules to treat mycobacterial-related diseases. *Int J Antimicrob Agents* **2018**, *51*, 651-654.

(39) Sarrazin, M.; Martin, B. P.; Avellan, R.; Gnawali, G. R.; Poncin, I.; Le Guenno, H.; Spilling, C. D.; Cavalier, J. F.; Canaan, S., Synthesis and Biological Characterization of Fluorescent Cyclipostins and Cyclophostin Analogues: New Insights for the Diagnosis of Mycobacterial-Related Diseases. *ACS Infect Dis* **2022**, *8* (12), 2564-2578.

(40) Santucci, P.; Point, V.; Poncin, I.; Guy, A.; Crauste, C.; Serveau-Avesque, C.; Galano, J. M.; Spilling, C. D.; Cavalier, J.-F.; Canaan, S., LipG a bifunctional phospholipase/thioesterase involved in mycobacterial envelope remodeling. *Bioscience Reports* **2018**, *38* (6), BSR20181953.

(41) Viljoen, A.; Richard, M.; Nguyen, P. C.; Fourquet, P.; Camoin, L.; Paudal, R. R.; Gnawali, G. R.; Spilling, C. D.; Cavalier, J.-F.; Canaan, S.; Blaise, M.; Kremer, L., Cyclipostins and Cyclophostin analogs inhibit the antigen 85C from *Mycobacterium tuberculosis* both *in vitro* and *in vivo*. *J. Biol. Chem.* **2018**, *293* (8), 2755–2769.

(42) Nguyen, P. C.; Nguyen, V. S.; Martin, B. P.; Fourquet, P.; Camoin, L.; Spilling, C. D.; Cavalier, J.-F.; Cambillau, C.; Canaan, S., Biochemical and structural characterization of TesA, a major thioesterase required for outer-envelope lipid biosynthesis in *M. tuberculosis*. *J Mol Biol.* **2018**, *430* (24), 5120-5136.

(43) Barelier, S.; Avellan, R.; Gnawali, G. R.; Fourquet, P.; Roig-Zamboni, V.; Poncin, I.; Point, V.; Bourne, Y.; Audebert, S.; Camoin, L.; Spilling, C. D.; Canaan, S.; Cavalier, J. F.; Sulzenbacher, G., Direct capture, inhibition and crystal structure of HsaD (Rv3569c) from *M. tuberculosis*. *FEBS J* **2023**, *290* (6), 1563-1582.

(44) Point, V.; Bénarouche, A.; Zarillo, J.; Guy, A.; Magnez, R.; Fonseca, L.; Raux, B.; Leclaire, J.; Buono, G.; Fotiadu, F.; Durand, T.; Carrière, F.; Vaysse, C.; Couëdelo, L.; Cavalier, J.-F., Slowing down fat digestion and absorption by an oxadiazolone inhibitor targeting selectively gastric lipolysis. *Eur J Med Chem.* **2016**, *123* (8), 834-848.

(45) Palomino, J. C.; Martin, A.; Camacho, M.; Guerra, H.; Swings, J.; Portaels, F., Resazurin microtiter assay plate: simple and inexpensive method for detection of drug resistance in *Mycobacterium tuberculosis*. *Antimicrob Agents Chemother* **2002**, *46* (8), 2720-2722.

(46) Delorme, V.; Dhouib, R.; Canaan, S.; Fotiadu, F.; Carrière, F.; Cavalier, J.-F., Effects of Surfactants on Lipase Structure, Activity and Inhibition. *Pharm. Res.* **2011**, *28* (8), 1831-1842.

(47) Goins, C. M.; Sudasinghe, T. D.; Liu, X.; Wang, Y.; O'Doherty, G. A.; Ronning, D. R., Characterization of Tetrahydrolipstatin and Stereoderivatives on the Inhibition of Essential *Mycobacterium tuberculosis* Lipid Esterases. *Biochemistry* **2018**, *57* (16), 2383-2393.

(48) Lehmann, J.; Cheng, T. Y.; Aggarwal, A.; Park, A. S.; Zeiler, E.; Raju, R. M.; Akopian, T.; Kandror, O.; Sacchettini, J. C.; Moody, D. B.; Rubin, E. J.; Sieber, S. A., An Antibacterial beta-Lactone Kills *Mycobacterium tuberculosis* by Disrupting Mycolic Acid Biosynthesis. *Angew Chem Int Ed Engl.* **2018**, *57* (1), 348-353.

(49) Lehmann, J.; Vomacka, J.; Esser, K.; Nodwell, M.; Kolbe, K.; Ramer, P.; Protzer, U.; Reiling, N.; Sieber, S. A., Human lysosomal acid lipase inhibitor lalistat impairs *Mycobacterium tuberculosis* growth by targeting bacterial hydrolases. *MedChemComm* **2016**, *7*, 1797-1801.

(50) Ravindran, M. S.; Rao, S. P.; Cheng, X.; Shukla, A.; Cazenave-Gassiot, A.; Yao, S. Q.; Wenk, M. R., Targeting lipid esterases in mycobacteria grown under different physiological conditions using activity-based profiling with tetrahydrolipstatin (THL). *Mol Cell Proteomics* **2014**, *13* (2), 435-48.

(51) Rens, C.; Laval, F.; Daffe, M.; Denis, O.; Frita, R.; Baulard, A.; Wattiez, R.; Lefevre, P.; Fontaine, V., Effects of lipid-lowering drugs on vancomycin susceptibility of mycobacteria. *Antimicrob Agents Chemother.* **2016**, *60* (10), 6193-6199.

(52) Ogata, H.; Goto, S.; Sato, K.; Fujibuchi, W.; Bono, H.; Kanehisa, M., KEGG: Kyoto Encyclopedia of Genes and Genomes. *Nucleic Acids Res* **1999**, *27* (1), 29-34.

(53) Kanehisa, M.; Sato, Y.; Kawashima, M.; Furumichi, M.; Tanabe, M., KEGG as a reference resource for gene and protein annotation. *Nucleic Acids Res* **2016**, *44* (D1), D457-62.

(54) Kapopoulou, A.; Lew, J. M.; Cole, S. T., The MycoBrowser portal: a comprehensive and manually annotated resource for mycobacterial genomes. *Tuberculosis (Edinb)* **2011**, *91* (1), 8-13.

(55) Koonin, E. V., Orthologs, paralogs, and evolutionary genomics. *Annu Rev Genet* **2005**, *39*, 309-38.

(56) UniProt, C., UniProt: the Universal Protein Knowledgebase in 2023. *Nucleic Acids Res* **2023**, *51* (D1), D523-D531.

(57) Rifat, D.; Chen, L.; Kreiswirth, B. N.; Nuermberger, E. L., Genome-Wide Essentiality Analysis of Mycobacterium abscessus by Saturated Transposon Mutagenesis and Deep Sequencing. *mBio* **2021**, *12* (3), e0104921.

(58) Dubois, V.; Pawlik, A.; Bories, A.; Le Moigne, V.; Sismeiro, O.; Legendre, R.; Varet, H.; Rodriguez-Ordonez, M. D. P.; Gaillard, J. L.; Coppee, J. Y.; Brosch, R.; Herrmann, J. L.; Girard-Misguich, F., *Mycobacterium abscessus* virulence traits unraveled by transcriptomic profiling in amoeba and macrophages. *PLoS Pathog* **2019**, *15* (11), e1008069.

(59) Trivedi, O. A.; Arora, P.; Sridharan, V.; Tickoo, R.; Mohanty, D.; Gokhale, R. S., Enzymic activation and transfer of fatty acids as acyl-adenylates in mycobacteria. *Nature* **2004**, *428* (6981), 441-5.

(60) Richard, M.; Gutierrez, A. V.; Viljoen, A.; Rodriguez-Rincon, D.; Roquet-Baneres, F.; Blaise, M.; Everall, I.; Parkhill, J.; Floto, R. A.; Kremer, L., Mutations in the MAB_2299c TetR Regulator Confer Cross-Resistance to Clofazimine and Bedaquiline in Mycobacterium abscessus. *Antimicrob Agents Chemother* **2019**, *63* (1).

(61) Daniel, J.; Deb, C.; Dubey, V. S.; Sirakova, T. D.; Abomoelak, B.; Morbidoni, H. R.; Kolattukudy, P. E., Induction of a novel class of diacylglycerol acyltransferases and triacylglycerol accumulation in *Mycobacterium tuberculosis* as it goes into a dormancy-like state in culture. *J Bacteriol* **2004**, *186* (15), 5017-30.

(62) Kapoor, N.; Pawar, S.; Sirakova, T. D.; Deb, C.; Warren, W. L.; Kolattukudy, P. E., Human granuloma in vitro model, for TB dormancy and resuscitation. *PLoS One* **2013**, *8* (1), e53657.

(63) Sirakova, T. D.; Dubey, V. S.; Deb, C.; Daniel, J.; Korotkova, T. A.; Abomoelak, B.; Kolattukudy, P. E., Identification of a diacylglycerol acyltransferase gene involved in accumulation of triacylglycerol in *Mycobacterium tuberculosis* under stress. *Microbiology (Reading)* **2006**, *152* (Pt 9), 2717-2725.

(64) Barisch, C.; Soldati, T., Breaking fat! How mycobacteria and other intracellular pathogens manipulate host lipid droplets. *Biochimie* **2017**, *141*, 54-61.

(65) Gago, G.; Arabolaza, A.; Diacovich, L.; Gramajo, H., Components and Key Regulatory Steps of Lipid Biosynthesis in Actinomycetes. In *Biogenesis of Fatty Acids, Lipids and Membranes*, Geiger, O., Ed. Springer International Publishing: Cham, 2019; pp 409-433. DOI: https://doi.org/10.1007/978-3-319-50430-8_65.

(66) Aguilar-Ayala, D. A.; Tilleman, L.; Van Nieuwerburgh, F.; Deforce, D.; Palomino, J. C.; Vandamme, P.; Gonzalez, Y. M. J. A.; Martin, A., The transcriptome of *Mycobacterium tuberculosis* in a lipid-rich dormancy model through RNAseq analysis. *Sci Rep* **2017**, *7* (1), 17665.

(67) Mekonnen, D.; Derbie, A.; Mihret, A.; Yimer, S. A.; Tonjum, T.; Gelaw, B.; Nibret, E.; Munshae, A.; Waddell, S. J.; Aseffa, A., Lipid droplets and the transcriptome of *Mycobacterium tuberculosis* from direct sputa: a literature review. *Lipids Health Dis* **2021**, *20* (1), 129.

(68) Schnappinger, D.; Ehrt, S.; Voskuil, M. I.; Liu, Y.; Mangan, J. A.; Monahan, I. M.; Dolganov, G.; Efron, B.; Butcher, P. D.; Nathan, C.; Schoolnik, G. K., Transcriptional Adaptation of *Mycobacterium tuberculosis* within Macrophages: Insights into the Phagosomal Environment. *J Exp Med* **2003**, *198* (5), 693-704.

(69) Larrouy-Maumus, G.; Biswas, T.; Hunt, D. M.; Kelly, G.; Tsodikov, O. V.; de Carvalho, L. P., Discovery of a glycerol 3-phosphate phosphatase reveals glycerophospholipid polar head recycling in *Mycobacterium tuberculosis*. *Proc Natl Acad Sci U S A* **2013**, *110* (28), 11320-5.

(70) Crotta Asis, A.; Savoretti, F.; Cabruja, M.; Gramajo, H.; Gago, G., Characterization of key enzymes involved in triacylglycerol biosynthesis in mycobacteria. *Sci Rep* **2021**, *11* (1), 13257.

(71) Cox, J.; Hein, M. Y.; Luber, C. A.; Paron, I.; Nagaraj, N.; Mann, M., Accurate proteome-wide label-free quantification by delayed normalization and maximal peptide ratio extraction, termed MaxLFQ. *Mol Cell Proteomics* **2014**, *13* (9), 2513-2526.

(72) Cox, J.; Mann, M., MaxQuant enables high peptide identification rates, individualized p.p.b.-range mass accuracies and proteome-wide protein quantification. *Nat Biotechnol.* **2008**, *26* (12), 1367-1372.

(73) Cox, J.; Neuhauser, N.; Michalski, A.; Scheltema, R. A.; Olsen, J. V.; Mann, M., Andromeda: a peptide search engine integrated into the MaxQuant environment. *J Proteome Res.* **2011**, *10* (4), 1794-1805.

(74) The UniProt, C., UniProt: the universal protein knowledgebase. *Nucleic Acids Res* **2017**, *45* (D1), D158-D169.

(75) Tusher, V. G.; Tibshirani, R.; Chu, G., Significance analysis of microarrays applied to the ionizing radiation response. *Proc Natl Acad Sci U S A* **2001**, *98* (9), 5116-21.

(76) Deutsch, E. W.; Bandeira, N.; Sharma, V.; Perez-Riverol, Y.; Carver, J. J.; Kundu, D. J.; Garcia-Seisdedos, D.; Jarnuczak, A. F.; Hewapathirana, S.; Pullman, B. S.; Wertz, J.; Sun, Z.; Kawano, S.; Okuda, S.; Watanabe, Y.; Hermjakob, H.; MacLean, B.; MacCoss, M. J.; Zhu, Y.; Ishihama, Y.; Vizcaino, J. A., The

ProteomeXchange consortium in 2020: enabling 'big data' approaches in proteomics. *Nucleic Acids Res* **2020**, *48* (D1), D1145-D1152.

(77) Perez-Riverol, Y.; Bai, J.; Bandla, C.; Garcia-Seisdedos, D.; Hewapathirana, S.; Kamatchinathan, S.; Kundu, D. J.; Prakash, A.; Frericks-Zipper, A.; Eisenacher, M.; Walzer, M.; Wang, S.; Brazma, A.; Vizcaino, J. A., The PRIDE database resources in 2022: a hub for mass spectrometry-based proteomics evidences. *Nucleic Acids Res* **2022**, *50* (D1), D543-D552.

(78) Woglar, A.; Yamaya, K.; Roelens, B.; Boettiger, A.; Kohler, S.; Villeneuve, A. M., Quantitative cytogenetics reveals molecular stoichiometry and longitudinal organization of meiotic chromosome axes and loops. *PLoS Biol* **2020**, *18* (8), e3000817.

(79) Li, Q.; Lau, A.; Morris, T. J.; Guo, L.; Fordyce, C. B.; Stanley, E. F., A syntaxin 1, Galpha(o), and N-type calcium channel complex at a presynaptic nerve terminal: analysis by quantitative immunocolocalization. *J Neurosci* **2004**, *24* (16), 4070-81.

(80) Bolte, S.; Cordelieres, F. P., A guided tour into subcellular colocalization analysis in light microscopy. *J Microsc* **2006**, *224* (Pt 3), 213-32.

(81) Costes, S. V.; Daelemans, D.; Cho, E. H.; Dobbin, Z.; Pavlakis, G.; Lockett, S., Automatic and quantitative measurement of protein-protein colocalization in live cells. *Biophys J* **2004**, *86* (6), 3993-4003.

(82) Viljoen, A.; Gutierrez, A. V.; Dupont, C.; Ghigo, E.; Kremer, L., A Simple and Rapid Gene Disruption Strategy in *Mycobacterium abscessus*: On the Design and Application of Glycopeptidolipid Mutants. *Front Cell Infect Microbiol* **2018**, *8*, 69.

Conclusions et perspectives

Les gouttelettes lipidiques sont des organites conservés dans tous les phyla. Chez les bactéries, notamment chez les actinobactéries, ces gouttelettes nommées ILI, participent chez les organismes pathogènes, en plus de leur rôle dans le stockage de l'énergie, à la virulence et l'adaptation des microorganismes aux conditions très stringentes rencontrées au cours d'une infection. Chez *Mycobacterium tuberculosis*, les ILI contribuent à l'entrée en dormance, à la persistance des bacilles au sein de l'hôte infecté, et à la tolérance contre divers agents anti-tuberculeux. Dans ce contexte, le décryptage du métabolisme des ILI conduisant à leur synthèse ou à leur dégradation, pourrait améliorer la compréhension de tous les processus de virulence chez les mycobactéries, et même le développement de nouvelles stratégies thérapeutiques permettant de contenir ou d'éliminer la propagation des bactéries ou les formes de latence chez des patients infectés.

I) Historique des ILI

Un aspect important de ma thèse a été de dresser une rétrospective historique de la découverte des ILI, les techniques conventionnelles utilisées pour les purifier, déterminer les protéines associées à ces organites et enfin établir un état des lieux des nouvelles avancées technologiques disponibles pour étudier la formation et la dégradation de ces organites en temps réel (**article I**).

II) Etude bioinformatique des protéomes

Cette première étude a stimulé notre curiosité sur l'existence possible d'un protéome commun des ILI chez les actinomycètes. Pour cela, nous avons réalisé une étude bioinformatique sur les trois seuls protéomes des ILI de *M. smegmatis*, *R. opacus* et *R. jostii* identifiés expérimentalement jusqu'à présent (**article II**). Ces protéines n'étaient pas exclusivement impliquées dans le métabolisme lipidique mais appartenaient à différentes catégories fonctionnelles. Une analyse des séquences de ces protéines interagissant potentiellement avec les ILI, nous a permis d'identifier la présence d'une hélice amphipathique commune à tous ces membres qui pourrait agir comme un signal permettant l'interaction avec les ILI.

Cette étude bioinformatique dont les résultats doivent être validés expérimentalement, nous a permis de proposer un « core ILIome » chez les mycobactéries.

Pour valider cette hypothèse, la fusion d'une hélice amphipathique avec une sonde fluorescente pourrait permettre de confirmer l'interaction des protéines sélectionnées avec les ILI. De même, une souche exprimant une Tgs1 dépourvue de cette hélice ou d'une hélice modifiée par mutagenèse dirigée, suivie d'une étude de quantification des ILI par microscopie ou des TAG par chromatographie sur couche mince pourrait être un outil intéressant pour valider les résidus ou éléments structuraux impliqués dans l'interaction. Une validation similaire a été effectuée sur l'hélice identifiée chez PspA, protéine appartenant aux ILI de *M. smegmatis* (Armstrong, Carter et al. 2018). Les auteurs ont démontré que PspA dépourvue de cette hélice aboutit à un déficit d'ILI chez *M. smegmatis*.

Si l'hélice amphipathique est un élément suffisant pour permettre l'interaction avec les ILI, la synthèse d'anticorps dirigés contre cette hélice pourrait être le point de départ d'un blocage de la formation des ILI. Cette étape pourrait réduire la virulence des mycobactéries acquise par les ILI, leur tolérance à certains antibiotiques, et leur accès aux éléments nutritifs stockés dans les ILI. Par conséquent, le traitement des infections mycobactériennes serait plus simple, et les antibiotiques seront plus efficaces.

III) Marquage de proximité par APEX2

Cependant ces résultats de bioinformatiques ne permettent pas de discriminer entre les enzymes impliquées dans la synthèse et la dégradation. Dans ce contexte, mon travail de thèse s'est orienté vers l'utilisation de techniques spécifiques permettant de rechercher les protéines impliquées dans ces deux processus en utilisant les modèles développés au laboratoire (Santucci, Johansen et al. 2019) et les techniques de marquage de proximité (Bersuker, Peterson et al. 2018).

Afin d'étudier plus spécifiquement les enzymes lipolytiques impliquées dans la biogénèse et la dégradation des ILI et s'affranchir des limitations et artefacts dues à la lyse des cellules décrites précédemment, nous avons décidé d'utiliser la technique de marquage de proximité APEX2. Grâce à celle-ci, j'ai pu identifier à 24 et 48 heures, 228 protéines impliquées dans la synthèse des ILI dont 38 protéines communes. Ces résultats montrent que la synthèse des ILI est un processus complexe et très dynamique au cours du temps.

Afin de valider le rôle des protéines identifiées dans le cycle de formation des ILI, des études de colocalisation ont été réalisés et des mutants de délétion ont été générés.

Parmi ces cibles, les MAB_3486 et MAB_4532c identifiées pendant la formation des ILI ont révélé un impact significatif sur la biogénèse des ILI (**article III**).

Pour compléter ce travail, des études biochimiques et des tests d'activité pourraient désormais être réalisés sur chacune des protéines identifiées afin de mieux comprendre leur mode d'action et leur importance physiologique. En effet, l'utilisation des souches mutées pour ces gènes dans des conditions d'infection *ex vivo* (Caire-Brändli, Papadopoulos et al. 2014) ou *in vivo* (chez le zebrafish ou la souris) permettrait d'établir le rôle de ces protéines et par conséquence, des ILI, dans la virulence de *M. abscessus*. Si les résultats *in vivo* révèlent une perte de virulence de la bactérie en absence de ces enzymes, alors des études d'inhibition des cibles identifiées permettraient d'envisager de nouvelles pistes thérapeutiques pour lutter contre les infections aux mycobactéries. Dans ce but, nous avons développé et validé des inhibiteurs spécifiques de de certaines enzymes lipolytiques impliquées dans la synthèse de ces ILI. J'ai participé à la caractérisation de certaines d'entre elles dans la dernière partie de ma thèse (**Article IV**) (Point, Malla et al. 2012; Viljoen, Richard et al. 2018; Barelier, Avellan et al. 2023).

Des études similaires pourraient être menées chez *M. tuberculosis* et l'identification des protéines associées aux ILI, serait une étape essentielle pour comprendre les acteurs de la dormance ainsi que ceux impliqués de la réactivation des bacilles.

D'autres modèles *in vitro* basés sur l'utilisation d'un milieu Sauton, riche en glycérol (Armstrong, Carter et al. 2018), ou limitant en fer (Bacon, Dover et al. 2007) ou des conditions hypoxiques (Wayne and Hayes 1996) peuvent induire la formation des ILI. Par conséquent, l'utilisation du marquage de proximité dans ces différents modèles et la comparaison des différents protéomes générés, permettraient d'identifier les protéines associées aux ILI propres à ces conditions. Cette stratégie pourrait éliminer les protéines en relation avec les métabolismes induits dans chaque modèle. De plus, établir un modèle hypoxique chez *M. abscessus* est particulièrement intéressant car il n'a jamais été étudié chez cette espèce.

Également, pour se rapprocher des conditions pathologiques, il serait intéressant de tester un milieu de composition similaire à l'environnement pulmonaire d'un patient atteint de mucoviscidose, et observer la capacité de *M. abscessus* à accumuler des ILI dans ces conditions, et dans un second temps, étudier son protéome. En outre, chez les personnes atteints de mucoviscidose, *M. abscessus* colonise les poumons avec 4 autres bactéries ; *S. aureus*, *P. aeruginosa*, *H. influenzae*, et *B. cenocepacia* (Surette 2014). Il y a quelques années, un modèle mucoviscidose-like a été développé pour étudier le génome de *P. aeruginosa* (Turner, Wessel et al. 2015). Récemment, Jaiyesimi *et al.* ont utilisé ce milieu d'expectoration synthétique de la mucoviscidose et ont pu étudier les variations des métabolomes de *B. cenocepacia* par rapport à un milieu de culture standard (Jaiyesimi, McAvoy et al. 2021). De même, l'équipe de M. Jackson a utilisé ce milieu pour étudier la formation de biofilms chez *M. abscessus* (Belardinelli, Li et al. 2021).

D'autre part, Il serait judicieux d'utiliser l'APEX2 fusionnée à nos appâts dans le modèle *ex vivo* d'accumulation des ILI développé au laboratoire (**Figure 24**) (Caire-Brändli, Papadopoulos et al. 2014). Pour rappel, dans ce modèle la bactérie accumule des lipides sous forme d'ILI à partir des lipides de l'hôte. Par conséquent, l'identification et la comparaison des deux protéomes des ILI obtenus dans le modèle *in vitro* et *ex vivo* qui miment ce qui se passe au cours de la formation du granulome permettrait de déterminer s'il s'agit des mêmes cibles qui interviennent dans les deux processus.

IV) Capture d'enzymes à Ser/Cys pendant l'accumulation des ILI par ABPP

Comme évoqué dans la partie précédente, les résultats issus de la capture par les CyC et les OX (**article IV**), pourraient être complétés par des tests d'activité sur chacune des protéines capturées. Une résolution tridimensionnelle de la structure de nos cibles complexées avec ces inhibiteurs permettrait de mieux comprendre la spécificité des OX et des CyC pour chacune d'elles. L'accès à ces structures pourrait guider la synthèse de nouveaux inhibiteurs qui cibleraient parfaitement ces acteurs du métabolisme des lipides et en un lien avec la virulence.

Dans la même perspective que celle d'APEX2, les études de capture d'enzyme à serine et cystéine dans le modèle d'accumulation *ex vivo* seraient innovantes.

Pour ce faire, à l'inverse de la technique de chimie click utilisée dans l'article IV, et en utilisant le cuivre comme catalyseur, nous avons adapté au laboratoire un protocole de chimie click différent, en utilisant le dibenzocyclooctyne (DBCO).

Ce protocole permet de réaliser de la chimie click bio-orthogonale *in vivo* sans affecter la viabilité des macrophages, ainsi que de la microscopie sur des cellules vivantes (Sletten and Bertozzi 2011).

D'autre part, l'effet multi-cible des CyC, leur activité antimicrobienne et leur faible toxicité sur les cellules de mammifères laissent présager que cette famille de molécule pourrait être un potentiel outil sélectif de traitement contre les mycobactéries. Cependant des tests *in vivo* complémentaires sont nécessaires pour étayer cette hypothèse. En revanche, nous avons montré au laboratoire que la spécificité des CyC pourraient servir d'outil de diagnostic rapide et dans ce cas les contraintes sont beaucoup moins importantes que dans le cas du développement d'une thérapie (Sarrazin, Martin et al. 2022).

V) Validation des cibles par APEX2

L'étude réalisée durant ce travail de thèse a permis d'identifier un large spectre de protéines pouvant intervenir dans le métabolisme des ILI. Il serait intéressant d'étudier le rôle de certaines familles d'enzymes en construisant des souches doublement ou triplement délétées, c'est-à-dire des souches bactériennes dépourvues de deux ou trois gènes codant pour des protéines appartenant à la même famille mais surexprimées à des moments différents du cycle. Ces études permettraient de mieux comprendre l'impact de l'absence de certaines familles protéiques et leur rôle sur le niveau de TAG accumulé, tout en éloignant la possibilité de redondance fonctionnelle de ces protéines. En effet, des phénomènes compensatoires pourraient survenir, car plusieurs protéines avec une redondance ont été identifiées dans le génome des mycobactéries. Cela est probablement attribuable à la dynamique de la biogénèse des ILI ou à l'abondance des enzymes impliquées dans le métabolisme des lipides chez les mycobactéries.

Des résultats préliminaires ont montré l'implication de quelques cibles dans des voies métaboliques de synthèse et/ou modification des lipides de membranes. Par exemple, une des protéines identifiées à 48 heures, est une alcool déshydrogénase C (AdhC / MAB_3400).

Cette protéine a été étudiée chez *M. smegmatis* (Galamba, Soetaert et al. 2001), *M. tuberculosis* (Gu, Chen et al. 2003), et *M. bovis* (Wilkin, Soetaert et al. 1999). Il semblerait que cette enzyme soit impliquée dans le maintien de la paroi.

L'adhC se trouve chez différentes espèces bactériennes (*B. subtilis, E. coli, H. pylori*) et joue un rôle dans la résistance au stress ainsi que dans la formation des biofilms. Il serait intéressant de comparer des souches délétées de l'*adhC* chez le morphotype S et R et vérifier leur capacité à former des biofilms.

Nos données préliminaires montrent que la souche Δ*MAB_3400* chez *M. abscessus* présente une croissance plus lente par rapport au WT, comme démontré précédemment chez *M. smegmatis* (Galamba, Soetaert et al. 2001). De plus, l'analyse des lipides polaires et apolaires par chromatographie sur couche mince a montré une réduction du PIM chez le mutant, alors que le niveau de TAG ne varie pas. Un fait intéressant serait de savoir si cette protéine se trouve sur les ILI, même si elle n'agit pas dans la voie des TAG. Toutes ces études seront approfondies dans le futur pour bien comprendre le rôle de l'AdhC et sa présence au moment de la synthèse des ILI.

Une autre protéine intéressante est l'acétyl-CoA-acétyltransferase (MAB_1463). Cette protéine a été identifiée à 48 heures par la technique de l'APEX2, mais aussi par les CyC et les OX. De plus, on la retrouve statistiquement abondante dans le protéome de dégradation. Elle intervient dans la voie de β-oxydation et la souche Δ*MAB_1463* présente 40% de réduction de TAG dans le MSM NL par rapport au WT. Il serait important de caractériser cette protéine en détail, de vérifier sa localisation sur les ILI, et de voir si elle a un effet sur les autres types de lipides de la membrane. Une enoyl hydratase (MAB_2737) impliquée également dans la β-oxydation a été retrouvée à 24 et 48 heures d'accumulation par APEX2. La construction d'une souche délétée des gènes codant pour ces deux protéines permettrait d'évaluer l'effet de leur absence sur cette voie métabolique. En outre, MAB_2737 a été également étudiée chez *M. tuberculosis* lors d'un stress oxydant et d'une carence en nutriment (Srivastava, Chaudhary et al. 2015). Cela est en cohérence avec notre modèle limitant en azote. Kanvatirth *et al*., ont proposé un lien entre cette enzyme et la résistance aux antibiotiques (Kanvatirth, Jeeves et al. 2019). Par conséquent, il serait intéressant d'étudier les CMI au florfenicol des souches Δ*MAB_2737*.

Par rapport aux lipides, il semblerait que cette protéine soit impliquée dans la synthèse des PIM ainsi que sur la longueur des PE dans la membrane. Des études de lipidomiques seront donc importantes pour valider le rôle de cette protéine chez *M. abscessus*.

Si MAB_2737 agit sur la voie de synthèse des PIM, une souche délétée de *MAB_2737* et *MAB_3400*, toutes les deux intervenant dans cette voie, serait intéressante pour étudier la viabilité du bacille, car il est bien connu que l'absence de PIM a un impact sur la virulence et la propagation de la bactérie.

Des tests de survie intracellulaire des souches délétées, accompagnés d'un dénombrement de CFU pourraient compléter cette étude. En effet, on suppose que les souches incapables d'accumuler des ILI seraient moins virulentes, et par la suite probablement éliminées par la phagocytose n'ayant pas la capacité de survivre, ni de contourner le système immunitaire.

De plus, dans notre modèle, la longueur des chaînes carbonées du TAG n'a jamais été étudiée. Une étude en LC MS/MS pourrait compléter nos recherches. En effet, il serait intéressant de comparer la composition en lipides neutres des ILI issus de différents modèles, cités en dessus, avec notre modèle, afin de savoir l'effet de chaque condition sur la longueur des chaines carbonées des TAG.

En outre, la quantification des TAG pour certains de nos mutants de délétion (gènes codant pour des protéines identifiées lors de la synthèse des ILI) n'a pas révélé de variation significative. Cependant, ces cibles pourraient induire une variation au niveau des types de TAG, des phospholipides, ou même des longueurs de chaînes des lipides contenus dans la paroi, comme cela a été montré avec la délétion d'une enoyl-CoA isomérase chez *M. tuberculosis* (Srivastava, Chaudhary et al. 2015).

Des investigations plus approfondies en LC MS/MS ou RMN seraient nécessaires. Il serait également intéressant d'analyser les lipides totaux pour vérifier si ces protéines n'auraient pas également un impact sur les autres lipides bactériens tels que les phospholipides, les PIM, les PE, et d'autres lipides de la paroi.

Enfin, il a été montré que les ILI chez les mycobactéries confèrent une virulence ainsi qu'une tolérance à certains antibiotiques (Santucci, Johansen et al. 2019).

Il serait, par conséquent, intéressant de comparer la sensibilité des souches accumulant des ILI, à celle des souches délétées des gènes identifiés, sur des antibiotiques de références.

Pour faire suite à nos études, des investigations supplémentaires seraient prévues. En effet, nos premiers critères de sélection étaient basés sur les protéines annotées et ayant des orthologues chez *M. tuberculosis*.

Cependant, plusieurs protéines n'ayant pas de voie métabolique assignée pourraient être essentielles à la virulence de *M. abscessus*. De plus, comme ayant développé l'outil de CRISPR interférence au laboratoire, des répressions des gènes chez *M. abscessus* mais annotés essentiels chez *M. tuberculosis* seront étudiés.

VI) Etude de la dégradation des ILI

Le modèle d'accumulation des ILI que j'ai utilisé au cours de mes travaux de thèse est un modèle réversible et les bactéries gorgées d'ILI, une fois dans un milieu minimal dépourvu de source en carbone (glycérol dans ce cas), consomment leurs ILI. Au cours de ma thèse j'ai également étudié les enzymes qui interviennent dans la dégradation.

En utilisant APEX2, cette fois couplée à une enzyme bifonctionnelle identifiée sur les ILI de *M. bovis* BCG au moment de la dégradation des ILI (BCG1721 / Rv1683 / MAB_2348), j'ai pu identifier, 252 protéines parmi lesquels 7 protéines sont communes avec la phase de synthèse. Les études sur la consommation ont été réalisées 18 heures après que les ILI aient atteints leur taille maximale, cependant ils n'ont pas totalement disparu. Pour compléter cette étude, des données complémentaires doivent être collectées à 24 et 36 heures. De la même façon, des études de capture par les CyC et les OX ont été effectués au moment de la dégradation, ce qui a permis d'identifier 33 protéines statistiquement abondantes, parmi lesquelles 19 étaient présentes au moment de la synthèse, dont MAB_1978c. Pour chacune des deux études, 20 cibles appartenant aux familles des lipases, des carboxylases, des cutinases, des thioestérases, et des hydrolases ont été sélectionnées. Les perspectives de ce travail sont donc d'étudier l'implication de ces protéines dans la consommation des lLI, leur importance physiologique en caractérisant la capacité des mutants de délétion à dégrader les ILI.

Les protéines seront donc soumises à une caractérisation biochimique complète (activité enzymatique, spécificité du substrat, et tests d'inhibition). La localisation de ces cibles sur les ILI ainsi que leur rôle physiologique pourraient être étudiés une complémentation et fusion GFP.

Une fois validée, la génération des souches de délétion des gènes correspondant sera prévue.

Cette étude permettra d'évaluer la viabilité des mutants générés et leur capacité à survivre et à consommer des lipides dans des modèles cellulaires établis dans les macrophages spumeux qui imitent la formation d'ILI dans les macrophages infectés, et des modèles animaux (embryon de zebrafish).

Après avoir accumulé les lipides des cellules hôtes, nous évaluerons la dégradation de l'ILI en utilisant la microscopie électronique à transmission et la microscopie confocale dans les macrophages spumeux infectés, comme mentionné précédemment.

Le modèle du zebrafish poisson zèbre est bien adapté à l'étude de la chronologie des événements dans l'infection par *M. abscessus* S en surveillant la charge bactérienne, la survie de l'embryon, la formation de cordes et de granulomes. Ces résultats aideront à élucider le rôle de ces enzymes lipolytiques dans la dégradation de l'ILI, ce qui permettra de mieux comprendre les mécanismes cellulaires et moléculaires impliqués dans les phases de croissance et de persistance qui sont cruciales pour la physiopathologie des mycobactéries. En effet, si la dégradation des ILI est bloquée, les bacilles seront incapables de se réactiver et de se disséminer vers d’autres personnes.

VII) Etudes supplémentaires

Pour affiner encore plus nos études, Il serait intéressant d’utiliser la méthode TransitID en couplant la technologie de l’APEX2 à une protéine membranaire et Turbo ID à une protéine des ILI pour pouvoir suivre le trajet des protéines recrutées durant toute la cinétique et limiter ainsi la biotinylation des voisins dans le cytoplasme.

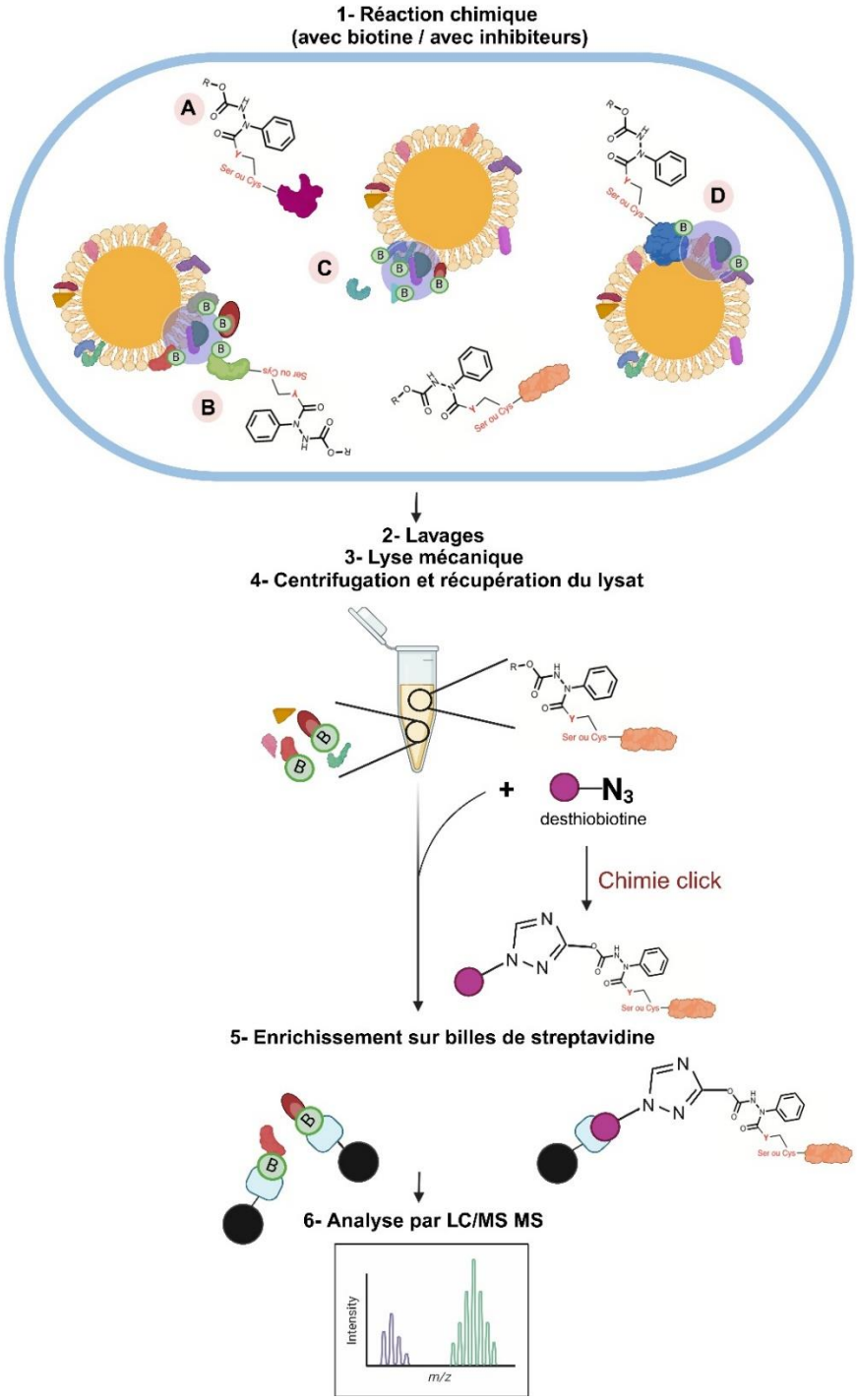

Figure 28. Complémentarité des deux études. *Représentation schématique d'une mycobactérie avec ses ILI. Les inhibiteurs sont représentés en formule chimique (avec R un alcyne terminal) avec la liaison covalente établie avec la serine (ser) ou la cystéine (cys) catalytique des enzymes dans le cytosol (A), en proximité des ILI (B), ou sur les ILI (D). L'APEX2 couplée à Tgs1 sont représentés à la surface des ILI en un complexe vert-mauve, biotinylant par un cercle vert les protéines localisées dans un rayon de 20 nm (cercle mauve). Certaines protéines sont biotinylées et interagissent avec les ILI. Des protéines sans ser/cys catalytique libres dans le cytosol (C) sont également représentées. Adaptée des deux manuscrits en préparation (article III, article IV).*

Les deux études précédemment évoquées ont fusionné deux approches distinctes, chacune ciblant des protéines selon des mécanismes différents. APEX2 a été employée pour viser l'ensemble des protéines à proximité de Tgs1, que ce soit directement sur les ILI ou dans un rayon de 20 nm. En revanche, la chimie click et les inhibiteurs peuvent identifier toutes les protéines du cytoplasme bactérien, qu'elles soient ou non localisées sur les ILI, en ciblant une sérine/cystéine catalytique. Les protéines communes ainsi identifiées sont celles qui pourraient être présentes sur les ILI tout en possédant une activité catalytique de type serine/cystéine (**Figure 28**).

En conclusion, l'ensemble des résultats de mes travaux de thèse permettent aujourd'hui d'ouvrir de nouvelles pistes pour comprendre le mécanisme de persistance et découvrir de nouvelles cibles d'intérêt thérapeutique. En effet, vu l'importance du métabolisme lipidique chez les mycobactéries, perturber une de ses voies ou inhiber quelques protéines pourrait avoir un impact sur la virulence des bacilles, la persistance, la croissance et le fitness, la fragilisation de la membrane et, par conséquent, la sensibilité probable à certains antibiotiques.

Une fois le mécanisme de formation et de dégradation de ces ILI avec tous ses acteurs seront définis, ces données peuvent être exploitées pour le développement des outils de lutte contre les mycobactéries. La synthèse des anticorps contre certaines protéines pourrait être envisageable afin d'inhiber l'interaction des cibles avec les ILI, et par la suite leur synthèse, leur maturation, et leur intégrité.

En résumé, mes travaux de thèse ont ouvert de nombreuses perspectives en lien avec le métabolisme lipidique chez les mycobactéries, la conservation d'un potentiel « core ILIome » au sein du genre *Mycobacterium*, et la compréhension d'un organite assez minuscule, les ILI, responsable en partie de la virulence de ces bactéries.

Références bibliographiques

Abate, G., F. Hamzabegovic, et al. (2019). "BCG Vaccination Induces M. avium and M. abscessus Cross-Protective Immunity." Front Immunol **10**(234).

Abdelaal, H. F. M., E. D. Chan, et al. (2022). "Mycobacterium abscessus: It's Complex." Microorganisms **10**(7).

Adékambi, T., P. Colson, et al. (2003). "rpoB-based identification of nonpigmented and late-pigmenting rapidly growing mycobacteria." J Clin Microbiol **41**(12): 5699-5708.

Adékambi, T., M. Reynaud-Gaubert, et al. (2004). "Amoebal coculture of "Mycobacterium massiliense" sp. nov. from the sputum of a patient with hemoptoic pneumonia." J Clin Microbiol **42**(12): 5493-5501.

Adjemian, J., T. B. Frankland, et al. (2017). "Epidemiology of Nontuberculous Mycobacterial Lung Disease and Tuberculosis, Hawaii, USA." Emerg Infect Dis **23**(3): 439-447.

Alibaud, L., Y. Rombouts, et al. (2011). "A Mycobacterium marinum TesA mutant defective for major cell wall-associated lipids is highly attenuated in Dictyostelium discoideum and zebrafish embryos." Mol Microbiol **80**(4): 919-934.

Alvarez, A. F., H. M. Alvarez, et al. (2008). "Cloning and characterization of a gene involved in triacylglycerol biosynthesis and identification of additional homologous genes in the oleaginous bacterium Rhodococcus opacus PD630." Microbiology **154**(Pt 8): 2327-2335.

Alvarez, H. M., R. Kalscheuer, et al. (2000). "Accumulation and mobilization of storage lipids by Rhodococcus opacus PD630 and Rhodococcus ruber NCIMB 40126." Appl Microbiol Biotechnol **54**(2): 218-223.

Alvarez, H. M., F. Mayer, et al. (1996). "Formation of intracytoplasmic lipid inclusions by Rhodococcus opacus strain PD630." Arch Microbiol **165**(6): 377-386.

Anderson, A. J. and E. A. Dawes (1990). "Occurrence, metabolism, metabolic role, and industrial uses of bacterial polyhydroxyalkanoates." Microbiol Rev **54**(4): 450-472.

Armstrong, D. T. and N. Parrish (2021). "Current Updates on Mycobacterial Taxonomy, 2018 to 2019." Journal of clinical microbiology **59**(7): e0152820.

Armstrong, R. M., D. C. Carter, et al. (2018). "Association of Mycobacterium Proteins with Lipid Droplets." J Bacteriol **200**(16): 00240-00218.

Bacon, J., L. G. Dover, et al. (2007). "Lipid composition and transcriptional response of Mycobacterium tuberculosis grown under iron-limitation in continuous culture: identification of a novel wax ester." Microbiology **153**(Pt 5): 1435-1444.

Bakala N'Goma, J. C., V. Le Moigne, et al. (2015). "Mycobacterium abscessus phospholipase C expression is induced during coculture within amoebae and enhances M. abscessus virulence in mice." Infect Immun **83**(2): 780-791.

Barelier, S., R. Avellan, et al. (2023). "Direct capture, inhibition and crystal structure of HsaD (Rv3569c) from M. tuberculosis." Febs J **290**(6): 1563-1582.

Barrow, W. W. and P. J. Brennan (1982). "Isolation in high frequency of rough variants of Mycobacterium intracellulare lacking C-mycoside glycopeptidolipid antigens." J Bacteriol **150**(1): 381-384.

Becker, J. T., A. A. Auerbach, et al. (2023). "APEX3 - An Optimized Tool for Rapid and Unbiased Proximity Labeling." J Mol Biol **435**(13): 13.

Belardinelli, J. M., W. Li, et al. (2021). "Unique Features of Mycobacterium abscessus Biofilms Formed in Synthetic Cystic Fibrosis Medium." Front Microbiol **12**(743126).

Belisle, J. T., M. R. McNeil, et al. (1993). "Expression of the core lipopeptide of the glycopeptidolipid surface antigens in rough mutants of Mycobacterium avium." J Biol Chem **268**(14): 10510-10516.

Benwill, J. L. and R. J. Wallace, Jr. (2014). "Mycobacterium abscessus: challenges in diagnosis and treatment." Curr Opin Infect Dis **27**(6): 506-510.

Bermúdez, M. A., M. A. Balboa, et al. (2021). "Lipid Droplets, Phospholipase A(2), Arachidonic Acid, and Atherosclerosis." Biomedicines **9**(12).

Bernut, A., J. L. Herrmann, et al. (2014). "Mycobacterium abscessus cording prevents phagocytosis and promotes abscess formation." Proc Natl Acad Sci U S A **111**(10): 24.

Bernut, A., J. L. Herrmann, et al. (2014). [Mycobacterial cording: a new mechanism of immune evasion?], Med Sci (Paris). 2014 May;30(5):499-502. doi: 10.1051/medsci/20143005008. Epub 2014 Jun 13.

Bernut, A., J. L. Herrmann, et al. (2017). "The Diverse Cellular and Animal Models to Decipher the Physiopathological Traits of Mycobacterium abscessus Infection." Front Cell Infect Microbiol **7**(100).

Bernut, A., M. Nguyen-Chi, et al. (2016). "Mycobacterium abscessus-Induced Granuloma Formation Is Strictly Dependent on TNF Signaling and Neutrophil Trafficking." PLoS Pathog **12**(11).

Bernut, A., A. Viljoen, et al. (2016). "Insights into the smooth-to-rough transitioning in Mycobacterium bolletii unravels a functional Tyr residue conserved in all mycobacterial MmpL family members." Mol Microbiol **99**(5): 866-883.

Bersuker, K., C. W. H. Peterson, et al. (2018). "A Proximity Labeling Strategy Provides Insights into the Composition and Dynamics of Lipid Droplet Proteomes." Dev Cell **44**(1): 97-112.

Bloch, H. and W. Segal (1956). "Biochemical differentiation of Mycobacterium tuberculosis grown in vivo and in vitro." J Bacteriol **72**(2): 132-141.

Boritsch, E. C. and R. Brosch (2016). "Evolution of Mycobacterium tuberculosis: New Insights into Pathogenicity and Drug Resistance." Microbiol Spectr **4**(5): 0020-2016.

Bosch, M., M. J. Sweet, et al. (2021). "Lipid droplets and the host-pathogen dynamic: FATal attraction?" J Cell Biol **220**(8): 24.

Bouley, D. M., N. Ghori, et al. (2001). "Dynamic nature of host-pathogen interactions in Mycobacterium marinum granulomas." Infect Immun **69**(12): 7820-7831.

Brennan, M. J. and U. Fruth (2001). Global Forum on TB Vaccine Research and Development. World Health Organization, June 7-8 2001, Geneva, Tuberculosis (Edinb). 2001;81(5-6):365-8. doi: 10.1054/tube.2001.0308.

Brennan, P. J. and H. Nikaido (1995). "The envelope of mycobacteria." Annu Rev Biochem **64**: 29-63.

Brown-Elliott, B. A. and R. J. Wallace, Jr. (2002). "Clinical and taxonomic status of pathogenic nonpigmented or late-pigmenting rapidly growing mycobacteria." Clin Microbiol Rev **15**(4): 716-746.

Bryant, J. M., D. M. Grogono, et al. (2013). "Whole-genome sequencing to identify transmission of Mycobacterium abscessus between patients with cystic fibrosis: a retrospective cohort study." Lancet **381**(9877): 1551-1560.

Bryant, J. M., D. M. Grogono, et al. (2016). "Emergence and spread of a human-transmissible multidrug-resistant nontuberculous mycobacterium." Science **354**(6313): 751-757.

Burian, J., S. Ramón-García, et al. (2012). "The mycobacterial transcriptional regulator whiB7 gene links redox homeostasis and intrinsic antibiotic resistance." J Biol Chem **287**(1): 299-310.

Byrd, T. F. and C. R. Lyons (1999). "Preliminary characterization of a Mycobacterium abscessus mutant in human and murine models of infection." Infect Immun **67**(9): 4700-4707.

Caire-Brändli, I., A. Papadopoulos, et al. (2014). "Reversible lipid accumulation and associated division arrest of Mycobacterium avium in lipoprotein-induced foamy macrophages may resemble key events during latency and reactivation of tuberculosis." Infect Immun **82**(2): 476-490.

Cambier, C. J., S. Falkow, et al. (2014). "Host evasion and exploitation schemes of Mycobacterium tuberculosis." Cell **159**(7): 1497-1509.

Camus, J. C., M. J. Pryor, et al. (2002). "Re-annotation of the genome sequence of Mycobacterium tuberculosis H37Rv." Microbiology **148**(Pt 10): 2967-2973.

Cantu, D. C., Y. Chen, et al. (2010). "Thioesterases: a new perspective based on their primary and tertiary structures." Protein Sci **19**(7): 1281-1295.

Casali, N. and L. W. Riley (2007). "A phylogenomic analysis of the Actinomycetales mce operons." BMC Genomics **8**(60): 1471-2164.

Casas-Godoy, L., F. Gasteazoro, et al. (2018). "Lipases: An Overview." Methods Mol Biol: 8672-8679_8671.

Catherinot, E., A. L. Roux, et al. (2009). "Acute respiratory failure involving an R variant of Mycobacterium abscessus." J Clin Microbiol **47**(1): 271-274.

Chadha, R., M. Grover, et al. (1998). "An outbreak of post-surgical wound infections due to Mycobacterium abscessus." Pediatr Surg Int **13**(5-6): 406-410.

Chan, E. D. and M. D. Iseman (2010). "Slender, older women appear to be more susceptible to nontuberculous mycobacterial lung disease." Gend Med **7**(1): 5-18.

Chan, E. D., A. M. Kaminska, et al. (2007). "Alpha-1-antitrypsin (AAT) anomalies are associated with lung disease due to rapidly growing mycobacteria and AAT inhibits Mycobacterium abscessus infection of macrophages." Scand J Infect Dis **39**(8): 690-696.

Charron, A. J. and L. D. Sibley (2002). "Host cells: mobilizable lipid resources for the intracellular parasite Toxoplasma gondii." J Cell Sci **115**(Pt 15): 3049-3059.

Chavadi, S. S., U. R. Edupuganti, et al. (2011). "Inactivation of tesA reduces cell wall lipid production and increases drug susceptibility in mycobacteria." J Biol Chem **286**(28): 24616-24625.

Chiaradia, L. (2018). Isolement et caractérisation de la mycomembrane des mycobactéries. PhD, Université Paul Sabatier à Toulouse.

Chiaradia, L., C. Lefebvre, et al. (2017). "Dissecting the mycobacterial cell envelope and defining the composition of the native mycomembrane." Sci Rep **7**(1): 017-12718.

Chiarelli, L. R., G. Degiacomi, et al. (2021). "Nitric oxide-releasing compounds for the treatment of lung infections." Drug Discov Today **26**(2): 542-550.

Chorlay, A. and A. R. Thiam (2020). "Neutral lipids regulate amphipathic helix affinity for model lipid droplets." J Cell Biol **219**(4): 201907099.

Cole, S. T., R. Brosch, et al. (1998). "Deciphering the biology of Mycobacterium tuberculosis from the complete genome sequence." Nature **393**(6685): 537-544.

Cole, S. T., K. Eiglmeier, et al. (2001). "Massive gene decay in the leprosy bacillus." Nature **409**(6823): 1007-1011.

Cook, G. M., M. Berney, et al. (2009). "Physiology of mycobacteria." Adv Microb Physiol **55**: 81-182.

Cortes, M. A., R. Nessar, et al. (2010). "Laboratory maintenance of Mycobacterium abscessus." Curr Protoc Microbiol **10**(1).

Cosma, C. L., D. R. Sherman, et al. (2003). "The secret lives of the pathogenic mycobacteria." Annu Rev Microbiol **57**: 641-676.

Costerton, J. W., R. T. Irvin, et al. (1981). "The bacterial glycocalyx in nature and disease." Annu Rev Microbiol **35**: 299-324.

Côtes, K., C. Bakala N'goma J, et al. (2008). "Lipolytic enzymes in Mycobacterium tuberculosis." Appl Microbiol Biotechnol **78**(5): 741-749.

Cowman, S., J. van Ingen, et al. (2019). "Non-tuberculous mycobacterial pulmonary disease." Eur Respir J **54**(1): 00250-02019.

Crick, D. C., S. Mahapatra, et al. (2001). "Biosynthesis of the arabinogalactan-peptidoglycan complex of Mycobacterium tuberculosis." Glycobiology **11**(9).

D'Avila, H., C. M. Maya-Monteiro, et al. (2008). "Lipid bodies in innate immune response to bacterial and parasite infections." Int Immunopharmacol **8**(10): 1308-1315.

Daffé, M. (2008). The Global Architecture of the Mycobacterial Cell Envelope. he Mycobacterial Cell Envelope, Wiley.

Daffé, M. and P. Draper (1998). "The envelope layers of mycobacteria with reference to their pathogenicity." Adv Microb Physiol **39**: 131-203.

Daher, W., L. D. Leclercq, et al. (2022). "Glycopeptidolipid glycosylation controls surface properties and pathogenicity in Mycobacterium abscessus." Cell Chem Biol **29**(5): 910-924.

Dal Molin, M., M. Gut, et al. (2017). "Molecular Mechanisms of Intrinsic Streptomycin Resistance in Mycobacterium abscessus." Antimicrob Agents Chemother **62**(1): 01427-01417.

Daleke, M. H., A. Cascioferro, et al. (2011). "Conserved Pro-Glu (PE) and Pro-Pro-Glu (PPE) protein domains target LipY lipases of pathogenic mycobacteria to the cell surface via the ESX-5 pathway." J Biol Chem **286**(21): 19024-19034.

Daniel, J., C. Deb, et al. (2004). "Induction of a novel class of diacylglycerol acyltransferases and triacylglycerol accumulation in Mycobacterium tuberculosis as it goes into a dormancy-like state in culture." J Bacteriol **186**(15): 5017-5030.

Daniel, J., H. Maamar, et al. (2011). "Mycobacterium tuberculosis uses host triacylglycerol to accumulate lipid droplets and acquires a dormancy-like phenotype in lipid-loaded macrophages." PLoS Pathog **7**(6): 23.

Dargham, T., I. Mallick, et al. (2023). "Intrabacterial lipid inclusion-associated proteins: a core machinery conserved from saprophyte Actinobacteria to the human pathogen Mycobacterium tuberculosis." FEBS Open Bio **23**(10): 2211-5463.

David, E. M., Y. C. L. Oona, et al. (2015). Pathophysiological Implications of Cell Envelope Structure in Mycobacterium tuberculosis and Related Taxa. Tuberculosis. R. Wellman. Rijeka, IntechOpen**:** Ch. 7.

Davidson, L. B., R. Nessar, et al. (2011). "Mycobacterium abscessus glycopeptidolipid prevents respiratory epithelial TLR2 signaling as measured by HβD2 gene expression and IL-8 release." PLoS One **6**(12): 21.

Dawrs, S. N., M. Kautz, et al. Mycobacterium abscessus and Gastroesophageal Reflux: An In Vitro Study, Am J Respir Crit Care Med. 2020 Aug 1;202(3):466-469. doi: 10.1164/rccm.202001-0011LE.

de Carvalho, L. P., S. M. Fischer, et al. (2010). "Metabolomics of Mycobacterium tuberculosis reveals compartmentalized co-catabolism of carbon substrates." Chem Biol **17**(10): 1122-1131.

De Groote, M. A. and G. Huitt (2006). "Infections due to rapidly growing mycobacteria." Clin Infect Dis **42**(12): 1756-1763.

Dedrick, R. M., C. A. Guerrero-Bustamante, et al. (2019). "Engineered bacteriophages for treatment of a patient with a disseminated drug-resistant Mycobacterium abscessus." Nat Med **25**(5): 730-733.

Degiacomi, G., J. C. Sammartino, et al. (2019). "Mycobacterium abscessus, an Emerging and Worrisome Pathogen among Cystic Fibrosis Patients." Int J Mol Sci **20**(23).

Delafont, V., F. Mougari, et al. (2014). "First evidence of amoebae-mycobacteria association in drinking water network." Environ Sci Technol **48**(20): 11872-11882.

Delorme, V., S. V. Diomandé, et al. (2012). "MmPPOX inhibits Mycobacterium tuberculosis lipolytic enzymes belonging to the hormone-sensitive lipase family and alters mycobacterial growth." PLoS One **7**(9): 28.

Demoulin, L., M. Médard, et al. (1983). "[Antibiogram of mycobacteria for erythromycin, tetracycline and cotrimoxazole]." Pathol Biol **31**(3): 195-197.

Deng, L., Y. Z. Luo, et al. Subcutaneous infection caused by Mycobacterium abscessus following cosmetic injections of botulinum toxin: A case report, World J Clin Cases. 2022 Jun 26;10(18):6141-6147. doi: 10.12998/wjcc.v10.i18.6141.

Dhiman, R., S. Caesar, et al. (2020). "Mechanisms of protein targeting to lipid droplets: A unified cell biological and biophysical perspective." Semin Cell Dev Biol **108**: 4-13.

Ding, Y., L. Yang, et al. (2012). "Identification of the major functional proteins of prokaryotic lipid droplets." J Lipid Res **53**(3): 399-411.

Drage, M. G., H. C. Tsai, et al. (2010). "Mycobacterium tuberculosis lipoprotein LprG (Rv1411c) binds triacylated glycolipid agonists of Toll-like receptor 2." Nat Struct Mol Biol **17**(9): 1088-1095.

Dubée, V., A. Bernut, et al. (2015). "β-Lactamase inhibition by avibactam in Mycobacterium abscessus." J Antimicrob Chemother **70**(4): 1051-1058.

Dubée, V., D. Soroka, et al. (2015). "Impact of β-lactamase inhibition on the activity of ceftaroline against Mycobacterium tuberculosis and Mycobacterium abscessus." Antimicrob Agents Chemother **59**(5): 2938-2941.

Dubnau, E., J. Chan, et al. (2000). "Oxygenated mycolic acids are necessary for virulence of Mycobacterium tuberculosis in mice." Mol Microbiol **36**(3): 630-637.

Dutta, N. K. and P. C. Karakousis (2014). "Latent tuberculosis infection: myths, models, and molecular mechanisms." Microbiol Mol Biol Rev **78**(3): 343-371.

Etienne, G., C. Villeneuve, et al. (2002). "The impact of the absence of glycopeptidolipids on the ultrastructure, cell surface and cell wall properties, and phagocytosis of Mycobacterium smegmatis." Microbiology **148**(Pt 10): 3089-3100.

Eustace, K., V. Jolliffe, et al. (2016). "Cutaneous Mycobacterium abscessus infection following hair transplant." Clin Exp Dermatol **41**(7): 768-770.

Falsey, R. R., M. H. Kinzer, et al. (2013). "Cutaneous inoculation of nontuberculous mycobacteria during professional tattooing: a case series and epidemiologic study." Clin Infect Dis **57**(6): 23.

Fifor, A., K. Krukowski, et al. (2022). "Sex, ancestry, senescence, and aging (SAnSA) are stark drivers of nontuberculous mycobacterial pulmonary disease." J Clin Tuberc Other Mycobact Dis **26**(100297).

Floto, R. A., K. N. Olivier, et al. (2016). "US Cystic Fibrosis Foundation and European Cystic Fibrosis Society consensus recommendations for the management of non-tuberculous mycobacteria in individuals with cystic fibrosis." Thorax **1**(Suppl 1): 2015-207360.

Freiberg, C., N. A. Brunner, et al. (2004). "Identification and characterization of the first class of potent bacterial acetyl-CoA carboxylase inhibitors with antibacterial activity." J Biol Chem **279**(25): 26066-26073.

Friesen, J. D. (1988). "Escherichia coli and Salmonella typhimurium: Cellular and Molecular Biology." Science **240**(4859): 1678+.

Fukuda, E. Y., S. P. Lad, et al. (2005). "Activation of lipid metabolism contributes to interleukin-8 production during Chlamydia trachomatis infection of cervical epithelial cells." Infect Immun **73**(7): 4017-4024.

Galamba, A., K. Soetaert, et al. (2001). "Disruption of adhC reveals a large duplication in the Mycobacterium smegmatis mc(2)155 genome." Microbiology **147**(Pt 12): 3281-3294.

Ganapathy, U. S., L. Bai, et al. (2018). "Compartment-Specific Labeling of Bacterial Periplasmic Proteins by Peroxidase-Mediated Biotinylation." ACS Infect Dis **4**(6): 918-925.

Gao, Q. and J. M. Goodman (2015). "The lipid droplet-a well-connected organelle." Front Cell Dev Biol **3**(49).

Garrett, C. K., L. J. Broadwell, et al. (2015). "Modulation of the Activity of Mycobacterium tuberculosis LipY by Its PE Domain." PLoS One **10**(8).

Garsia, R. J., L. Hellqvist, et al. (1989). "Homology of the 70-kilodalton antigens from Mycobacterium leprae and Mycobacterium bovis with the Mycobacterium tuberculosis 71-kilodalton antigen and with the conserved heat shock protein 70 of eucaryotes." Infect Immun **57**(1): 204-212.

Garton, N. J., H. Christensen, et al. (2002). "Intracellular lipophilic inclusions of mycobacteria in vitro and in sputum." Microbiology **148**(Pt 10): 2951-2958.

Gengenbacher, M. and S. H. Kaufmann (2012). "Mycobacterium tuberculosis: success through dormancy." FEMS Microbiol Rev **36**(3): 514-532.

Gerasimova, A., A. E. Kazakov, et al. (2011). "Comparative genomics of the dormancy regulons in mycobacteria." J Bacteriol **193**(14): 3446-3452.

Ghon, A. (1912). "Der primäre Lungenherd bei der Tuberkulose der Kinder." Digital Public Library of America.

Gilleron, M., J. Nigou, et al. (1999). "Structural study of the lipomannans from Mycobacterium bovis BCG: characterisation of multiacylated forms of the phosphatidyl-myo-inositol anchor." J Mol Biol **285**(5): 2147-2160.

Gilleron, M., V. F. Quesniaux, et al. (2003). "Acylation state of the phosphatidylinositol hexamannosides from Mycobacterium bovis bacillus Calmette Guerin and mycobacterium tuberculosis H37Rv and its implication in Toll-like receptor response." J Biol Chem **278**(32): 29880-29889.

Goins, C. M., C. M. Schreidah, et al. (2018). "Structural basis for lipid binding and mechanism of the Mycobacterium tuberculosis Rv3802 phospholipase." J Biol Chem **293**(4): 1363-1372.

Goodman, J. M. (2018). "Understanding the Lipid Droplet Proteome and Protein Targeting." Dev Cell **44**(1): 1-2.

Greenberg, A. S., J. J. Egan, et al. (1991). "Perilipin, a major hormonally regulated adipocyte-specific phosphoprotein associated with the periphery of lipid storage droplets." J Biol Chem **266**(17): 11341-11346.

Griffin, I., A. Schmitz, et al. (2019). "Outbreak of Tattoo-associated Nontuberculous Mycobacterial Skin Infections." Clin Infect Dis **69**(6): 949-955.

Griffith, D. E., T. Aksamit, et al. (2007). "An official ATS/IDSA statement: diagnosis, treatment, and prevention of nontuberculous mycobacterial diseases." Am J Respir Crit Care Med **175**(4): 367-416.

Griffith, D. E. and C. L. Daley (2022). "Treatment of Mycobacterium abscessus Pulmonary Disease." Chest **161**(1): 64-75.

Griffith, D. E., W. M. Girard, et al. (1993). "Clinical features of pulmonary disease caused by rapidly growing mycobacteria. An analysis of 154 patients." Am Rev Respir Dis **147**(5): 1271-1278.

Gu, S., J. Chen, et al. (2003). "Comprehensive proteomic profiling of the membrane constituents of a Mycobacterium tuberculosis strain." Mol Cell Proteomics **2**(12): 1284-1296.

Guerin, M. E., J. Korduláková, et al. (2010). "Molecular basis of phosphatidyl-myo-inositol mannoside biosynthesis and regulation in mycobacteria." J Biol Chem **285**(44): 33577-33583.

Guillemin, I., V. Jarlier, et al. (1998). "Correlation between quinolone susceptibility patterns and sequences in the A and B subunits of DNA gyrase in mycobacteria." Antimicrob Agents Chemother **42**(8): 2084-2088.

Gupta, R. S., B. Lo, et al. (2018). "Phylogenomics and Comparative Genomic Studies Robustly Support Division of the Genus Mycobacterium into an Emended Genus Mycobacterium and Four Novel Genera." Front Microbiol **9**(67).

Gutiérrez, A. V., A. Viljoen, et al. (2018). "Glycopeptidolipids, a Double-Edged Sword of the Mycobacterium abscessus Complex." Front Microbiol **9**(1145).

Halloum, I., S. Carrère-Kremer, et al. (2016). "Deletion of a dehydratase important for intracellular growth and cording renders rough Mycobacterium abscessus avirulent." Proc Natl Acad Sci U S A **113**(29): 6.

Hammond, R. J., V. O. Baron, et al. (2015). "Phenotypic resistance in mycobacteria: is it because I am old or fat that I resist you?" J Antimicrob Chemother **70**(10): 2823-2827.

Han, D., K. S. Lee, et al. (2003). "Radiographic and CT findings of nontuberculous mycobacterial pulmonary infection caused by Mycobacterium abscessus." AJR Am J Roentgenol **181**(2): 513-517.

Hanks, J. H. (1961). "Significance of capsular components of Mycobacterium leprae and other mycobacteria." Int J Lepr **29**: 74-83.

Haworth, C. S., J. Banks, et al. (2017). "British Thoracic Society guidelines for the management of non-tuberculous mycobacterial pulmonary disease (NTM-PD)." Thorax **72**(Suppl 2): 2017-210927.

Hernández, M. A., A. Arabolaza, et al. (2013). "The atf2 gene is involved in triacylglycerol biosynthesis and accumulation in the oleaginous Rhodococcus opacus PD630." Appl Microbiol Biotechnol **97**(5): 2119-2130.

Hernàndez Pando, R., L. D. Aguilar, et al. (2006). "The use of mutant mycobacteria as new vaccines to prevent tuberculosis." Tuberculosis **86**(3-4): 203-210.

Hoffmann, C., A. Leis, et al. (2008). "Disclosure of the mycobacterial outer membrane: cryo-electron tomography and vitreous sections reveal the lipid bilayer structure." Proc Natl Acad Sci U S A **105**(10): 3963-3967.

Howard, S. T. (2013). "Recent progress towards understanding genetic variation in the Mycobacterium abscessus complex." Tuberculosis **93**(20): 70005-70002.

Howard, S. T., E. Rhoades, et al. (2006). "Spontaneous reversion of Mycobacterium abscessus from a smooth to a rough morphotype is associated with reduced expression of glycopeptidolipid and reacquisition of an invasive phenotype." Microbiology **152**(Pt 6): 1581-1590.

Hunter, R. L., M. Olsen, et al. (2006). "Trehalose 6,6'-dimycolate and lipid in the pathogenesis of caseating granulomas of tuberculosis in mice." Am J Pathol **168**(4): 1249-1261.

Jackson, C. L. (2019). "Lipid droplet biogenesis." Curr Opin Cell Biol **59**: 88-96.

Jackson, M. (2014). "The mycobacterial cell envelope-lipids." Cold Spring Harb Perspect Med **4**(10).

Jackson, M., C. Raynaud, et al. (1999). "Inactivation of the antigen 85C gene profoundly affects the mycolate content and alters the permeability of the Mycobacterium tuberculosis cell envelope." Mol Microbiol **31**(5): 1573-1587.

Jain, M., C. J. Petzold, et al. (2007). "Lipidomics reveals control of Mycobacterium tuberculosis virulence lipids via metabolic coupling." Proc Natl Acad Sci U S A **104**(12): 5133-5138.

Jaiyesimi, O. A., A. C. McAvoy, et al. (2021). "Metabolomic profiling of Burkholderia cenocepacia in synthetic cystic fibrosis sputum medium reveals nutrient environment-specific production of virulence factors." Sci Rep **11**(1): 021-00421.

Jankute, M., V. Nataraj, et al. (2017). "The role of hydrophobicity in tuberculosis evolution and pathogenicity." Sci Rep **7**(1): 017-01501.

Jarlier, V. and H. Nikaido (1990). "Permeability barrier to hydrophilic solutes in Mycobacterium chelonei." J Bacteriol **172**(3): 1418-1423.

Jeong, Y. J., K. S. Lee, et al. (2004). "Nontuberculous mycobacterial pulmonary infection in immunocompetent patients: comparison of thin-section CT and histopathologic findings." Radiology **231**(3): 880-886.

Johansen, M. D., J. L. Herrmann, et al. (2020). "Non-tuberculous mycobacteria and the rise of Mycobacterium abscessus." Nat Rev Microbiol **18**(7): 392-407.

Jönsson, B. E., M. Gilljam, et al. (2007). "Molecular epidemiology of Mycobacterium abscessus, with focus on cystic fibrosis." J Clin Microbiol **45**(5): 1497-1504.

Joyce, P., I. Kempson, et al. (2016). "Orientating lipase molecules through surface chemical control for enhanced activity: A QCM-D and ToF-SIMS investigation." Colloids Surf B Biointerfaces **142**: 173-181.

Kalscheuer, R., A. Palacios, et al. (2019). "The Mycobacterium tuberculosis capsule: a cell structure with key implications in pathogenesis." Biochem J **476**(14): 1995-2016.

Kalscheuer, R. and A. Steinbüchel (2003). "A novel bifunctional wax ester synthase/acyl-CoA:diacylglycerol acyltransferase mediates wax ester and triacylglycerol biosynthesis in Acinetobacter calcoaceticus ADP1." J Biol Chem **278**(10): 8075-8082.

Kalscheuer, R., M. Wältermann, et al. (2001). "Preparative isolation of lipid inclusions from Rhodococcus opacus and Rhodococcus ruber and identification of granule-associated proteins." Arch Microbiol **177**(1): 20-28.

Kanvatirth, P., R. E. Jeeves, et al. (2019). "Utilisation of the Prestwick Chemical Library to identify drugs that inhibit the growth of mycobacteria." PLoS One **14**(3).

Kerem, B., J. M. Rommens, et al. (1989). "Identification of the cystic fibrosis gene: genetic analysis." Science **245**(4922): 1073-1080.

Ketter, E. and G. Randall (2019). "Virus Impact on Lipids and Membranes." Annu Rev Virol **6**(1): 319-340.

Kim, H. Y., Y. Kook, et al. (2008). "Proportions of Mycobacterium massiliense and Mycobacterium bolletii strains among Korean Mycobacterium chelonae-Mycobacterium abscessus group isolates." J Clin Microbiol **46**(10): 3384-3390.

Kim, J. J. and K. P. Battaile (2002). "Burning fat: the structural basis of fatty acid beta-oxidation." Curr Opin Struct Biol **12**(6): 721-728.

Knight, M., J. Braverman, et al. (2018). "Lipid droplet formation in Mycobacterium tuberculosis infected macrophages requires IFN-γ/HIF-1α signaling and supports host defense." PLoS Pathog **14**(1).

Koh, W. J. (2017). "Nontuberculous Mycobacteria-Overview." Microbiol Spectr **5**(1): 0024-2016.

Koh, W. J., B. H. Jeong, et al. (2017). "Mycobacterial Characteristics and Treatment Outcomes in Mycobacterium abscessus Lung Disease." Clin Infect Dis **64**(3): 309-316.

König, B., I. Tammer, et al. (2005). "Intra- and interpatient variability of the hsp65 and 16S-23S intergenic gene region in Mycobacterium abscessus strains from patients with cystic fibrosis." J Clin Microbiol **43**(7): 3500-3503.

Kubo, K., Y. Yamazaki, et al. (1998). "Pulmonary infection with Mycobacterium avium-intracellulare leads to air trapping distal to the small airways." Am J Respir Crit Care Med **158**(3): 979-984.

Kusunoki, S. and T. Ezaki (1992). "Proposal of Mycobacterium peregrinum sp. nov., nom. rev., and elevation of Mycobacterium chelonae subsp. abscessus (Kubica et al.) to species status: Mycobacterium abscessus comb. nov." Int J Syst Bacteriol **42**(2): 240-245.

Kwon, Y. S., A. Levin, et al. (2019). "Efficacy and safety of tigecycline for Mycobacterium abscessus disease." Respir Med **158**: 89-91.

L. Marsollier, A. A., E. Carbonnelle, S. Canaan, E. Cambau, J.-L. Herrmann (2020). "Mycobactérioses cutanées dues à Mycobacterium ulcerans, M. marinum, M. abscessus, M. chelonae et autres mycobactéries non tuberculeuses." EM Consulte.

Lam, S. S., J. D. Martell, et al. (2015). "Directed evolution of APEX2 for electron microscopy and proximity labeling." Nat Methods **12**(1): 51-54.

Lamrabet, O., F. Mba Medie, et al. (2012). "Acanthamoeba polyphaga-enhanced growth of Mycobacterium smegmatis." PLoS One **7**(1): 11.

Laufman, O., J. Perrino, et al. (2019). "Viral Generated Inter-Organelle Contacts Redirect Lipid Flux for Genome Replication." Cell **178**(2): 275-289.

Laval, T., L. Chaumont, et al. (2021). "Not too fat to fight: The emerging role of macrophage fatty acid metabolism in immunity to Mycobacterium tuberculosis." Immunol Rev **301**(1): 84-97.

Le Chevalier, F., A. Cascioferro, et al. (2015). "Revisiting the role of phospholipases C in virulence and the lifecycle of Mycobacterium tuberculosis." Sci Rep **5**(16918).

Le Moigne, V., C. Belon, et al. (2016). "MgtC as a Host-Induced Factor and Vaccine Candidate against Mycobacterium abscessus Infection." Infect Immun **84**(10): 2895-2903.

Le Moigne, V., M. Rottman, et al. (2015). "Bacterial phospholipases C as vaccine candidate antigens against cystic fibrosis respiratory pathogens: the Mycobacterium abscessus model." Vaccine **33**(18): 2118-2124.

Le Moigne, V., A. L. Roux, et al. (2020). "A TLR2-Activating Fraction From Mycobacterium abscessus Rough Variant Demonstrates Vaccine and Diagnostic Potential." Front Cell Infect Microbiol **10**(432).

Le Moigne, V., A. L. Roux, et al. (2022). "Serological biomarkers for the diagnosis of Mycobacterium abscessus infections in cystic fibrosis patients." J Cyst Fibros **21**(2): 353-360.

Lee, M. R., A. Cheng, et al. (2012). "CNS infections caused by Mycobacterium abscessus complex: clinical features and antimicrobial susceptibilities of isolates." J Antimicrob Chemother **67**(1): 222-225.

Lee, M. R., W. H. Sheng, et al. (2015). "Mycobacterium abscessus Complex Infections in Humans." Emerg Infect Dis **21**(9): 1638-1646.

Lee, S. J., Y. J. Ryu, et al. (2014). "The impact of low subcutaneous fat in patients with nontuberculous mycobacterial lung disease." Lung **192**(3): 395-401.

Lee, S. Y., H. Y. Kim, et al. (2017). "Effect of amikacin on cell wall glycopeptidolipid synthesis in Mycobacterium abscessus." J Microbiol **55**(8): 640-647.

Lemassu, A., A. Ortalo-Magné, et al. (1996). "Extracellular and surface-exposed polysaccharides of non-tuberculous mycobacteria." Microbiology **142**(Pt 6): 1513-1520.

Levy, Z. D., V. Du, et al. (2016). "Ventriculoperitoneal Shunt Infection with Mycobacterium abscessus: A Rare Cause of Ventriculitis." World Neurosurg **86**(510): 10.

Lin, T. W., M. M. Melgar, et al. (2006). "Structure-based inhibitor design of AccD5, an essential acyl-CoA carboxylase carboxyltransferase domain of Mycobacterium tuberculosis." Proc Natl Acad Sci U S A **103**(9): 3072-3077.

Liu, J., C. E. Barry, 3rd, et al. (1996). "Mycolic acid structure determines the fluidity of the mycobacterial cell wall." J Biol Chem **271**(47): 29545-29551.

Liu, J., E. Y. Rosenberg, et al. (1995). "Fluidity of the lipid domain of cell wall from Mycobacterium chelonae." Proc Natl Acad Sci U S A **92**(24): 11254-11258.

Lopeman, R. C., J. Harrison, et al. (2019). "Mycobacterium abscessus: Environmental Bacterium Turned Clinical Nightmare." Microorganisms **7**(3).

Low, K. L., G. Shui, et al. (2010). "Lipid droplet-associated proteins are involved in the biosynthesis and hydrolysis of triacylglycerol in Mycobacterium bovis bacillus Calmette-Guerin." J Biol Chem **285**(28): 21662-21670.

Luppa, H. and J. Andrä (1983). "The histochemistry of carboxylester hydrolases: problems and possibilities." Histochem J **15**(2): 111-137.

Machowski, E. E., S. Senzani, et al. (2014). "Comparative genomics for mycobacterial peptidoglycan remodelling enzymes reveals extensive genetic multiplicity." BMC Microbiol **14**(75): 1471-2180.

Maeda, S. and Y. Kashiwabara (1996). "Purification and properties of a membrane-bound phospholipase B from Mycobacterium lepraemurium." Biochim Biophys Acta **6**(1): 31-38.

Magnet, S. and J. S. Blanchard (2005). "Molecular insights into aminoglycoside action and resistance." Chem Rev **105**(2): 477-498.

Mallick, I., P. Santucci, et al. (2021). "Intrabacterial lipid inclusions in mycobacteria: unexpected key players in survival and pathogenesis?" FEMS Microbiol Rev **45**(6).

Marakalala, M. J., R. M. Raju, et al. (2016). "Inflammatory signaling in human tuberculosis granulomas is spatially organized." Nat Med **22**(5): 531-538.

Mariano, M. (1995). "The experimental granuloma. A hypothesis to explain the persistence of the lesion." Rev Inst Med Trop Sao Paulo **37**(2): 161-176.

Martinot, A. J., M. Farrow, et al. (2016). "Mycobacterial Metabolic Syndrome: LprG and Rv1410 Regulate Triacylglyceride Levels, Growth Rate and Virulence in Mycobacterium tuberculosis." PLoS Pathog **12**(1).

Maurer, F. P., V. Rüegger, et al. (2012). "Acquisition of clarithromycin resistance mutations in the 23S rRNA gene of Mycobacterium abscessus in the presence of inducible erm(41)." J Antimicrob Chemother **67**(11): 2606-2611.

McNeil, M., M. Daffe, et al. (1990). "Evidence for the nature of the link between the arabinogalactan and peptidoglycan of mycobacterial cell walls." J Biol Chem **265**(30): 18200-18206.

McNeil, M., S. J. Wallner, et al. (1987). "Demonstration that the galactosyl and arabinosyl residues in the cell-wall arabinogalactan of Mycobacterium leprae and Mycobacterium tuberculosis are furanoid." Carbohydr Res **166**(2): 299-308.

Medjahed, H., J. L. Gaillard, et al. (2010). "Mycobacterium abscessus: a new player in the mycobacterial field." Trends Microbiol **18**(3): 117-123.

Medjahed, H. and J. M. Reyrat (2009). "Construction of Mycobacterium abscessus defined glycopeptidolipid mutants: comparison of genetic tools." Appl Environ Microbiol **75**(5): 1331-1338.

Meehan, C. J., R. A. Barco, et al. (2021). "Reconstituting the genus Mycobacterium." International journal of systematic and evolutionary microbiology **71**(9).

Middlebrook (1945). "Pathogenic components of the tubercle bacillus." Am Rev Tuberc **51**: 244-259

Minnikin, D. E., S. M. Minnikin, et al. (1982). "The mycolic acids of Mycobacterium chelonei." J Gen Microbiol **128**(4): 817-822.

Mishra, K. C., C. de Chastellier, et al. (2008). "Functional role of the PE domain and immunogenicity of the Mycobacterium tuberculosis triacylglycerol hydrolase LipY." Infect Immun **76**(1): 127-140.

Miyanari, Y., K. Atsuzawa, et al. (2007). "The lipid droplet is an important organelle for hepatitis C virus production." Nat Cell Biol **9**(9): 1089-1097.

Mojica, J. E., C. J. Richards, et al. (2018). "Case 40-2018: A 47-Year-Old Woman with Recurrent Sinusitis, Cough, and Bronchiectasis." N Engl J Med **379**(26): 2558-2565.

Moore, M. and J. B. Frerichs (1953). "An unusual acid-fast infection of the knee with subcutaneous, abscess-like lesions of the gluteal region; report of a case with a study of the organism, Mycobacterium abscessus, n. sp." J Invest Dermatol **20**(2): 133-169.

Moorey, A. R. and G. S. Besra (2022). "The role of triacylglycerols and repurposing DGAT1 inhibitors for the treatment of Mycobacterium tuberculosis." Cell Surf **8**(100083).

Możejko-Ciesielska, J. and R. Kiewisz (2016). "Bacterial polyhydroxyalkanoates: Still fabulous?" Microbiol Res **192**: 271-282.

Nakagawa, H., Y. Kashiwabara, et al. (1976). "Metabolism of triacylglycerol in Mycobacterium smegmatis." J Biochem **80**(5): 923-928.

Nakanaga, K., Y. Hoshino, et al. (2011). "Multiple cases of cutaneous Mycobacterium massiliense infection in a "hot spa" in Japan." J Clin Microbiol **49**(2): 613-617.

Nash, K. A., B. A. Brown-Elliott, et al. (2009). "A novel gene, erm(41), confers inducible macrolide resistance to clinical isolates of Mycobacterium abscessus but is absent from Mycobacterium chelonae." Antimicrob Agents Chemother **53**(4): 1367-1376.

Nazarova, E. V., C. R. Montague, et al. (2019). "The genetic requirements of fatty acid import by Mycobacterium tuberculosis within macrophages." Elife **8**(8): 43621.

Nazarova, E. V., C. R. Montague, et al. (2017). "Rv3723/LucA coordinates fatty acid and cholesterol uptake in Mycobacterium tuberculosis." Elife **27**(6): 26969.

Neetika Jaisinghani, M. L. P., Joshua Andrade, Manor Askenazi, Beatrix Ueberheide, View ORCID ProfileJessica C. Seeliger (2023). "Cell wall proteomics in live Mycobacterium tuberculosis uncovers exposure of ESX substrates to the periplasm."

Ng, H. F. and Y. F. Ngeow (2022). "Genetic Determinants of Tigecycline Resistance in Mycobacteroides abscessus." Antibiotics **11**(5).

Nguyen, P. C., V. S. Nguyen, et al. (2018). "Biochemical and Structural Characterization of TesA, a Major Thioesterase Required for Outer-Envelope Lipid Biosynthesis in Mycobacterium tuberculosis." J Mol Biol **430**(24): 5120-5136.

Nolan, S. J., J. D. Romano, et al. (2017). "Host lipid droplets: An important source of lipids salvaged by the intracellular parasite Toxoplasma gondii." PLoS Pathog **13**(6).

Noone, P. G., M. W. Leigh, et al. (2004). "Primary ciliary dyskinesia: diagnostic and phenotypic features." Am J Respir Crit Care Med **169**(4): 459-467.

Okazaki, A., H. Takato, et al. (2013). "Successful treatment with chemotherapy and corticosteroids of pulmonary Mycobacterium abscessus infection accompanied by pleural effusion." J Infect Chemother **19**(5): 964-968.

Ollis, D. L., E. Cheah, et al. (1992). "The alpha/beta hydrolase fold." Protein Eng **5**(3): 197-211.

Orgeur, M. and R. Brosch (2018). "Evolution of virulence in the Mycobacterium tuberculosis complex." Curr Opin Microbiol **41**: 68-75.

Ortalo-Magné, A., A. Lemassu, et al. (1996). "Identification of the surface-exposed lipids on the cell envelopes of Mycobacterium tuberculosis and other mycobacterial species." J Bacteriol **178**(2): 456-461.

Pai, M., M. A. Behr, et al. (2016). "Tuberculosis." Nat Rev Dis Primers **2**(16076): 76.

Pandey, A. K. and C. M. Sassetti (2008). "Mycobacterial persistence requires the utilization of host cholesterol." Proc Natl Acad Sci U S A **105**(11): 4376-4380.

Parbhoo, T., S. L. Sampson, et al. (2020). "Recent Developments in the Application of Flow Cytometry to Advance our Understanding of Mycobacterium tuberculosis Physiology and Pathogenesis." Cytometry A **97**(7): 683-693.

Park, I. K., A. P. Hsu, et al. (2015). "Clonal Diversification and Changes in Lipid Traits and Colony Morphology in Mycobacterium abscessus Clinical Isolates." J Clin Microbiol **53**(11): 3438-3447.

Parker, S. K., R. M. Barkley, et al. (2009). "Mycobacterium tuberculosis Rv3802c encodes a phospholipase/thioesterase and is inhibited by the antimycobacterial agent tetrahydrolipstatin." PLoS One **4**(1): 26.

Parmar, S. and E. I. Tocheva (2023). "The cell envelope of Mycobacterium abscessus and its role in pathogenesis." PLoS Pathog **19**(5).

Pawlik, A., G. Garnier, et al. (2013). "Identification and characterization of the genetic changes responsible for the characteristic smooth-to-rough morphotype alterations of clinically persistent Mycobacterium abscessus." Mol Microbiol **90**(3): 612-629.

Peyron, P., J. Vaubourgeix, et al. (2008). "Foamy macrophages from tuberculous patients' granulomas constitute a nutrient-rich reservoir for M. tuberculosis persistence." PLoS Pathog **4**(11): 11.

Pfyffer, G. E., H. M. Welscher, et al. (1997). "Comparison of the Mycobacteria Growth Indicator Tube (MGIT) with radiometric and solid culture for recovery of acid-fast bacilli." J Clin Microbiol **35**(2): 364-368.

Piersimoni, C. and C. Scarparo (2009). "Extrapulmonary infections associated with nontuberculous mycobacteria in immunocompetent persons." Emerg Infect Dis **15**(9): 1351-1358.

Point, V., R. K. Malla, et al. (2012). "Synthesis and kinetic evaluation of cyclophostin and cyclipostins phosphonate analogs as selective and potent inhibitors of microbial lipases." J Med Chem **55**(22): 10204-10219.

Portillo, K. and J. Morera (2012). "Nutritional status and eating disorders: neglected risks factor for nontuberculous mycobacterial lung disease?" Med Hypotheses **78**(1): 39-41.

Prados-Rosales, R., L. J. Carreño, et al. (2016). "The Type of Growth Medium Affects the Presence of a Mycobacterial Capsule and Is Associated With Differences in Protective Efficacy of BCG Vaccination Against Mycobacterium tuberculosis." J Infect Dis **214**(3): 426-437.

Prevots, D. R. and T. K. Marras (2015). "Epidemiology of human pulmonary infection with nontuberculous mycobacteria: a review." Clin Chest Med **36**(1): 13-34.

Rabhi, S., I. Rabhi, et al. (2016). "Lipid Droplet Formation, Their Localization and Dynamics during Leishmania major Macrophage Infection." PLoS One **11**(2).

Rao, A. and A. Ranganathan (2004). "Interaction studies on proteins encoded by the phthiocerol dimycocerosate locus of Mycobacterium tuberculosis." Mol Genet Genomics **272**(5): 571-579.

Rastogi, N., E. Legrand, et al. (2001). "The mycobacteria: an introduction to nomenclature and pathogenesis." Rev Sci Tech **20**(1): 21-54.

Raynaud, C., C. Guilhot, et al. (2002). "Phospholipases C are involved in the virulence of Mycobacterium tuberculosis." Mol Microbiol **45**(1): 203-217.

Recht, J. and R. Kolter (2001). "Glycopeptidolipid acetylation affects sliding motility and biofilm formation in Mycobacterium smegmatis." J Bacteriol **183**(19): 5718-5724.

Remm, S., D. De Vecchis, et al. (2023). "Structural basis for triacylglyceride extraction from mycobacterial inner membrane by MFS transporter Rv1410." Nature Communications **14**(1): 6449.

Rhee, H. W., P. Zou, et al. (2013). "Proteomic mapping of mitochondria in living cells via spatially restricted enzymatic tagging." Science **339**(6125): 1328-1331.

Rhoades, E. R., A. S. Archambault, et al. (2009). "Mycobacterium abscessus Glycopeptidolipids mask underlying cell wall phosphatidyl-myo-inositol mannosides blocking induction of human macrophage TNF-alpha by preventing interaction with TLR2." J Immunol **183**(3): 1997-2007.

Richard, M., A. V. Gutiérrez, et al. (2018). "Mutations in the MAB_2299c TetR Regulator Confer Cross-Resistance to Clofazimine and Bedaquiline in Mycobacterium abscessus." Antimicrob Agents Chemother **63**(1): 01316-01318.

Richard, M., A. V. Gutiérrez, et al. (2018). "Mechanistic and Structural Insights Into the Unique TetR-Dependent Regulation of a Drug Efflux Pump in Mycobacterium abscessus." Front Microbiol **9**(649).

Richter, L. and B. Saviola (2009). "The lipF promoter of Mycobacterium tuberculosis is upregulated specifically by acidic pH but not by other stress conditions." Microbiol Res **164**(2): 228-232.

Ripoll, F., S. Pasek, et al. (2009). "Non mycobacterial virulence genes in the genome of the emerging pathogen Mycobacterium abscessus." PLoS One **4**(6): 0005660.

Rodriguez, G. M., M. I. Voskuil, et al. (2002). "ideR, An essential gene in mycobacterium tuberculosis: role of IdeR in iron-dependent gene expression, iron metabolism, and oxidative stress response." Infect Immun **70**(7): 3371-3381.

Romano, M., F. Squeglia, et al. (2023). "A Structural View at Vaccine Development against M. tuberculosis." Cells **12**(2).

Roux, A. L., A. Viljoen, et al. (2016). "The distinct fate of smooth and rough Mycobacterium abscessus variants inside macrophages." Open Biol **6**(11): 160185.

Ruis, C., J. M. Bryant, et al. (2021). "Dissemination of Mycobacterium abscessus via global transmission networks." Nat Microbiol **6**(10): 1279-1288.

Runyon, E. H. (1959). "Anonymous mycobacteria in pulmonary disease." Med Clin North Am **43**(1): 273-290.

Russell, D. G., C. E. Barry, 3rd, et al. (2010). "Tuberculosis: what we don't know can, and does, hurt us." Science **328**(5980): 852-856.

Russell, D. G., P. J. Cardona, et al. (2009). "Foamy macrophages and the progression of the human tuberculosis granuloma." Nat Immunol **10**(9): 943-948.

Rutschmann, M., N. Redinger, et al. (2023). "Amikacin@SiO(2) core@shell nanocarriers to treat pulmonal bacterial infections." J Mater Chem B **10**(10).

Safi, R., M. Sánchez-Álvarez, et al. (2023). "Defensive-lipid droplets: Cellular organelles designed for antimicrobial immunity." Immunol Rev **317**(1): 113-136.

Salaemae, W., A. Azhar, et al. (2011). "Biotin biosynthesis in Mycobacterium tuberculosis: physiology, biochemistry and molecular intervention." Protein Cell **2**(9): 691-695.

Salipante, S. J. and B. G. Hall (2011). "Towards the molecular epidemiology of Mycobacterium leprae: strategies, successes, and shortcomings." Infect Genet Evol **11**(7): 1505-1513.

Sánchez-Chardi, A., F. Olivares, et al. (2011). "Demonstration of cord formation by rough Mycobacterium abscessus variants: implications for the clinical microbiology laboratory." J Clin Microbiol **49**(6): 2293-2295.

Sani, M., E. N. Houben, et al. (2010). "Direct visualization by cryo-EM of the mycobacterial capsular layer: a labile structure containing ESX-1-secreted proteins." PLoS Pathog **6**(3): 1000794.

Santucci, P., F. Bouzid, et al. (2016). "Experimental Models of Foamy Macrophages and Approaches for Dissecting the Mechanisms of Lipid Accumulation and Consumption during Dormancy and Reactivation of Tuberculosis." Front Cell Infect Microbiol **6**(122).

Santucci, P., S. Diomandé, et al. (2018). "Delineating the Physiological Roles of the PE and Catalytic Domains of LipY in Lipid Consumption in Mycobacterium-Infected Foamy Macrophages." Infect Immun **86**(9): 00394-00318.

Santucci, P., M. D. Johansen, et al. (2019). "Nitrogen deprivation induces triacylglycerol accumulation, drug tolerance and hypervirulence in mycobacteria." Sci Rep **9**(1): 019-45164.

Santucci, P., V. Point, et al. (2018). "LipG a bifunctional phospholipase/thioesterase involved in mycobacterial envelope remodeling." Biosci Rep **38**(6): 21.

Santucci, P., N. Smichi, et al. (2019). "Dissecting the membrane lipid binding properties and lipase activity of Mycobacterium tuberculosis LipY domains." Febs J **286**(16): 3164-3181.

Sardiña, L. A., U. Kaw, et al. (2020). "Diagnosis of Mycobacterium abscessus/chelonae complex cutaneous infection: Correlation of tissue culture and skin biopsy." J Cutan Pathol **47**(4): 321-327.

Sarmiento, M. E., N. Alvarez, et al. (2019). "Tuberculosis vaccine candidates based on mycobacterial cell envelope components." Tuberculosis **115**: 26-41.

Sarrazin, M., B. P. Martin, et al. (2022). "Synthesis and Biological Characterization of Fluorescent Cyclipostins and Cyclophostin Analogues: New Insights for the Diagnosis of Mycobacterial-Related Diseases." ACS Infect Dis **8**(12): 2564-2578.

Sassi, M. and M. Drancourt (2014). "Genome analysis reveals three genomospecies in Mycobacterium abscessus." BMC Genomics **15**(1): 1471-2164.

Schmalstig, A. A., A. Wiggins, et al. (2023). "Bacteriophage infection and killing of intracellular Mycobacterium abscessus." mBio **7**(10): 02924-02923.

Schué, M., L. G. Dover, et al. (2009). "Sequence and analysis of a plasmid-encoded mercury resistance operon from Mycobacterium marinum identifies MerH, a new mercuric ion transporter." J Bacteriol **191**(1): 439-444.

Schué, M., D. Maurin, et al. (2010). "Two cutinase-like proteins secreted by Mycobacterium tuberculosis show very different lipolytic activities reflecting their physiological function." Faseb J **24**(6): 1893-1903.

Shahraki, A. H., P. Heidarieh, et al. (2015). ""Multidrug-resistant tuberculosis" may be nontuberculous mycobacteria." Eur J Intern Med **26**(4): 279-284.

Shallom, S. J., P. J. Gardina, et al. (2013). "New rapid scheme for distinguishing the subspecies of the Mycobacterium abscessus group and identifying Mycobacterium massiliense isolates with inducible clarithromycin resistance." J Clin Microbiol **51**(9): 2943-2949.

Sharma, S. K. and V. Upadhyay (2020). "Epidemiology, diagnosis & treatment of non-tuberculous mycobacterial diseases." Indian J Med Res **152**(3): 185-226.

Shen, G., K. Singh, et al. (2012). "LipC (Rv0220) is an immunogenic cell surface esterase of Mycobacterium tuberculosis." Infect Immun **80**(1): 243-253.

Shteinberg, M., I. J. Haq, et al. (2021). "Cystic fibrosis." Lancet **397**(10290): 2195-2211.

Silva Miranda, M., A. Breiman, et al. (2012). "The tuberculous granuloma: an unsuccessful host defence mechanism providing a safety shelter for the bacteria?" Clin Dev Immunol **139127**(10): 3.

Simcox, B. S., B. R. Tomlinson, et al. (2023). "Mycobacterium abscessus DosRS two-component system controls a species-specific regulon required for adaptation to hypoxia." Front Cell Infect Microbiol **13**(1144210).

Simmon, K. E., J. I. Pounder, et al. (2007). "Identification of an emerging pathogen, Mycobacterium massiliense, by rpoB sequencing of clinical isolates collected in the United States." J Clin Microbiol **45**(6): 1978-1980.

Sirakova, T. D., V. S. Dubey, et al. (2006). "Identification of a diacylglycerol acyltransferase gene involved in accumulation of triacylglycerol in Mycobacterium tuberculosis under stress." Microbiology **152**(Pt 9): 2717-2725.

Sletten, E. M. and C. R. Bertozzi (2011). "From mechanism to mouse: a tale of two bioorthogonal reactions." Acc Chem Res **44**(9): 666-676.

Somoskovi, A. and M. Salfinger (2014). "Nontuberculous mycobacteria in respiratory infections: advances in diagnosis and identification." Clin Lab Med **34**(2): 271-295.

Soroka, D., V. Dubée, et al. (2014). "Characterization of broad-spectrum Mycobacterium abscessus class A β-lactamase." J Antimicrob Chemother **69**(3): 691-696.

Sousa, P. P., R. C. Cruz, et al. (2015). "Mycobacterium abscessus skin infection after tattooing--Case report." An Bras Dermatol **90**(5): 741-743.

Srivastava, S., S. Chaudhary, et al. (2015). "Unsaturated Lipid Assimilation by Mycobacteria Requires Auxiliary cis-trans Enoyl CoA Isomerase." Chem Biol **22**(12): 1577-1587.

Srivastava, S., S. Dey, et al. (2023). "Vaccines against Tuberculosis: Where Are We Now?" Vaccines **11**(5).

Stehr, M., A. A. Elamin, et al. (2012). "Cytosolic lipid inclusions formed during infection by viral and bacterial pathogens." Microbes Infect **14**(13): 1227-1237.

Steindor, M., F. Stehling, et al. (2021). "Species-Specific Interferon-Gamma Release Assay for the Diagnosis of Mycobacterium abscessus Complex Infection." Front Microbiol **12**(692395).

Surette, M. G. (2014). "The cystic fibrosis lung microbiome." Ann Am Thorac Soc **11**(1): 201306-201159MG.

Swarbrick, C. M., G. V. Bythrow, et al. (2017). "Mycobacteria Encode Active and Inactive Classes of TesB Fatty-Acyl CoA Thioesterases Revealed through Structural and Functional Analysis." Biochemistry **56**(10): 1460-1472.

Swenson, J. M., R. J. Wallace, Jr., et al. (1985). "Antimicrobial susceptibility of five subgroups of Mycobacterium fortuitum and Mycobacterium chelonae." Antimicrob Agents Chemother **28**(6): 807-811.

Talley, J. T. and S. S. Mohiuddin (2023). Biochemistry, Fatty Acid Oxidation.

Tauchi-Sato, K., S. Ozeki, et al. (2002). "The surface of lipid droplets is a phospholipid monolayer with a unique Fatty Acid composition." J Biol Chem **277**(46): 44507-44512.

Tazi, A., J. R. Araujo, et al. (2018). "Disentangling Host-Microbiota Regulation of Lipid Secretion by Enterocytes: Insights from Commensals Lactobacillus paracasei and Escherichia coli." mBio **9**(5): 01493-01418.

Teng, S. H., C. M. Chen, et al. (2013). "Matrix-assisted laser desorption ionization-time of flight mass spectrometry can accurately differentiate between Mycobacterium masilliense (M. abscessus subspecies bolletti) and M. abscessus (sensu stricto)." J Clin Microbiol **51**(9): 3113-3116.

Thomson, R., C. Tolson, et al. (2013). "Isolation of nontuberculous mycobacteria (NTM) from household water and shower aerosols in patients with pulmonary disease caused by NTM." J Clin Microbiol **51**(9): 3006-3011.

Thomson, R., C. Tolson, et al. (2013). "Mycobacterium abscessus isolated from municipal water - a potential source of human infection." BMC Infect Dis **13**(241): 1471-2334.

To, K., R. Cao, et al. (2020). "General Overview of Nontuberculous Mycobacteria Opportunistic Pathogens: Mycobacterium avium and Mycobacterium abscessus." J Clin Med **9**(8).

Tortoli, E., B. A. Brown-Elliott, et al. (2019). "Same meat, different gravy: ignore the new names of mycobacteria." The European respiratory journal **54**(1).

Tortoli, E., T. Fedrizzi, et al. (2017). "The new phylogeny of the genus Mycobacterium: The old and the news." Infect Genet Evol **56**: 19-25.

Touré, H., L. A. Galindo, et al. (2023). "Mycobacterium abscessus resists the innate cellular response by surviving cell lysis of infected phagocytes." PLoS Pathog **19**(3).

Trias, J. and R. Benz (1994). "Permeability of the cell wall of Mycobacterium smegmatis." Mol Microbiol **14**(2): 283-290.

Trias, J., V. Jarlier, et al. (1992). "Porins in the cell wall of mycobacteria." Science **258**(5087): 1479-1481.

Turner, K. H., A. K. Wessel, et al. (2015). "Essential genome of Pseudomonas aeruginosa in cystic fibrosis sputum." Proc Natl Acad Sci U S A **112**(13): 4110-4115.

Varghese, B., S. E. Shajan, et al. (2012). "First case report of chronic pulmonary lung disease caused by Mycobacterium abscessus in two immunocompetent patients in Saudi Arabia." Ann Saudi Med **32**(3): 312-314.

Vielemeyer, O., M. T. McIntosh, et al. (2004). "Neutral lipid synthesis and storage in the intraerythrocytic stages of Plasmodium falciparum." Mol Biochem Parasitol **135**(2): 197-209.

Vilchèze, C. and L. Kremer (2017). "Acid-Fast Positive and Acid-Fast Negative Mycobacterium tuberculosis: The Koch Paradox." Microbiol Spectr **5**(2): 0003-2015.

Viljoen, A., M. Blaise, et al. (2016). "MAB_3551c encodes the primary triacylglycerol synthase involved in lipid accumulation in Mycobacterium abscessus." Mol Microbiol **102**(4): 611-627.

Viljoen, A., M. Richard, et al. (2018). "Cyclipostins and cyclophostin analogs inhibit the antigen 85C from Mycobacterium tuberculosis both in vitro and in vivo." J Biol Chem **293**(8): 2755-2769.

Waddell, S. J., G. A. Chung, et al. (2005). "Inactivation of polyketide synthase and related genes results in the loss of complex lipids in Mycobacterium tuberculosis H37Rv." Lett Appl Microbiol **40**(3): 201-206.

Wakamatsu, K., N. Nagata, et al. (2015). "Patients with MAC Lung Disease Have a Low Visceral Fat Area and Low Nutrient Intake." Pulm Med **218253**(10): 29.

Wallace, R. J., Jr., B. A. Brown, et al. (1997). Mycobacterium chelonae vs. abscessus, Pediatr Infect Dis J. 1997 Aug;16(8):829. doi: 10.1097/00006454-199708000-00027.

Wältermann, M., A. Hinz, et al. (2005). "Mechanism of lipid-body formation in prokaryotes: how bacteria fatten up." Mol Microbiol **55**(3): 750-763.

Wang, S. H. and P. Pancholi (2014). "Mycobacterial skin and soft tissue infection." Curr Infect Dis Rep **16**(11): 014-0438.

Wayne, L. G. and L. G. Hayes (1996). "An in vitro model for sequential study of shiftdown of Mycobacterium tuberculosis through two stages of nonreplicating persistence." Infect Immun **64**(6): 2062-2069.

West, N. P., F. M. Chow, et al. (2009). "Cutinase-like proteins of Mycobacterium tuberculosis: characterization of their variable enzymatic functions and active site identification." Faseb J **23**(6): 1694-1704.

Whang, J., Y. W. Back, et al. (2017). "Mycobacterium abscessus glycopeptidolipids inhibit macrophage apoptosis and bacterial spreading by targeting mitochondrial cyclophilin D." Cell Death Dis **8**(8): 420.

WHO (2023). Global tuberculosis report.

Wilburn, K. M., R. A. Fieweger, et al. (2018). "Cholesterol and fatty acids grease the wheels of Mycobacterium tuberculosis pathogenesis." Pathog Dis **76**(2).

Wilkin, J. M., K. Soetaert, et al. (1999). "Overexpression, purification and characterization of Mycobacterium bovis BCG alcohol dehydrogenase." Eur J Biochem **262**(2): 299-307.

Wilmers, M. J., H. M. Mackay, et al. (1950). "Five cases of cystic fibrosis of the pancreas." Proc R Soc Med **43**(11): 829-832.

Wipperman, M. F., M. Yang, et al. (2013). "Shrinking the FadE proteome of Mycobacterium tuberculosis: insights into cholesterol metabolism through identification of an α2β2 heterotetrameric acyl coenzyme A dehydrogenase family." J Bacteriol **195**(19): 4331-4341.

Wongkitisophon, P., P. Rattanakaemakorn, et al. (2011). Cutaneous Mycobacterium abscessus Infection Associated with Mesotherapy Injection, Case Rep Dermatol. 2011 Feb 18;3(1):37-41. doi: 10.1159/000324766.

Wu, M. L., D. B. Aziz, et al. (2018). "NTM drug discovery: status, gaps and the way forward." Drug Discov Today **23**(8): 1502-1519.

Xu, W. Q., J. S. Cheah, et al. (2023). Dynamic mapping of proteome trafficking within and between living cells by TransitID, bioRxiv. 2023 Feb 8:2023.02.07.527548. doi: 10.1101/2023.02.07.527548. Preprint.

Yang, D., G. Vandenbussche, et al. (2020). "Methyl arachidonyl fluorophosphonate inhibits Mycobacterium tuberculosis thioesterase TesA and globally affects vancomycin susceptibility." FEBS Lett **594**(1): 79-93.

Yuan, T. and N. S. Sampson (2018). "Hit Generation in TB Drug Discovery: From Genome to Granuloma." Chem Rev **118**(4): 1887-1916.

Zapun, A., C. Contreras-Martel, et al. (2008). "Penicillin-binding proteins and beta-lactam resistance." FEMS Microbiol Rev **32**(2): 361-385.

Zaunbrecher, M. A., R. D. Sikes, Jr., et al. (2009). "Overexpression of the chromosomally encoded aminoglycoside acetyltransferase eis confers kanamycin resistance in Mycobacterium tuberculosis." Proc Natl Acad Sci U S A **106**(47): 20004-20009.

Zhang, C. and P. Liu (2019). "The New Face of the Lipid Droplet: Lipid Droplet Proteins." Proteomics **19**(10): 8.

Zhang, M., J. D. Wang, et al. (2005). "Expression and characterization of the carboxyl esterase Rv3487c from Mycobacterium tuberculosis." Protein Expr Purif **42**(1): 59-66.

Zuber, B., M. Chami, et al. (2008). "Direct visualization of the outer membrane of mycobacteria and corynebacteria in their native state." J Bacteriol **190**(16): 5672-5680.